NASA CR-168,417

OLD DOMINION UNIVERSITY RESEARCH FOUNDATION

DEPARTMENT OF MECHANICAL ENGINEERING
AND MECHANICS
SCHOOL OF ENGINEERING
OLD DOMINION UNIVERSITY
NORFOLK, VIRGINIA

NASA-CR-168417
1982 000 9839

EFFECTS OF MULTIPLE SCATTERING AND SURFACE ALBEDO ON THE PHOTOCHEMISTRY OF THE TROPOSPHERE

By

T. R. Augustsson

and

S. N. Tiwari, Principal Investigator

Final Report
For the period ending November 30, 1981

Prepared for the
National Aeronautics and Space Administration
Langley Research Center
Hampton, Virginia 23665

LIBRARY COPY

1984

LANGLEY RESEARCH CENTER
LIBRARY, NASA
HAMPTON, VIRGINIA

Under
Cooperative Agreement NCCI-30
Joel S. Levine, Technical Monitor
Atmospheric Environmental Sciences Division

December 1981

3 1176 00511 3320

DEPARTMENT OF MECHANICAL ENGINEERING
AND MECHANICS
SCHOOL OF ENGINEERING
OLD DOMINION UNIVERSITY
NORFOLK, VIRGINIA

EFFECTS OF MULTIPLE SCATTERING AND SURFACE ALBEDO ON THE PHOTOCHEMISTRY OF THE TROPOSPHERE

By

T. R. Augustsson

and

S. N. Tiwari, Principal Investigator

Final Report
For the period ending November 30, 1981

Prepared for the
National Aeronautics and Space Administration
Langley Research Center
Hampton, Virginia 23665

Under
Cooperative Agreement NCCI-30
Joel S. Levine, Technical Monitor
Atmospheric Environmental Sciences Division

Submitted by the
Old Dominion University Research Foundation
P.O. Box 6369
Norfolk, Virginia 23508-0369

December 1981

N82-17707 #

FOREWORD

This is a comprehensive report of the work done on the project "Coupled Radiative-Chemical Studies of the Earth's Troposphere." The report emphasizes the work completed during the period December 1, 1980 through November 30, 1981. The study was supported by the NASA/Langley Research Center (Atmospheric Sciences Branch of the Atmospheric Environmental Sciences Division) under Cooperative Agreement NCCI-30. The cooperative agreement was monitored by Dr. Joel S. Levine of the Atmospheric Environmental Sciences Division.

TABLE OF CONTENTS

	Page
FOREWORD	iii
SUMMARY	1
INTRODUCTION	3
LIST OF SYMBOLS	5
BASIC FORMULATION	8
Introduction	8
The Species Continuity Equation	8
Photolysis Rate Calculations	12
Heterogeneous Losses	21
RADIATION MODEL	22
RESULTS AND DISCUSSION	24
Introduction	24
Comparison of Calculated Photodissociation Frequencies Using the Leighton Approxiation and the Matrix Inversion Technique	24
The Nitrogen Group	52
Introduction	52
Molecular nitrogen (N_2)	55
Ammonia (NH_3)	55
Nitrogen oxides ($NO_x = NO + NO_2$)	61
Nitric acid (HNO_3)	69
Nitrous acid (HNO_2)	74
Hydrazine (N_2H_4)	78
Nitrogen trioxide (NO_3)	81

Page

Amino radical (NH_2) 85

Dinitrogen pentoxide (N_2O_5) 87

Imino radical (NH). 92

Nitroxyl radical (HNO). 95

Hydrazine derivative (N_2H_3) 98

Hydrazine derivative (N_2H_2) 98

Future perturbations to the nitrogen budget. 102

The Oxygen Group. 104

Introduction. 104

Molecular oxygen (O_2) 105

Ozone (O_3). 105

Atomic oxygen [$O(^3p)$] 112

Excited oxygen atom [$O(^1D)$] 116

Future perturbations to the oxygen budget. 121

The Hydrogen Group. 122

Introduction. 122

Water vapor (H_2O) 122

Molecular hydrogen (H_2) 124

Hydrogen peroxide (H_2O_2). 125

Hydroperoxyl radical (HO_2). 126

Hydroxyl radical (OH) 129

Atomic hydrogen (H) 137

Future perturbations to the hydrogen budget. 141

The Carbon Group. 142

Page

Introduction. 142

Methane (CH_4) 144

Carbon monoxide (CO). 145

Methylhydroperoxy (CH_3OOH). 146

Formaldehyde (CH_2O) 149

Methylperoxy radical (CH_3O_2). 151

Methoxy radical (CH_3O). 153

Methyl radical (CH_3). 159

Formyl radical (HCO). 161

Future perturbations to the carbon budget. 165

The Sulfur Group. 166

Introduction. 166

Sulfur dioxide (SO_2). 168

Carbonyl sulfide (COS). 173

Hydrogen sulfide (H_2S). 177

Carbon disulfide (CS_2). 180

Sulfuric acid (H_2SO_4) 182

Sulfuric acid radical (HSO_3). 187

Sulfoxy (SO). 190

Thiohydroxyl radical (HS) 194

Carbon sulfide (CS) 196

Sulfur trioxide (SO_3) 200

Atomic sulfur [$S(^3p)$] 202

Methanethiol (CH_3SH). 205

Dimethyl sulfide (CH_3SCH_3). 209

Page

Future perturbations to the sulfur budget. 212

CONCLUSIONS. 214

REFERENCES 217

APPENDIX A: PHOTOCHEMICAL AND KINETIC DATA. 231

APPENDIX B: THE CONTINUIY EQUATION. 243

APPENDIX C: BOUNDARY CONDITIONS 247

APPENDIX D: CONVERGENCE CRITERIA. 251

LIST OF TABLES

Table Page

1 Photodissociation frequencies of O_3 and ratios of photodissociation frequencies for multiple scattering for various albedos and the Leighton approximation. 27

2 Photodissociation frequencies of O_3 and ratios for multiple scattering for various albedos and the Leighton approximation 29

3 Photodissociation frequencies of NO_2 and ratios for multiple scattering for various albedos and the Leighton approximation 32

4 Photodissociation frequencies of NO_3 and ratios for multiple scattering for various albedos and the Leighton approximation 35

5 Photodissociation frequencies of NO_3 and ratios for multiple scattering for various albedos and the Leighton approximation 36

6 Photodissociation frequencies of N_2O_5 and ratios for multiple scattering for various albedos and the Leighton approximation 39

7 Photodissociation frequencies of HNO_3 and ratios for multiple scattering for various albedos and the Leighton approximation 42

8 Photodissociation frequencies of HNO_2 and ratios for multiple scattering for various albedos and the Leighton approximation 45

9 Photodissociation frequencies of H_2O_2 and CH_3OOH and ratios for multiple scattering for various albedos and the Leighton approximation. 47

Table		Page
10	Photodissociation frequencies of CH_2O and ratios for multiple scattering for various albedos and the Leighton approximation	50
11	Photodissociation frequencies of CH_2O and ratios for multiple scattering for various albedos and the Leighton approximation	51
12	Production and destruction terms of NH_3 and percent of total production and destruction.	58
13	Production and destruction terms of NO_x and percent of total production and destruction.	67
14	Production and destruction terms of HNO_3 and percent of total production and destruction.	71
15	Production and destruction terms of HNO_2 and percent of total production and destruction.	75
16	Production and destruction terms of N_2H_4 and percent of total production and destruction.	79
17	Production and destruction terms of NO_3 and percent of total production and destruction.	82
18	Production and destruction terms of NH_2 and percent of total production and destruction.	86
19	Production and destruction terms of N_2O_5 and percent of total production and destruction.	90
20	Production and destruction terms of NH and percent of total production and destruction.	93
21	Production and destruction terms of HNO and percent of total production and destruction.	96
22	Production and destruction terms of N_2H_3 and percent of total production and destruction.	99
23	Production terms of N_2H_2 and percent of total production.	101
24	Production and destruction terms of $O(^3p)$ and percent of total production and destruction.	114
25	Production and destruction terms of $O(^1D)$ and percent of total production and destruction.	119

Table		Page
26	Production and destruction terms of HO_2 and percent of total production and destruction.	127
27	Production and destruction terms of OH and percent of total production and destruction.	132
28	Production and destruction terms of H and percent of total production and destruction.	139
29	Production and destruction terms of CH_3OOH and percent of total production and destruction.	147
30	Production and destruction terms of CH_2O and percent of total production and destruction.	150
31	Production and destruction terms of CH_3O_2 and percent of total production and destruction.	154
32	Production and destruction terms of CH_3O and percent of total production and destruction.	157
33	Production and destruction terms of CH_3 and percent of total production and destruction.	160
34	Production and destruction terms of HCO and percent of total production and destruction.	163
35	Production and destruction terms of SO_2 and percent of total production and destruction.	170
36	Production and destruction terms of COS and percent of total production and destruction.	174
37	Production and destruction terms of H_2S and percent of total production and destruction.	178
38	Production and destruction terms of CS_2 and percent of total production and destruction.	181
39	Production and destruction terms of H_2SO_4 and percent of total production and destruction.	185
40	Production and destruction terms of HSO_3 and percent of total production and destruction.	188
41	Production and destruction terms of SO and percent of total production and destruction.	191
42	Production and destruction terms of HS and percent of total production and destruction.	195

Table | Page

43 Production and destruction terms of CS and percent of total production and destruction. 198

44 Production and destruction terms of SO_3 and percent of total production and destruction. 201

45 Production and destruction terms of $S(^3p)$ and percent of total production and destruction. 204

46 Destruction terms of CH_3SH and percent of total destruction 207

47 Destruction terms of CH_3SCH_3 and percent of total destruction 210

A1 Photolytic reactions included in the model. 232

A2 Chemical reactions included in the model. 233

LIST OF FIGURES

Figure | Page

1 Solar flux versus wavelength for the spectral region from 270 to 730 nm. 15

2 Absorption cross sections versus wavelength for O_3, CH_2O, CH_3OOH, and H_2O_2. 16

3 Quantum efficiency for ozone photolysis ($\lambda < 320$ nm) and branching ratios for CH_2O and NO_2 photolysis. 17

4 Absorption cross sections versus wavelength for NO_2, NO_3, N_2O_5, HNO_2, and HNO_3. 19

5 Photodissociation frequencies of O_3 for the multiple scattering cases with various albedos and the Leighton approximation 26

6 Photodissociation frequencies of O_3 for the multiple scattering cases with various albedos and the Leighton approximation 28

7 Photodissociation frequencies of NO_2 for the multiple scattering cases with various albedos and the Leighton approximation 33

8 Photodissociation frequencies of NO_3 for the multiple scattering cases with various albedos and the Leighton approximation 37

9 Photodissociation frequencies of NO_3 for the multiple scattering cases with various albedos and the Leighton approximation 38

Figure		Page
10	Photodissociation frequencies of N_2O_5 for the multiple scattering cases with various albedos and the Leighton approximation	41
11	Photodissociation frequencies of HNO_3 for the multiple scattering cases with various albedos and the Leighton approximation	43
12	Photodissociation frequencies of HNO_2 for the multiple scattering cases with various albedos and the Leighton approximation	46
13	Photodissociation frequencies of H_2O_2 and CH_3OOH for the multiple scattering cases with various albedos and the Leighton approximation.	48
14	Photodissociation frequencies of CH_2O for the multiple scattering cases with various albedos and the Leighton approximation	53
15	Photodissociation frequencies of CH_2O for the multiple scattering cases with various albedos and the Leighton approximation	54
16	Reaction paths of the nitrogen family	56
17	Vertical distributions of NH_3 for the multiple scattering cases with various albedos and the Leighton approximation.	60
18	Vertical distributions of NO for the multiple scattering cases with various albedos and the Leighton approximation.	65
19	Vertical distributions of NO_2 for the multiple scattering cases with various albedos and the Leighton approximation.	66
20	Vertical distributions of HNO_3 for the multiple scattering cases with various albedos and the Leighton approximation.	73
21	Vertical distributions of HNO_2 for the multiple scattering cases with various albedos and the Leighton approximation.	77
22	Vertical distributions of N_2H_4 for the multiple scattering cases with various albedos and the Leighton approximation.	80
23	Vertical distributions of NO_3 for the multiple scattering cases with various albedos and the Leighton approximation.	84
24	Vertical distributions of NH_2 for the multiple scattering cases with various albedos and the Leighton approximation.	88
25	Vertical distributions of N_2O_5 for the multiple scattering cases with various albedos and the Leighton approximation.	91
26	Vertical distributions of NH for the multiple scattering cases with various albedos and the Leighton approximation.	94

Figure		Page
27	Vertical distributions of HNO for the multiple scattering cases with various albedos and the Leighton approximation.	97
28	Vertical distributions of N_2H_3 for the multiple scattering cases with various albedos and the Leighton approximation.	100
29	Vertical distributions of N_2H_2 for the multiple scattering cases with various albedos and the Leighton approximation.	103
30	Reaction paths of the oxygen family	106
31	Vertical distributions of O_3 for the multiple scattering cases with various albedos and the Leighton approximation.	111
32	Vertical distributions of $O(^3P)$ for the multiple scattering cases with various albedos and the Leighton approximation	117
33	Vertical distributions of $O(^1D)$ for the multiple scattering cases with various albedos and the Leighton approximation	120
34	Reaction paths of the hydrogen family	123
35	Vertical distributions of NO_2 for the multiple scattering cases with various albedos and the Leighton approximation.	130
36	Vertical distributions of OH for the multiple scattering cases with various albedos and the Leighton approximation.	136
37	Vertical distributions of H for the multiple scattering cases with various albedos and the Leighton approximation.	140
38	Reaction paths of the carbon family	143
39	Vertical distributions of CH_3OOH for the multiple scattering cases with various albedos and the Leighton approximation	148
40	Vertical distributions of CH_2O for the multiple scattering cases with various albedos and the Leighton approximation.	152
41	Vertical distributions of CH_3O_2 for the multiple scattering cases with various albedos and the Leighton approximation	155
42	Vertical distributions of CH_3O for the multiple scattering cases with various albedos and the Leighton approximation.	158
43	Vertical distributions of CH_3 for the multiple scattering cases with various albedos and the Leighton approximation.	162
44	Vertical distributions of HCO for the multiple scattering cases with various albedos and the Leighton approximation.	164

Figure		Page
45	Reaction paths of the sulfur family	167
46	Vertical distributions of SO_2 for the multiple scattering cases with various albedos and tne Leighton approximation.	171
47	Vertical distributions of COS for the multiple scattering cases with various albedos and the Leighton approximation.	176
48	Vertical distributions of H_2S for the multiple scattering cases with various albedos and the Leighton approximation.	179
49	Vertical distributions of CS_2 for the multiple scattering cases with various albedos and the Leighton approximation.	183
50	Vertical distributions of H_2SO_4 for the multiple scattering cases with various albedos and the Leighton approximation	186
51	Vertical distributions of HSO_3 for the multiple scattering cases with various albedos and the Leighton approximation.	189
52	Vertical distributions of SO for the multiple scattering cases with various albedos and the Leighton approximation.	193
53	Vertical distributions of HS for the multiple scattering cases with various albedos and tne Leighton approximation.	197
54	Vertical distributions of CS for the multiple scattering cases with various albedos and tne Leighton approximation.	199
55	Vertical distributions of SO_3 for the multiple scattering cases with various albedos and the Leighton approximation.	203
56	Vertical distributions of $S(^3p)$ for the multiple scattering cases with various albedos and the Leighton approximation	206
57	Vertical distributions of CH_3SH for the multiple scattering cases with various albedos and the Leighton approximation	208
58	Vertical distributions of CH_3SCH_3 for the multiple scattering cases with various albedos and the Leighton approximation	211

EFFECT OF MULTIPLE SCATTERING AND SURFACE ALBEDO ON THE PHOTOCHEMISTRY OF THE TROPOSPHERE

By

T. R. Augustsson[1] and S. N. Tiwari[2]

SUMMARY

A one-dimensional photochemical model of the troposhere containing the species of the nitrogen, oxygen, carbon, hydrogen, and sulfur families has been developed and used to investigate the vertical profiles and the natural (including atmospheric chemical reactions) and anthropogenic sources and sinks of these species. The species continuity equations are solved numerically by applying prescribed boundary conditions. The vertical flux is simulated by use of the parameterized eddy diffusion coefficients. Heterogeneous losses (e.g. rainout, gas-to-particle chemistry, and dry deposition) are parameterized to make calculated profiles consistent with measurements. The photochemical model is coupled to a radiative transfer model that calculates the radiation field due to the incoming solar radiation which initiates much of the photochemistry of the troposphere. Comparisons of vertical profiles of tropospheric species are made between the Leighton approximation, widely used in most tropospheric models, and the detailed, radiative transfer, matrix inversion model used in this study. The radiative transfer code includes the effects of multiple scattering due to molecules and aerosols, pure absorption, and surface albedo on the transfer of incoming solar radiation. The results indicate that significant differences exist for several key photolysis frequencies and species number density profiles between the Leighton approximation and the profiles generated with the more detailed, radiative transfer, matrix inversion technique used in this study. Most species show enhanced vertical profiles when the more realistic treatment of the incoming solar radiation field is included.

[1]Graduate Research Assistant, Department of Mechanical Engineering and Mechanics, Old Dominion University, Norfolk, Virginia 23508.

[2]Eminent Professor, Department of Mechanical Engineering and Mechanics, Old Dominion University, Norfolk, Virginia 23508.

Furthermore, most species increase in concentration as a function of increasing surface albedo. A few species, notably ozone, exhibit decreased levels of concentration when the realistic radiative transfer model is used. The effect of the detailed treatment of incoming solar radiation on the photochemistry of the troposphere is discussed.

INTRODUCTION

Atmospheric modeling involves an attempt to simulate the physical, chemical, and dynamical processes in the atmosphere with the aid of mathematical formulations and numerical techniques. A goal of many models is to investigate the effects of anthropogenic activities on the composition and structure of the atmosphere. The field of atmospheric modeling is not new. By the end of the last century scientists utilized the concept of atmospheric modeling (ref. 1), but is has been only in the era of the modern day high-speed computers that rapid advancements have been made. Most atmospheric chemistry studies are performed with one-dimensional (vertical) models, whereas two- and three-dimensional models are usually used for studies of atmospheric flow, dynamics, and circulation. Since atmospheric chemistry is initiated by photodissociation of various molecules (which varies as a function of altitude), the vertical coordinate is the most important one in atmospheric chemistry studies. One-dimensional models are globally averaged models, because all parameters in these models are globally averaged. Vertical transport is parameterized in terms of an empirical constant K_z, usually called the "eddy diffusion coefficient."

Two-dimensional models, or zonally averaged models, employ an averaging technique whereby parameters are averaged in a given latitudinal band usually on the order of 5° to 10° wide. These models have been used mostly to study certain flow phenomena of zonal character. Two-dimensional models are usually formulated from a phenomenological point of view rather than from first principles. The eddy mixing model is usually developed by using the mixing length theory. Hence, despite increasing the model by one dimension, the transport coupling still relies on the choice of eddy coefficients.

Three-dimensional models have been under development during the last decade but have yet to be used extensively because of their nearly prohibitive cost. The three-dimensional models in existence today have been used mostly for dynamic studies. The most sophisticated three-dimensional model in existence uses a mere nine chemical reactions and considers only seven species (ref. 2). It has been found that each time seven new species are included, the com-

putational cost rises by an order of magnitude. Also, the largest digital computers available still do not have adequate storage to fully describe vertical transport. Hence, three-dimensional models must still rely on parameterized vertical eddy diffusivities. In one-dimensional models, a lot of storage is available to incorporate vast amounts of chemistry, which have their major variations in the vertical dimension. Furthermore, most chemical interactions are more easily studied with one-dimensional models.

The troposphere, which is the lowest region of the atmosphere (from the surface to about 10 km), contains about 75 percent of the total atmospheric mass. It is the region where nearly all of man's activities take place. The field of tropospheric photochemistry originated early in the 1970's, when it was suggested that the so-called "odd hydrogen" radicals ought to exist in the unpolluted troposphere (refs. 3-5). During the last decade, photochemical modeling has become an important tool to assess the natural state and perturbed troposphere. During the last few years, a one-dimensional global tropospheric photochemical model has been under development at NASA/Langley Research Center (LaRC). The existing model consists of five major chemical families: oxygen, nitrogen, hydrogen, carbon, and sulfur. The model consists of a total of 114 chemical reactions and 12 photolytic reactions. The existing model covers the range from 0 to 10 km with grid steps of 1 km.

The present model was developed as a tool to assess natural background concentrations as well as to assess the anthropogenic effect of environmentally significant gases. Man's activities might significantly alter the very delicate balance of the atmosphere (refs. 6-12). Ultimately, the distributions and abundances of tropospheric gases are governed by interactions of four reservoirs: the atmosphere, the hydrosphere, the biosphere, and the lithosphere (the crust).

The radiative quantity of primary interest to a photochemical modeler is the source function, which is the amount that the radiation incident at the top of the atmosphere is attenuated by various atmospheric processes such as scattering and absorption. Most one-dimensional photochemical models of the troposphere have used the Leighton approximation to calculate the source function.

Recently, Anderson and Meier (ref. 13) pointed out that the Leighton approximation is correct only when the optical depth due to pure absorption is much greater than the optical depth due to scattering. This occurs primarily for wavelengths less than 320 nm. Various methods have been used to improve on the Leighton approximation. Luther and Gelinas (ref. 14), Luther et al. (ref. 15), and Crutzen et al. (ref. 16) used the so-called two-stream approximation to calculate the source function. Callis et al. (ref. 17) used a parameterization technique whereby correction factors were applied to photodissociation rates. Anderson and Meier (ref. 13) also noted that "the two-stream approximation is in general not a good approximation for $S(\tau)$, the equation of radiative transfer. For $\lambda > 320$ nm, the two-stream model works well, due primarily to the dominance of pure absorption and not to its ability to describe multiple scattering." A recent model development to determine the source function involves a so-called matrix inversion technique (ref. 13). This technique accounts for the flux of photons into a volume element from all directions, contrary to the Leighton and two-steam approximation. The matrix inversion, radiative transfer model (ref. 13) is the first model that gives a realistic treatment of the radiation field, since it accounts for multiple scattering by particles and molecules, pure absorption, and surface albedo.

The objectives of this study are twofold: first, to investigate the sources and sinks (chemical and anthropogenic) of tropospheric gases in a systematic manner for all 38 species included in this model; and, second, once the governing chemistry is established, to investigate the effects of multiple scattering and surface albedo.

In subsequent sections of this report, the basic formulations of the governing equations are presented, followed by a discussion of the radiative transfer equations, and the results and discussion of the study.

LIST OF SYMBOLS

$A(\tau)$	coefficient to determine ozone photolysis
a	albedo

$B(\tau)$	coefficient to determine ozone photolysis
$C(\tau)$	coefficient to determine ozone photolysis
E_1	first exponential integral
E_2	second exponential integral
f	mixing ratio
g	constant of gravitational acceleration
H	scale height
h	Planck constant
I_0	radiative intensity
I_∞	solar flux at the top of the atmosphere
J	photolytic frequency
j	rate of absorption
k_{het}	heterogeneous loss frequency
K_z	eddy diffusion parameter
L	chemical loss term
M	total number density
n_j	number density of the ith species
P	chemical source term
R	universal gas constant
r	directional vector
S	source function
s	directional vector
T	temperature
t	time
z	altitude

Δ	chemical decomposition
δ	solar declination angle
Θ	solar zenith angle
λ	wavelength
μ	cosine of the solar zenith angle
ν	frequency
σ	molecular absorption cross section
τ	optical depth
Φ	vertical flux
ϕ	latitude

Subscripts

a	albedo
atm	atmospheric pressure
Diff	diffuse component of radiation
Dir	direct component of radiation
g	ground
het	heterogeneous
i	ith species
j	jth species
L	Leighton approximation
ms	multiple scattering
O_3	ozone
p	particle

R	Rayleigh scattering
sc	scattering
z	altitude
∞	infinity

BASIC FORMULATION

Introduction

In this section, the governing continuity and flux equations are derived along with appropriate boundary conditions. The calculations of photolysis rates are also described, as is the formulation of heterogeneous (gas-to-particle) losses. Table A1 (see Appendix A) lists the 12 photolytic processes that are included with these photolysis frequencies at the surface for a solar zenith angle of 45°. Table A2 lists the 114 chemical reactions with appropriate rate coefficients.

The Species Continuity Equation

The vertical profiles of the rapdily reacting species are determined by chemistry alone, while the vertical profiles of the more long-lived species are determined by the combined effects of chemistry and eddy transport, utilizing a steady-state continuity equation. The species continuity equation for the ith constituent of the atmosphere can be written in either number density form or mixing ratio form. In the present model, the mixing ratio form is used. The vertical profiles of long-lived species are then expressed as

$$\frac{\partial n_i}{\partial t} + \frac{\partial \phi_i}{\partial z} = P_i(n_j) - L_i(n_j)\, M\, f_i \qquad (1)$$

where ϕ_i is the vertical flux ($cm^{-2}s^{-1}$) of the ith species, $P_i(n_j)$ is chemical production, $L_i(n_j)$ is chemical loss, n_i is the number density of ith species, f_i is the mixing ratio of the ith species, and M is the total number density (molecules cm^{-3}).

The quantities n_i and f are related by

$$f_i = \frac{n_i}{M} \tag{2}$$

The vertical flux of the ith species, ϕ_i, is usually written in terms of a parameterization with altitude as

$$\phi_i = K_z \, M \left(\frac{\partial f_i}{\partial z} \right) \tag{3}$$

where K_z is an empirical constant ($cm^2 \, s^{-1}$), usually called the "eddy diffusion coefficient." The value of K_z in the present model is taken to be 1×10^5 and is assumed to be constant throughout the troposphere. The use of the word "eddy" is somewhat of a misnomer, since it indicates that the diffusive process occurs on a small scale. On the contrary, most vertical transport in the troposphere takes place on a very large scale. Inserting equation (1) into equation (3) yields the final form of the species continuity equation (in steady-state form) as

$$\frac{\partial}{\partial_z} \left[K_z M \left(\frac{\partial f_i}{\partial z} \right) \right] = - P_i(n_j) + L_i(n_j) M f_i \tag{4}$$

Because equation (4) usually depends on many species other than the ith, it is a highly coupled, nonlinear, differential equation that has to be solved numerically. For the short-lived species, chemistry dominates the vertical distribution, and therefore the transport term [i.e., the left-hand side of equation (4)] can be neglected. This condition is known as photochemical equilibrium (PCE). If PCE is justified, equation (4) is simplified considerably, and it is possible to solve explicitly for the mixing ratio as

$$f_i = \frac{P_i(n_j)}{L_i(n_j) M} \tag{5}$$

The one-dimensional steady-state equation in mixing ratio form is expressed as

$$K_z \frac{\partial^2 f_i}{\partial z^2} + \frac{1}{M} \frac{\partial (K_z M)}{\partial z} \frac{\partial f_i}{\partial z} - L_i f_i = - \frac{P_i}{M} \tag{6}$$

Since equation (6) is a second-order differential equation, two boundary conditions are necessary. Three kinds of boundary conditions which are commonly employed are

(1) PCE, which depends on the lifetime of the species under consideration;

(2) Constant number density, which should only be used if a species has been measured accurately at the boundaries; and

(3) Prescribed flux, which is perhaps the most interesting kind of boundary condition, since it allows the number density at the boundary to respond to any specified external forcing.

Equation (4) is identical to the original form of the species continuity equation developed in the early part of the 1950's (ref. 18). This can be shown by writing equation (3) in the form

$$\phi_i = - M K_z \frac{\partial}{\partial z} \left(\frac{n_i}{M}\right) \tag{7}$$

This can be expanded upon to yield

$$\phi_i = - K_z \left[\frac{\partial n_i}{\partial z} - n_i \frac{\partial \ln M}{\partial z}\right] \tag{8}$$

The equation of state can now be introduced

$$p = MkT \tag{9}$$

In thermodynamics, this equation is written as $p = nkT$, but the field of atmospheric sciences traditionally uses the letter M to denote total number density. Equation (9) can be differentiated logarithmically to yield

$$\frac{\partial \ln M}{\partial z} = \frac{\partial \ln p}{\partial z} - \frac{\partial \ln T}{\partial z} \tag{10}$$

The hydrostatic equation can be expressed as

$$dp = \frac{pg}{RT}\, dz \tag{11}$$

where g is the constant of gravitational acceleration and R represents the universal gas constant.

If we make the assumption that the atmosphere is isothermal, then equation (11) can be integrated as

$$\int_{p_o}^{p} \frac{dp}{p} = -\frac{g}{RT} \int_{0}^{z} dz \tag{12}$$

This can also be written as

$$\ln \left[\frac{p}{p_o}\right] = -\frac{gz}{RT} \tag{13}$$

The pressure scale height, H, is defined as

$$H = \frac{RT}{g} \tag{14}$$

Thus, equation (13) can now be expressed as

$$p = p_o\, e^{-z/H} \tag{15}$$

Substituting this into equation (8) yields the original form of the flux equation:

$$\phi_i = -K_z \left[\frac{\partial n_i}{\partial z} + n_i \left(\frac{1}{T}\frac{\partial T}{\partial z} + \frac{1}{H}\right)\right] \tag{16}$$

The continuity equation (in one-dimensional form) can now be expressed as

$$\frac{\partial}{\partial z}\left\{-K_z\left[\frac{\partial n_i}{\partial z}+n_i\left(\frac{1}{T}\frac{\partial T}{\partial z}+\frac{1}{H}\right)\right]\right\} - P_i + L_i n_i = 0 \qquad (17)$$

Hence, in the cases where PCE can be used, a high degree of computational efficiency, both in terms of time and money, can be reached. Numerically, the continuity equation is solved using a finite-difference form known as the "central difference scheme." The details of the numerical schemes are discussed in Appendix B. The boundary conditions for the continuity equation can be either specified number density or a specified flux. This is elaborated on in Appendix C. The convergence criteria imposed on the numerical solution are given in Appendix D.

The vertical mixing flux, ϕ_i, in general, includes advection by atmospheric winds, molecular diffusion, and turbulent diffusion (often referred to as the eddy flux). Molecular diffusion is not important below the turbopause (100 km) and, therefore, can be disregarded in tropospheric models (ref. 19). Horizontal wind (advection) is also disregarded in one-dimensional models and only the eddy flux is retained. Most models use a constant value of 1×10^5 ($cm^2\ s^{-1}$) to simulate the very turbulent nature of the troposphere (refs. 8, 9, 11, 20-22). There are a couple of different methods available to obtain values for the eddy diffusivities. One method involves tracking the dispersion of radioactive carbon-14 (ref. 23). Another method of obtaining K_z profiles is to use natural tracers (chemically inert gases), such as methane (CH_4) and nitrous oxide (N_2O). These gases are formed biogenically, i.e. by microbial activity in the soil, and are transported upwards. By measuring their number densities versus altitude, information about their rates of mixing can be obtained (ref. 24).

Photolysis Rate Calculations

In order to calculate the photolysis rates for the 12 photolytic expressions, the amount of incoming radiation must be determined first. The incident radiation is a function of wavelength λ, altitude z, and solar zenith angle

θ [i.e., $I = I(\lambda, z, \theta)$]. The expression for the incident solar radiation is given by Leighton (ref. 25) as

$$I(\lambda,z,\theta) = I_o(\lambda)\exp\left[-\tau O_3(\lambda)\sec\theta\right] \times \left\{\exp\left[-\tau_p(\lambda) - \tau_R(\lambda)\right]\sec\theta + \left[1 - \exp\left[-\tau_p(\lambda) - \tau_R(\lambda)\right]\sec\theta\right]\cos\theta\right\} \tag{18}$$

In this equation, $I_o(\lambda)$ represents the incident solar flux at the top of the atmosphere and has been tabulated by Ackerman (ref. 26). The term $\exp[\tau O_3(\lambda)\sec\theta]$ is the attenuation of solar radiation due to ozone absorption. The next term, $\exp[-\tau_p(\lambda) - \tau_R(\lambda)]\sec\theta$ is the direct solar attenuation due to aerosol particle scattering (τ_p) and Rayleigh scattering (τ_R), The last term, $\left[1 - \exp\left[-\tau_p(\lambda) - \tau_R(\lambda)\right]\right]\sec\theta$ is the diffuse solar radiation attenuated by aerosol and Rayleigh scattering, respectively. Values for $\tau O_3(\lambda)$, $\tau_p(\lambda)$, and $\tau_R(\lambda)$ have been tabulated by Elterman (ref. 27) and are used as standard input in most models. Once the incident solar radiation $I(\lambda, z, \theta)$ is known, the photodissociation rates J_i can be calculated by

$$J_i(\lambda, z, \theta) \Big| \sum_{\lambda=1}^{N} \Delta I_j(\lambda, z, \theta)\,\sigma_i(\lambda) \tag{19}$$

where $\sigma_i(\lambda)$ is the molecular cross section of the ith species. The solar zenith angle θ is calculated by using the relation

$$\cos\theta = \cos\phi\cos\delta\cos t + \sin\phi\sin\delta \tag{20}$$

where ϕ is the latitude, δ is the solar declination angle, and t is the local hour angle of the Sun. For a given latitude and solar declination angle, the local hour angle of the sun varies from -180° to 180° with each hour corresponding to a 15° increment, i.e., local noon is 0°, 11 a.m. is -15°, 1 p.m. is +15°, etc.

Certain long-lived species that are chemically inert are treated as specified inputs: i.e., their vertical profiles are specified. Examples of this

group include: molecular nitrogen (N_2), which has a lifetime of 10^6 years; molecular oxygen (O_2) which has a lifetime of several million years; molecular hydrogen (H_2) with a lifetime of 10 years; methane (CH_4) with a lifetime of 4 years; and carbon monoxide (CO), which has an average tropospheric lifetime of 4 months. Water vapor (H_2O) has an average tropospheric lifetime of only about one week, but it is specified since its profile is primarily a function of the temperature profile and rainout rate. In the present model, the water vapor profile was obtained by taking the average values of January and July from reference 28 at 30° N. The incident solar fluxes at the top of the atmosphere used in this model are the values tabulated by Ackerman (ref. 26). Figure 1 shows a graph of solar flux versus wavelength. The model covers the wavelength region from 270 to 730 nm. The incident solar radiation is needed in order to calculate the so-called source function. This, in turn, is used to calculate the photodissociation rates as per equation (19). In all, nine species are photolyzed in 12 different paths (see table A1). The absorption cross sections, which are needed to calculate photodissociation rates, are generally the values recommended in The Stratosphere: Present and Future (ref. 29). The ozone absorption cross sections shown in figure 2 are taken from Ackerman (ref. 26). The spectral region up to 310 nm contains the so-called O_3 Hartley bands, while the spectral range of the Huggins bands is from 310 to 360 nm. From 400 to 850 nm is a set of O_3 absorbing bands called the "Chappius bands." The Hartley-Huggins bands are stronger absorbers than are the Chappius bands. Ozone will photolyze to either the ground state oxygen atom, $O(^3p)$, or the excited metastable oxygen atom, $O(^1D)$, depending on the wavelength. For wavelengths greater than 320 nm, O_3 photolysis yields $O(^3p)$ while, for wavelengths less thhan 320 nm, $O(^1D)$ is formed.

The quantum efficiency of ozone photodissociation yielding $O(^1D)$ has been and continues to be a source of uncertainty. For wavelengths shorter than 300 nm, a quantum yield of unity (refs. 30-35) has been reported as well as a value of 0.9 for this quantum efficiency (refs. 36, 37). Figure 3 shows graphically the quantum efficiency for ozone photolysis. In the present model, a mathemat-

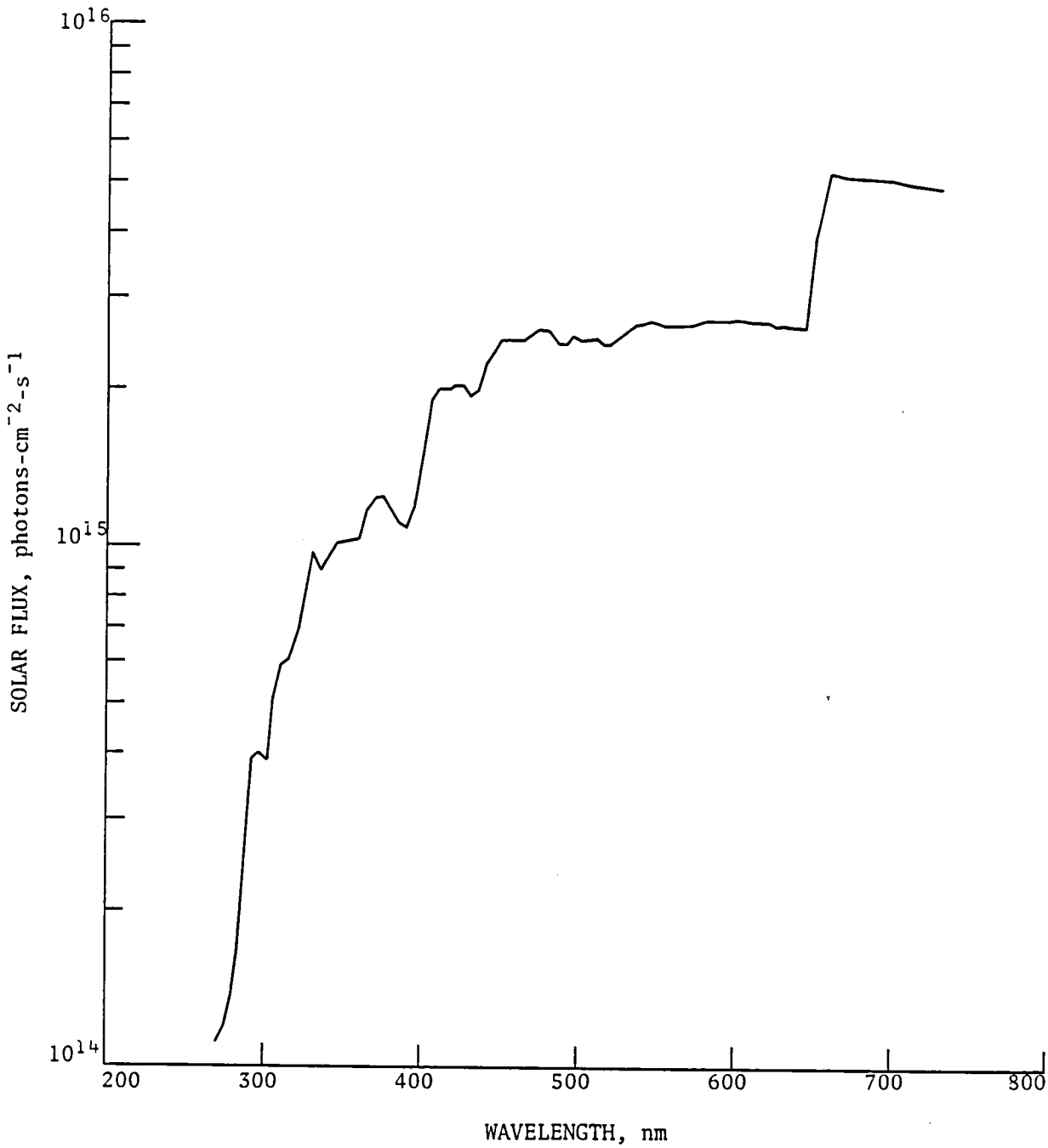

Figure 1. Solar flux versus wavelength for the spectral region from 270 to 730 nm.

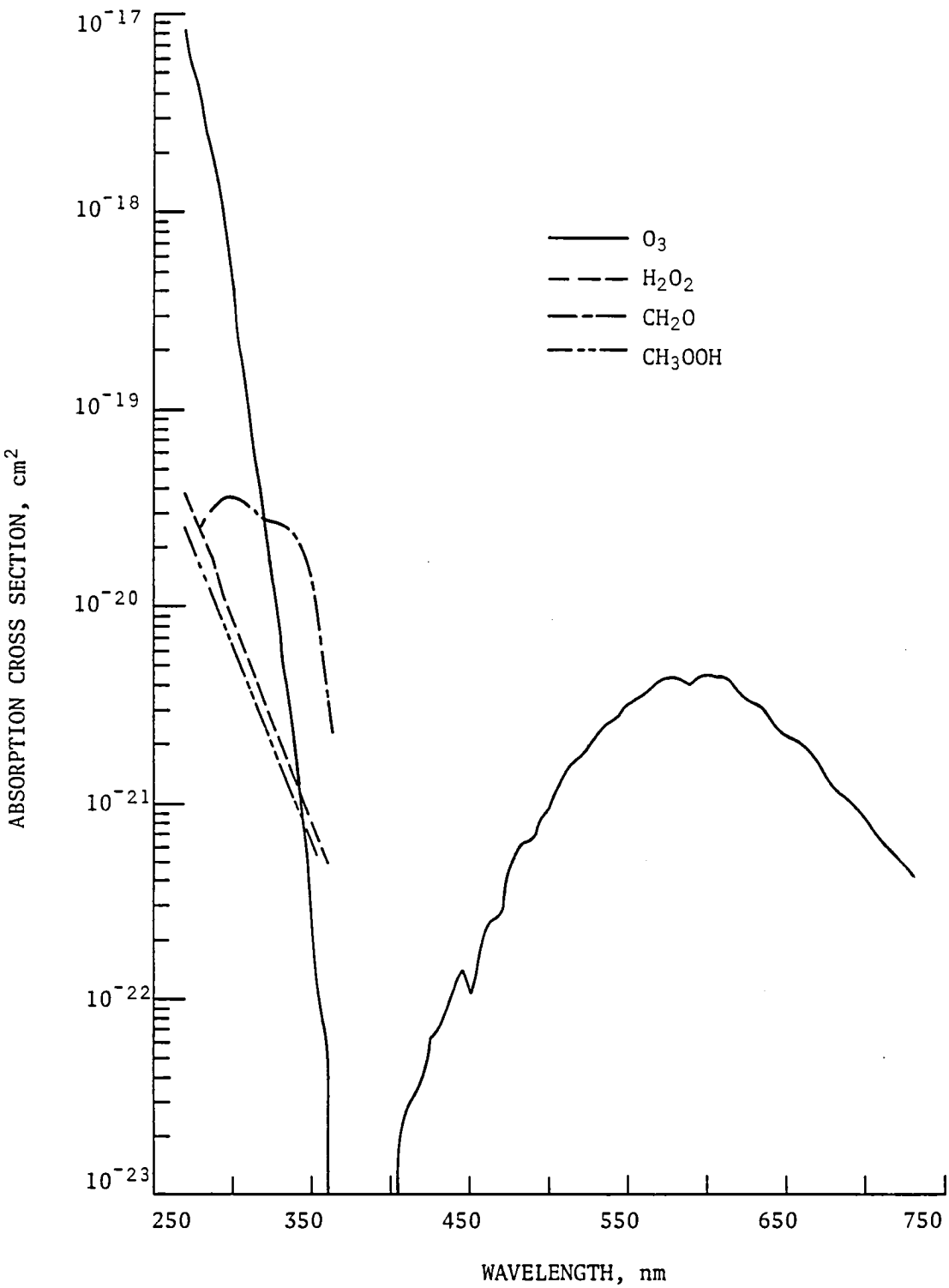

Figure 2. Absorption cross sections versus wavelength for O_3, CH_2O, CH_3OOH, and H_2O_2.

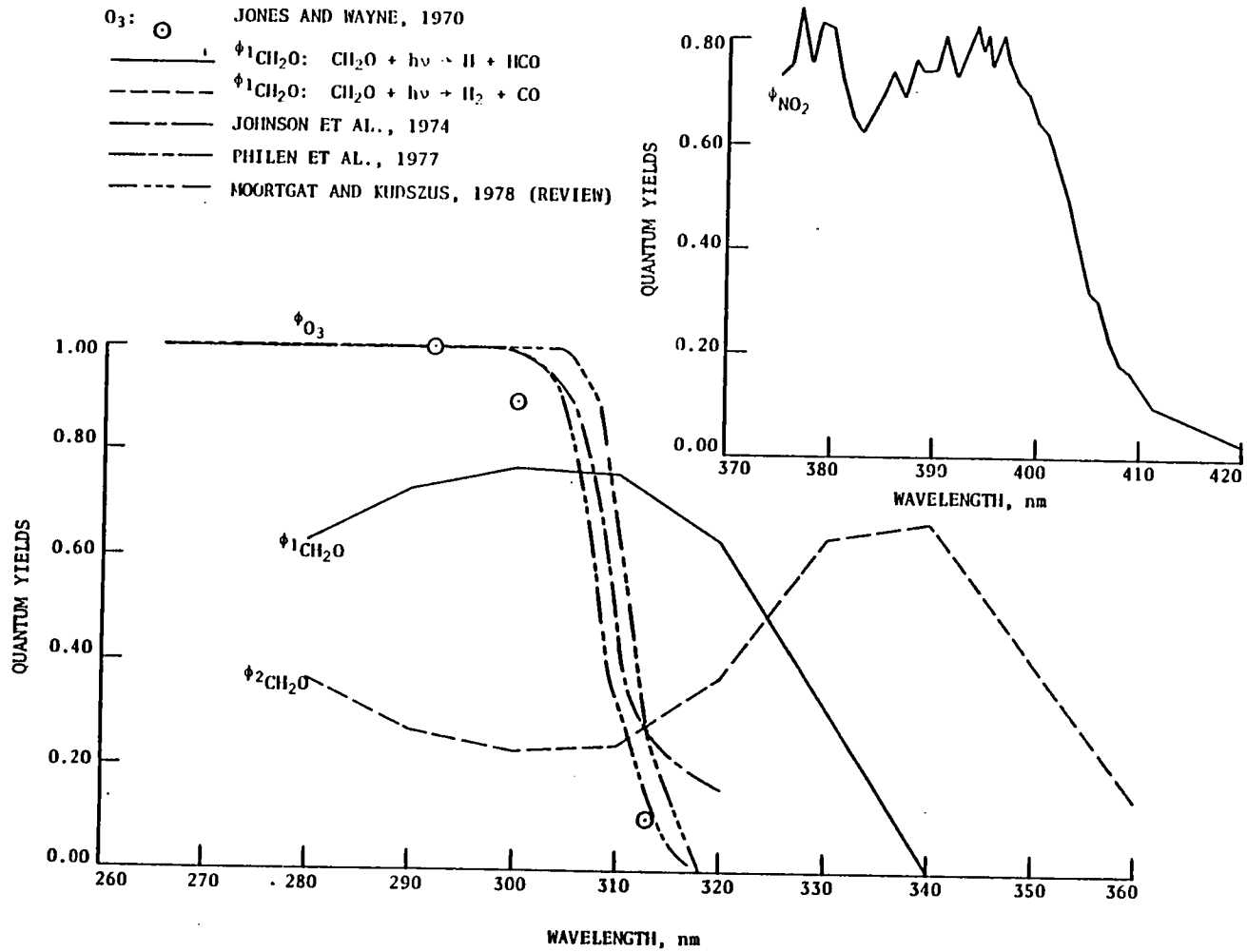

Figure 3. Quantum efficiency for ozone photolysis ($\lambda < 320$ nm) and branching ratios for CH_2O and NO_2 photolysis.

ical expression developed by Moortgat and Kudszus (ref. 33) is used, and this is given by

$$\phi(\lambda, T) = A(\tau) \text{ arc tan } \left\{B(\tau) \; [\lambda-\lambda_0(\tau)]\right\} + C(\tau) \qquad (21)$$

In this equation, $\tau = T - 230$ and T is expressed in degrees Kelvin, λ is given in nanometers, and arc tan in radians. A third-order interpolation polynomial is used for the coefficients as

$$A(\tau) = 0.369 + 2.85 \times 10^{-4} \tau + 1.28 \times 10^{-5} \tau^2 + 2.57 \times 10^{-8} \tau^3$$

$$B(\tau) = -0.575 + 5.59 \times 10^{-3} \tau - 1.439 \times 10^{-5} \tau^2 - 3.27 \times 10^{-8} \tau^3$$

$$\lambda_0(\tau) = 308.20 + 4.487 \times 10^{-2} \tau + 6.9380 \times 10^{-5} \tau^2 - 2.5452 \times 10^{-6} \tau^3$$

$$C(\tau) = 0.518 + 9.87 \times 10^{-4} \tau - 3.94 \times 10^{-5} \tau^2 + 3.9 \times 10^{-7} \tau^3$$

In the limits where $\phi(\lambda, T) > 1$, the quantum efficiency is set identical to one; and, for the cases where $\phi(\lambda, T) < 0$, the quantum efficiency is set to zero. A graphical depiction to the numerical solution of equation (21) is shown as a dashed line in figure 3. The photolysis of O_3 for wavelengths shorter than 320 nm is a key reaction in the troposphere, and the uncertainty surrounding the quantum yield is obviously a question that merits further investigation. Nitrogen dioxide (NO_2) is another species with quantum yields different than unity, as shown in the right-hand portion of figure 3. These quantum yields are taken from a tabulation by Harker and Johnston (ref. 38). Quantum efficiencies for NO_2 are generally between 0.7 to 0.8 for the wavelength region from 375 to 400 nm and decrease nearly monotomically to 0.0 at 420 nm. The absorption cross sections for NO_2 taken from a study by Bass et al. (ref. 39) are depicted as a dotted line in figure 4. Formaldehyde (CH_2O) photodissociates via two different paths. One path leads to atomic hydrogen (H) and the formyl radical (HCO) while the other path leads to molecular hydrogen (H_2) and carbon monoxide (CO). The branching ratios for formaldehyde photolysis are shown in figure 3. Initially, the branch leading to atomic hydrogen and the formyl radical dominates. At 325 nm, both paths have equal

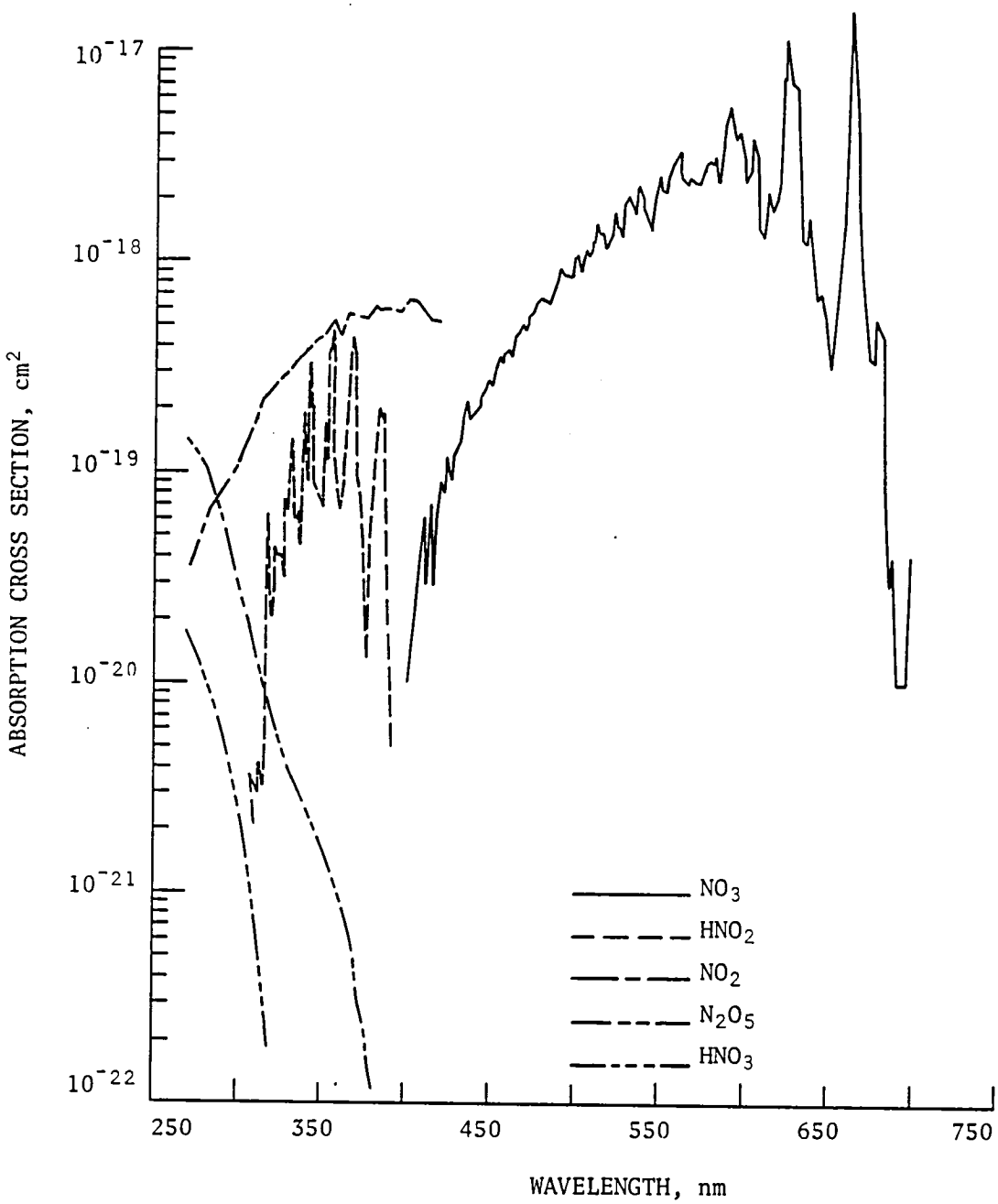

Figure 4. Absorption cross sections versus wavelength for NO_2, NO_3, N_2O_5, HNO_2, and HNO_3.

while at wavelengths greater than 325 nm the path leading to H_2 + CO shows a modest increase until 340 nm, where it starts a monotomic decrease reaching 0.14 at 360 nm. The other path, leading to H + HCO, intercepts the abscissa at 340 nm. Both the branching ratios and the absorption cross sections are taken from Moortgad and Warneck (ref. 40). Nitrogen trioxide (NO_3) absorbs in the spectral region 400 to 700 nm. The absorption cross sections are taken from a study by Graham and Johnston (ref. 41) and shown in figure 4. It shows a relatively smooth increase versus wavelength from 400 to 600 nm. From 600 to 700 nm, NO_3 absorption cross sections vary rapidly with wavelength, but generally show a decrease. The quantum yield for NO_3 photolysis is assumed to be unity. Dinitrogen pentoxide, N_2O_5, has absorption cross sections that decrease nearly linearly from 270 nm to 380 nm as shown in figure 4. The molecular data is taken from Graham and Johnson (ref. 41). The quantum efficiencies for N_2O_5 are unknown and assumed to be unity. Nitric acid (HNO_3) absorbs molecularly between 270 and 320 nm. The cross sections decrease linearly in this spectral range, as seen in figure 4. The absorption data is from Johnston and Graham (ref. 42), while the information concerning quantum yields found to be unity is from Johnston et al. (ref. 43). The spectral data for nitrous acid (HNO_2) which has rapidly changing absorption cross sections in the region from 300 to 400 nm, is taken from an extensive tabulation by Stockwell and Calvert (ref. 44). No recommendations exist for wavelengths shorter than 300 nm. The quantum yields for the spectral region from 300 to 400 nm are found to be unity. Hydrogen peroxide (H_2O_2) absorbs in the region from 270 to 360 nm. The cross-sectional data shown in figure 4 is the mean of two studies, one by Molina et al. (ref. 45) and the other by Lin et al. (ref. 46). Quantum yields are assumed to be unity. The methylhydroperoxy radical (CH_3OOH) recently had its cross sections measured by Arguello and Molina (ref. 47). The data for CH_3OOH shows similar characteristics to that of H_2O_2 (see fig. 4) and, in fact, nearly overlaps it. No data exists for the quantum efficiency for CH_3OOH, and it is assumed to be one.

Heterogeneous Losses

Certain species are subject to loss mechanisms other than gas phase chemistry. The mechanisms include rainout, aerosol formation, and dry deposition. A heterogeneous loss can be described as a chemical process that includes two phases (i.e., gas-solid, gas-liquid, or liquid-solid). Little is known about the physics and chemistry of these changes, and hence they are not modeled explicitly. The heterogeneous losses are expressed in the units of inverse time, and it is therefore possible to arrive at a characteristic time constant using the relation

$$K_{het} = \frac{1}{\tau_{het}} \tag{22}$$

where K_{het} is the heterogeneous loss constant and τ_{het} is the characteristic time for heterogeneous loss. Ammonia (NH_3) and sulfur dioxide (SO_2) are examples of gases in the present model that have heterogeneous loss terms. Rainout affects the distribution of certain soluble gases (ref. 48). The most obvious molecule undergoing rainout is water vapor, H_2O. In fact, the chemical lifetime of tropospheric water vapor is almost entirely governed by precipitation processes. An order of magnitude estimate of the average tropospheric lifetime of H_2O can be obtained by dividing the total number of H_2O molecules in the atmosphere by the mean annual precipitation rate. The total number of H_2O molecules has been estimated to be 2.7×10^{43} (ref. 49), while the mean annual precipitation rate is 200.9 mm year^{-1}, which can be expressed as 1.1×10^{38} H_2O molecules s^{-1} (ref. 50). Using these two values, an average tropospheric lifetime for water vapor of about 3 days is obtained. It is important to know this lifetime because certain other species, notably nitric acid (HNO_3) and, to some extent, ammonia (NH_3) and sulfur dioxide (SO_2), are believed to be sufficiently water soluble for their vertical profiles to resemble that of water vapor (ref. 48). In addition to H_2O, HNO_3, NH_3, and SO_2, rainout losses have been included for the methylhydroperoxy radical (CH_3OOH) (ref. 51) and for sulfuric acid (H_2SO_4) and the sulfurous acid radical (HSO_3) (ref. 52). A vast amount of data is available to determine rainout rates for water vapor. The

data base for the other species, on the other hand, is very sparse, and it is difficult to accurately determine their rainout factors. Definitive studies of rainout processes, both theoretical and experimental, are relevant topics deserving further elucidation.

RADIATION MODEL

As discussed in the previous section, the radiation model usually employed in photolytic frequency calculations is the Leighton approximation (see "Photolysis Rate Calculations"). Several limitations to this widely used approximation have recently been noted in the literature (ref. 13). The Leighton approximation is, in effect, a one-stream approximation. Hence, it does not account for the flux of photons from all sides into a volume element. Furthermore, the Leighton approximation does not consider the effects of multiple scattering and surface albedo. Recently, Anderson and Meier (ref. 13) have proposed a more realistic mode; a brief description of this model is presented in this section.

For a plane-parallel, isotropically scattering atmosphere, the radiative flux at a given altitude z can be expressed as

$$I(Z) = I_\infty \, T(\vec{r}, r_0) + \frac{1}{2} \int_Q^\infty j(Z') \, E_2(Z,Z') \, dZ' \qquad (23)$$

where I_∞ is the solar flux at the top of the atmosphere, $T(r,r_0)$ is the transmission function which describes the attenuation of incoming solar radiation due to molecular and particle scattering in addition to pure absorption. The quantity $j(Z')$ is the rate of absorption of the incoming solar radiation by particle and molecular scatterers, and E_2 is the second exponential integral. The rate of absorption $j(Z')$ can be written in terms of optical depth, τ as

$$J(Z') = I(Z') \, (\tau_p + \tau_R) \qquad (24)$$

where τ_R is the optical depth due to Rayleigh (molecular) scattering and τ_p

is the optical depth due to Mie (particle) scattering. In terms of the optical depths, equation (23) can be written as

$$I(Z) = I_\infty T(\vec{r}, r_0) + \frac{1}{2} \int_0^\infty S(\tau') \, E1(\Delta\tau) \, d\tau' \qquad (25)$$

Since $dZ' = \mu ds$, where $\mu = \cos\theta$ and $\vec{s} = \vec{r}' - \vec{r}$, equation (25) can now be expressed as

$$I(Z) = I_0(Z) + \frac{1}{2} \int S(\tau') \, E_1 \, (\Delta\tau) \, d\tau' \qquad (26)$$

where $I_0(Z) = I_\infty \, T(\vec{r}, r_0)$ and $\Delta\tau = |\tau_{sc} - \tau'_{sc}| + \tau_a - \tau'_a$. The quantity $S(\tau')$, which is the source function, can be defined as

$$S(r') = \frac{I(Z')}{I_\infty} \qquad (27)$$

In the above equations, the subscript sc stands for scattering (both Rayleigh and Mie) and a stands for absorption. The two different scattering terms can be combined into a single term that represents the total scattering. Albedo is defined as the fraction of the incident light that is reflected back from a surface into the atmosphere, i.e.,

$$a = \frac{I\uparrow}{I\downarrow} \qquad (28)$$

The globally averaged value for the albedo was measured extensively by the Nimbus family of spacecraft and determined to be about 0.30. The incident direct solar flux at the surface of the Earth is given in terms of an exponential attenuation by

$$I_s = I_\infty \cos\theta \exp\left[-(\tau_{sc} + \tau_a) \sec\theta\right] \qquad (29)$$

If a Lambertian surface is assumed, integration of this yields

$$S_{DIR} = 2a \cos\theta \exp\left[-(\tau_{sc} + \tau_a) \sec\theta\right] E_2 \, (\Delta\tau_s) \qquad (30)$$

where E_2 is the exponential integral of second order. The diffuse (or scattered) component can be calculated similarly such that

$$S_{DIFF} = aE_2(\Delta\tau_s) \int_0^\infty S(\tau') E_2 (\Delta\tau_g') d\tau \tag{31}$$

Adding the direct and diffuse components into the radiative transfer equation yields an integral equation for $S(\tau)$ as

$$S(\tau) = S_0(\tau) + S_{DIR}(\tau) + \int_0^\infty S(\tau') \left\{ \frac{E_1(\Delta\tau')}{2} + aE_2 (\Delta\tau_s) E_2 (\Delta\tau_s') \right\} d\tau' \tag{32}$$

As mentioned in reference 13, a matrix inversion technique can be applied to solve equation (32). The effects of including multiple scattering and surface albedo on the photochemistry of the troposphere will be compared to the effects of the Leighton approximation in the next section.

RESULTS AND DISCUSSION

Introduction

The results of the present study are presented in this section. First the model-calculated photodissociation frequencies with and without the inclusion of multiple scattering are compared. A systematic investigation of the chemical source and destruction terms as well as the effects of multiple scattering and surface albedo on the vertical profiles of the 38 tropospheric species is then presented.

Comparison of Calculated Photodissociation Frequencies Using the Leighton Approximation with the Matrix Inversion Technique

Photolysis of ozone in the wavelength region from 295 to 320 nm is a pivotal reaction in tropospheric photochemistry. This O_3 photolysis:

$$O_3 + h\nu \rightarrow O_2 + O(^1D) \quad [295 \text{ nm} \leq \lambda \leq 320 \text{ nm}] \tag{33}$$

results in excited, metastable $O(^1D)$ atoms which very rapidly react with water vapor molecules to form the hydroxyl radical (OH). The OH molecules are the main tropospheric scavenger; hence, it is of utmost importance to learn the

distribution of this molecule. Figure 5 shows the photodissociation frequencies of ozone versus altitude for the spectral region from 295 to 320 nm. The solid line represents the distribution obtained using the Leighton approximation according to equation (18). The five curves on the right-hand side represent the vertical profiles for various values of the surface albedo using the more realistic treatment of the radiation field. The numerical values of the photolysis frequencies are given in table 1, which also shows the ratios of photodissociation frequencies for multiple scattering to the Leighton approximation for various albedos, i.e., J_{ms}/J_L. For all cases, a solar zenith angle of 45° is used. For a surface albedo of 0.00, which shows the effects of multiple scattering alone, an increase in the photolysis frequency by a factor of 2.1 was calculated at the surface compared to the Leighton approximation. For the midtropospheric level (5 km), the increase in this ratio was 4.36, and for the tropopause (10 km) it was found to be 4.29. For an albedo of 0.25, which is close to the globally averaged value, a photolytic frequency of 1.94×10^{-5} s^{-1} was calculated at the surface (0 km). This is in close agreement with a measured value of $1.9\ (\pm 0.3) \times 10^{-5}\ s^{-1}$ for a solar zenith angle of 45 degrees and cloudless sky obtained by Dickerson et al. (ref. 53) even when the elevation of Dickerson's measurement (1.8 km) is considered. The recent measurements by Hanser and Sellers (ref. 54) at an altitude of 5.5 km are also in good agreement with the multiple scattering calculations. For an albedo of 0.50, we notice an increase in the photolysis frequencies of the multiple scattering case of 4 to 5 times compared to the results using the Leighton approximation. For an albedo of 0.75, this increase is generally 5 to 6 times and, for the case of a perfect reflector, i.e. an albedo of 1.00, the photolysis frequencies are enhanced by a factor of 6 to 8. For the photolysis of O_3 for wavelengths > 320 nm, smaller variations result when comparing the Leighton approximation and the Anderson-Meier calculations. The photolysis frequencies versus altitude for O_3 for $\lambda > 320$ nm have been plotted in figure 6. The corresponding numerical values and the ratios of the multiple scattering results to Leighton approximation are given in table 2. For the case of a surface albedo of 0.00, we find increases in the photodissociation frequencies for the multiple scattering calculations as compared to the Leighton approximation ranging from a factor of

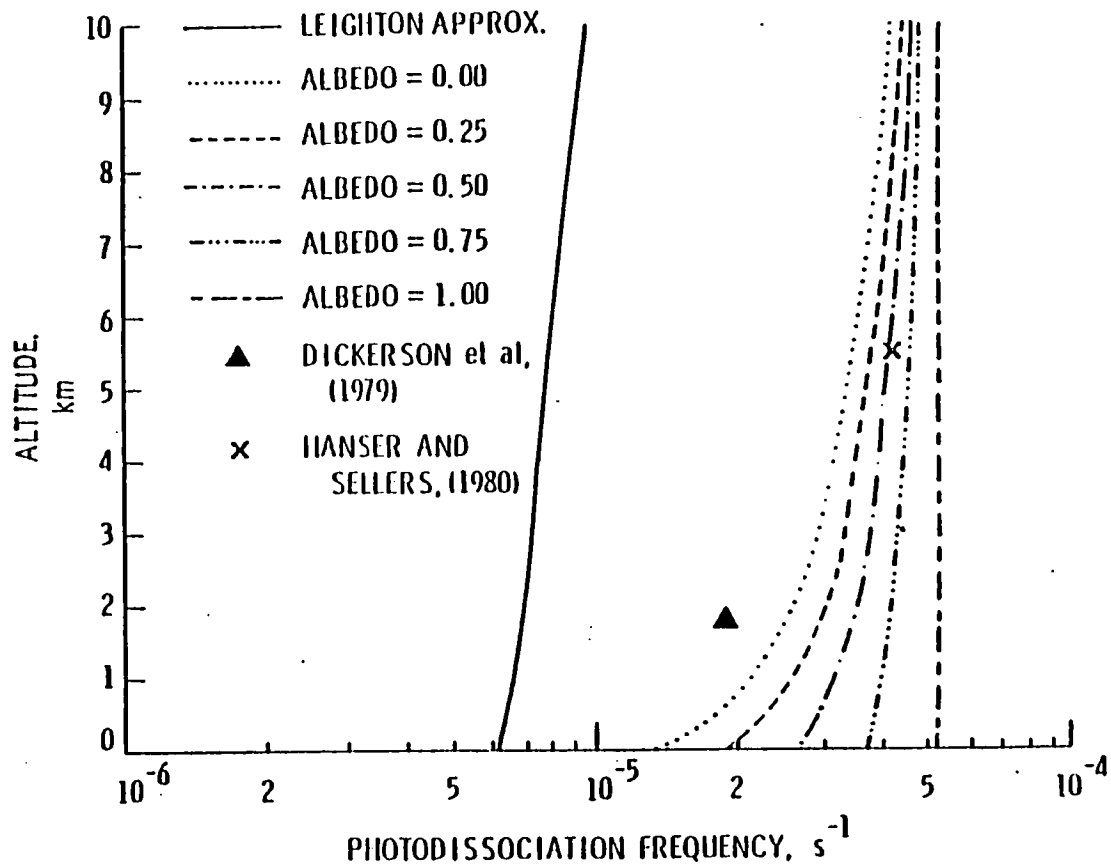

Figure 5. Photodissociation frequencies of O_3 for the multiple scattering cases with various albedos and the Leighton approximation.

Table 1. Photodissociation frequencies of O_3 and ratios of photodissociation frequencies for multiple scattering for various albedos and the Leighton approximation.

$$O_3 + h\nu \rightarrow O_2 + O(^1D) \quad (\lambda < 320 \text{ nm})$$

Photodissociation Frequencies, s^{-1}

Altitude, km	J_L	$J_{ms}(a = 0.00)$	$J_{ms}(a = 0.25)$	$J_{ms}(a = 0.50)$	$J_{ms}(a = 0.75)$	$J_{ms}(a = 1.00)$
10	9.74 E-6	4.18 E-5	4.37 E-5	4.62 E-5	4.94 E-5	5.41 E-5
5	7.98 E-6	3.48 E-5	3.77 E-5	4.16 E-5	4.67 E-5	5.39 E-5
0	6.32 E-6	1.33 E-5	1.94 E-5	2.73 E-5	3.80 E-5	5.29 E-5

Ratios of Photodissociation Frequencies for Multiple Scattering and the Leighton Approximation for Various Albedos

Altitude, km	$\frac{J_{ms}(a = 0.00)}{J_L}$	$\frac{J_{ms}(a = 0.25)}{J_L}$	$\frac{J_{ms}(a = 0.50)}{J_L}$	$\frac{J_{ms}(a = 0.75)}{J_L}$	$\frac{J_{ms}(a = 1.00)}{J_L}$
10	4.29	4.49	4.74	5.07	5.55
5	4.36	4.72	5.21	5.85	6.75
0	2.10	3.07	4.32	6.01	8.37

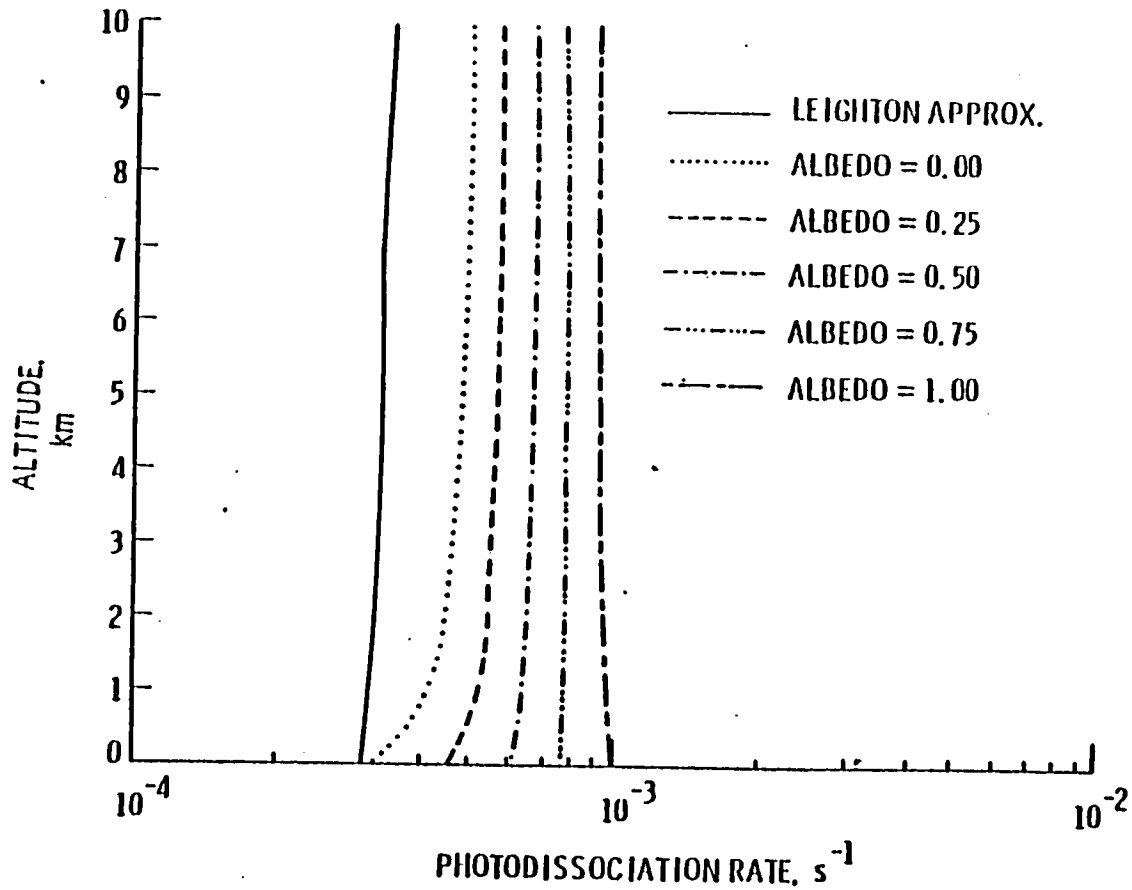

Figure 6. Photodissociation frequencies of O_3 for the multiple scattering cases with various albedos and the Leighton approximation.

Table 2. Photodissociation frequencies of O_3 and ratios for multiple scattering for various albedos and the Leighton approximation.

$$O_3 + h\nu \rightarrow O_2 + O(^3p) \quad (\lambda > 320 \text{ nm})$$

Photodissociation Frequencies, s^{-1}

Altitude, km	J_L	$J_{ms}(a = 0.00)$	$J_{ms}(a = 0.25)$	$J_{ms}(a = 0.50)$	$J_{ms}(a = 0.75)$	$J_{ms}(a = 1.00)$
10	3.40 E-4	4.97 E-4	5.78 E-4	6.70 E-4	7.75 E-4	8.98 E-4
5	3.31 E-4	4.79 E-4	5.69 E-4	6.71 E-4	7.89 E-4	9.27 E-4
0	3.05 E-4	3.26 E-4	4.60 E-4	6.13 E-4	7.90 E-4	1.00 E-3

Ratios of Photodissociation Frequencies for Multiple Scattering and the Leighton Approximation for Various Albedos

Altitude, km	$\frac{J_{ms}(a = 0.00)}{J_L}$	$\frac{J_{ms}(a = 0.25)}{J_L}$	$\frac{J_{ms}(a = 0.50)}{J_L}$	$\frac{J_{ms}(a = 0.75)}{J_L}$	$\frac{J_{ms}(a = 1.00)}{J_L}$
10	1.46	1.70	1.97	2.28	2.64
5	1.45	1.72	2.03	2.38	2.80
0	1.07	1.51	2.01	2.59	3.28

1.07 at the surface to a factor of 1.46 at the tropopause. For an albedo of 0.25, the increase in the ratio ranges from a factor of 1.51 at the surface to 1.70 at the tropopause. When the albedo is 0.50, we generally observe a doubling in the ratio of J_{ms}/J_L. For higher values of surface albedo, we notice slightly more than a doubling of this ratio. Specifically, when the surface albedo is 0.75, the increase at the surface is 2.59; at the midtropospheric level (5 km), the factor increases by 2.38, and at the tropopause (10 km) we observe a factor of 2.28. For the case of a perfect reflector (a = 1.00), the increase in the ratio ranges from 3.28 at the surface to 2.64 at the tropopause pause. It is not surprising that smaller differences are observed for the ozone photolysis for $\lambda > 320$ nm than for $\lambda < 320$ nm. Rayleigh scattering is inversely proportional to the fourth power of the wavelength; hence, a greater effect was found for reaction (33) than for reaction (34):

$$O_3 + h\nu \rightarrow O_2 + O(^1D) \quad [295 \text{ nm} < \lambda < 320 \text{ nm}] \qquad (33)$$

$$O_3 + h\nu \rightarrow O_2 + O(^3p) \quad [\lambda > 320 \text{ nm}] \qquad (34)$$

Most of the molecular scattering occurs in the troposphere, since more than 75 percent of the total mass of the atmosphere resides in this atmospheric region. Consequently, the amount of the backscattered radiation increases from the tropopause to the surface, resulting in a decrease in the downward flux component. This decrease is especially noticeable in the ratios of multiple scattering to the Leighton approximation for low values of the surface albedo. In general, if the albedo is less than 0.50, the ratio J_{ms}/J_L is lower at the surface than in the mid and upper troposphere. For larger surface albedo, say 0.75 to 1.00, the large reflectance at the surface is able to compensate for the decrease in downward flux due to backscattering.

For the photodissociation of nitrogen dioxide (NO_2):

$$NO_2 + h\nu \rightarrow NO + O \quad [270 < \lambda < 420 \text{ nm}] \qquad (35)$$

We find differences that are similar in magnitude to those we found from process (34). The numerical values of the photolytic process [eq. (35)] for vari-

ous values of the surface albedo along with the ratio J_{ms}/J_L are reproduced in table 3. For the case of an albedo of 0.00, we can hardly see any difference in the photolysis frequency at the surface between the multiple scattering calculations and the Leighton approximation. If anything, there is a slight decrease in the ratio of J_{ms}/J_L. In the mid to upper regions of the troposphere, this ratio is about 1.7. For higher values of the surface albedo, the ratio was found to increase. When a = 0.25, we calculate values ranging from 1.44 at the surface to nearly 2.00 at the tropopause. We observe factors slightly more than doubled through the entire troposphere when the albedo is 0.50. For higher values of the albedo, the surface reflection is able to compensate for the decrease in downward flux, similar to process (34). Hence, for the case of a = 0.75, the ratio J_{ms}/J_L ranges from 2.75 at the surface to 2.52 at 10 km. When the surface is asssumed to be a perfect reflector (a = 1.00), the values range from 3.74 at the surface to slightly less than 3 at the tropopause. Experimental values for process (35) are available (ref. 55) as a function of local time. For local noon, most of the values at the surface are about 0.7×10^{-3} s^{-1}, which agrees very well with our calculated value of 1.1×10^{-3} s^{-1} for an albedo of 0.25. The photolysis frequency for reaction (35) has also been measured by Harvey et al. (ref. 56) and found to be 0.8×10^{-3} s^{-1} at an altitude of 0.3 km. Stedman and Smith (ref. 57) measured values ranging from 0.75 to 0.9×10^{-3} s^{-1} during the "CHON" experiment in rural Colorado. The calculated values for process (35) are illustrated in figure 7.

Nitrogen trioxide (NO_3) photodissociates along two different paths with one path leading to

$$NO_3 + h\nu \rightarrow NO_2 + O \quad [400 < \lambda < 700 \text{ nm}] \qquad (36)$$

and the other branching to

$$NO_3^- + h\nu \rightarrow NO + O_2 \quad [400 < \lambda < 700 \text{ nm}] \qquad (37)$$

Table 3. Photodissociation frequencies of NO_2 and ratios for multiple scattering for various albedos and the Leighton approximation.

$NO_2 + h\nu \rightarrow NO + O$ ($270 < \lambda < 420$ nm)

Photodissociation Frequencies, s^{-1}

Altitude, km	J_L	$J_{ms}(a = 0.00)$	$J_{ms}(a = 0.25)$	$J_{ms}(a = 0.50)$	$J_{ms}(a = 0.75)$	$J_{ms}(a = 1.00)$
10	8.93 E-3	1.59 E-2	1.76 E-2	1.97 E-2	2.25 E-2	2.62 E-2
5	8.48 E-3	1.45 E-2	1.66 E-2	1.93 E-2	2.27 E-2	2.73 E-2
0	7.57 E-3	7.48 E-3	1.09 E-2	1.52 E-2	2.08 E-2	2.83 E-2

Ratios of Photodissociation Frequencies for Multiple Scattering and the Leighton Approximation for Various Albedos

Altitude, km	$\frac{J_{ms}(a = 0.00)}{J_L}$	$\frac{J_{ms}(a = 0.25)}{J_L}$	$\frac{J_{ms}(a = 0.50)}{J_L}$	$\frac{J_{ms}(a = 0.75)}{J_L}$	$\frac{J_{ms}(a = 1.00)}{J_L}$
10	1.78	1.97	2.21	2.52	2.93
5	1.71	1.96	2.28	2.68	3.22
0	0.99	1.44	2.01	2.75	3.74

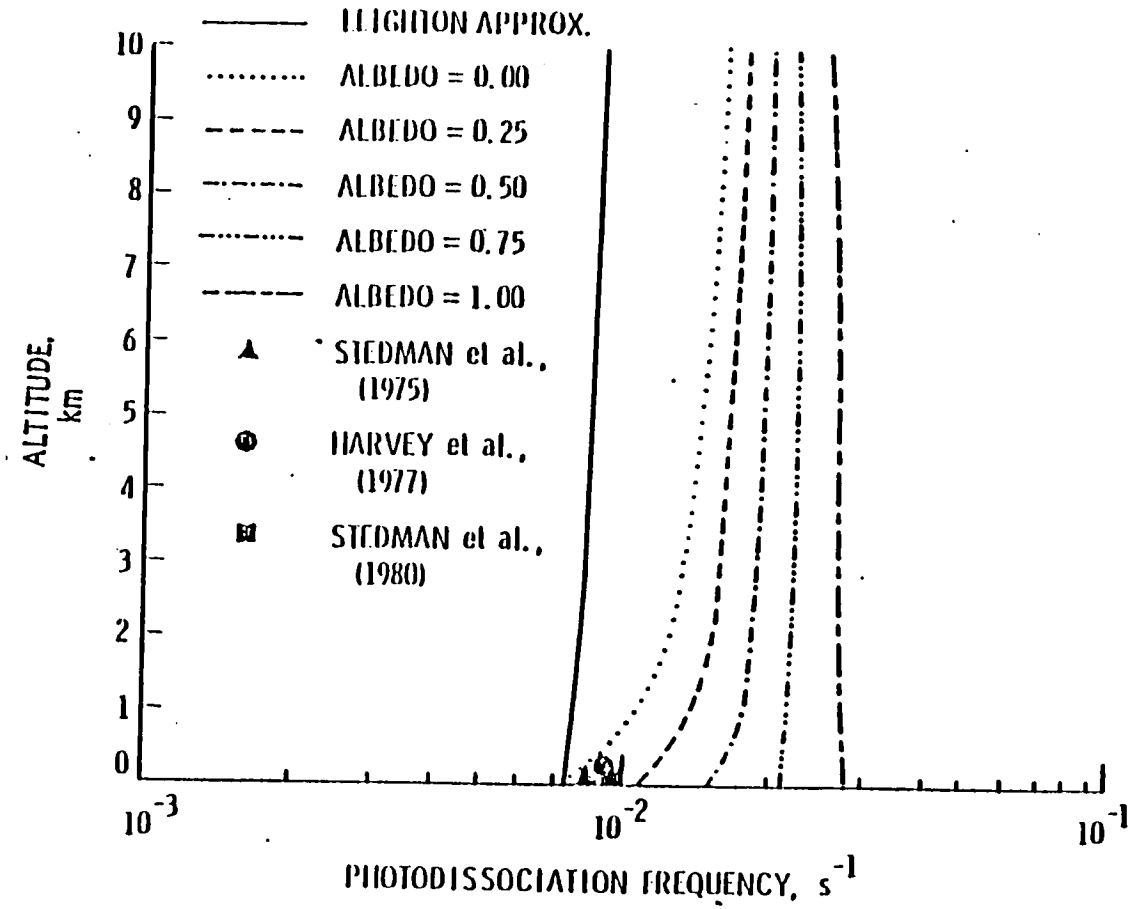

Figure 7. Photodissociation frequencies of NO_2 for the multiple scattering cases with various albedos and the Leighton approximation.

The branching ratios for these photolytic processes were discussed under "Photolysis Rate Calculations" and illustrated in figure 4. The photolysis frequencies for process (36) are generally 4 times faster than those for process (37). The calculated values for NO_3 photolysis are tabulated in table 4 for the branch leading to NO_2 + O and in table 5 for the NO + O_2 branch. Inspection of these tables shows that the ratios of J_{ms}/J_L are very similar, albeit not identical, for comparable albedos. For the case showing the effects of the multiple scattering alone, i.e. a = 0.00, the inclusion of the multiple scattering code increases the photolytic frequency at the surface by 8 percent for both processes. In the mid and upper troposphere, the factor is increased about 40 percent. For a surface albedo of 0.25, the ratio of J_{ms}/J_L is about 1.5 throughout the troposphere for both processes. The ratio is approximately doubled when the albedo is 0.50 and varies from about 2.6 at the surface to 2.2 at the tropopause for an albedo of 0.75. When the surface is perfectly reflecting, i.e. a = 1.00, the ratio ranges from approximately 3.2 at the surface to 2.6 at 10 km. The vertical profiles of the photolytic processes (36) and (37) are shown in figures 8 and 9, respectively, for the Leighton approximation as well as for the multiple scattering cases for different albedos. Also included on these figures are measurements by Graham and Johnston (ref. 58) and Magnotta and Johnston (ref. 59).

Dinitrogen pentoxide (N_2O_5) undergoes photolysis in the spectral region from 270 to 380 nm. Its photolytic products are nitrogen dioxide (NO_2) and nitrogen trioxide (NO_3) according to

$$N_2O_5 + h\nu \rightarrow NO_2 + NO_3 \quad [270 \text{ nm} < \lambda > 380 \text{ nm}] \qquad (38)$$

The values for the photodissociation frequencies for process (38) are given in table 6 along with the ratios of J_{ms}/J_L. Since N_2O_5 is photolytically active at short wavelengths, i.e. $\lambda < 300$ nm, the ratio J_{ms}/J_L should be larger than for species that are not active in this region, at least for large values of the surface albedo. This is verified by inspecting the lower half of table 6. For a = 0.00, no difference is found at the surface for values calculated using the Leighton approximation to those obtained with the multiple scattering rou-

Table 4. Photodissociation frequencies of NO_3 and ratios for multiple scattering for various albedos and the Leighton approximation.

$NO_3 + h\nu \rightarrow NO_2 + O$ ($400 < \lambda < 700$ nm)

Photodissociation Frequencies, s^{-1}

Altitude, km	J_L	$J_{ms}(a = 0.00)$	$J_{ms}(a = 0.25)$	$J_{ms}(a = 0.50)$	$J_{ms}(a = 0.75)$	$J_{ms}(a = 1.00)$
10	9.11 E-3	1.29 E-2	1.51 E-2	1.76 E-2	2.05 E-2	2.38 E-2
5	8.93 E-3	1.26 E-2	1.50 E-2	1.78 E-2	2.09 E-2	2.46 E-2
0	8.21 E-3	8.83 E-3	1.24 E-2	1.65 E-2	2.12 E-2	2.66 E-2

Ratios of Photodissociation Frequencies for Multiple Scattering and the Leighton Approximation for Various Albedos

Altitude, km	$\frac{J_{ms}(a = 0.00)}{J_L}$	$\frac{J_{ms}(a = 0.25)}{J_L}$	$\frac{J_{ms}(a = 0.50)}{J_L}$	$\frac{J_{ms}(a = 0.75)}{J_L}$	$\frac{J_{ms}(a = 1.00)}{J_L}$
10	1.42	1.66	1.93	2.25	2.61
5	1.41	1.68	1.99	2.34	2.75
0	1.08	1.51	2.01	2.58	3.24

Table 5. Photodissociation frequencies of NO_3 and ratios for multiple scattering for various albedos and the Leighton approximation.

$NO_3 + h\nu \rightarrow NO + O_2$ ($400 < \lambda < 700$ nm)

Photodissociation Frequencies, s^{-1}

Altitude, km	J_L	$J_{ms}(a = 0.00)$	$J_{ms}(a = 0.25)$	$J_{ms}(a = 0.50)$	$J_{ms}(a = 0.75)$	$J_{ms}(a = 1.00)$
10	2.25 E-3	3.10 E-3	3.66 E-3	4.28 E-3	4.99 E-3	5.79 E-3
5	2.21 E-3	3.04 E-3	3.65 E-3	4.33 E-3	5.10 E-3	5.97 E-3
0	2.04 E-3	2.20 E-3	3.09 E-3	4.09 E-3	5.22 E-3	6.50 E-3

Ratios of Photodissociation Frequencies for Multiple Scattering and the Leighton Approximation for Various Albedos

Altitude, km	$\frac{J_{ms}(a = 0.00)}{J_L}$	$\frac{J_{ms}(a = 0.25)}{J_L}$	$\frac{J_{ms}(a = 0.50)}{J_L}$	$\frac{J_{ms}(a = 0.75)}{J_L}$	$\frac{J_{ms}(a = 1.00)}{J_L}$
10	1.38	1.63	1.90	2.22	2.57
5	1.38	1.65	1.96	2.31	2.70
0	1.08	1.51	2.00	2.56	3.19

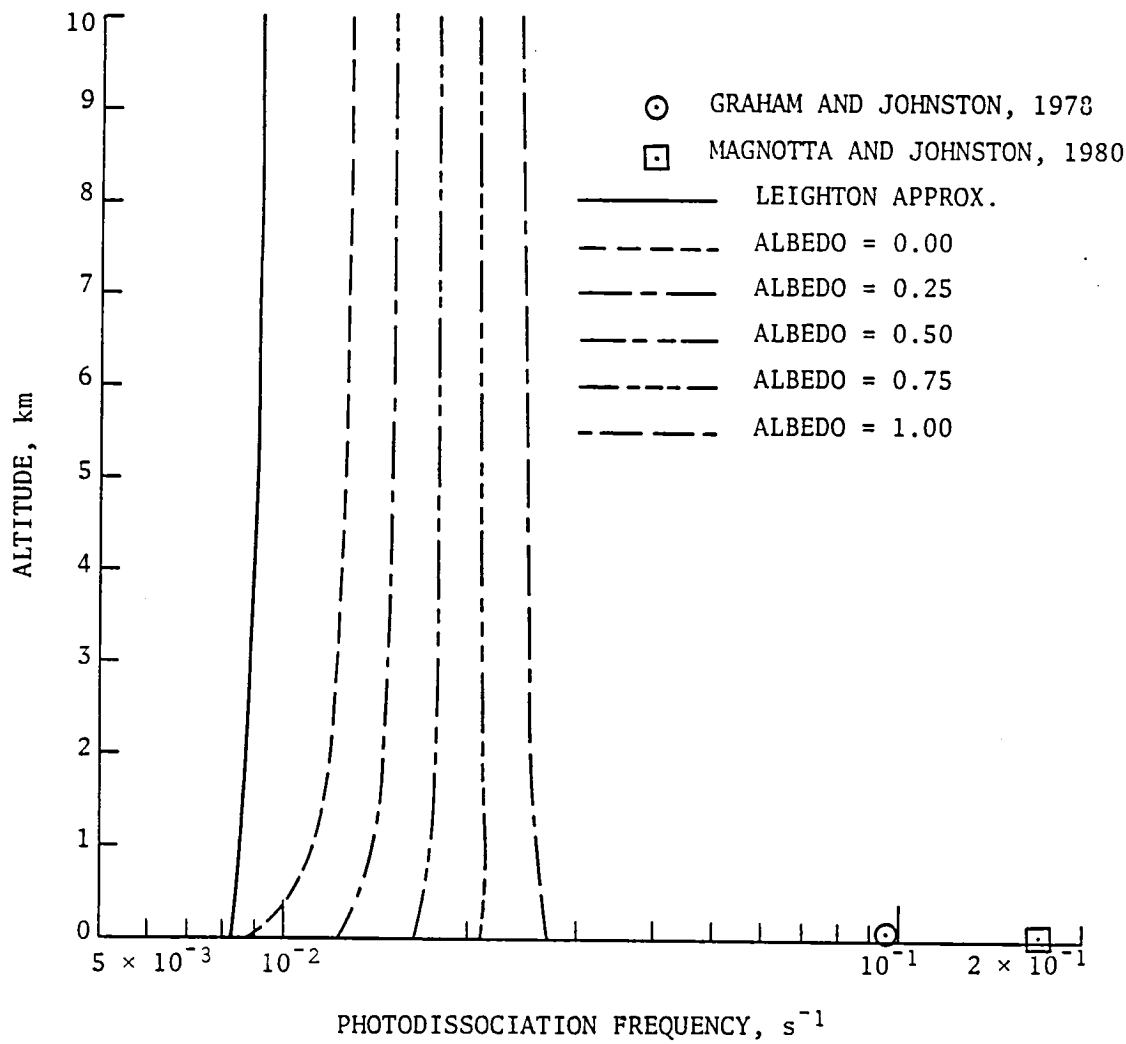

Figure 8. Photodissociation frequencies of NO_3 for the multiple scattering cases with various albedos and the Leighton approximation.

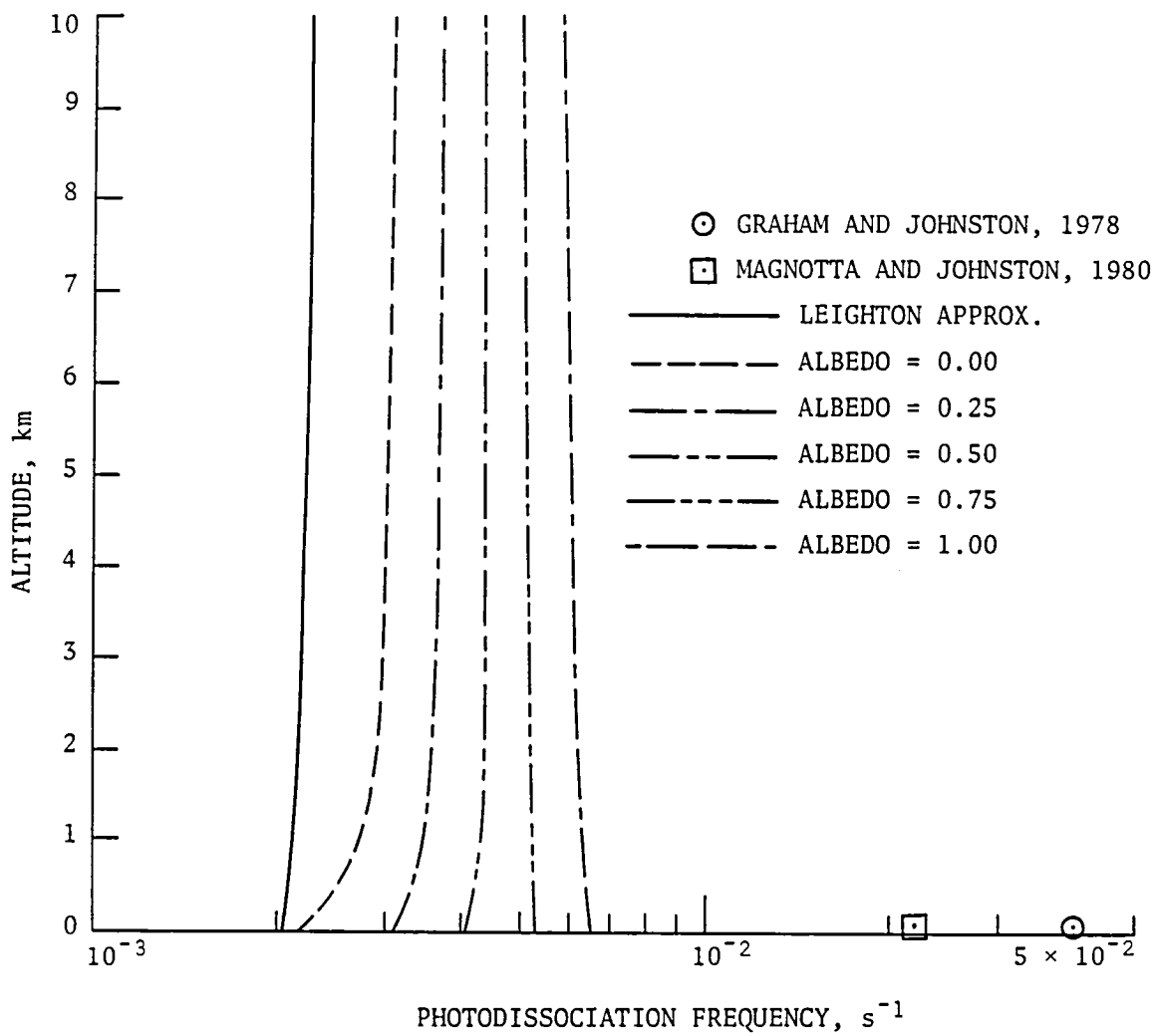

Figure 9. Photodissociation frequencies of NO_3 for the multiple scattering cases with various albedos and the Leighton approximation.

Table 6. Photodissociation frequencies of N_2O_5 and ratios for multiple scattering for various albedos and the Leighton approximation.

$N_2O_5 + h\nu \rightarrow NO_2 + NO_3$ ($270 < \lambda < 380$ nm)

Photodissociation Frequencies, s^{-1}

Altitude, km	J_L	$J_{ms}(a = 0.00)$	$J_{ms}(a = 0.25)$	$J_{ms}(a = 0.50)$	$J_{ms}(a = 0.75)$	$J_{ms}(a = 1.00)$
10	2.41 E-5	4.98 E-5	5.38 E-5	5.91 E-5	6.62 E-5	7.64 E-5
5	2.22 E-5	4.40 E-5	4.93 E-5	5.62 E-5	6.57 E-5	7.91 E-5
0	1.96 E-5	1.96 E-5	2.88 E-5	4.08 E-5	5.72 E-5	8.07 E-5

Ratios of Photodissociation Frequencies for Multiple Scattering and the Leighton Approximation for Various Albedos

Altitude, km	$\frac{J_{ms}(a = 0.00)}{J_L}$	$\frac{J_{ms}(a = 0.25)}{J_L}$	$\frac{J_{ms}(a = 0.50)}{J_L}$	$\frac{J_{ms}(a = 0.75)}{J_L}$	$\frac{J_{ms}(a = 1.00)}{J_L}$
10	2.07	2.23	2.45	2.75	3.17
5	1.98	2.22	2.53	2.96	3.56
0	1.00	1.47	2.08	2.92	4.12

tine. At the tropopause, however, the ratio of J_{ms}/J_L is doubled. When the albedo is 0.25, the ratio at the surface is about 1.5 increasing to approximately 2.2 at 10 km. For an albedo of 0.50, the ratio is slightly more than doubled at the surface and almost 2.5 at the tropopause. For yet higher values of the surface albedo, the ratio of J_{ms}/J_L increases such that when a = 0.75 the ratio varies between 2.9 and 2.8. Finally, when a = 1.00, the ratio varies between 4.1 at the surface to 3.2 at the tropopause level. The vertical profiles of the photodissociation frequencies for N_2O_5 photolysis are shown in figure 10.

Nitric acid (HNO_3) is another species that is very active in the shorter end of the spectrum. Hence, we would expect large ratios for J_{ms}/J_L similar to the case of N_2O_5. Nitric acid undergoes photolysis according to

$$HNO_3 + h\nu \rightarrow OH + NO_2 \quad [270 < \lambda < 320 \text{ nm}] \qquad (39)$$

with the numerical values given in table 7. The upper half of this table shows the photodissociation frequencies for process (39) to be on the order of 10^{-7} s^{-1}. The lower half lists the ratios of J_{ms}/J_L. These ratios are generally higher than any of the previously discussed processes except process (33). Even at low values for the surface albedo, the ratios are relatively high, with a factor of 1.5 increase at the surface for an albedo of 0.00 increasing to a factor of 3.2 at the tropopause. With an albedo of 0.25, the increases range from 2.2 at the surface to 3.4 at 10 km. For the case of a = 0.50, we notice more than a tripling of the ratio of J_{ms}/J_L. When the albedo is 0.75, the ratio is more than quadrupled at the surface and nearly quadrupled at 10 km. Finally, for a = 1.00, the factor is larger than 6 at the surface and decreases with altitude to a value of 4.4 at the tropopause. The photolytic process (39) has its frequencies displayed graphically in figure 11.

Nitrous acid (HNO_2) undergoes photolysis in the spectral region from 300 to 400 nm according to

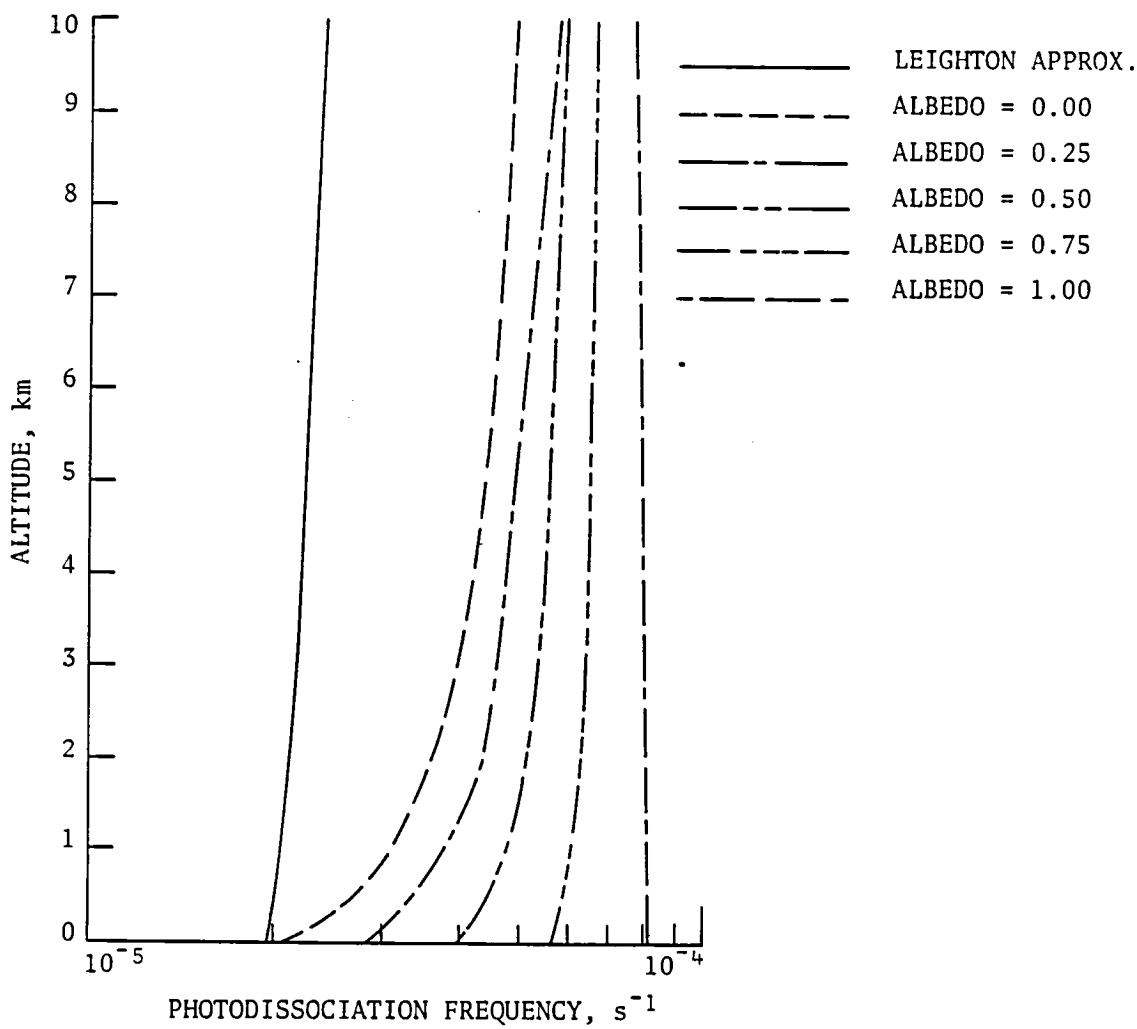

Figure 10. Photodissociation frequencies of N_2O_5 for the multiple scattering cases with various albedos and the Leighton approximation.

Table 7. Photodissociation frequencies of HNO_3 and ratios for multiple scattering for various albedos and the Leighton approximation.

$HNO_3 + h\nu \rightarrow OH + NO_2$ ($270 < \lambda < 320$ nm)

Photodissociation Frequencies, s^{-1}

Altitude, km	J_L	$J_{ms}(a = 0.00)$	$J_{ms}(a = 0.25)$	$J_{ms}(a = 0.50)$	$J_{ms}(a = 0.75)$	$J_{ms}(a = 1.00)$
10	2.20 E-7	7.02 E-7	7.41 E-7	7.92 E-7	8.61 E-7	9.60 E-7
5	1.91 E-7	5.96 E-7	6.54 E-7	7.28 E-7	8.30 E-7	9.76 E-7
0	1.61 E-7	2.37 E-7	3.48 E-7	4.93 E-7	6.90 E-7	9.74 E-7

Ratios of Photodissociation Frequencies for Multiple Scattering and the Leighton Approximation for Various Albedos

Altitude, km	$\frac{J_{ms}(a = 0.00)}{J_L}$	$\frac{J_{ms}(a = 0.25)}{J_L}$	$\frac{J_{ms}(a = 0.50)}{J_L}$	$\frac{J_{ms}(a = 0.75)}{J_L}$	$\frac{J_{ms}(a = 1.00)}{J_L}$
10	3.19	3.37	3.60	3.91	4.36
5	3.12	3.42	3.81	4.35	5.11
0	1.47	2.16	3.06	4.29	6.05

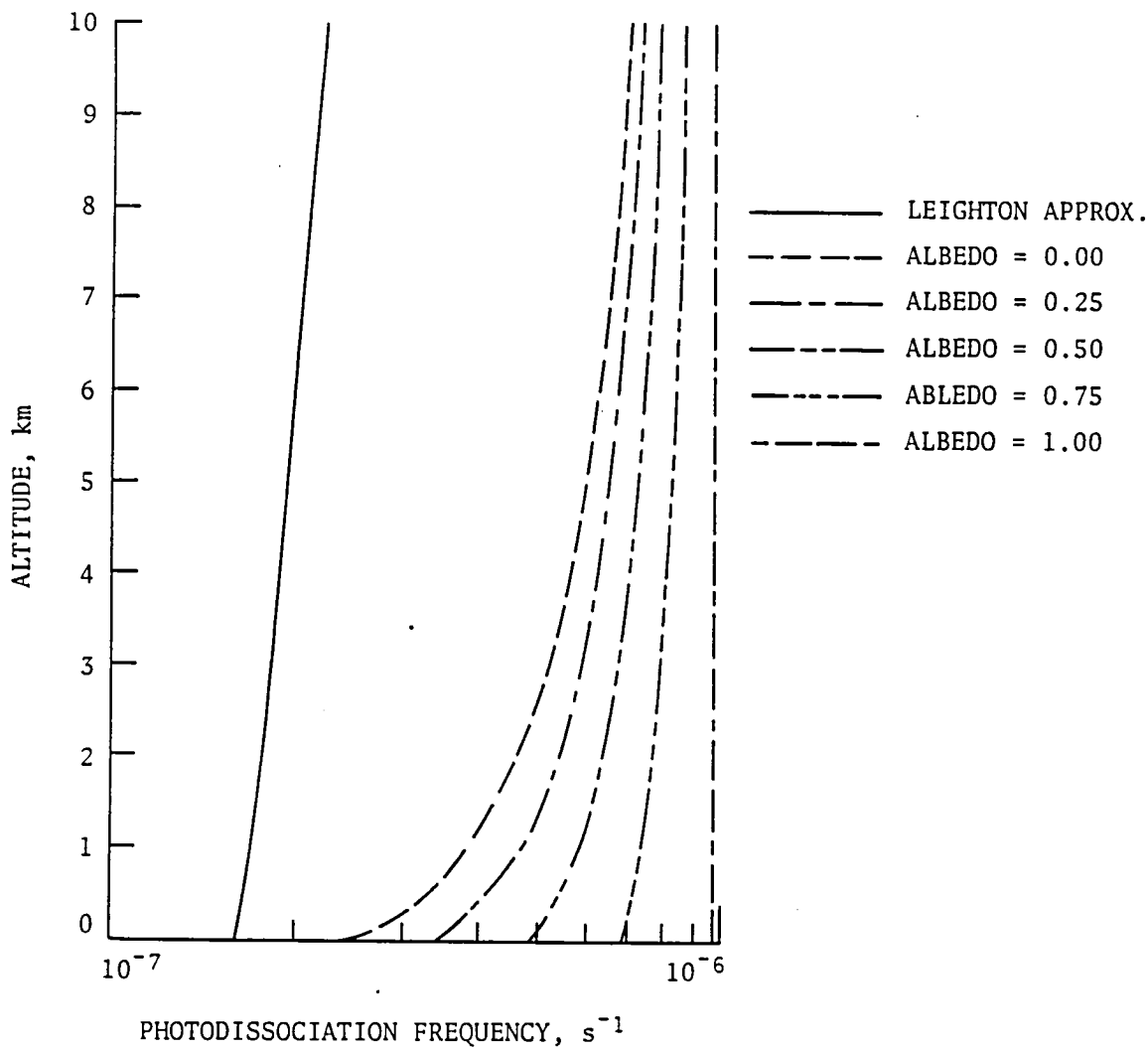

Figure 11. Photodissociation frequencies of HNO_3 for the multiple scattering cases with various albedos and the Leighton approximation.

$$HNO_2 + h\nu \rightarrow OH + NO \; [300 \text{ nm} < \lambda < 400 \text{ nm}] \qquad (40)$$

The model calculated values for this process are given in table 8 along with ratios of J_{ms}/J_L. For nitrous acid there is only a small effect noticeable at low albedos between the multiple scattering results and those obtained with the Leighton approximation. In fact, we observe a slight decrease below unity in the ratio J_{ms}/J_L at the surface for an albedo of 0.00. At higher altitudes, however, the ratio is slightly more than doubled. For an albedo of 0.25, the surface level ratio is about 1.3 and the midtropospheric and tropopause levels have values of 2.0. When a = 0.50, values range from 1.8 at the surface to 2.3 in the upper regions of the troposphere. The ratio J_{ms}/J_L is more than doubled for a = 0.75, with a value of 2.5 at the surface, 2.7 at 5 km, and 2.5 at the tropopause. Finally, when the albedo is unity, there is more than a tripling of the ratio at the surface with a value of 3.4, decreasing with altitude to 3.0 at 10 km. The vertical profiles of the photodissociation frequencies of process (40) are shown in figure 12.

Hydrogen peroxide, H_2O_2, and methylhydroperoxy, CH_3OOH, undergo photolysis between 270 and 360 nm according to

$$H_2O_2 + h\nu \rightarrow 2\,OH \; [270 \text{ nm} < \lambda < 360 \text{ nm}] \qquad (41)$$

and

$$CH_3OOH + h\nu \rightarrow CH_3 + OH \; [270 \text{ nm} < \lambda < 360 \text{ nm}] \qquad (42)$$

Both of these species are assumed to have nearly identical absorption and quantum efficiency parameters and can, therefore, be assumed to have identical photodissociation frequencies (see discussion under "Photolysis Rate Calculations"). These frequencies, as well as the ratios of the multiple scattering results to the results using the Leighton approximation, are given in table 9. The vertical profiles of the photolysis frequencies are illustrated in figure 13. Initially, at the surface for an albedo of 0.00, only a slight difference between the Leighton approximation calculations and the multiple scattering calculations are noticeable. The multiple scattering calculations increase the

Table 8. Photodissociation frequencies of HNO_2 and ratios for multiple scattering for various albedos and the Leighton approximation.

$HNO_2 + h\nu \rightarrow OH + NO$ ($300 < \lambda < 400$ nm)

Photodissociation Frequencies, s^{-1}

Altitude, km	J_L	$J_{ms}(a = 0.00)$	$J_{ms}(a = 0.25)$	$J_{ms}(a = 0.50)$	$J_{ms}(a = 0.75)$	$J_{ms}(a = 1.00)$
10	5.74 E-4	1.05 E-3	1.15 E-3	1.29 E-3	1.46 E-3	1.71 E-3
5	5.42 E-4	9.52 E-4	1.08 E-3	1.25 E-3	1.47 E-3	1.78 E-3
0	4.84 E-4	4.70 E-4	6.86 E-4	9.64 E-4	1.33 E-3	1.84 E-3

Ratios of Photodissociation Frequencies for Multiple Scattering and the Leighton Approximation for Various Albedos

Altitude, km	$\frac{J_{ms}(a = 0.00)}{J_L}$	$\frac{J_{ms}(a = 0.25)}{J_L}$	$\frac{J_{ms}(a = 0.50)}{J_L}$	$\frac{J_{ms}(a = 0.75)}{J_L}$	$\frac{J_{ms}(a = 1.00)}{J_L}$
10	1.83	2.00	2.25	2.54	2.98
5	1.76	1.99	2.31	2.71	3.28
0	0.97	1.27	1.78	2.45	3.39

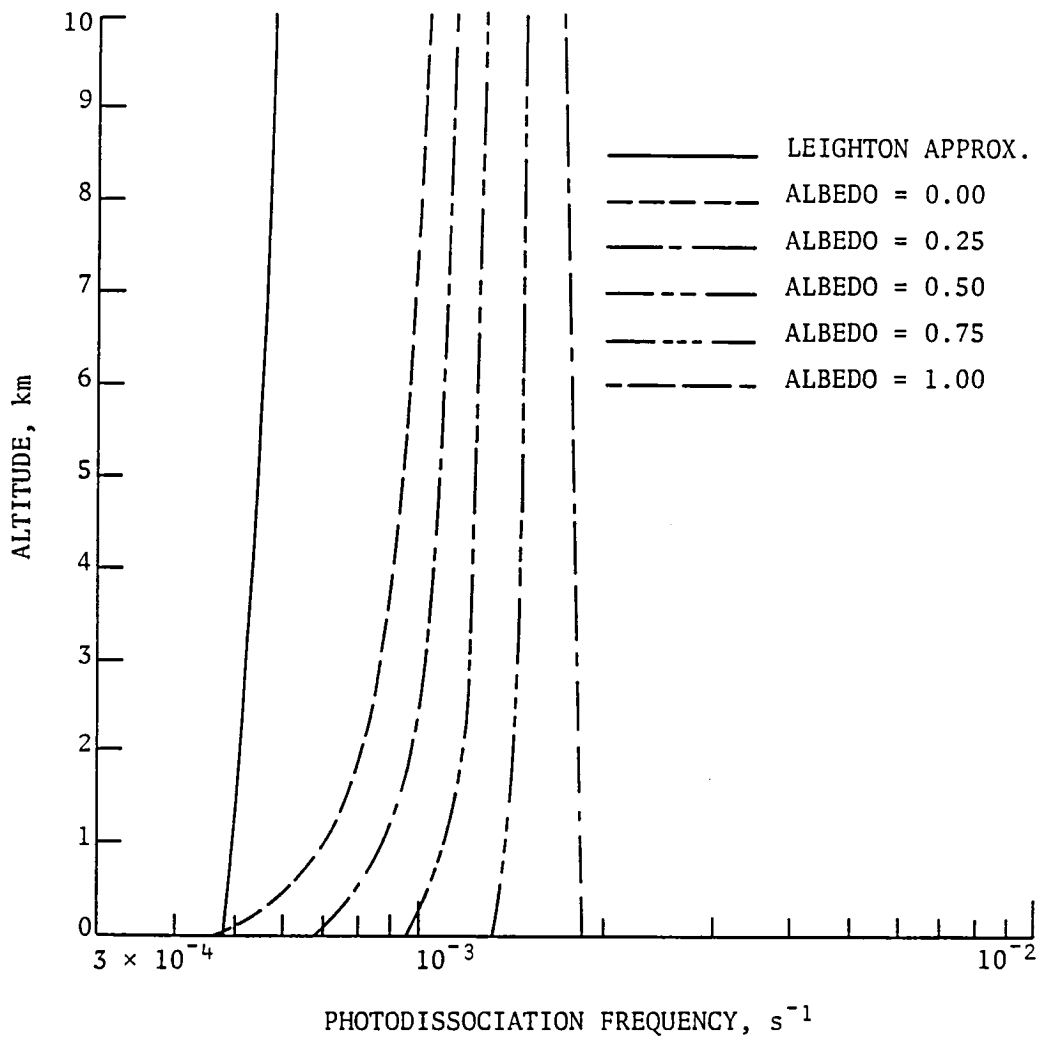

Figure 12. Photodissociation frequencies of HNO_2 for the multiple scattering cases with various albedos and the Leighton approximation.

Table 9. Photodissociation frequencies of H_2O_2 and CH_3OOH ratios for multiple scattering for various albedos and the Leighton approximation.

$H_2O_2 + h\nu \rightarrow 2\ OH\ (270 < \lambda < 360\ nm)$

and

$CH_3OOH + h\nu \rightarrow CH_3 + OH\ (270 < \lambda < 360\ nm)$

Photodissociation Frequencies, s^{-1}

Altitude, km	J_L	$J_{ms}(a = 0.00)$	$J_{ms}(a = 0.25)$	$J_{ms}(a = 0.50)$	$J_{ms}(a = 0.75)$	$J_{ms}(a = 1.00)$
10	2.00 E-6	4.54 E-6	4.87 E-6	5.30 E-6	5.88 E-6	6.73 E-6
5	1.82 E-6	3.96 E-6	4.41 E-6	4.99 E-6	5.79 E-6	6.95 E-6
0	1.60 E-6	1.69 E-6	2.48 E-6	3.53 E-6	4.97 E-6	7.04 E-6

Ratios of Photodissociation Frequencies for Multiple Scattering and the Leighton Approximation for Various Albedos

Altitude, km	$\frac{J_{ms}(a = 0.00)}{J_L}$	$\frac{J_{ms}(a = 0.25)}{J_L}$	$\frac{J_{ms}(a = 0.50)}{J_L}$	$\frac{J_{ms}(a = 0.75)}{J_L}$	$\frac{J_{ms}(a = 1.00)}{J_L}$
10	2.27	2.44	2.65	2.94	3.37
5	2.18	2.42	2.74	3.18	3.82
0	1.06	1.55	2.21	3.11	4.40

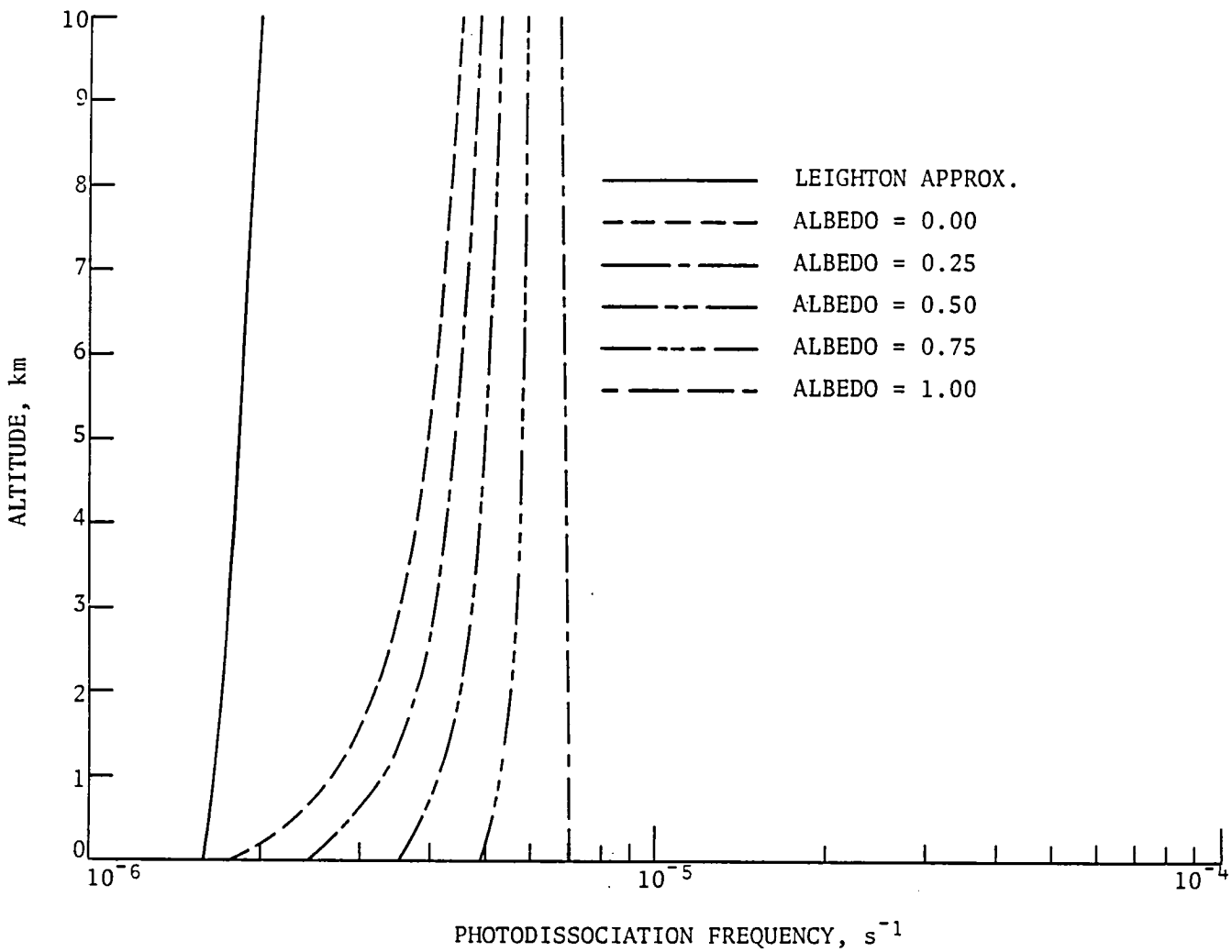

Figure 13. Photodissociation frequencies of H_2O_2 and CH_3OOH for the multiple scattering cases with various albedos and the Leighton approximation.

photolysis frequency by about 6 percent. At higher altitudes, still for the case of a = 0.00, the photolysis frequencies are more than doubled. For an increase in the albedo to 0.25, the ratio J_{ms}/J_L is 1.6 at the surface and 2.4 at both 5 and 10 km. More than a doubling is noticed for an albedo of 0.5. Specifically, a value of 2.2 is obtained at the surface, and 2.7 in the mid and upper tropospheric regions. When the albedo is 0.75, the ratio is more than tripled at the surface and at 5 km with values of 3.1 and 3.2, respectively. At the tropopause it is nearly tripled, reaching a value of 2.9. When the assumption is made that the surface is a perfect reflector (a = 1.00), well over a quadrupling is seen with a value of 4.4. In the midtroposphere (5 km) the ratio is nearly quadrupled (3.82), and at the tropopause (10 km) the ratio is more than tripled (3.4).

Formaldehyde (CH_2O) photodissociates in two different branches with one branch leading to atomic hydrogen (H) and the formyl radical (HCO) according to

$$CH_2O + h\nu \rightarrow H + HCO \quad [280 < \lambda < 340 \text{ nm}] \qquad (43)$$

and the other branch leading to molecular hydrogen (H_2) and carbon monoxide (CO) in accordance with

$$CH_2O + h\nu \rightarrow H_2 + CO \quad [280 < \lambda < 360 \text{ nm}] \qquad (44)$$

The branching of formaldehyde photolysis has been discussed (see "Photolysis Rate Calculations") and shown graphically in figure 3. The photolysis frequencies for process (44) are generally 3 times faster than those for process (43). The calculated photolysis frequencies are given in table 10 for the branch leading to H + HCO and in table 11 for the H_2 + CO branch. Inspection of tables 10 and 11 shows that the values of the ratio of J_{ms}/J_L are similar in magnitude and range, with the ratios due to process (43) slightly higher than those due to process (44). For a surface albedo of 0.00, no difference is seen at the surface for process (43) while a 5 percent decrease is observed for

Table 10. Photodissociation frequencies of CH_2O and ratios for multiple scattering for various albedos and the Leighton approximation.

$CH_2O + h\nu \rightarrow HCO + H$ ($280 < \lambda < 340$ nm)

Photodissociation Frequencies, s^{-1}

Altitude, km	J_L	$J_{ms}(a = 0.00)$	$J_{ms}(a = 0.25)$	$J_{ms}(a = 0.50)$	$J_{ms}(a = 0.75)$	$J_{ms}(a = 1.00)$
10	2.53 E-5	5.36 E-5	5.77 E-5	6.31 E-5	7.04 E-5	8.11 E-5
5	2.32 E-5	4.70 E-5	5.26 E-5	5.98 E-5	6.97 E-5	8.40 E-5
0	2.05 E-5	2.04 E-5	3.01 E-5	4.28 E-5	6.02 E-5	8.54 E-5

Ratios of Photodissociation Frequencies for Multiple Scattering and the Leighton Approximation for Various Albedos

Altitude, km	$\frac{J_{ms}(a = 0.00)}{J_L}$	$\frac{J_{ms}(a = 0.25)}{J_L}$	$\frac{J_{ms}(a = 0.50)}{J_L}$	$\frac{J_{ms}(a = 0.75)}{J_L}$	$\frac{J_{ms}(a = 1.00)}{J_L}$
10	2.12	2.28	2.49	2.78	3.21
5	2.03	2.27	2.58	3.00	3.62
0	1.00	1.47	2.09	2.94	4.17

Table 11. Photodissociation frequencies of CH_2O and ratios for multiple scattering for various albedos and the Leighton approximation.

$CH_2O + h\nu \rightarrow H_2 + CO$ ($280 < \lambda < 360$ nm)

Photodissociation Frequencies, s^{-1}

Altitude, km	J_L	$J_{ms}(a = 0.00)$	$J_{ms}(a = 0.25)$	$J_{ms}(a = 0.50)$	$J_{ms}(a = 0.75)$	$J_{ms}(a = 1.00)$
10	8.03 E-5	1.57 E-4	1.71 E-4	1.89 E-4	2.12 E-4	2.47 E-4
5	7.47 E-5	1.40 E-4	1.58 E-4	1.80 E-4	2.11 E-4	2.56 E-4
0	6.63 E-5	6.30 E-5	9.29 E-5	1.32 E-4	1.85 E-4	2.62 E-4

Ratios of Photodissociation Frequencies for Multiple Scattering and the Leighton Approximation for Various Albedos

Altitude, km	$\frac{J_{ms}(a = 0.00)}{J_L}$	$\frac{J_{ms}(a = 0.25)}{J_L}$	$\frac{J_{ms}(a = 0.50)}{J_L}$	$\frac{J_{ms}(a = 0.75)}{J_L}$	$\frac{J_{ms}(a = 1.00)}{J_L}$
10	1.96	2.13	2.35	2.64	3.08
5	1.87	2.12	2.41	2.82	3.43
0	0.95	1.40	1.99	2.79	3.95

process (44). At higher altitudes, slightly more than a doubling is seen for proces (43) while process (44) shows slightly less than a doubling. When the albedo is 0.25, process (43) shows almost a 50 percent increase in J_{ms}/J_L at surface while process (44) exhibits an increase of 40 percent. In the mid and upper tropospheric regions, process (43) has a ratio of 2.3 while it is 2.1 for process (44). For an albedo of 0.50, the ratio is 2.1 for process (43) and exactly doubled for process (44). The midtropospheric and tropopause values are also very similar with ratios ranging from 2.4 to 2.6. Even when the ratios of J_{ms}/J_L for higher albedos are calculated, processes (43) and (44) exhibit similar numerical values. For a = 0.75, the values range from 2.8 to 3.0 for the branch leading to HCO + H [process (43)] and from 2.6 to 2.8 for the H_2 + CO branch [process (44)]. Finally, when an albedo of 1.00 is used, the ratio is J_{ms}/J_L ranges from 3.2 to 4.2 for process (43) and from 3.1 to 4.0 for process (44). The vertical profiles for the photodissociation frequencies for processes (43) and (44) are displayed in figures 14 and 15, respectively.

The Nitrogen Group

Introduction - In this subsection, a systematic approach is used to identify the chemical production and loss terms and the percent contribution of each reaction to the formation and destruction of each species calculated in the present model. A solar zenith angle of 45° is used throughout this study. The species are discussed within the framework of their chemical families with the nitrogen family first, followed by the oxygen, hydrogen, carbon, and sulfur families. Finally, the calculated vertical profiles for each species are shown for the Leighton approximation and for the multiple scattering calculations based on the Anderson-Meier model for various albedos. Whenever possible, the calculated vertical profiles have been compared with available measurements.

The nitrogen group consists of a total of 14 species with wide ranges of lifetimes and abundances. The most abundant species in the Earth's atmosphere, molecular nitrogen, is a member of this group. Also, some pivotal photochemical species in the troposphere such as odd nitrogen (nitric oxide and nitrogen dioxide), ammonia, and nitric acid are members of this group. The reaction

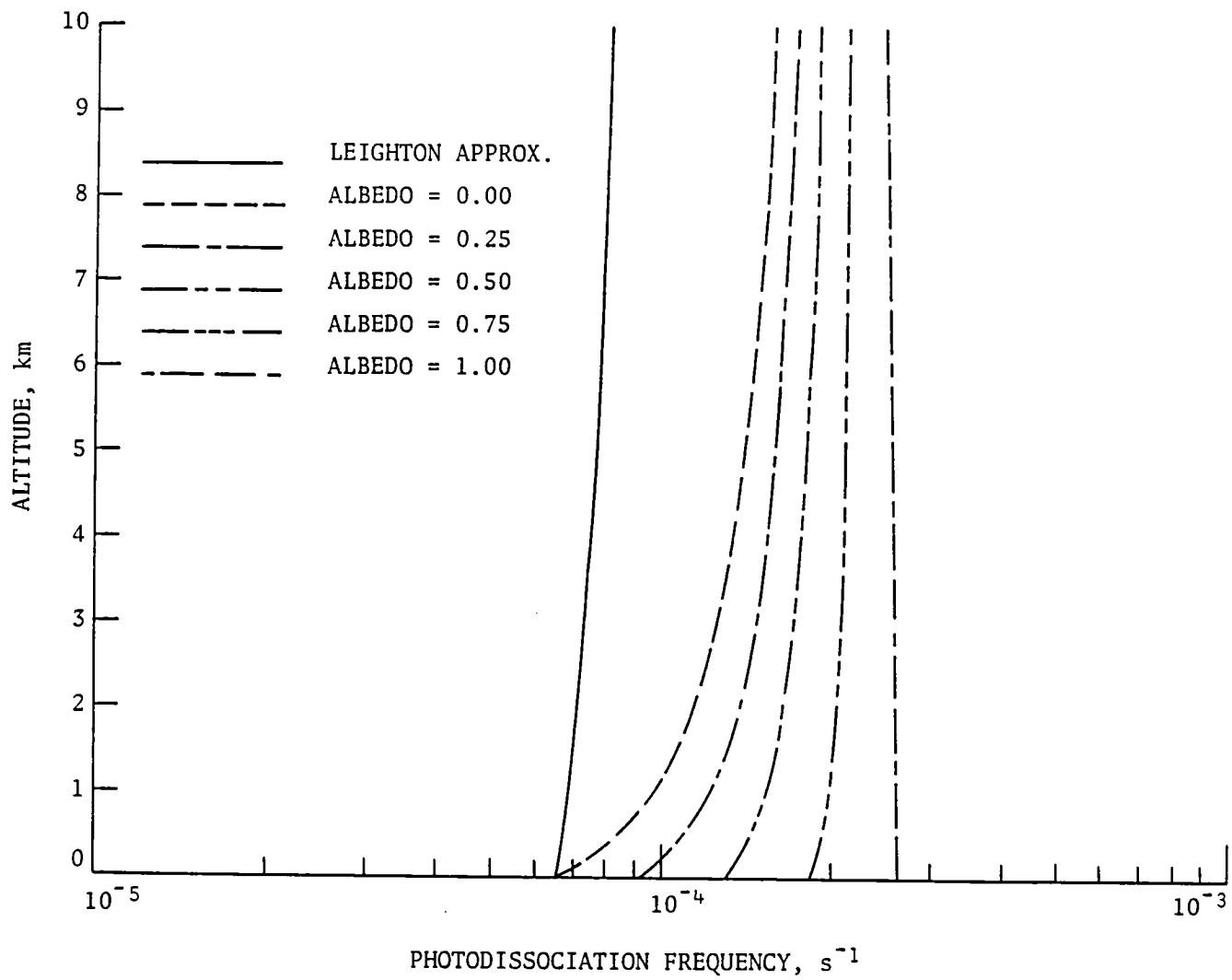

Figure 14. Photodissociation frequencies of CH_2O for the multiple scattering cases with various albedos and the Leighton approximation.

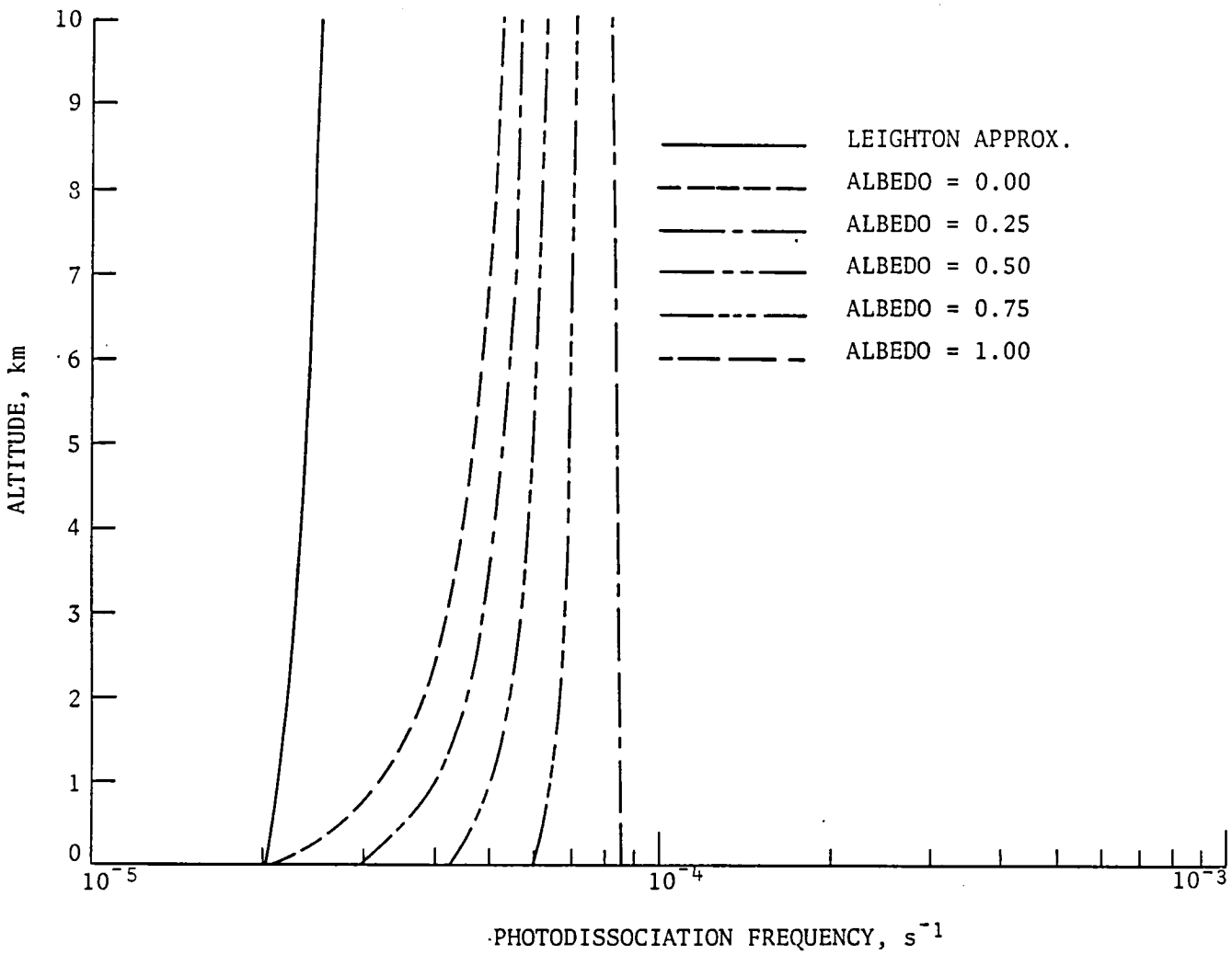

Figure 15. Photodissociation frequencies of CH_2O for the multiple scattering cases with various albedos and the Leighton approximation.

paths of the nitrogen family are shown in figure 16. The species are arranged in decreasing order of their tropospheric abundances, and within the framework of each species the chemical reactions are arranged in order of their importance.

Molecular nitrogen (N_2). - Although molecular nitrogen is the most abundant species in the Earth's atmosphere from a photochemical point of view, it is uninteresting. This is due to its radiative and chemical inertness. Molecular nitrogen has a concentration of 78.08 percent by volume and a lifetime of several million years. It derives its primary importance in the atmosphere from the fact that 78 percent of the time it serves as the third body in chemical reaction of the type:

$$A + B + M \rightarrow AB + M$$

where M is the third body. Consequently, in the present model, molecular nitrogen is only included as an input with a specified vertical profile. Nitrogen is only important chemically, since atmospheric lightning can decompose it forming atomic nitrogen, which can recombine with oxygen atoms to form nitric oxide (NO).

Ammonia (NH_3). -

Production	Destruction
K53: $NH_2 + H_2 \rightarrow NH_3 + H$	K48: $NH_3 + OH \rightarrow NH_2 + H_2O$
K52: $NH_2 + OH \rightarrow NH_3 + O$	K47: $NH_3 + O(1D) \rightarrow NH_2 + OH$
	K46: $NH_3 + O \rightarrow NH_2 + OH$
	K49: $NH_3 + H \rightarrow NH_2 + H_2$

Ammonia, which is the only common gaseous base in the atmosphere, is formed primarily as a result of microbial activity in the soil. Chemically, two reactions contribute to the production. Reaction of the amino radical

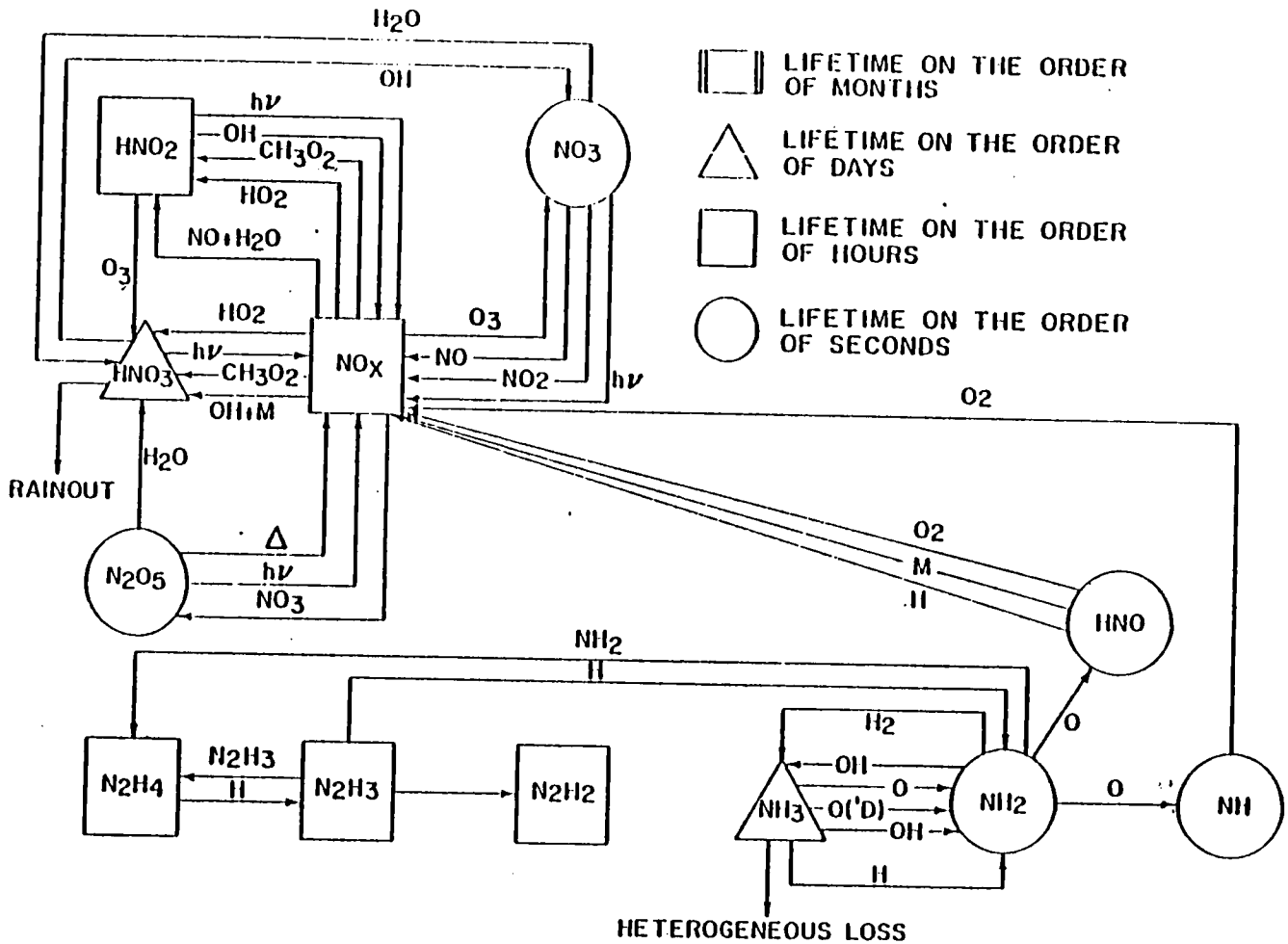

Figure 16. Reaction paths of the nitrogen family.

(NH_2) with molecular hydrogen (H_2) (reaction 53) provides for nearly all of the atmospheric chemical production, with only minute fractions produced as a result of reaction 52 (see table 12). The overwhelming chemical sink for ammonia is the reaction with hydroxyl (reaction 48). The reaction of ammonia with excited oxygen (reaction 47) accounts for a minor sink (0.01 percent) at the tropopause, while the remaining two destruction terms for ammonia are 6 to 10 orders of magnitude smaller than the primary destruction path. The chemical equilibrium concentration of NH_3 has been calculated to $10^{-54.5}$ (ppb) (ref. 11), while the actual ammonia mixing ratio is in the ppb range (ref. 60). The large difference between the calculated and actual levels of ammonia is due to microbial activity in the soil. Hence, the most important source of atmospheric NH_3 appears to be the surface with different processes controlling ammonia production in different geographical locations. In the industrialized parts of the world, coal conversion and combustion proceses appear to emit large quantities of NH_3 (refs. 61, 62). Volatilization from fertilized and nonfertilized land is also an ammonia source (ref. 63). In England, urine from domestic animals is reportedly the dominant source of NH_3 (ref. 64). With an ever-increasing industrial activity, a greater dependence on coal, and an increase in the use of fertilizers to enhance crop yields, the prospect of large anthropogenic emissions of NH_3 is very real indeed. Until recently, the only vertical measurements of NH_3 available were those by Georgii and Muller (ref. 65). They found large spatial and temporal variabilities partly as a function of surface temperature. Recently a remote instrument, the Infrared Heterodyne Radiometer (IHR), has been developed and used to make routine measurements of NH_3 (ref. 60). Furthermore, in situ aircraft measurements of ammonia in the same general location as the IHR (NASA/LaRC) have yielded excellent agreement with IHR (ref. 66). The typical background level of ammonia is generally about 1 ppb at the surface decreasing to about 0.5 ppb at 10 km. Measurements obtained during the spring (March to early April) have exhibited about an order of magnitude larger values for the surface mixing ratio than the background level. It is believed that the enhanced level of ammonia in the springtime is the result of rapid volatilization of ammonium nitrate fertilizer that is applied to agricultural fields prior to the start of the growing season (ref.

Table 12. Production and destruction terms of NH_3 and percent of total production and destruction.

Production Rate (molecules-cm^{-3}-s^{-1}) and Percent of Total Production

Altitude, km	K53	%	K52	%	Total	%
10	5.796 E-1	99.97	1.755 E-2	0.03	5.798 E-1	100.00
5	3.182 E-2	99.98	7.929 E-2	0.02	3.183 E-2	100.00
0	1.709 E-3	99.98	3.243 E-1	0.02	1.709 E-3	100.00

Destruction Frequency (s^{-1}) and Percent of Total Destruction

Altitude, km	K48	%	K47	%	K46	%	K49	Total	%
10	8.319 E-8	99.99	8.805 E-12	0.01	4.893 E-14	-	1.857 E-17	8.319 E-8	100.00
5	1.919 E-7	100.00	3.515 E-12	-	1.152 E-13	-	2.319 E-17	1.919 E-7	100.00
0	3.466 E-7	100.00	1.272 E-12	-	1.798 E-13	-	2.855 E-17	3.466 E-7	100.00

11). In the summer, the level of ammonia decreases to its background level again. Similar temporal variations were observed in 1976 on Long Island, New York during engineering tests of the Infrared Heterodyne Spectrometer (IHS), which was the predecessor of the IHR. The homogeneous loss of NH_3 occurs primarily by the reaction of ammonia with the hydroxyl radical (reaction 48). The homogeneous lifetime of ammonia based on this reaction is nearly 40 days. Ammonia, which is water soluble and is also involved in aerosol formation, has a heterogeneous loss time of about 10 days (ref. 11). The effect of varying the heterogeneous loss term and eddy diffusion on the vertical distribution of ammonia has been investigated by Levine et al. (ref. 11). This study shows that an eddy diffusion coefficient of about 2×10^5 cm^2 s^{-1} is needed to obtain a good fit with the measured data. It should be pointed out, however, that the IHR uses the Sun as a radiation source, and measurements can only be taken on clear sunny days. This might lead to a bias, since sunny days increase the local convection. The study by Levine et al. also found that the heterogeneous loss term has a time constant in excess of 10 days, which is somewhat longer than was previously believed. The amount of ammonia emitted from the soil is a function of soil moisture as well as soil temperature (ref. 63). Lower ammonia levels were observed in 1980 than in 1979 (ref. 67). Part of the explanation for this might be that in 1979, through September, the Hampton, Virginia area experienced a 57 percent enhancement in total precipitation amount as compared to the mean. In 1980, on the other hand, the total precipitation was 21 percent below the mean through September, which resulted in much lower soil moisture value than did the frequent precipitation patterns in 1979. The measurement envelope for background levels of ammonia is indicated by cross-hatches in figure 17, together with in situ aircraft measurements at 1.6 and 3.0 km (refs. 11, 66). The lower boundary condition was held constant at 1.25 ppb, which corresponds to about 3.2×10^{10} molecules cm^{-3}. At the upper boundary a constant mixing ratio of 0.5 ppb was imposed. This corresponds to an ammonia number density of 3.3×10^9 molecules cm^{-3}. The resulting vertical profiles for the Leighton approximation as well as the multiple scattering cases are shown in figure 17. The multiple scattering profiles decrease more rapidly with altitude than does the Leighton approximation. This is a result

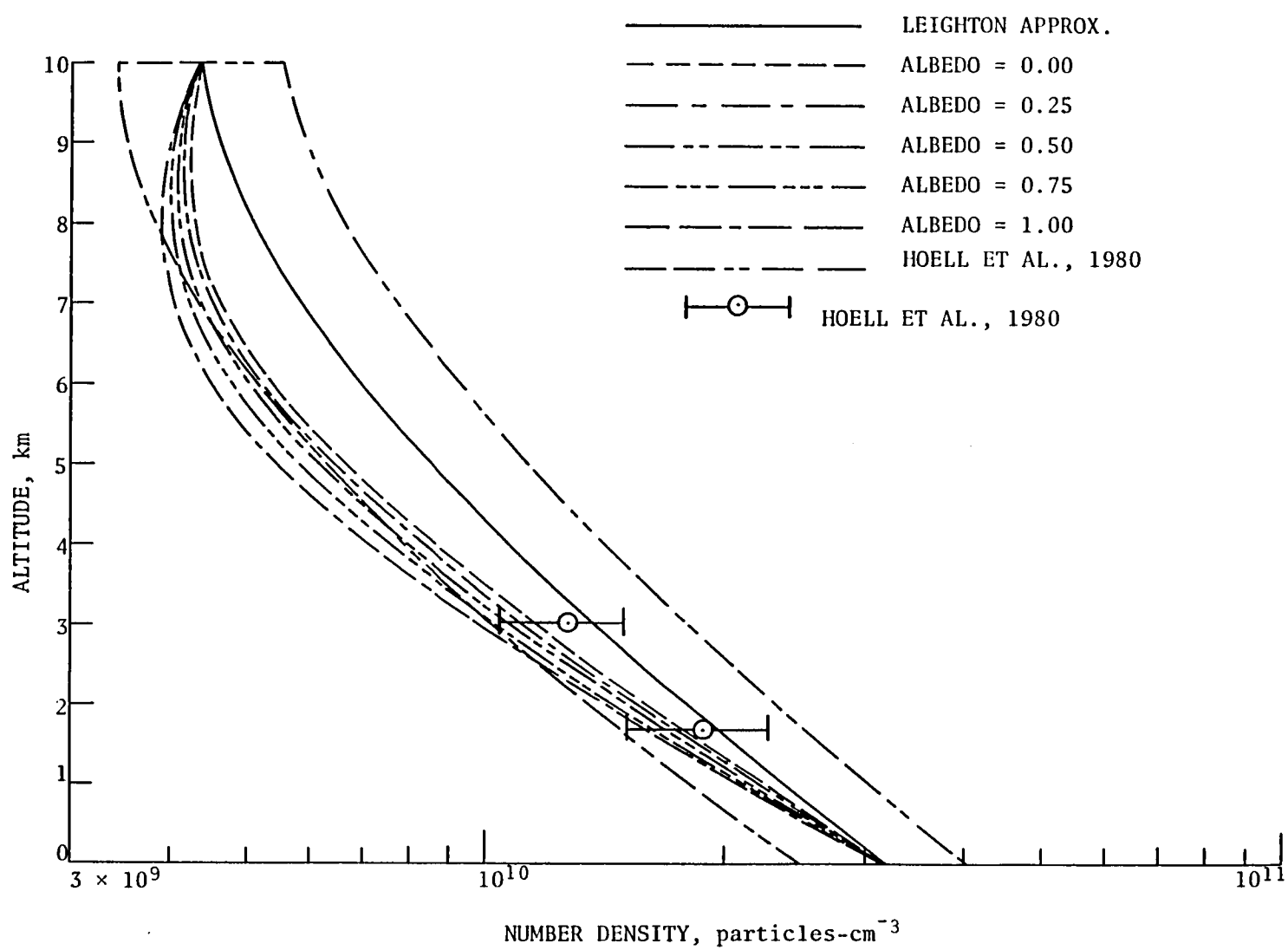

Figure 17. Vertical distributions of NH_3 for the multiple scattering cases with various albedos and the Leighton approximation.

of the enhanced OH level resulting from the multiple scattering calculations. From 8 to 10 km, the multiple scattering calculations appear to be turning back into the center of the measurement envelope. This is a numerical artifact as opposed to an atmospheric source of NH_3, due to the imposed upper boundary condition. The multiple scattering calculations with high albedos, notably 1.00 and 0.75, fall outside the measurement envelope in the midtroposphere. The case of an albedo of 0.50 falls just on the lower limit of the measurement envelope, while the cases of albedos of 0.25 and 0.00 fall entirely within the measurement envelope, albeit not by very much. The Leighton approximation shows the best fit of any calculated vertical profile, but it should be kept in mind that the heterogeneous loss frequencies were determined by applying the code in the Leighton approximation mode.

Nitrogen oxides ($NO_x = NO + NO_2$). -

Production	Destruction
J4 : $NO_3 + h\nu \rightarrow NO_2 + O$	K24 : $NO_2 + OH \rightarrow HNO_3$
K32: $NO_3 + NO \rightarrow 2NO_2$	K28 : $NO_2 + O_3 \rightarrow NO_3 + O_2$
J5 : $NO_3 + h\nu \rightarrow NO + O_2$	K112: $NO + HO_2 \rightarrow HNO_3$
K35: $N_2O_5 \rightarrow NO_3 + NO_2$	K54 : $NO + NH_2 \rightarrow N_2 + H_2O$
J7 : $HNO_3 + h\nu \rightarrow NO_2 + OH$	K23 : $NO_2 + HO_2 \rightarrow HNO_2 + O_2$
J8 : $HNO_2 + h\nu \rightarrow NO + OH$	K30 : $NO_2 + NO_3 \rightarrow N_2O_5$
K40: $HNO_2 + OH \rightarrow NO_2 + H_2O$	K7 : $NO_2 + CH_3O_2 \rightarrow HNO_3 + CH_3O$
K31: $NO_3 + NO_2 \rightarrow NO + NO_2 + O_2$	K25 : $NO + OH \rightarrow HNO_2$
J6 : $N_2O_5 + h\nu \rightarrow NO_2 + NO_3$	K33 : $NO + NO_2 + H_2O \rightarrow 2HNO_2$
K59: $HNO + O_2 \rightarrow NO + HO_2$	K56 : $NO + NH \rightarrow N_2 + O + H$
K61: $HNO + H \rightarrow NO + H_2$	K58 : $NO + NH \rightarrow N_2 + OH$
K60: $HNO + M \rightarrow NO + H + M$	K67 : $NO + HS \rightarrow$ Products

Due to the rapid cycling that occurs between nitric oxide (NO) and nitrogen dioxide (NO_2), they are commonly grouped together into an entity called "odd nitrogen" or NO_x. This grouping is made in order to avoid numerical stiffness. Thus, the code calculates the production and destruction of NO_x and subsequently partitions it with the so-called photostationary state equation (ref. 25). This equation yields the ratio $[NO_2]/[NO]$ according to

$$\frac{[NO_2]}{[NO]} = \frac{K29\ [O_3]}{J3}$$

The photostationary state equation is commonly employed in tropospheric models to obtain the abundances of NO and NO_2, although some recent measurements indicate that this relation tends to breakdown for low concentrations of NO_x (ref. 68). It is important to note that the production and destruction terms of NO_x listed above represent the net chemical production and destruction of NO_x. In other words, many other reactions listed in table A2 contain either NO or NO_2 or both, but if no net production or destruction of NO_x occurs they are excluded from table 13. For example, reaction 8 destroys one NO molecule but produces one NO_2, hence there is no net change of NO_x; the same is true for reaction 22. It should also be noted that the photochemical equilibrium value of NO_x, in this study of less than 10 ppt at the surface, is lower than measurements indicate. It is therefore evident that other processes such as industrial emissions, lightning, and forest fires contribute to the NO_x budget (ref. 69).

The anthropogenic source of NO_x has been estimated to be 20 Mt/yr (ref. 70), while the source due to lightning was thought to be 40 to 80 Mt/yr (refs. 71-74). These estimates were based on measurements of NO_2 by Noxon before, during, and after a thunderstorm (ref. 71). Subsequent theoretical calculations by Hill et al. indicate that only NO, and not NO_2, is formed during lightning discharges (ref. 75). The theoretical arguments by Hill et al. were confirmed in some recent laboratory experiments by Levine et al. (ref. 76).

These experimental results indicate that only NO is instantaneously produced during lightning discharges. During a laboratory discharge, neither NO_2 nor O_3 was measured, contrary to common belief. Ozone has always been thought to be formed as a result of lightning discharges, primarily on "aromatic evidence." (The odor of ozone is detected around welding and electric discharge machinery.) It is quite possible that the enhanced levels of NO_2 measured by Noxon during a thunderstorm could be due to two things. First, the enhanced level of NO produced by lightning is converted by the natural background level of O_3 to NO_2 according to the reaction

$$NO + O_3 \rightarrow NO_2 + O_2$$

Secondly, the very turbulent nature of a thunderstorm causes rapid convection, and enhanced levels of upper tropospheric-lower stratospheric NO_2 could be brought down to the surface. The laboratory experiments by Levine et al. yielded a global source of NO due to lightning of 1.8 Mt/yr, much less than previous estimates, but in very good agreement with recent theoretical calculations of 3 Mt/yr by Dawson (ref. 77). Hence, it appears that anthropogenic sources dominate the NO_x production.

Measurements of tropospheric NO_2 range from 1 to 4 ppb in the more polluted areas such as the Central and Eastern United States. Specifically, values of 1 to 2 ppb were measured in Florida and Hawaii (ref. 78), 4.6 ppb in North Carolina (ref. 79), and 1 to 3 ppb in the central United States (ref. 80). Lower values have been obtained in more pristine air: for example, 0.1 to 0.3 ppb in Boulder, Colorado (ref. 81), 0.2 to 0.7 ppb in the Tropics (ref. 82), and less than 0.1 ppb at Fritz Peak, Colorado (ref. 83) and in North America and Peru (ref. 84). More recent measurements at Loop Head on the West Coast of Ireland have yielded values in the range of 0.1 to 2.6 ppb (ref. 85).

Nitric oxide (NO) has also been measured and generally shows lower values than NO_2. Values ranging from 0.1 to 0.7 ppb were obtained in the Tropics (ref. 82) and less than 0.05 ppb over the Pacific Ocean at altitudes between 8 to 12 km (ref. 86). Measurements in Laramie, Wyoming indicate very low levels

of NO, ranging from 0.01 to 0.05 ppb (ref. 87), as do measurements on the Niwot Ridge, Colorado, where NO levels between 0.02 to 0.05 ppb were obtained in a recent experiment (ref. 68). Air samples in clean background air at an altitude of 7 km in the vicinity of Mt. St. Helens were found to contain between 0.015 to 0.029 ppb of NO (ref. 88). Both the studies by Drummond at Laramie, Wyoming (ref. 87) and by Kelly et al. at the Niwot Ridge, Colorado (ref. 68) found that the ratio of NO_2/NO was typically much greater than the photostationary state equation would predict. Kelly et al. (ref. 68) reported that only 10 to 25 percent of the NO_x was in the form of NO. Similarly, Drummond (ref. 87) found that NO molecules comprised only 5 to 27 percent of the total NO_x with the smallest percentage for the lowest NO_x measurements. For this study, a lower boundary condition of 0.03 ppb (or 30 ppt) of NO_x was selected. The amount of NO_x was then partitioned with the photostationary state equation, and the resulting vertical profiles of NO and NO_2 are shown in figures 18 and 19, respectively. The vertical profiles of NO are in reasonably good agreement with the measured values at pristine locations (refs. 86-89), but the calculated values of NO_2 are lower than measured values due to the breakdown of the photostationary state equation. The contributions due to chemistry are listed in table 13. Again, it should be emphasized that the photochemical production accounts for only a small fraction of the total NO_x chemistry.

The primary sink for NO_x is the reaction of NO_2 with OH forming HNO_3 (reaction 24). Since nitric acid has a longer lifetime than NO_x, it has been argued that the NO_x observed in clean background air, away from anthropogenic sources, is due to the photolysis of nitric acid molecules that were formed according to reaction 24 and subsequently transported away (ref. 90). Other important chemical sinks for NO_x include the reaction of NO_2 with ozone (reaction 28) and the reaction of NO with O_2 (reaction 112) (see table 13).

One of the objectives of this study was to investigate the effects of a detailed radiative transfer code on the photochemistry of the troposphere. In order to faciliate this, it was desirable to maintain a constant lower boundary condition. In addition to the boundary condition, it was necessary to augment the chemical production with a source term to account for surface anthropogenic

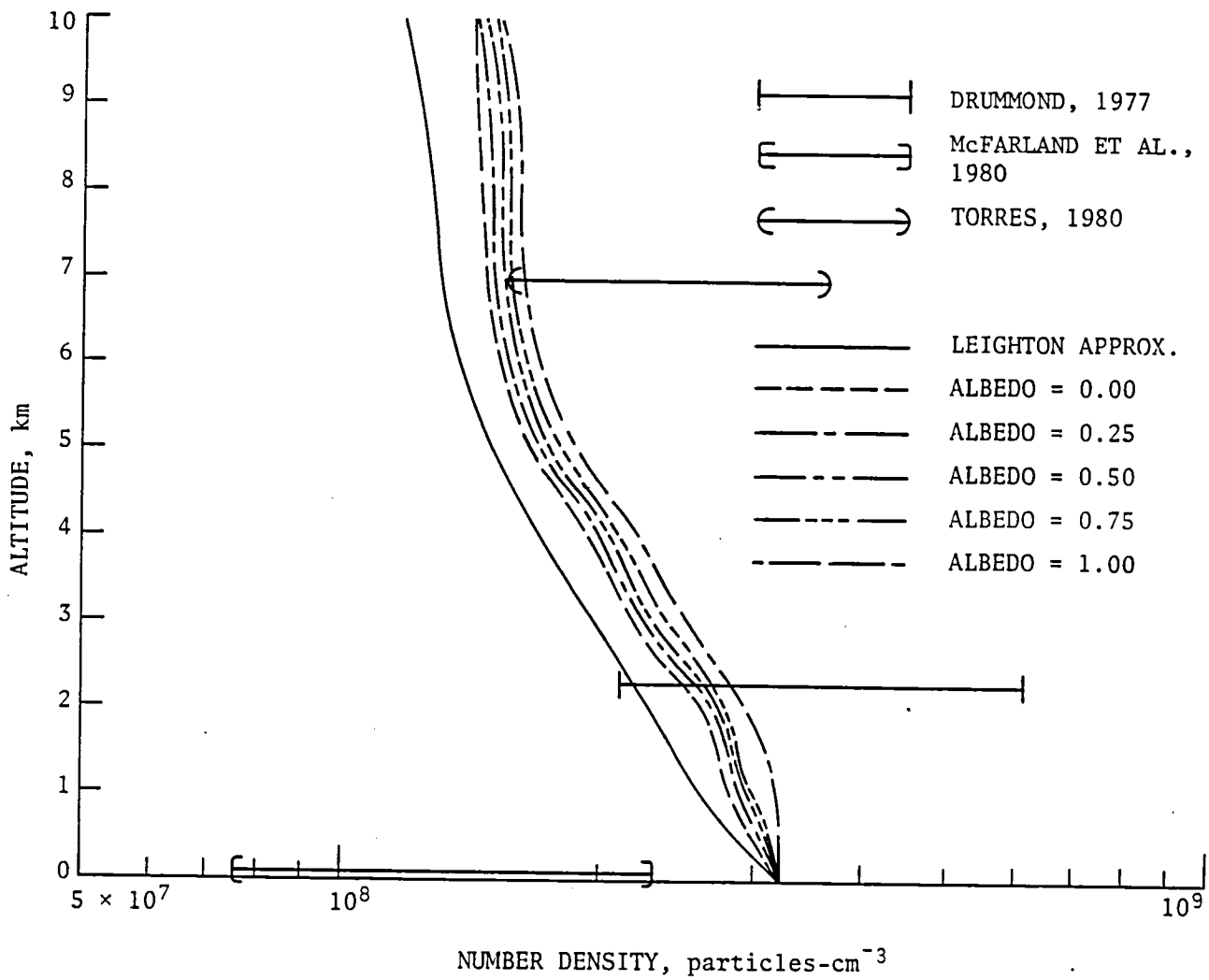

Figure 18. Vertical distributions of NO for the multiple scattering cases with various albedos and the Leighton approximation.

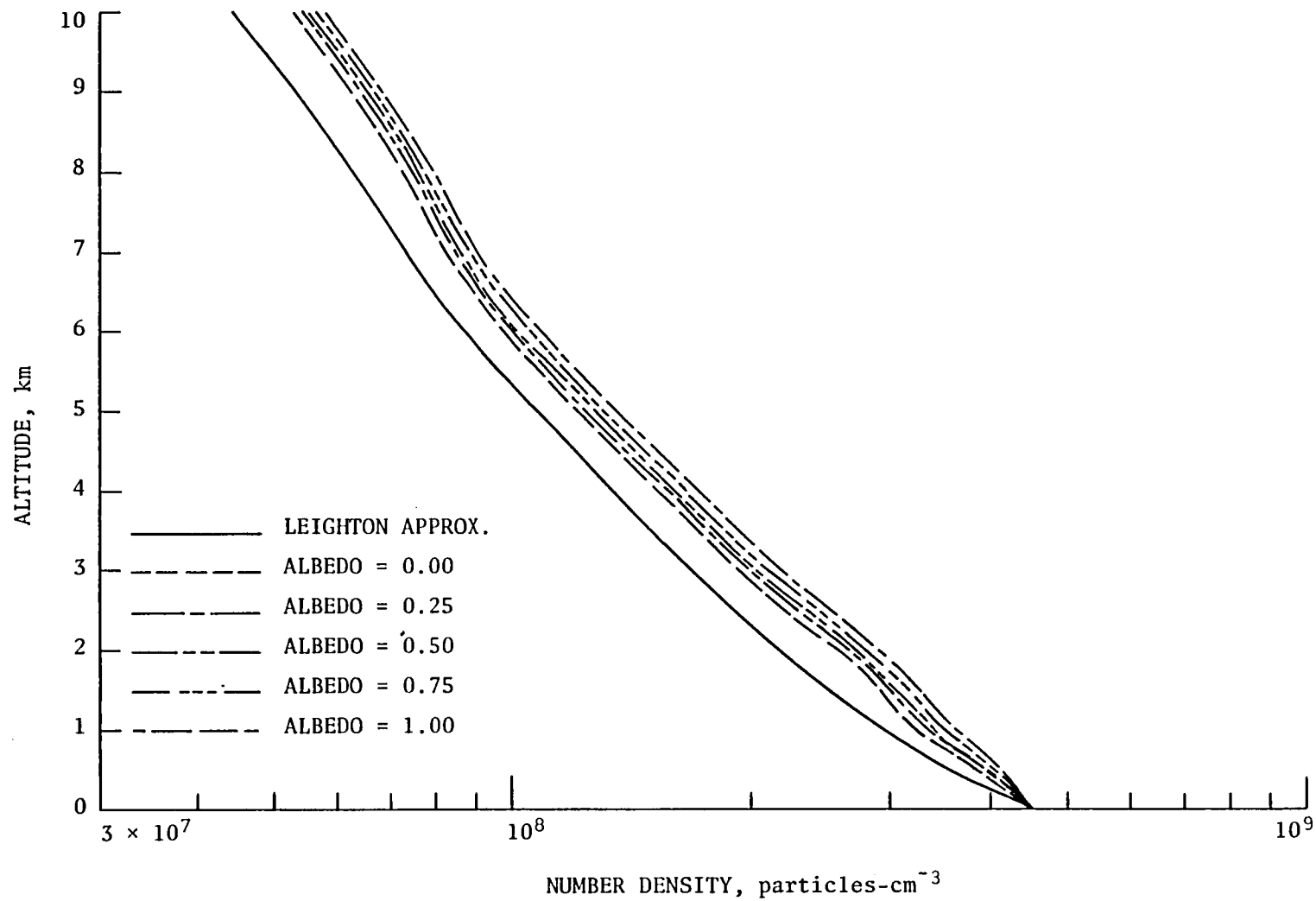

Figure 19. Vertical distributions of NO_2 for the multiple scattering cases with various albedos and the Leighton approximation.

Table 13. Production and destruction terms of NO_x and percent of total production and destruction.

Production Rate (molecules-cm^{-3}-s^{-1}) and Percent of Total Chemical Production

Altitude, km	J4	%	K32	%	J5	%	K35	%	J7	%	J8	%
10	1.017 E-3	48.08	1.131 E-2	5.35	2.509 E-2	11.86	4.808 E-1	0.03	4.398 E-2	20.79	2.841 E-2	13.43
5	4.885 E-3	59.38	7.066 E-2	8.58	1.208 E-3	14.68	1.170 E-2	1.42	7.649 E-2	9.29	5.457 E-2	6.63
0	3.127 E-4	49.30	1.478 E-4	23.30	7.772 E-3	12.25	5.596 E-3	8.82	2.460 E-3	3.88	1.527 E-3	2.41

Altitude, km	K40	%	K31	%	J6	%	K59	%	K61	%	K60	%	Total	%
10	1.353 E-0	0.06	1.293 E-2	-	8.466 E-0	0.40	4.703 E-3	-	1.157 E-15	-	1.170 E-37	-	2.115 E-3	100.00
5	4.027 E-0	0.02	2.707 E-1	-	4.617 E-1	-	5.242 E-3	-	9.050 E-16	-	1.442 E-31	-	8.231 E-3	100.00
0	1.605 E-1	0.03	1.215 E-1	0.01	1.943 E-0	-	6.159 E-3	-	7.856 E-16	-	8.321 E-27	-	6.434 E-4	100.00

(continued)

Table 13. (Concluded.)

Destruction Frequency (s^{-1}) and Percent of Total Chemical Destruction

Altitude, km	K24	%	K28	%	K112	%	K54	%	K23	%	K30	%
10	6.859 E-5	70.34	2.052 E-6	2.10	1.663 E-5	17.05	2.831 E-6	2.90	3.564 E-6	3.65	4.225 E-7	0.44
5	1.205 E-4	62.78	7.368 E-6	3.84	3.827 E-5	19.94	8.734 E-6	4.55	8.007 E-6	4.17	2.078 E-6	1.08
0	1.804 E-4	44.97	8.127 E-5	20.26	7.063 E-5	17.61	2.816 E-5	7.02	1.514 E-5	3.77	1.448 E-5	3.61

Altitude, km	K7	%	K25	%	K33	%	K56	%	K58	%	K67	%	Total	%
10	8.270 E-7	0.85	2.604 E-6	2.67	3.125 E-13	-	4.309 E-11	-	3.567 E-11	-	3.131 E-16	-	9.752 E-5	100.00
5	3.157 E-6	1.65	3.812 E-6	1.99	1.130 E-11	-	3.651 E-11	-	3.029 E-11	-	1.122 E-15	-	1.919 E-4	100.00
0	6.264 E-6	1.56	4.843 E-6	1.20	2.295 E-10	-	1.940 E-11	-	1.645 E-11	-	1.210 E-13	-	4.012 E-4	100.00

emissions and lightning production of NO_x. (Incidentally, this could also be accomplished by a flux boundary condition.) The inclusion of a detailed radiative transfer code enhanced the levels of NO and NO_2 only slightly. In fact, odd nitrogen was less affected than any other species in this study. At the tropopause there was a factor of 1.3 difference between the multiple scattering calculations and the Leighton approximation. Since the NO_x species are important presursors to ozone production, it is essential that the background level of NO_x be established. Odd nitrogen participates in the catalytic cycle

$$NO + O_3 \rightarrow NO_2 + O_2$$

$$NO_2 + h\nu \rightarrow NO + O$$

$$O + O_2 + M \rightarrow O_3 + M$$

which governs the photostationary state equation. The departure of the NO_2/NO ratio from the photostationary state value indicates that free peroxy radicals, which constitute a competing mechanism to ozone for reaction with nitric oxide, may play a more significant role in the clean troposphere, as recently suggested by Kelly et al. (ref. 68).

Nitric acid (HNO_3). -

Production		Destruction	
K24 :	$NO_2 + OH \rightarrow HNO_3$	K26 :	$HNO_3 + OH \rightarrow NO_3 + H_2O$
K112:	$NO + HO_2 \rightarrow HNO_3$	J7 :	$HNO_3 + h\nu \rightarrow NO_2 + OH$
K7 :	$NO_2 + CH_3O_2 \rightarrow HNO_3 + CH_2O$	K110:	$HNO_3 + O \rightarrow NO_3 + OH$
K34 :	$NO + NO_2 + H_2O \rightarrow 2HNO_3$	K114:	$HNO_3 + H \rightarrow$ Products
K111:	$HNO_2 + O_3 \rightarrow HNO_3 + O_2$		
K113:	$NO_3 + H_2O \rightarrow HNO_3 + OH$		

Nitric acid is an important molecule in the troposphere because it acts as a reservoir for reactive nitrogen species. It is formed by six reactions, but primarily by nitrogen dioxide reacting with hydroxyl in the presence of a third body (reaction 24) and by nitric oxide reacting with hydroperoxyl (reaction 112). Together these two reactions are responsible for 97 to 99 percent of all tropospheric HNO_3 production depending on altitude (see table 14). Minor HNO_3 sources include reactions of NO_2 with CH_3O_2 (reaction 7) and NO_2 with NO and H_2O (reaction 34); together they account for one to three percent of total production. The two remaining reactions are between four and nine orders of magnitude smaller than the primary chemical sources. Nitric acid is a very water soluble gas and, hence, is subject to heterogeneous removal by rainout and washout. Nitric acid is also lost by dry deposition. An attempt to quantify this loss was made during the CHON Experiment in rural Colorado (ref. 91). Yet another removal mechanism of HNO_3 is the conversion to aerosol nitrates. In addition to these physical sinks, there are also chemical reactions that remove HNO_3. The two primary chemical sinks are the reaction of HNO_3 with OH (reaction 26) and HNO_3 photolysis (J7) (see table 14). The two remaining chemical reactions removing HNO_3 are six to seven orders of magnitude smaller than the two primary chemical loss terms and, thus, need not be considered. The chemical lifetime of HNO_3 based solely on the reaction scheme above is much too long to account for the relatively low abundances that have been measured lately. Clearly, heterogeneous removal must play an important part in controlling the tropospheric level of nitric acid.

Measurements of HNO_3 have ben obtained in both urban and rural environments. Okita et al. (ref. 92) found HNO_3 levels in Tokyo, Japan varying between 0.2 and 8 ppb. Huebert and Lazrus (ref. 93) measured levels in the 0.4 to 0.9 ppb range over the continental United States. As expected, lower values of nitric acid are present in rural air. Okita et al. (ref. 9) obtained levels between 0.0 and 0.7 ppb on Mt. Tsukuba, Japan, while Huebert and Lazrus found values of 0.02 to 0.3 ppb over a wide range of latitudes and altitudes. Those measurements have been transposed to figure 20 and are compared to the present calculations. Shipboard measurements taken during a voyage in the equatorial Pacific region found low values of HNO_3; the average concentration

Table 14. Production and destruction terms of HNO_3 and percent of total production and destruction.

Production Rate (molecules-cm^{-3}-s^{-1}) and Percent of Total Production

Altitude, km	K24	%	K112	%	K7	%	K34	%	K111	%	K113	%	Total	%
10	3.043 E-3	60.13	1.936 E-3	38.62	3.669 E-1	0.73	1.760 E-1	0.52	2.468 E-1	-	6.423 E-6	-	5.060 E-3	100.00
5	1.296 E-4	68.07	5.549 E-3	29.14	3.394 E-2	1.78	1.910 E-2	1.01	4.478 E-1	-	5.786 E-4	-	1.904 E-4	100.00
0	8.043 E-4	75.35	2.253 E-4	21.11	2.794 E-3	2.62	9.890 E-2	0.92	1.184 E-0	-	4.379 E-2	-	1.067 E-5	100.00

Destruction Frequency (s^{-1}) and Percent of Total Destruction

Altitude, km	K26	%	J8	%	K110	%	K114	%	Total	%
10	1.107 E-7	33.48	2.199 E-7	66.52	5.844 E-13	-	1.857 E-14	-	3.306 E-7	100.00
5	1.620 E-7	45.87	1.912 E-7	54.13	2.110 E-13	-	2.318 E-14	-	3.532 E-7	100.00
0	2.057 E-7	56.13	1.608 E-7	43.87	7.680 E-14	-	2.855 E-14	-	3.665 E-7	100.00

was 0.030 ppb (ref. 94). Kelly et al. (ref. 68) measured values of 0.03 to 0.01 ppb at the Niwot Ridge at an elevation of 3 km in the Rocky Mountains of Colorado. They also found that NO_x levels were always greater than HNO_3 levels, perhaps invalidating the photostationary state equation. More research is needed on this point. The measurements by Huebert and Lazrus during the GAMETAG flights seem to indicate higher concentrations in the rural free troposphere than in the boundary layer, contrary to the prediction of photochemical models (ref. 95). At 5.5 km, HNO_3 concentrations of 0.08 to 0.2 ppb were found, while in the boundary layer (0.27 to 0.37 km) concentrations ranged from less than 0.05 to 0.09 ppb. The present study, similar to other tropospheric calculations, found decresing levels of HNO_3 with altitude.

The heterogeneous loss frequency, which is a composite of dry and wet deposition, is taken from a study of sulfuric acid by Turco et al. (ref. 52). The characteristic lifetime for heterogeneous removal at the surface is 0.5 day, somewhat shorter than the 1.7 days for wet deposition suggested by Huebert and Lazrus (ref. 93). As noted by Huebert and Lazrus, there are several reasons the heterogeneous removal time is shorter than the average rain-fall frequency. The heterogeneous removal by dry deposition could be higher in areas with large anthropogenic sources. This would decrease the amount of HNO_3 that would have to be rained out. Also, the average rainfall could remove larger amounts of HNO_3 per event than is comonly believed. Furthermore, some NO_2 might be scavenged directly, which would reduce the amount of NO_x available for HNO_3 formation. It should also be noted that the heterogeneous removal frequency in this study incorporates both dry and wet deposition and that the characteristic time constant is larger than 1.7 days in the mid and upper troposphere. It has also been postulated that a step-function might be needed to correctly represent the heterogeneous removal of HNO_3 (ref. 93).

For this study, the nitric acid concentration at the lower boundary was fixed at 0.6 ppb. The calculated vertical profiles of HNO_3 decreased in concentration with altitude, in agreement with measurements over the continental United States (see fig. 20), but in disagreement with the measurements of rural air. The more refined treatment of the radiation field in this study increased

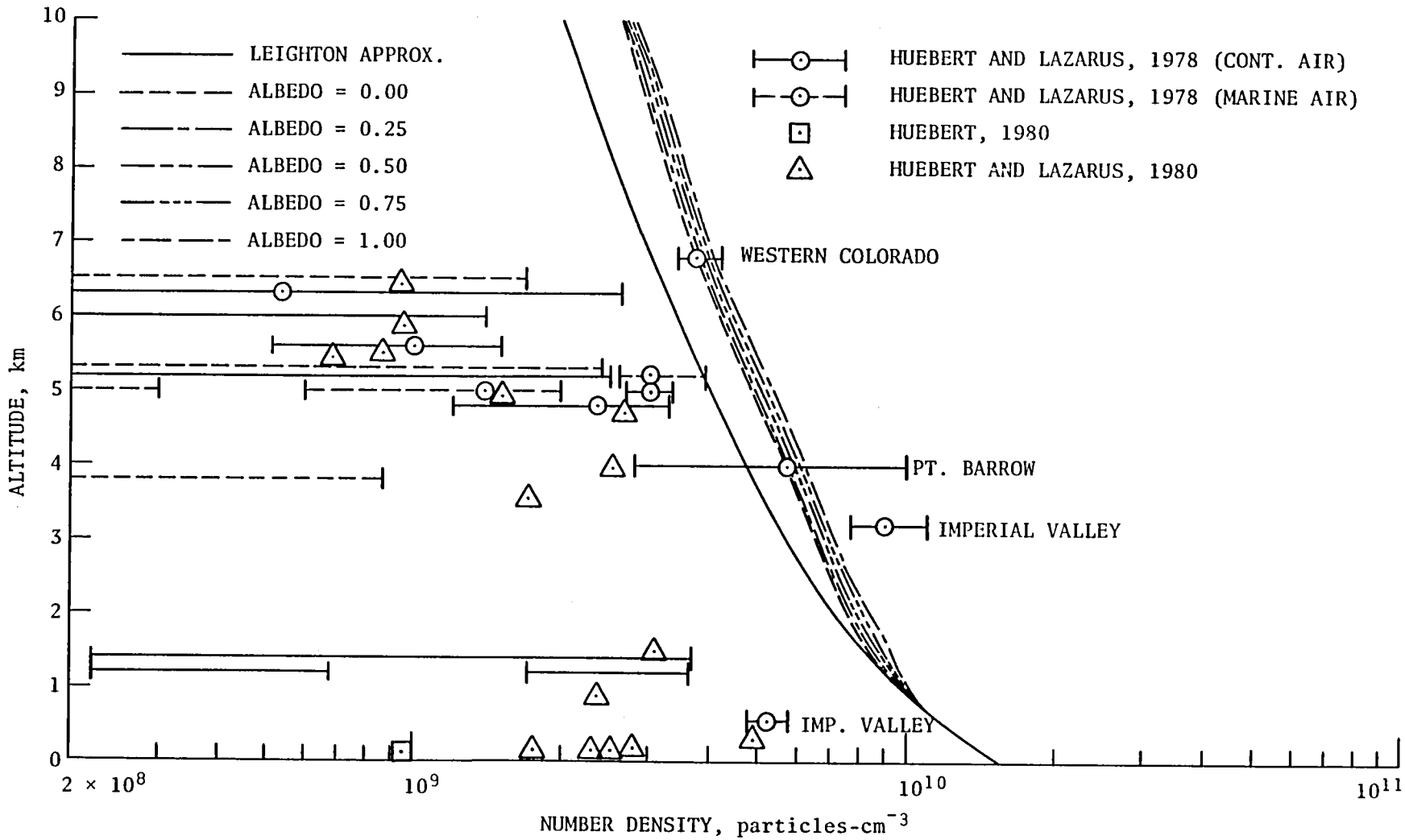

Figure 20. Vertical distributions of HNO_3 for the multiple scattering cases with various albedos and the Leighton approximation.

the level of HNO_3 by a factor of 1.3 at the tropopause, similar to NO_x. Due to the rapid interconversion of HNO_3 to NO_x, similar responses to the multiple scattering calculations are expected. Obviously, there is a great need for further research on the HNO_3-NO_x-O_3 cycles on a global scale.

Nitrous acid (HNO_2). -

Production	Destruction
K25: $NO + OH \rightarrow HNO_2$	J8 : $HNO_2 + h\nu \rightarrow OH + NO$
K33: $NO_2 + NO + H_2O \rightarrow 2HNO_2$	K40 : $HNO_2 + OH \rightarrow NO_2 + H_2O$
	K111: $HNO_2 + O_3 \rightarrow HNO_3 + O_2$

Nitrous acid (HNO_2) is formed chemically by two reactions and destroyed by three. The primary mechanism for production of HNO_2 is the reaction of NO with OH in the presence of a third body M (reaction 25). This reaction is five to seven orders of magnitude larger than the secondary reaction path of NO_2 combining with NO and H_2O (reaction 33) (see table 15). There are also indications that HNO_2 is emitted anthropogenically in automobile exhaust and in effluents from industral and residential chimneys (ref. 96); the magnitude of the anthropogenic emissions is very uncertain, however.

Chemically, destruction of nitrous acid occurs primarily by photolysis (J8). About 99 percent of all HNO_2 is destroyed in this manner. Roughly one percent at the surface is lost as a result of HNO_2 reacting with OH (reaction 40). At the tropopause this reaction is responsible for approximatly 0.5 percent of all HNO_2 loss. The reaction of HNO_2 with O_3 (reaction 115) constitutes a very minor sink for nitrous acid with less than 0.1 percent of all HNO_2 molecules destroyed in this manner. The lifetime of HNO_2 based on the photochemistry described above in about 0.5 hour. Nitrous acid is highly water soluble and should, therefore, be subject to heterogeneous removal by rainout, which would further decrease its lifetime.

Table 15. Production and destruction terms of $HNO_2^{\cdot}$ and percent of total production and destruction.

Production Rate (molecules-cm^{-3}-s^{-1}) and Percent of Total Production

Altitude, km	K25	%	K33	%	Total	%
10	3.031 E-2	100.00	1.053 E-5	-	3.031 E-2	100.00
5	5.661 E-2	100.00	7.088 E-4	-	5.661 E-2	100.00
0	1.545 E-3	100.00	4.268 E-2	-	1.545 E-3	100.00

Destruction Frequency (s^{-1}) and Percent of Total Destruction

Altitude, km	J8	%	K40	%	K111	%	Total	%
10	5.742 E-4	99.44	2.738 E-6	0.47	4.998 E-7	0.09	5.774 E-4	100.00
5	5.424 E-4	99.19	4.003 E-6	0.73	4.454 E-7	0.08	5.648 E-4	100.00
0	4.838 E-4	98.88	5.084 E-6	1.04	3.750 E-7	0.08	4.893 E-4	100.00

The first tropospheric measurements of HNO_2 were made by Nash in southern England using a wet chemistry technique (ref. 97). The levels of HNO_2 measured by Nash ranged from 0.4 to 11 ppb. Subsequent measurements of nitrous acid by Platt and Perner (refs. 85 and 96) yielded much lower values. These studies (refs. 85 and 96) used a differential optical absorption technique where the sensitivity of the apparatus is a function of prevailing visibility: i.e., in clear, unpolluted air, lower levels of HNO_2 can be detected than during episodes of pollution. The studies by Perner and Platt report on measurements of nitrous acid at three different locations in Europe. The levels of HNO_2 at the moderate-to-heavy polluted site at Jülich, West Germany were generally less than 0.1 ppb, although values as high as 0.8 ppb were observed just prior to sunrise before the initiation of photolytic decomposition. At Deuselbach in the German mountains, the level of HNO_2 was found to be always below the detection limit, which ranged from 0.02 to 0.13 ppb. At the Loop Head site on the Irish west coast, nitrous acid was also always below the detection limit, which varied between 0.003 and 0.13 ppb. Due to the much cleaner air at the Loop Head site, the sensitivity was much higher.

The detection limit of the differential optical absorption technique is a strong function of prevailing visibility. The concentrations of HNO_2 calculated in this study are generally about an order of magnitude lower than the lowest measurements at Loop Head (see fig. 21). It should be remembered, however, that the concentration of nitrous acid never reeached the detection limit, which on occasion was as low as 3 ppt. Hence, the only thing that can be concluded with any certainty is that during pristine conditions 3 ppt is an upper limit of HNO_2 concentration and the existence of considerably lower levels cannot be ruled out. When the more detailed radiation code is coupled into the photochemical calculations, the vertical profiles of HNO_2 are enhanced by factors ranging from 1.2 to 1.5 at the surface, depending on albedo, to factors of 1.35 to 1.75 at the tropopause, again as a function of albedo. The largest enhancement occurs for the case with an albedo of 0.00 and smallest for an albedo of 1.00.

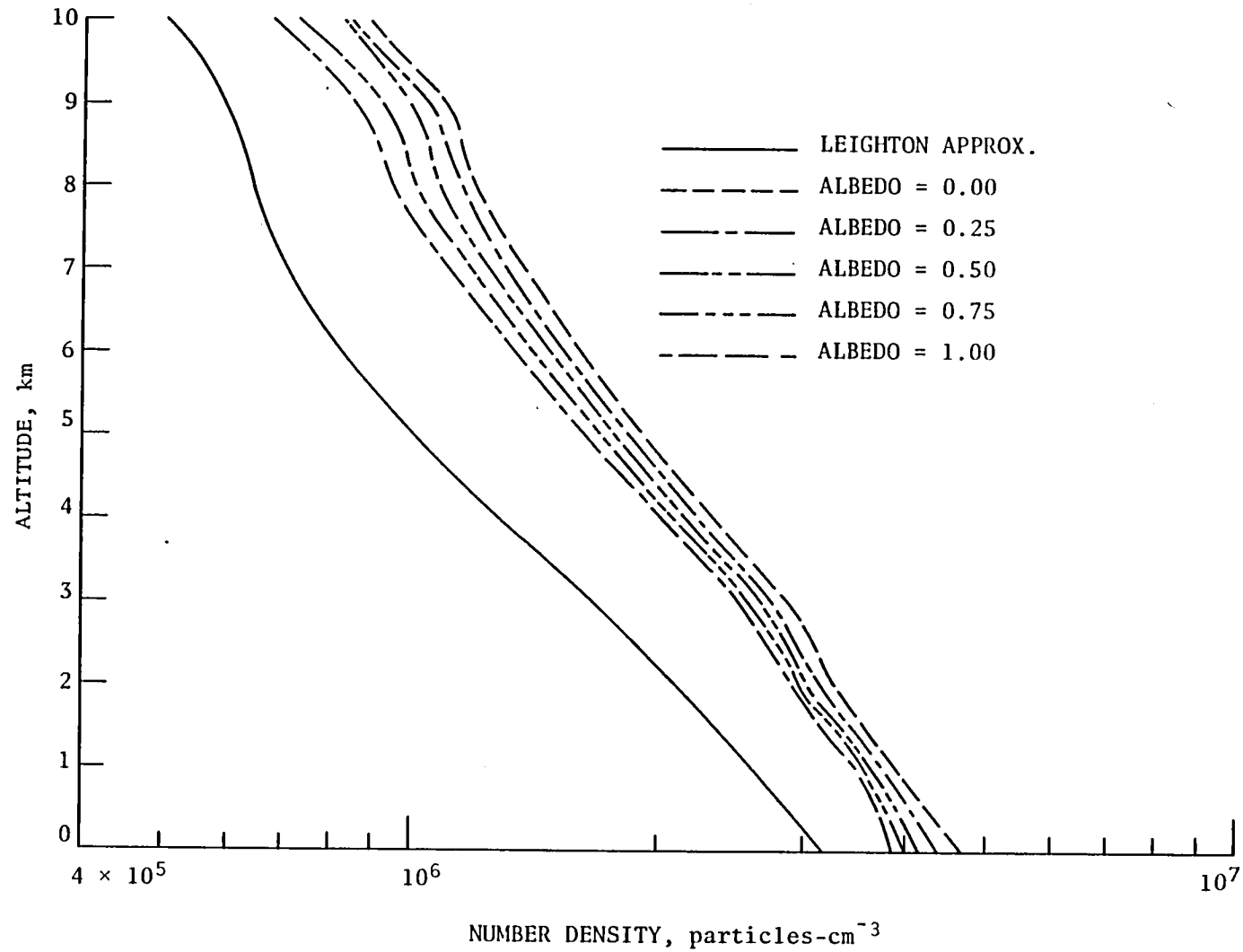

Figure 21. Vertical distributions of HNO_2 for the multiple scattering cases with various albedos and the Leighton approximation.

This is contrary to the behavior of many other tropospheric trace gases. The enhanced levels of NO and OH resulting from the multiple scattering calculations produce larger amounts of HNO_2 than does the Leighton approximation. Destruction by photolysis is also affected by multiple scattering; the relative amounts can be seen in table 8. From this table it can be seen that the photolytic frequency for HNO_2 decomposition varies strongly as a function of albedo. For an albedo of 1.00, the ratio of J_{ms}/J_L is greater than three, while the ratio is slightly less than 1 for an albedo of 0.00. Consequently, the enhanced levels of HNO_2 due to reaction 25 are readjusted downward by photolysis in greater amounts for the high albedo values than for the low.

Hydrazine (N_2H_4). -

Production	Destruction
K55: $NH_2 + NH_2 \rightarrow N_2H_4$	K42: $N_2H_4 + H \rightarrow N_2H_3 + H_2$
K44: $N_2H_3 + N_2H_3 \rightarrow N_2H_4 + N_2H_2$	

Hydrazine (N_2H_4) is a very stable compound that is formed primarily when the amino radical (NH_2) reacts with itself (reaction 55). The secondary source of hydrazine (N_2H_3) reacting with itself (reaction 44) is between 10 to 15 orders of magnitude smaller (see table 16). Loss of N_2H_4 occurs when it reacts with the hydrogen atom to form N_2H_3 and H_2 (reaction 42). The chemical lifetime of hydrazine based on the chemistry above is extremely long: 7×10^5 years. It is very likely that hydrazine is involved in additional, hitherto unidentified chemistry. Furthermore, in all likelihood, hydrazine is subject to rainout similar to NH_3 (ref. 11) and NH_2 (ref. 21). No atmospheric measurements exist of hydrazine, so boundary conditions have to be asssigned somewhat arbitrarily. A lower boundary condition of a few parts per trillion (ppt) was adopted with a condition of zero flux at the tropopause with the resulting vertical profiles shown in figure 22. The vertical profiles of N_2H_4 that have undergone the more detailed treatment of the radiative transfer equation are, in general, enhanced two to three times compared to the Leighton approximation.

Table 16. Production and destruction terms of N_2H_4 and percent of total production and destruction.

Production Rate (molecules-cm^{-3}-s^{-1}) and Percent of Total Production

Altitude, km	K55	%	K44	%	Total	%
10	1.817 E-0	100.00	6.617 E-10	-	1.817 E-0	100.00
5	1.731 E-1	100.00	1.393 E-9	-	1.731 E-1	100.00
0	1.796 E-2	100.00	3.901 E-13	-	1.796 E-2	100.00

Destruction Frequency (s^{-1}) and Percent of Total Destruction

Altitude, km	K42	%
10	8.525 E-15	100.00
5	2.103 E-14	100.00
0	4.392 E-14	100.00

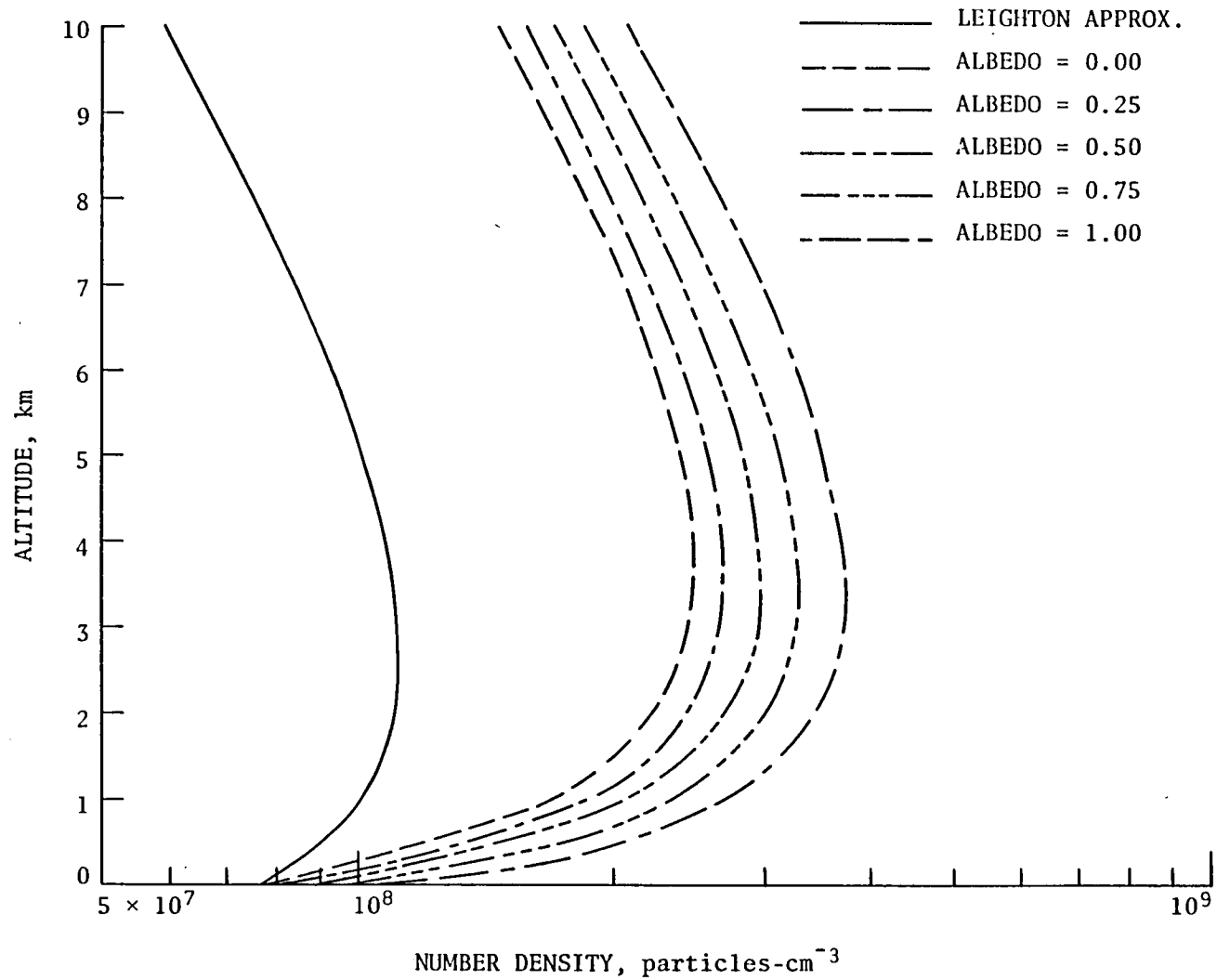

Figure 22. Vertical distributions of N_2H_4 for the multiple scattering cases with various albedos and the Leighton approximation.

This occurs because the amino radical (NH_2) is approximately doubled, and when multiplied by itself yields four times as much N_2H_4. Atomic hydrogen (H), which is involved in the destruction, is also increased as a result of including multiple scattering, and the profiles of hydrazine are adjusted accordingly.

Nitrogen trioxide (NO_3). -

Production		Destruction	
K28 :	$NO_2 + O_3 \rightarrow NO_3 + O_2$	J4 :	$NO_3 + h\nu \rightarrow NO_2 + O$
K35 :	$N_2O_5 \rightarrow NO_3 + NO_2$	K32 :	$NO_3 + NO \rightarrow 2NO_2$
K26 :	$HNO_3 + OH \rightarrow NO_3 + H_2O$	J5 :	$NO_3 + h\nu \rightarrow NO + O_2$
J6 :	$N_2O_5 + h\nu \rightarrow NO_3 + NO_2$	K30 :	$NO_3 + NO_2 \rightarrow N_2O_5$
K110:	$HNO_3 + O \rightarrow NO_3 + OH$	K31 :	$NO_3 + NO_2 \rightarrow NO + NO_2 + O_2$
		K113:	$NO_3 + H_2O \rightarrow HNO_3 + O_2$

Nitrogen trioxide is formed by five chemical reactions and destroyed by six. The primary path for NO_3 production is the oxidation of nitrogen dioxide by ozone (reaction 28). At the surface almost 55 percent of all NO_3 production occurs via this path (see table 17). In the midtroposphere nearly 75 percent of NO_3 is formed by reaction 28, and at the tropopause almost 50 percent by this reaction. Reaction 35 offers a secondary path to NO_3 production, providing over 38 percent at the surface, almost 11 percent at 5 km, and 28 percent at the tropopause. The reaction of nitric acid with hydroxyl accounts for NO_3 production in amounts varying from 6.8 percent at the surface to 17.7 percent at the tropopause. Photolysis of dinitrogen pentoxide (N_2O_5) produces about 0.01 percent of the NO_3 at the surface, increasing to approximately 4.5 percent at the tropopause. The reaction of HNO_3 with ground-state oxygen, $O(^3p)$ (reaction 110), can be neglected as an NO_3 source.

Table 17. Production and destruction terms of NO_3 and percent of total production and destruction.

Production Rate (molecules-cm^{-3}-s^{-1}) and Percent of Total Production

Altitude, km	K28	%	K35	%	K26	%	J6	%	K110	%	Total	%
10	9.281 E-1	49.74	5.234 E-1	28.05	3.296 E-1	17.66	8.466 E-0	4.54	1.163 E-2	-	1.866 E-2	100.00
5	7.921 E-2	74.21	1.170 E-2	10.96	1.536 E-2	14.39	4.617 E-0	0.44	2.001 E-4	-	1.067 E-3	100.00
0	8.417 E-3	54.56	5.958 E-3	38.62	1.050 E-3	6.81	1.943 E-0	0.01	3.924 E-4	-	1.543 E-4	100.00

Destruction Frequency (s^{-1}) and Percent of Total Destruction

Altitude, km	J4	%	K32	%	J5	%	K30	%	K31	%	K113	%	Total	%
10	9.107 E-3	72.65	1.013 E-3	8.08	2.246 E-3	17.92	1.686 E-4	1.35	1.157 E-7	-	5.750 E-11	-	1.253 E-2	100.00
5	8.932 E-3	69.56	1.292 E-3	10.06	2.209 E-3	17.20	4.085 E-4	3.18	4.949 E-7	-	1.058 E-9	-	1.284 E-2	100.00
0	8.211 E-3	55.76	2.775 E-3	18.85	2.041 E-3	13.86	1.695 E-3	11.51	3.191 E-6	0.02	1.150 E-8	-	1.473 E-2	100.00

Destruction of NO_3 occurs primarily as a result of two photolytic reactions, one leading to NO_2 and O (J4), the other to NO and O_2 (J5). At the surface these two photolytic processes destroy about 70 percent of all the NO_3 molecules, and at the tropopause more than 90 percent. The reaction of NO_3 with NO provides an appreciable sink with amounts varying from nearly 19 percent at the surface to 8 percent at the tropopause. The reaction of NO_3 with NO_2 accounts for 11.5 percent of the NO_3 loss at the surface, decreasing to slightly more than 1 percent at 10 km. Reaction 31 provides a minute sink (0.02 percent) at the surface, while reaction 113 can be neglected. The lifetime of nitrogen trioxide based on the chemistry desribed above is approximately one minute.

NO_3 has been measured in the troposphere at night in slightly polluted air in Colorado (ref. 98) and during twilight and at night on the west coast of Ireland in clean air (ref. 85). The measurements in Colorado were in the range from a few ppt to about 75 ppt depending on the background level of NO_2. The measurements of NO_3 at Loop Head, Ireland were always below the detection limit regardless of the level of NO_2. Most of the nitrogen trioxide concentrations at night were in the 2 to 14 ppt range. Two measurements taken just at sunrise had exceptionally low detection limits, 0.5 and 0.8 ppt, respectively. Despite this, NO_3 was not observed. It should be kept in mind that the nighttime chemistry differs radically from the daytime; therefore only the measurements during daylight hours can be considered truly representative of a photochemical system. As a consequence, only the 0.8 ppt and 0.5 ppt measurements have been transposed to figure 23 and compared to the model calculated NO_3 profiles. The surface level concentration of NO_3 based on photochemistry is about 0.2 ppt, decreasing to about 0.03 ppt at the tropopause. The clean air masurements by Platt and Perner (ref. 85) do not exclude these levels of NO_3. At the surface the profiles of the multiple scattering calculations are closely grouped together independent of albedo. The enhancement over the Leighton approximation is about a factor of 1.3. In the upper regions of the troposphere, the differences between the various profiles are more pronounced. Like HNO_3 the greatest enhancement was found for an albedo of 0.00 and the smallest increase for a = 1.00. This can be explained from the data in tables 4 and 5.

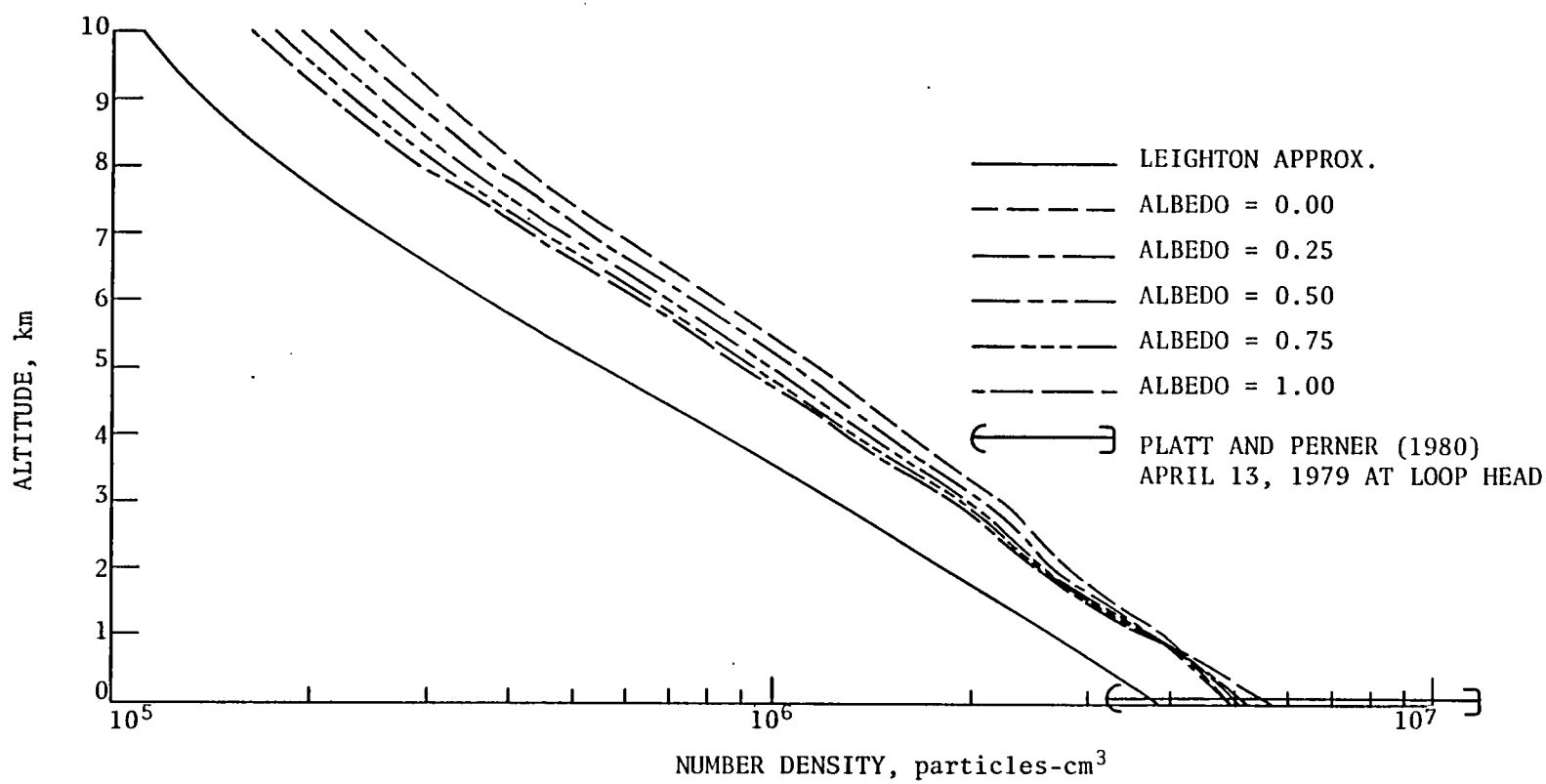

Figure 23. Vertical distributions of NO_3 for the multiple scattering cases with various albedos and the Leighton approximation.

Photolysis provides the largest destruction of NO_3, and the ratios of J_{ms}/J_L at the tropopause for an albedo of 0.00 are about 1.4; for an albedo of 1.00 the ratios of J_{ms}/J_L from tables 4 and 5 are approximately 2.6 at the tropopause. Hence, more NO_3 is photolyzed, and therefore lost, when the albedo is high.

Amino radical (NH_2). -

Production	Destruction
K48: $NH_3 + OH \rightarrow NH_2 + H_2O$	K54: $NH_2 + NO \rightarrow N_2 + H_2O$
K47: $NH_3 + O(^1D) \rightarrow NH_2 + OH$	K53: $NH_2 + H_2 \rightarrow NH_3 + H$
K46: $NH_3 + O \rightarrow NH_2 + OH$	K55: $NH_2 + NH_2 \rightarrow N_2H_4$
K49: $NH_3 + H \rightarrow NH_2 + H_2$	K52: $NH_2 + OH \rightarrow NH_3 + O$
K45: $N_2H_3 + H \rightarrow 2NH_2$	K50: $NH_2 + O \rightarrow HNO + H$
	K51: $NH_2 + O \rightarrow NH + OH$

The amino radical (NH_2) is produced by five tropospheric reactions and destroyed by six. Virtually all amino radicals that are present in the troposphere are formed as a result of ammonia reacting with hydroxyl (reaction 48) (see table 18). The only other production term yielding a noticeable contribution is the reaction of ammonia with excited oxygen, reaction 47, which provides for a minute 0.01 percent of the total NH_2 production. The remaining 3′ terms producing NH_2 are between 7 and 17 orders of magnitude smaller than the primary production term. The loss of NH_2 occurs primarily as a result of the reaction of NH_2 with NO (reaction 54) and with H_2 (reaction 53). At the surface more than 81 percent of all NH_2 molecules are destroyed due to reaction 54. About 15.5 percent are lost as a result of reaction 53, while 3.25 percent are destroyed when NH_2 reacts with itself (reaction 55). At higher altitudes, the reaction with molecular hydrogen (reaction 53) becomes the predominant loss mechanism, and the reaction with nitric oxide (reaction 54) becomes secondary. Since H_2 is well-mixed in the troposphere, its relative abundance at higher

Table 18. Production and destruction terms of NH_2 and percent of total production and destruction.

Production Rate (molecules-cm^{-3}-s^{-1}) and Percent of Total Production

Altitude, km	K48	%	K47	%	K46	%	K49	%	K45	%	Total	%
10	3.744 E-2	99.99	3.938 E-2	0.01	2.247 E-5	-	8.305 E-8	-	3.330 E-12	-	3.744 E-2	100.00
5	1.619 E-3	100.00	2.967 E-2	-	9.721 E-4	-	1.957 E-7	-	6.033 E-13	-	1.619 E-3	100.00
0	1.105 E-4	100.00	4.055 E-2	-	5.732 E-3	-	9.102 E-7	-	3.931 E-13	-	1.105 E-4	100.00

Destruction Frequency (s^{-1}) and Percent of Total Destruction

Altitude, km	K54	%	K53	%	K55	%	K52	%	K50	%	K51	%	Total	%
10	2.444 E-3	36.10	4.300 E-3	63.51	2.696 E-5	0.39	1.302 E-7	-	3.506 E-8	-	3.506 E-8	-	6.771 E-3	100.00
5	3.119 E-3	28.74	7.650 E-3	70.49	8.319 E-5	0.77	1.906 E-7	-	1.266 E-8	-	1.266 E-8	-	1.085 E-2	100.00
0	6.699 E-3	81.28	1.275 E-3	15.47	2.682 E-4	3.25	2.421 E-7	-	4.615 E-9	-	4.615 E-9	-	8.242 E-3	100.00

altitudes is greater than NO, which decrease fairly rapidly with altitude. Consequently, in the mid and upper troposphere, reaction 53 provides approximately two-thirds of the total NH_2 destruction, while one-third is due to reaction 54. The reaction of NH_2 with itself (reaction 55) accounts for less than 1 percent of the total NH_2 loss in the upper troposphere. The remaining three loss terms are between four to six orders of magnitude smaller than the primary loss mechanisms. The photochemical lifetime of NH_2 based on the kinetic scheme above, is on the order of a couple of minutes. The vertical profiles of NH_2 (see fig. 24) decrease about an order of magnitude from the surface to the tropopause. The choice of surface albedo significantly affects the NH_2 profiles in the lower troposphere. Number density enhancements, due to inclusion of multiple scattering, compared to the Leighton approximation range from 1.4 for an albedo of 0.00 to 4.2 when the albedo is 1.00. In the mid and upper troposphere, the choice of albedo becomes less significant and the vertical profiles, due to multiple scattering, are closely grouped together at approximately twice the value of the Leighton approximation. No atmospheric measurements of NH_2 are available. It has been postulated that NH_2 is lost heterogeneously, but this has not been supported by loss rates (ref. 21).

Dinitrogen pentoxide (N_2O_5). -

Production:	Destruction
K30: $NO_2 + NO_3 \rightarrow N_2O_5$	K35: $N_2O_5 \rightarrow NO_3 + NO_2$
	K34: $N_2O_5 + H_2O \rightarrow 2HNO_3$
	J6 : $N_2O_5 + h\nu \rightarrow NO_2 + NO_3$

The only atmospheric reaction known to produce dinitrogen pentoxide (N_2O_5) is the reaction of nitrogen dioxide with nitrogen trioxide (reaction 30). Losses of N_2O_5 include decomposition (K35), reaction of N_2O_5 with H_2O (reaction 34), and photolysis (J6). The decomposition is strongly temperature dependent and manifests itself in a very rapdily decreasing loss frequency with altitude

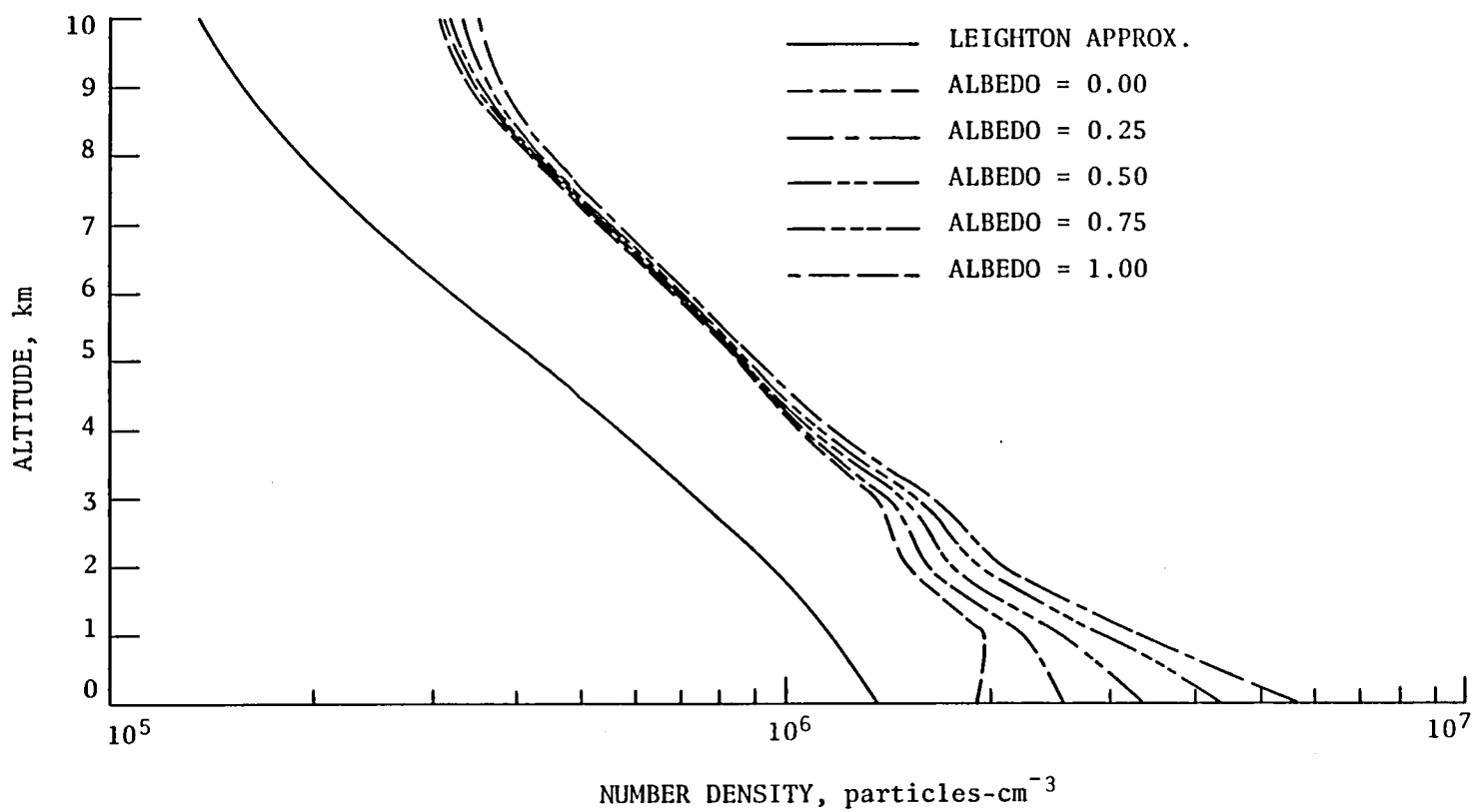

Figure 24. Vertical distributions of NH_2 for the multiple scattering cases with various albedos and the Leighton approximation.

(see table 19). At the surface, more than 92 percent of all N_2O_5 is destroyed by decomposition, in the midtroposphere about 54 percent, and at the tropopause less than 3 percent. The reaction of water vapor with N_2O_5 (reaction 74) destroys less than 8 percent at the surface, about 44 percent at 5 km, and almost 50 percent at the tropopause. Photolysis of N_2O_5 (J6) destroys only a minute 0.03 percent at the surface, about 2 percent in the midtroposphere, and more than 47 percent at 10 km. Hence, the loss mechanisms of N_2O_5 are very altitude dependent. At the surface, the overwhelming path of N_2O_5 destruction is thermal decomposition. In the midtroposphere both decomposition and the reaction of H_2O with N_2O_5 (reaction 34) are important. At the tropopause, it is photolysis (J6) and reaction 34 that dominate.

The lifetime of N_2O_5 is about 15 s; thus, the PCE formulation is used. The vertical profiles generated by the model are shown in figure 25. In general, the number density of dinitrogen pentoxide increases with altitude, except at the tropopause. In the lower regions of the troposphere, the vertical profiles, calculated with the Anderson-Meier code, are closely grouped together independent of the choice of surface albedo. This is not surprising since the primary loss mechanism in the low troposphere is decomposition, which is a function of atmospheric temperature. Above 5 km, there are noticeable differences in the vertical profiles as a function of albedo. In fact, the number density of N_2O_5 calculated using the Leighton approximation to describe the radiation field is greater than the number densities for the multiple scattering calculations with albedos of 1.00 and 0.75. The number densitites at the tropopause for albedos in the range of 0.00 to 0.50 are greater than the Leighton approximation; with the calculation using a 0.00 albedo, they are enhanced by a factor of 1.5. The reason some profiles are greater than the Leighton approximation and others are smaller can be understood by inspection of tables 6 and 19. The ratio of the photodissociation frequencies J_{ms}/J_L is doubled at the tropopause for an albedo of 1.00 (see table 6). As indicated in table 19, photolysis becomes increasingly important with altitude, and at the tropopause almost half of all N_2O_5 molecules are destroyed this way. As a result, the vertical profiles for the various albedos are more spread out in

Table 19. Production and destruction terms of N_2O_5 and percent of total production and destruction.

Production Rate (molecules-cm^{-3}-s^{-1}) and Percent of Total Production

Altitude, km	K30	%
10	1.883 E-1	100.00
5	2.234 E-2	100.00
0	6.455 E-3	100.00

Destruction Frequency (s^{-1}) and Percent of Total Destruction

Altitude, km	K35	%	K34	%	J6	%	Total	%
10	1.487 E-6	2.94	2.500 E-5	49.47	2.405 E-5	47.59	5.054 E-5	100.00
5	5.635 E-4	53.89	4.600 E-4	43.99	2.224 E-5	2.12	1.046 E-3	100.00
0	6.022 E-2	92.31	5.000 E-3	7.66	1.964 E-5	0.03	6.524 E-2	100.00

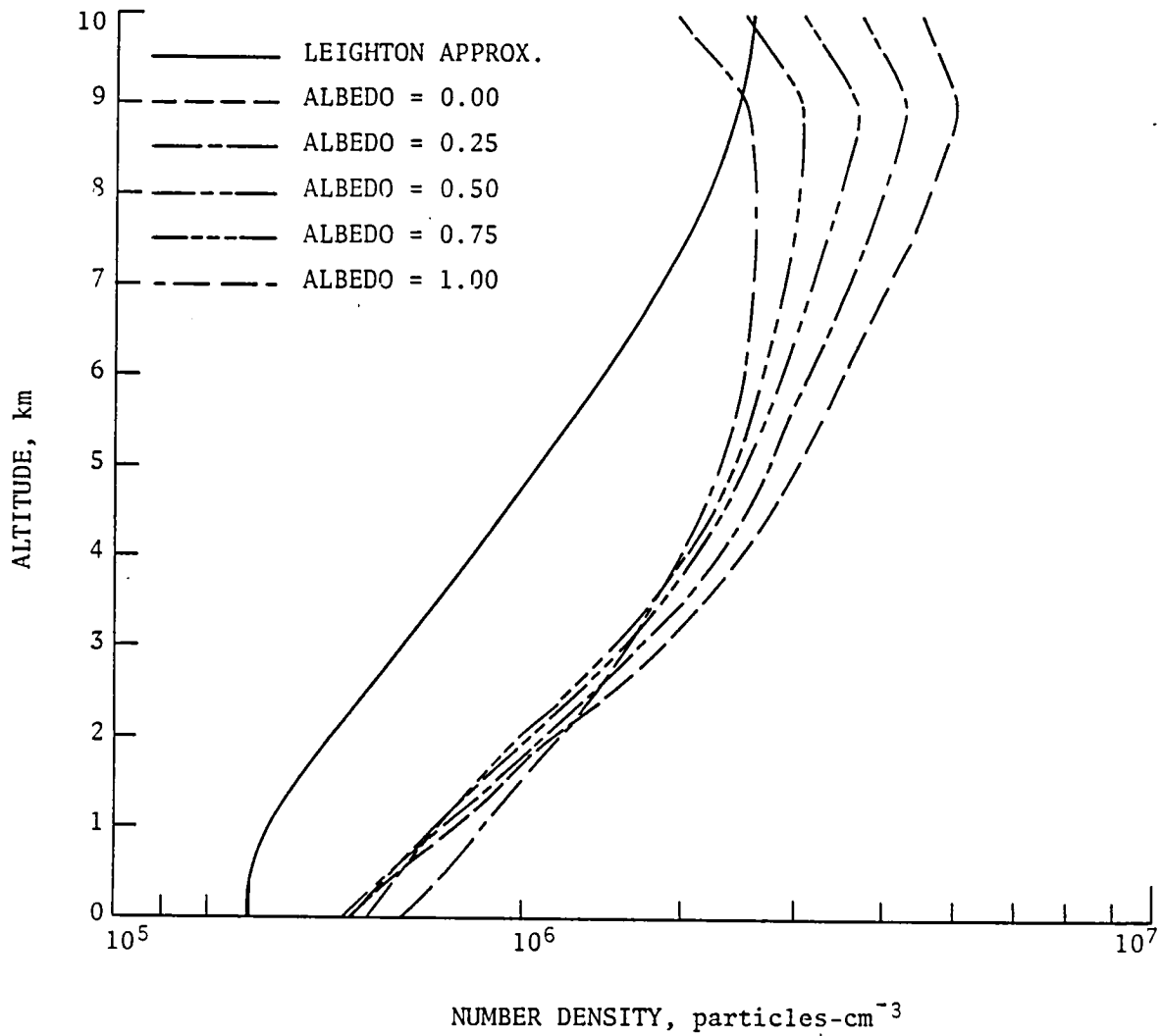

Figure 25. Vertical distributions of N_2O_5 for the multiple scattering cases with various albedos and the Leighton approximation.

the upper troposphere. No measurements of N_2O_5 to compare with the theoretical calculations have been made.

Imino radical (NH). -

Production	Destruction
K51: $NH_2 + O \rightarrow NH + OH$	K56: $NH + NO \rightarrow N_2 + O + H$

The imino radical (NH) is formed by the reaction of the amino radical (NH_2) with ground-state oxygen, $O(^3p)$ (see table 20). Some other reaction paths for the formation of NH have been proposed, but none has been supported by kinetic data (ref. 21). In particular, the reaction of NH with O_2 (reaction 57), which has a proposed rate constant of 6.0E-13, has not been included since that rate is probably several orders of magnitude too high. At that high a rate and with the large abundance of O_2 reaction 57 would, for example, dominate the chemical production of NO_x. For these reasons reaction 57 has been deleted from the chemical scheme.

Destruction of NH occurs as a result of the reaction of nitric oxide with the imino radical forming molecular nitrogen, ground-state oxygen, and atomic hydrogen (reaction 56). The lifetime of NH is about 10 minutes, hence the PCE formulation was used to calculate its vertical profile. The imino radical is greatly influenced by multiple scattering and choice of surface albedo. The number densisites at the surface are enhanced by a factor of 1.5 for albedo of 0.00 compared to the Leighton approximation; for an albedo of 1.00, the enhancement is a factor of about 14 (see fig. 26). Even at the tropopause, there are large differences between the profiles obtained with the Leighton approximation and those with the more refined multiple scattering calculations. There is almost a factor of 5 difference for an albedo of 0.00, and more than a factor of 5.5 difference when the albedo is 1.00. The vertical profiles of NH are strongly dependent on the profiles of NH_2 and $O(^3p)$ (see figs. 24 and 32, respectively). Both ground-state oxygen and the amino radical are enhanced when multiple scattering is introduced into the radiation calculations, and

Table 20. Production and destruction terms of NH and percent of total production and destruction.

Production Rate (molecules-cm^{-3}-s^{-1}) and Percent of Total Production

Altitude,km	K51	%
10	4.731 E-3	100.00
5	5.266 E-3	100.00
0	6.175 E-3	100.00

Destruction Frequency (s^{-1}) and Percent of Total Destruction

Altitude, km	K56	%
10	5.471 E-3	100.00
5	6.980 E-3	100.00
0	1.499 E-3	100.00

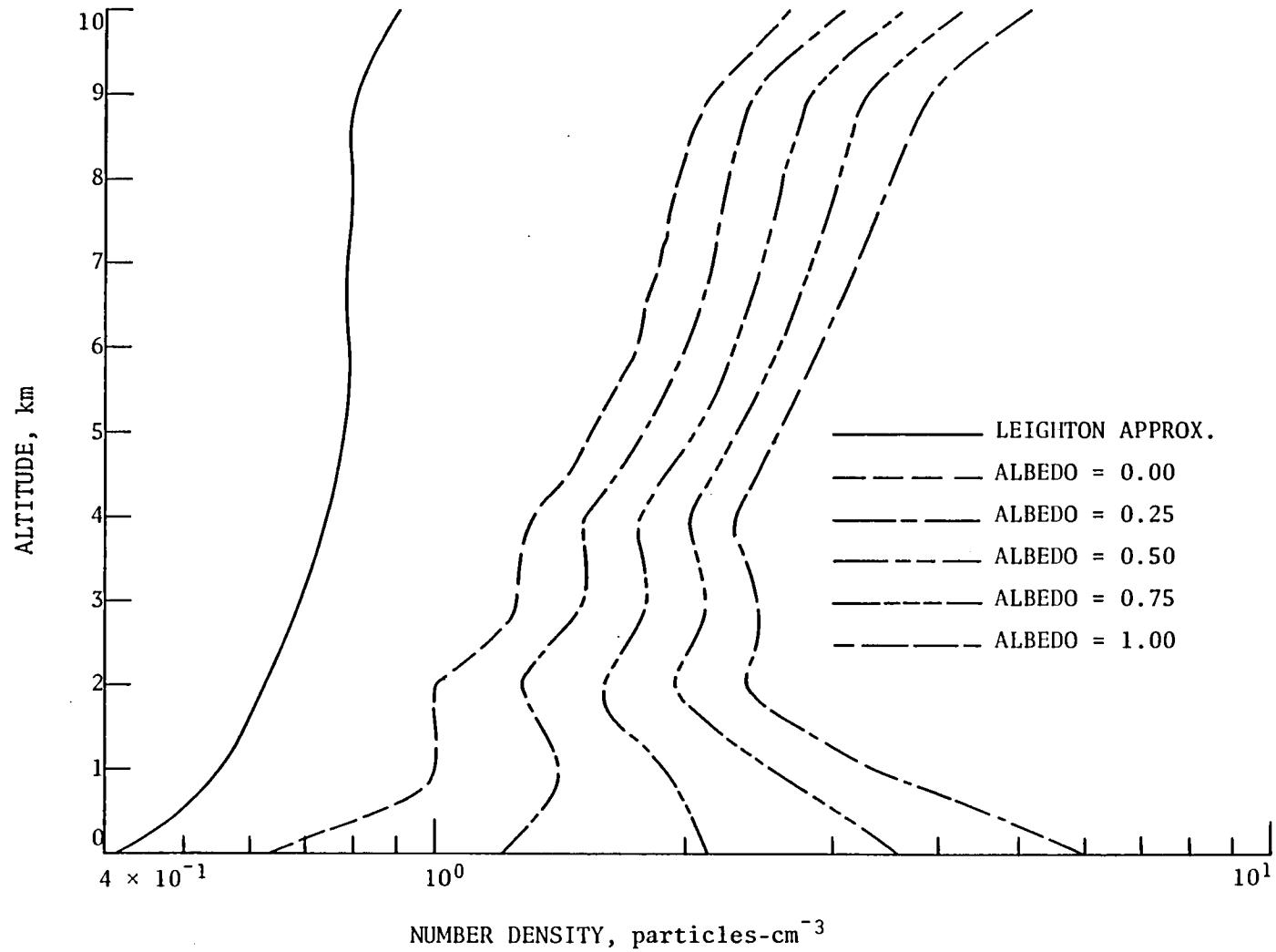

Figure 26. Vertical distributions of NH for the multiple scattering cases with various albedos and the Leighton approximation.

both compounds show large variations in the number densities close to the surface as a function of albedo. These variations are propagated into the calculation of the vertical profiles of NH.

Nitroxyl radical (HNO). -

Production	Destruction
K50: $NH_2 + O \rightarrow HNO + H$	K59: $HNO + O_2 \rightarrow NO + HO_2$
	K61: $HNO + H \rightarrow NO + H_2$
	K62: $HNO + HNO \rightarrow N_2O + H_2O$

The nitroxyl radical (HNO) is formed by the same reactants that produced NH, and at the same rate. Only the end products vary between reactions 50 and 51. Chemically, HNO is lost by three reactions, but the primary destruction path (reaction 59) totally deminates the loss mechanism of HNO. In fact, this reaction is anywhere from 13 to 16 orders of magnitude larger than the minor loss mechanisms (reactions 61 and 62) (see table 21). The lifetime of the nitroxyl radical based on the scheme above is about 10 s, well justifying the PCE assumption. The reaction of the nitroxyl radical with molecular oxygen is reportedly endothermic and should therefore occur very slowly in the atmosphere (ref. 21). The fact that this reaction deominates the destruction of HNO is due to the large abundance of molecular oxygen. The vertical profiles of HNO are very similar to the NH profiles (see fig. 27). In fact, if the horizontal scale is shifted approximately an order of magnitude, the HNO profiles form almost a perfect overlay to the NH profiles. Since both NH and HNO are formed by the same reactants and at identical rates, their vertical profiles should be nearly identical. At the tropopause, some small differences in the profiles of NH and HNO are noticeable. This is due to the loss terms. The nitroxyl radical is destroyed primarily when it combines with molecular oxygen, which has a constant mixing ratio. The imino radical, on the other hand, is lost when it reacts with nitric oxide, which does not have a constant mixing ratio, but rather decreases with altitude.

Table 21. Production and destruction terms of HNO and percent of total production and destruction.

Production Rate (molecules-cm^{-3}-s^{-1}) and Percent of Total Production

Altitude, km	K50	%
10	4.727 E-3	100.00
5	5.266 E-3	100.00
0	6.185 E-3	100.00

Destruction Frequency (s^{-1}) and Percent of Total Destruction

Altitude, km	K59	%	K61	%	K62	%	Total	%
10	3.775 E-2	100.00	9.250 E-15	-	9.968 E-16	-	3.775 E-2	100.00
5	6.715 E-2	100.00	1.159 E-14	-	6.244 E-15	-	6.715 E-2	100.00
0	1.119 E-1	100.00	1.428 E-14	-	4.400 E-16	-	1.119 E-1	100.00

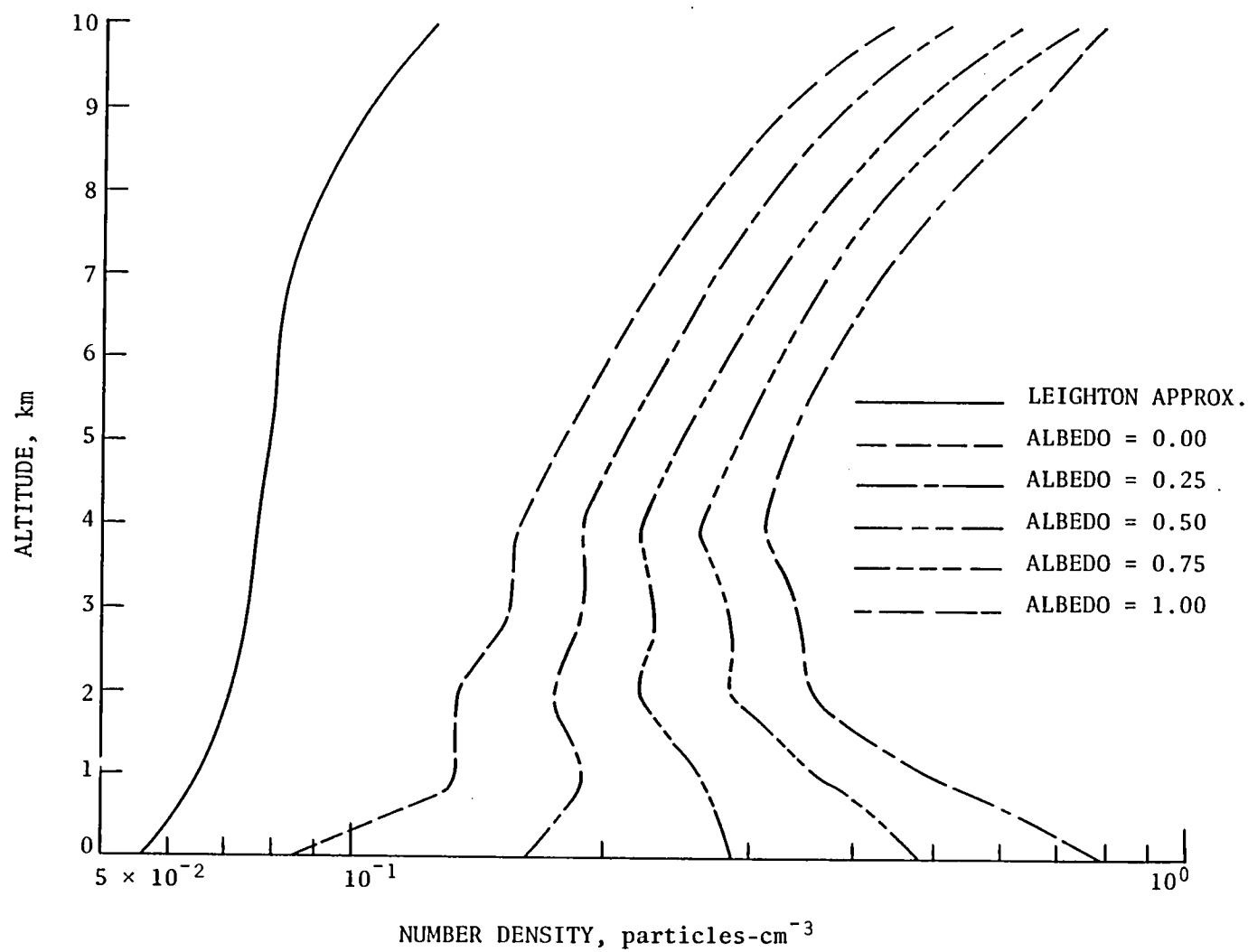

Figure 27. Vertical distributions of HNO for the multiple scattering cases with various albedos and the Leighton approximation.

Hydrazine derivative (N_2H_3). -

Production	Destruction
K42: $N_2H_4 + H \rightarrow N_2H_3 + H_2$	K45: $N_2H_3 + H \rightarrow 2NH_2$
	K44: $N_2H_3 + N_2H_3 \rightarrow N_2H_4 + N_2H_2$

In order to complete a very detailed ammonia package, two rather obscure hydrazine derivatives, N_2H_3 and N_2H_2, were included. The first compound (H_2H_3) is formed when hydrazine reacts with atomic hydrogen (reaction 42). Two loss terms are specified for N_2H_3. The reaction with H (reaction 45) dominates near the surface while the reaaction of N_2H_3 with itself (reaction 44) is the predominant loss in the upper troposphere (see table 22). The calculated lifetime for N_2H_3 is very long, about 1.5×10^3 years. It is clear that unidentified chemical processes, and possibly heterogeneous mechanisms as well, must affect N_2H_3. The vertical profiles of N_2H_3 are very similar to the hydrazine profiles (see fig. 28), and the same reasoning for the variations in the profiles applies here. The lower boundary condition was chosen in much the same way as was the lower boundary condition for N_2H_4. At the upper boundary, a condition of zero flux was used.

Hydrazine derivative (N_2H_2). -

Production
K44: $N_2H_3 + N_2H_3 \rightarrow N_2H_2 + N_2H_4$

The second hydrazine derivative (H_2H_2) is formed when N_2H_3 reacts with itself yielding hydrazine in addition to N_2H_2 (reaction 44) (see table 23). No destruction mechanisms have been postulated for N_2H_2, although clearly some must exist. Since N_2H_2 only has a production term, its atmospheric abundance in the troposphere will basically be a constant mixing ratio with the possible exception near the lower boundary, where the boundary condition must again be

Table 22. Production and destruction terms of N_2H_3 and percent of total production and destruction.

Production Rate (molecules-cm^{-3}-s^{-1}) and Percent of Total Production

Altitude, km	K42	%
10	5.038 E-6	100.00
5	2.110 E-6	100.00
0	3.360 E-6	100.00

Destruction Frequency (s^{-1}) and Percent of Total Destruction

Altitude, km	K45	%	K44	%	Total	%
10	1.114 E-11	2.72	3.985 E-10	97.28	4.096 E-10	100.00
5	1.391 E-11	2.35	5.782 E-10	97.65	5.921 E-10	100.00
0	1.713 E-11	84.84	3.060 E-12	15.16	2.019 E-11	100.00

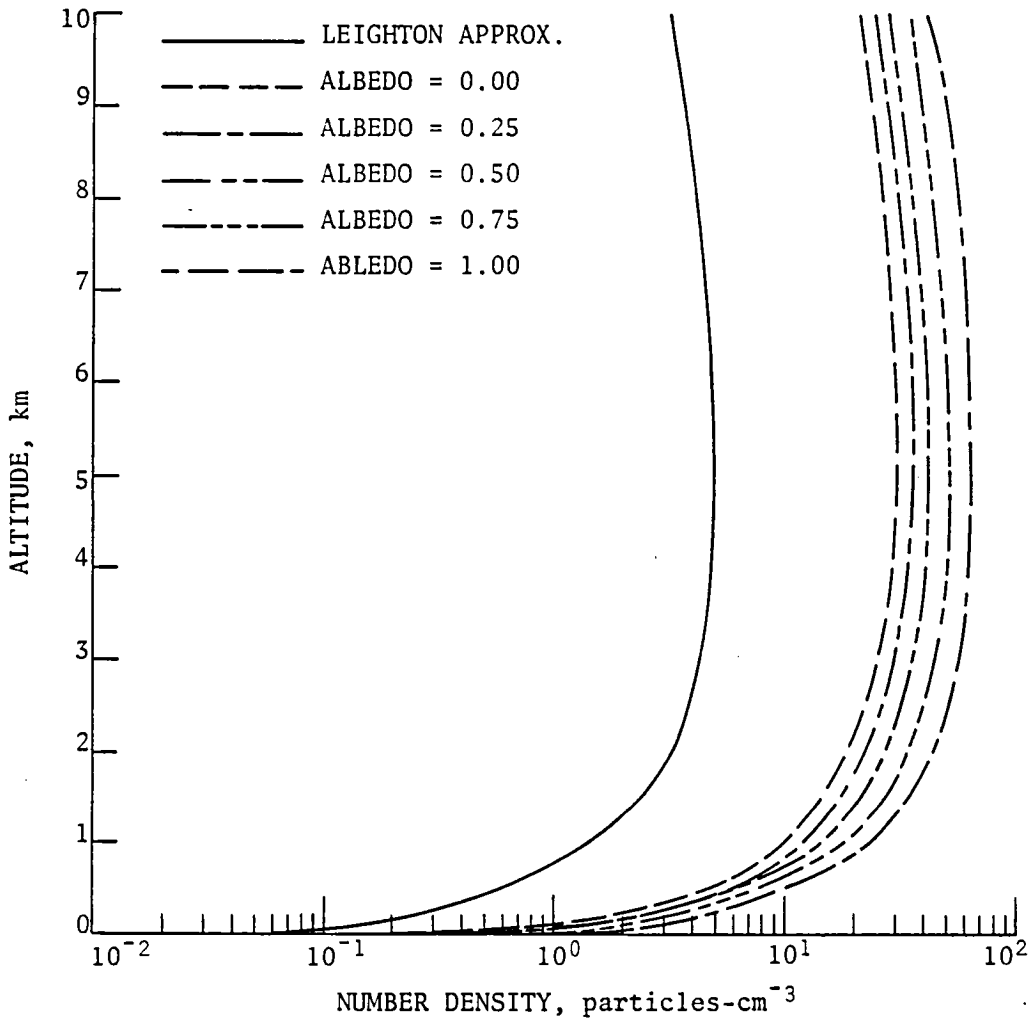

Figure 28. Vertical distributions of N_2H_3 for the multiple scattering cases with various albedos and the Leighton approximation.

Table 23. Production terms for N_2H_2 and percent of total production.

Altitude, km	K44	%
10	6.617 E-10	100.00
5	1.393 E-9	100.00
0	3.902 E-12	100.00

assigned somewhat arbitrarily. The main advantage of including N_2H_2, therefore, is that it can be used as a tracer to ensure that the numerical techniques of the problem are operating correctly. The model generated profiles of N_2H_2 are given in figure 29.

Future perturbations to the nitrogen budget. - Most of the concern over future perturbations to nitrogen species has centered around two issues: (1) the global increase in the usage of nitrogen based fertilizers and subsequent nitrification, denitrification, and volatilzation gas production, and (2) the increasing industrial output of NO_x. Biological systems are unable to use nitrogen species with a double bond, e.g. N_2, as nutrients. Instead, single-bonded nitrogen species such as ammonia (NH_3), ammonium (NH_4^+), nitrate (NO_3^-), and nitrite (NO_2^-) are applied to agricultural fields as fertilizers. The process of forming single-bonded nitrogen species is known as nitrogen fixation. The opposite of this, i.e., production of double-bonded nitrogen species in the soil by bacteria and other microorganisms, is called denitrification. The increase in crop yields during the last few decades as a result of advances in agricultural technology has been impressive. Some of these techniques include irrigation, selection of higher yield strains, application of herbicides and insecticides, and last, but not least, the increased application of fertilizers. The adverse effects of indiscriminate use of pesticides (e.g., DDT and Kepone) are well documented, but only recently have the effects of large and widespread use of fertilizers been considered.

In 1959, the amount of nitrogen fixation due to fertilizer use was 3.5 million tons per year (3.5 Mt/yr). In 1974, this had increased to 40 Mt/yr and has been projected to reach 200 Mt/yr by the year 2000 (ref. 70). The natural fixation of nitrogen in the soil which occurs due to activities of micro-organisms has been estimated to be 44 Mt/yr in one study (ref. 99) and 175 Mt/yr in another (ref. 100). The marine biosphere is thought to fix 10 Mt/yr (ref. 101). Regardless of which estimate of nitrogen fixation in the land biomass is used, by the turn of the century anthropogenic input will exceed the natural cycle. The effects of this massive fertilizer application are at least two-

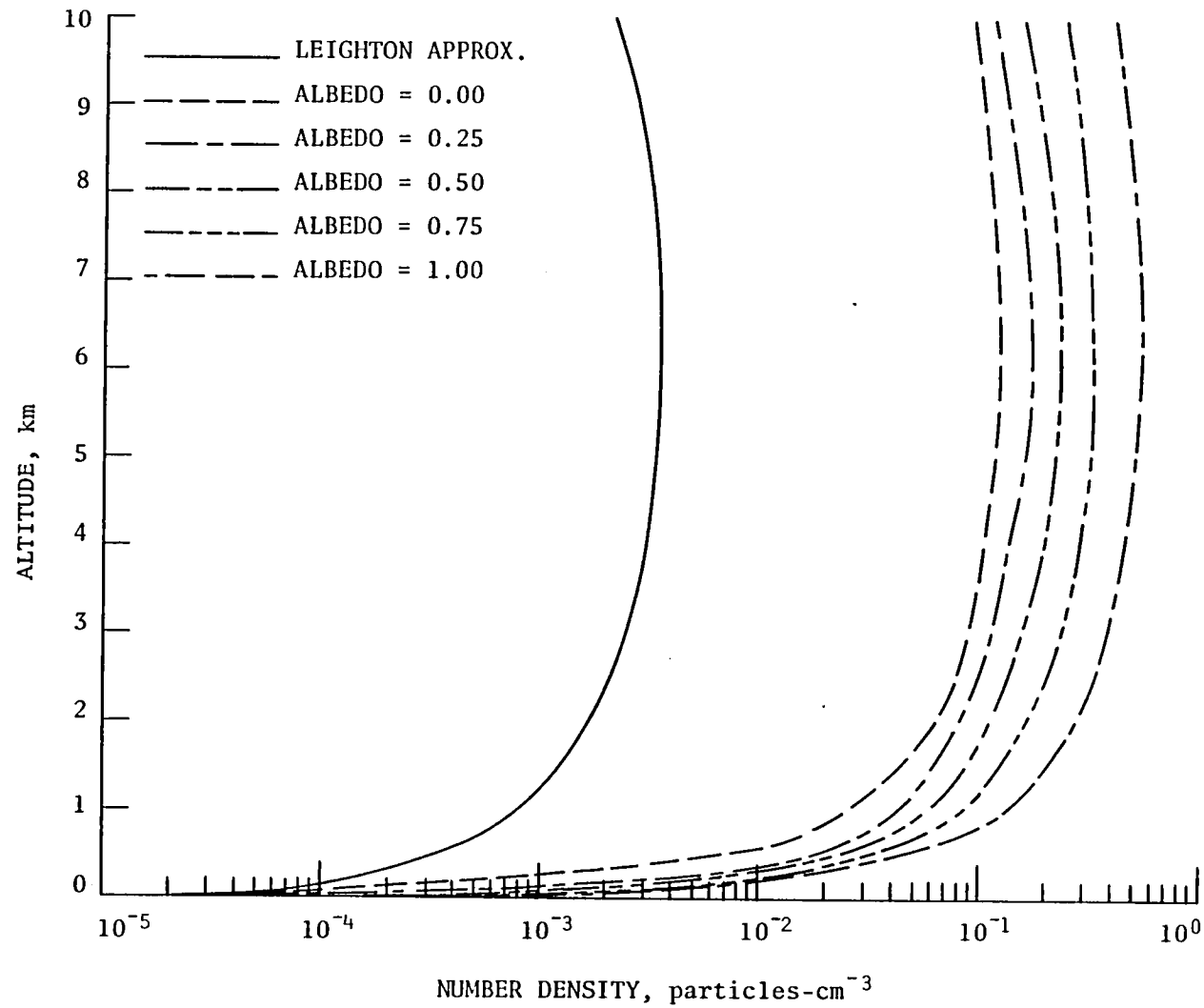

Figure 29. Vertical distributions of N_2H_2 for the multiple scattering cases with various albedos and the Leighton approximation.

fold. Large amounts of the ammonium nitrate fertilizers that are applied are volatilized rapidly and diffuse upward. During extreme conditions, as much as 50 percent of the fertilizer is emitted into the troposphere in gaseous form, and, thus, from an agricultural point of view this portion of the fertilizer is useless (ref. 63). The tropospheric effects of ammonia fluxes have recently been discussed by Levine et al. (refs. 11, 102). The second effect is that the large levels of fertilizer input will increase the rate of bacterial denitrification, which causes larger amounts of nitrous oxide (N_2O) to be produced and emitted into the atmosphere. This species diffuses upward into the stratosphere where it reacts with the excited oxygen atom, $O(^1D)$, forming two nitric oxide molecules. This initiates a catalytic cycle of ozone destruction in the stratosphere. Naturally, any large-scale perturbation of the stratosphere would propagate into the troposphere.

The anthropogenic emissions of NO_x are currently about 20 Mt/hr (ref. 70). As discussed earlier (see "Nitrogen oxides"), the anthropogenic emissions of NO_x are greater than the natural. The manmade emissions of NO_x are primarily in the form of NO, which is formed during high-temperature combustion. The NO_x species are active participants in the formation of HNO_3, which is one of the components of acid rain. Another species of the nitrogen group, NH_3, plays an important role in controlling the acidity of the troposphere, since it is the only common base in the atmosphere.

The Oxygen Group

Introduction. - Only four species are members of this group. Despite this, there is a large degree of variability between the individual species, both in terms of their lifetimes and their concentrations. For example, molecular oxygen has a long lifetime, on the order of millions of years, and is very abundant with an atmospheric concentration of almost 21 percent. The excited oxygen atom $[O(^1D)]$, on the other hand, has a very short lifetime (10^{-9} s) and a low number density. Other members of the oxygen group are ozone and ground-state oxygen $[O(^3p)]$. Photolysis of ozone initiates most of the tropospheric

photochemistry; and, consequently, O_3 is a pivotal molecule in the atmosphere. The reaction paths of the oxygen family are shown in figure 30.

Molecular oxygen (O_2). - Molecular oxygen (O_2) is the second most abundant species in the Earth's atmosphere, comprising about 20.9 percent. The atmospheric lifetime of O_2 is on the order of 10^6 years, although there are 2 separate time scales involving oxygen. One is a fairly short time scale that involves the exchange of oxygen between the biosphere and the atmosphere. This occurs as a result of photosynthesis, respiration, and oxidation of dead organic carbon. The longer of the two time scales involves a cycling of oxygen between the atmosphere and the lithosphere. The characteristic time constant for this cycling is very long indeed, on the order of several million years. The early atmosphere had only trace amounts of oxygen compared to the present level of nearly 21 percent. The chronology for the rise of atmospheric oxygen and, hence, ozone has been the subject of intense studies (ref. 103). The most recent investigations of the evolution of oxygen are those of Kasting and Donahue (ref. 104) and Levine et al. (ref. 105). It has been calculated that only a three percent decrease in the O_2 level would result if all fossil fuel reserves were burned (ref. 106). Furthermore, if all photosynthetic activity ceased and respiration of man and animals continued at the present level, only a fraction of the total amount of oxygen would be destroyed (ref. 107). Thus, it would appear that the present level of atmospheric oxygen is fairly stable.

In a sense, oxygen can be regarded as the greatest pollutant in the history of the Earth. The terrestial atmosphere changed from a chemically reducing one to an oxidating one with profound implications for biological evolution.

Ozone (O_3). - Ozone, the molecule that initiates a great deal of tropospheric photochemistry, is calculated somewhat differently from most of the other species in this study. Ozone is included as a part of odd oxygen (O_3, $O(^3p)$, and $O(^1D)$) and formulated similarly to the expressions given by

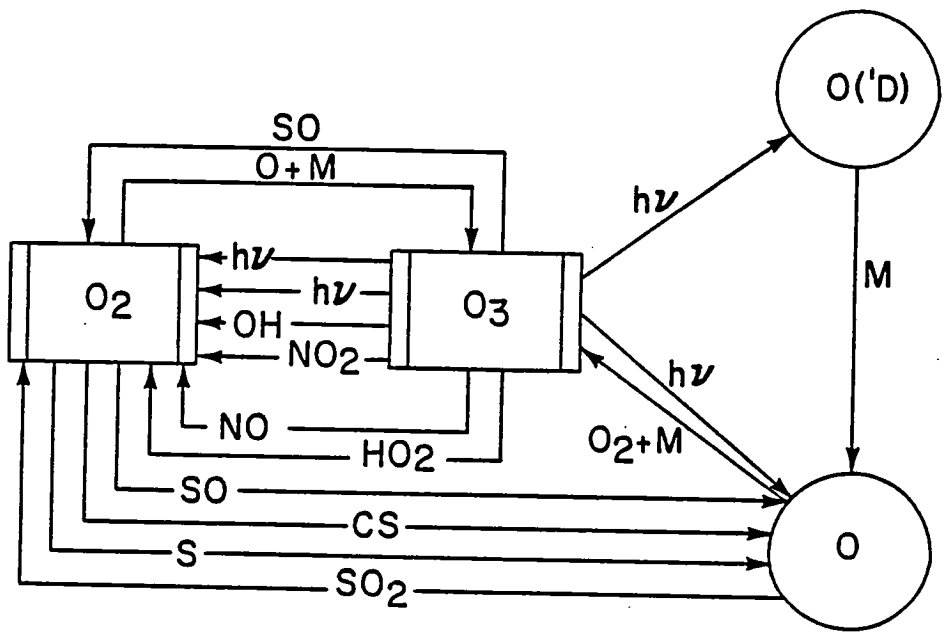

Figure 30. Reaction paths of the oxygen family.

Chameides and Walker (ref. 6) and by Stewart et al. (ref. 7). The steady-state equation for ozone is given by

$$0 = K36\ [O]\ [O_2]\ [M] - [O_3]\ \{K28\ [NO_2] + K29\ [NO] + K38\ [OH] + K39\ [HO_2] + K103\ [SO] + J1 + J2\}$$

where the J's and K's refer to photodissociation frequencies and reaction rates in tables A1 and A2, respectively. For ground-state oxygen the expression would be

$$0 = K19\ [OH]^2 + K37\ [O(^1D)]\ [M] + K52\ [NH_2]\ [OH] + K75\ [CS]\ [O_2] + K76\ [S]\ [O_2] + J2\ [O_3] + J3\ [NO_2] + J4\ [NO_3] + K68\ [SO]\ [O_2] + K56\ [NH]\ [NO] - O(^3p)\ \{K36\ [O_2]\ [M] + K46\ [NH_3] + K50\ [NH_2] + K51\ [NH_2] + K65\ [HS] + K70\ [CS_2] + K71\ [CS_2] + K72\ [CS_2] + K73\ [CS] + K81\ [SO_2] + K94\ [CH_3SH] + K95\ [CH_3SH] + K96\ [CH_3SH] + K98\ [CH_3SCH_3] + K99\ [CH_3SCH_3] + K101\ [COS] + K102\ [H_2S] + K104\ [SO_2]\ [M] + K110\ [HNO_3]\}.$$

For the excited oxygen atom $[O(^1D)]$, the equivalent expression would be

$$0 = J1\ [O_3] - O(^1D)\ \{K2\ [CH_4] + K16\ [H_2O] + K17\ [H_2] + K37\ [M] + K41\ [CH_4] + K47\ [NH_3]\}.$$

The ratio of $[O(^3p)]/[O_3]$ called "f_1," can then be written as $f_1 = [O(^3p)]/[O_3]$ where f_1 is given by

$$f_1 = \{K28\ [NO_2] + K29\ [NO] + K38\ [OH] + K39\ [HO_2] + K103\ [SO] + J1 + J2\ \ K36\ [O_2]\ [M]\}^{-1}$$

Similarly, the ratio of $[O(^1D)]/[O_3]$, denoted "f_2," is written in the form $f_2 = [O(^1D)]/[O_3]$, with f_2 expressed as

$$f_2 = J1 \; \{K2\,[CH_4] + K16\,[H_2O] + K17\,[H_2] + K37\,[M] + K43\,[CH_4] + K47\,[NH_3]\}^{-1}.$$

Since the concentration of ozone is very dependent on the cycling of odd nitrogen (see discussion under "Nitrogen oxides"), it is necessary to define a ratio F which is an expression for the fraction of nitrogen dioxide molecules that is destroyed by photolysis, i.e.

$$F = \frac{D[NO_2]_{J3}}{D[NO_2]_{tot}}$$

The complete expression for F is

$$F = J3 \; \{J3 + K23\,[HO_2] + K24\,[OH] + K28\,[O_3] + K30\,[NO_3] + K33\,[NO]\,[H_2O] + K69\,[SO]\}^{-1}$$

The destruction of nitrogen dioxide is dominated by photolysis. Consequently the fraction F is typically near unity. Values of F range from 0.95 to 0.99 depending on altitude. Hence, the abundance of ozone can be calculated according to

$$[O_3] = \{J4\,[NO_3] + J6\,[N_2O_5] + J7\,[HNO_3] + [NO]\,(K8\,[CH_3O_2]\,K22\,[HO_2] + 2\,K32\,[NO_3]) + K35\,[N_2O_5] + K40\,[HNO_2]\,[OH]\} \times F\,\{f_2\,(K2\,[CH_4] + K16\,[H_2O] + K17\,[H_2] + K37\,[M] + K43\,[CH_4] + K47\,[NH_3]) + K28\,[NO_2] + K38\,[OH] + K39\,[HO_2] + K103\,[SO] + K29\,[NO]\,(1-F)\}^{-1}.$$

The first set of braces contains the terms that produce NO_2 and are multiplied by the fraction (F) that is photodissociated. The second set of braces (to the -1 power) contains the terms that destroy odd oxygen (O_x); in addition, reaction 29 must be included. The term K29 [NO] (1-F) expresses the destruction of odd oxygen due to nitric oxide molecules that are formed by processes other than photolysis of nitrogen dioxide.

Because of the central role ozone occupies in tropospheric photochemistry, most of the early studies concentrated on this molecule. The classical view of tropospheric ozone contended that O_3 is essentially inert in this region and is transported down from the stratosphere by intrusion (refs. 108, 109). During the last decade, several studies have suggested that ozone is photochemically very active in the troposphere (refs. 6, 20, 110, 111). Some studies have suggested that the troposphere is a region where ozone is photochemically produced (ref. 112). Another study suggests that additional sources augment the photochemical levels of O_3 (ref. 7), while yet other studies contend that ozone is photochemically lost in the troposphere (refs. 20, 111). Photochemical production of ozone maximizes for an NO_x level of 0.5 ppb. For high NO_x levels, the photostationary state equation discussed earlier (see "Nitrogen oxides") dominates the cycling of odd oxygen. For NO_x levels between 0.5 and 1.0 ppb, the level of O_3 is decreased because odd hydrogen (NO_x) reacts very efficiently with NO_x (ref. 7). At very low levels of NO_x, it is not possible to photochemically produce ozone (ref. 113). Fishman et al. (ref. 112) critically assessed the photochemical production of tropospheric ozone as a function of NO concentration and found that the level of nitric oxide determines the concentration of ozone in the troposphere since O_3 is formed when a peroxy radical, RO_2, converts NO to NO_2. Specifically, it was determined that the "critical level" of NO is about 10 ppt. Below this level peroxy radicals preferentially react with O_3 rather than NO, thus enhancing the ozone destruction. At NO concentrations exceeding 10 pptv, peroxy radicals react with NO more often than with O_3, which results in conversion to NO_2 and later enhanced levels of ozone. Obviously, the background level of NO_x is a key parameter

in determining the photochemistry of ozone. Some of the early NO_x measurements (see "Nitrogen oxides") indicated background levels in the ppb (ref. 79). Subsequent measurements yielded concentrations on the order of 0.1 ppb, while the most recent measurements of NO resulted in yet lower concentrations, on the order of a few parts per trillion by volume (pptv) (refs. 84, 85, 87).

The dialogue of in situ production, destruction, and transport of tropospheric ozone was recently rekindled in a paper by Singh et al. (ref. 113). This paper argues that most of the ozone that is present in the troposphere is stratospheric in origin and is transported downward by a mechanism known as tropopause folding. Furthermore, they point out that the vertical gradient of ozone is consistent with a downward transport of O_3 from the stratosphere. Finally, they note that the seasonal variability of ozone is out of phase with the solar flux, i.e., ozone concentrations tend to maximize in the springtime while the maximum amount of solar flux, and therefore greatest photochemical efficiency, occurs during the summer.

The question of whether ozone in the troposphere is produced photochemically in the troposphere or is stratospheric in origin cannot be settled until the important presursor NO_x has been measured more extensively in clean, background tropospheric air. In particular, vertical profiles of the concentrations of odd nitrogen are highly desirable. Ozone concentrations are monitored routinely at many stations throughout the world. However, most of these stations are located in large, metropolitan areas with a high degree of air pollution and, hence, have a photochemistry that is different from the more pristine background tropospheric air.

Some measurements of O_3, even vertical profiles of clean tropospheric air, are available (see fig. 31). Both the measurements by Krueger and Minzner (ref. 114) and Chatfield and Harrison (ref. 115) are generally between 6-10 × 10^{11} molecules-cm^{-3}. The average of measurements at 2.0 and 5.5 km by Routhier et al. (ref. 116) are also in that range, while the vertical profile by Routhier et al. has a steeper gradient than those presented in references 114 and 115.

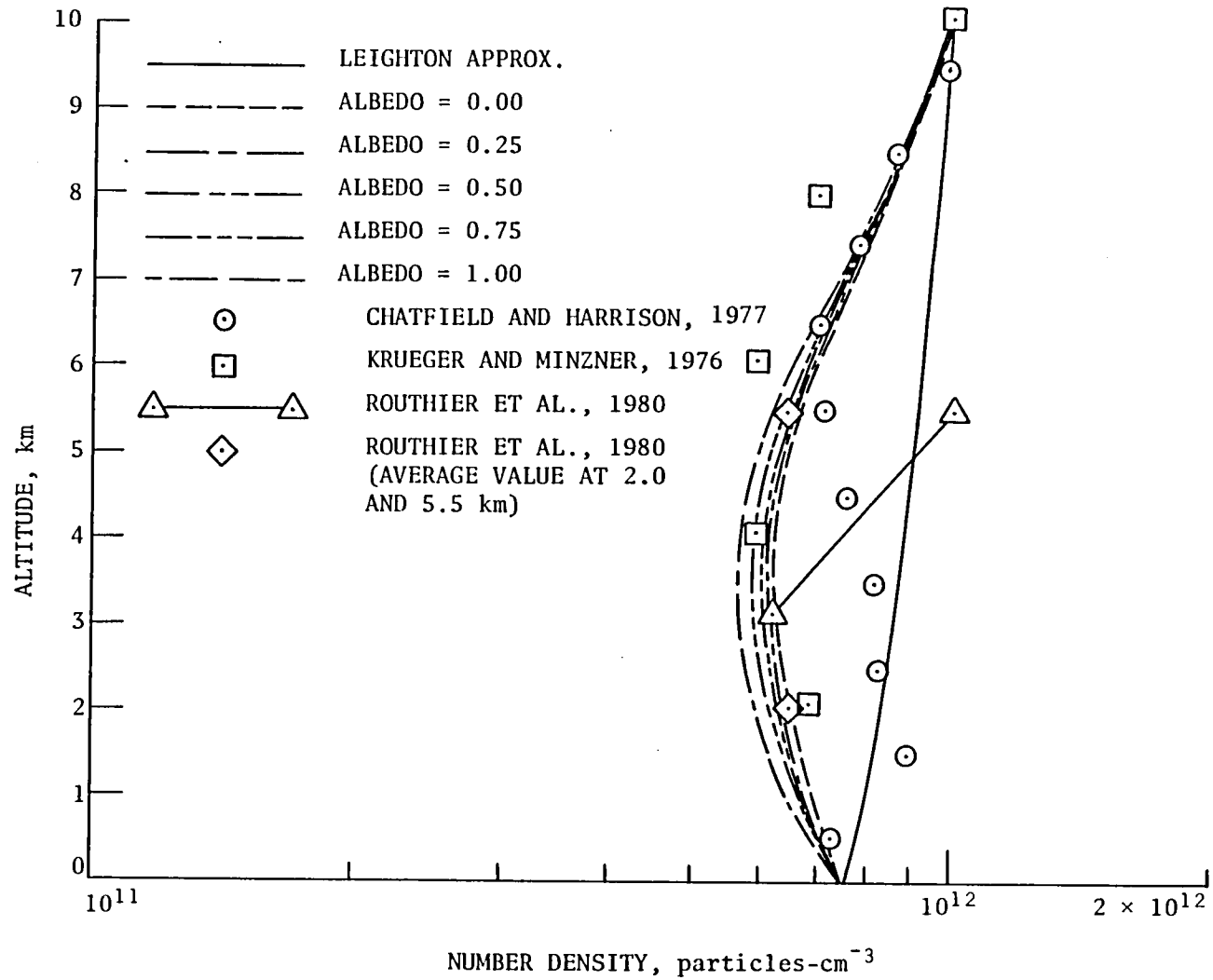

Figure 31. Vertical distributions of O_3 for the multiple scattering cases with various albedos and the Leighton approximation.

In the present study, the number density of ozone was held constant at 7.5 5 × 10^{11} molecules cm^{-3} at the surface and 10 × 10^{11} molecules cm^{-3} at the tropopause. Inclusion of multiple scattering and surface albedo to the calculations of the radiation field causes drastic changes compared to the profile calculated using the Leighton approximation. With the Leighton approximation, a gradual increase from 7.5 × 10^{11} molecules of O_3 per cm^3 (corresponding to 29 ppbv) at the surface to 10 × 10^{11} O_3 molecules per cm^3 (corresponding to 166 pbbv) at the tropopause is obtained. The vertical profiles of the multiple scattering calculations, on the other hand, minimize at four km and are generally lower than the Leighton approximation. It should also be noted that the selection of a particular value of the surface albedo has less of an effect than using the more detailed treatment of the radiation equation in the first place. It should come as no surprise that the ozone concentration decreases when a multiple scattering routine is used. The photolysis of O_3, processes J1 and J2, becomes more efficient. In addition, the enhanced levels of OH and HO_2 cause a further decrease in the O_3 concentration. The hydroxyl and hydroperoxy radicals, together with surface deposition, have been identified as the major loss mechanisms for ozone (ref. 9).

Atomic oxygen [$O(^3p)$]. -

Production		Destruction	
J2 :	$O_3 + h\nu \rightarrow O + O_2$	K36 :	$O + O_2 + M \rightarrow O_3 + M$
K37:	$O(^1D) + M \rightarrow O + M$	K99 :	$O + CH_3SCH_3 \rightarrow CH_2S + CH_3O$
J3 :	$NO_2 + h\nu \rightarrow O + NO$	K70 :	$O + CS_2 \rightarrow SO + CS$
K68:	$SO + O_2 \rightarrow O + SO_2$	K71 :	$O + CS_2 \rightarrow S + COS$
J4 :	$NO_3 + h\nu \rightarrow O + NO_2$	K72 :	$O + CS_2 \rightarrow S_2 + CO$
K75:	$CS + O_2 \rightarrow O + COS$	K104:	$O + SO_2 + M \rightarrow SO_3 + M$
K19:	$OH + OH \rightarrow O + H_2O$	K102:	$O + H_2S \rightarrow HS + OH$
K76:	$S + O_2 \rightarrow O + SO$	K101:	$O + COS \rightarrow SO + CO$

Production (concl'd)	Destruction (concl'd)
K52: $NH_2 + OH \rightarrow O + NH_3$	K50 : $O + NH_2 \rightarrow HNO + H$
K56: $NH + NO \rightarrow O + N_2 + H$	K51 : $O + NH_2 \rightarrow NH + OH$
	K46 : $O + NH_3 \rightarrow NH_2 + OH$
	K98 : $O + CH_3SCH_3 \rightarrow CH_3SO + CH_3$
	K110: $O + HNO_3 \rightarrow NO_3 + OH$
	K94 : $O + CH_3SH \rightarrow CH_3 + HSO$
	K95 : $O + CH_3SH \rightarrow CH_3SO + H$
	K96 : $O + CH_3SH \rightarrow CH_3SOH$
	K81 : $O + SO_2 \rightarrow SO + O_2$
	K65: $O + HS \rightarrow SO + H$

Ground-state atomic oxygen [$O(^3p)$] is produced by a total of 10 reactions and destroyed by 19. However, of the 10 reactions that produce ground-state oxygen, only 3 are of real importance. Atomic oxygen is produced primarily by ozone photolysis at wavelengths greater than 320 nm. This process accounts for approximately 97 percent of all tropospheric $O(^3p)$ that is produced (see table 24). Between two and three percent of atomic oxygen production is due to quenching of the excited oxygen atom $O(^1D)$ in the presence of a third body (reaction 37). Photolysis of nitrogen dioxide (NO_2) produces about 1.75 percent of all $O(^3p)$ atoms at the surface, decreasing to 0.1 percent at the tropopause. The remaining 7 reactions that produce ground-state atomic oxygen are anywhere from 4 to 11 orders of magnitude smaller than the primary path of $O(^3p)$ production. In all, 19 reactions contribute to the destruction of $O(^3p)$, but nearly all of the destruction occurs by reaction of atomic oxygen with molecular oxygen in the presence of a third body forming ozone (reaction 36). In fact, so dominating is this one term that the next largest destruction term is five orders of magnitude smaller at the surface. The remaining 17 loss terms of $O(^3p)$ are anywhere from 5 to as much as 24 orders of magnitude smaller

Table 24. Production and destruction terms of $O(^3p)$ and percent of total production and destruction.

Production Rate (molecules-cm^{-3}-s^{-1}) and Percent of Total Production

Altitude, km	J2	%	K37	%	J3	%	K68	%	J4	%	K75	%
10	3.388 E-8	97.11	9.693 E-6	2.78	3.962 E-5	0.11	8.804 E-1	-	1.107 E-3	-	2.083 E-1	-
5	2.952 E-8	97.43	6.884 E-6	2.27	9.111 E-5	0.30	4.207 E-2	-	4.885 E-3	-	1.972 E-1	-
0	2.287 E-8	96.81	4.152 E-6	1.76	3.378 E-6	1.43	6.471 E-4	-	3.127 E-4	-	1.677 E-1	-

Altitude, km	K19	%	K76	%	K52	%	K56	%	Total	%
10	1.813 E-0	-	4.998 E-1	-	1.755 E-2	-	5.016 E-3	-	3.489 E-8	100.00
5	5.140 E-0	-	4.735 E-0	-	7.929 E-2	-	5.421 E-3	-	3.030 E-8	100.00
0	1.033 E-1	-	4.025 E-0	-	3.247 E-1	-	6.188 E-3	-	2.362 E-8	100.00

(continued)

Table 24. (Concluded.)

Destruction Frequency (s^{-1}) and Percent of Total Destruction

Altitude, km	K36	%	K99	%	K70	%	K71	%	K72	%	K104	%	K102	%
10	1.776 E-4	100.00	2.673 E-6	-	2.181 E-3	-	2.594 E-4	-	2.594 E-4	-	2.017 E-7	-	6.848 E-9	-
5	4.243 E-4	100.00	4.600 E-4	-	5.638 E-3	-	6.766 E-4	-	6.766 E-4	-	3.579 E-6	-	3.821 E-7	-
0	9.170 E-4	100.00	6.426 E-1	-	1.314 E-2	-	1.577 E-3	-	1.577 E-3	-	2.190 E-4	-	1.344 E-4	-

Altitude, km	K101	%	K50	%	K51	%	K46	%	K98	%	K110	%	K94	%
10	4.654 E-4	-	2.426 E-7	-	2.426 E-7	-	1.153 E-8	-	3.659 E-15	-	1.530 E-7	-	1.448 E-16	-
5	2.895 E-5	-	7.488 E-7	-	7.488 E-7	-	1.382 E-7	-	1.225 E-11	-	3.060 E-7	-	4.845 E-13	-
0	1.294 E-4	-	2.414 E-6	-	2.414 E-6	-	2.235 E-6	-	1.224 E-6	-	4.590 E-7	-	4.845 E-8	-

Altitude, km	K95	%	K96	%	K81	%	K65	%	K73	%	Total	%
10	1.488 E-16	-	1.488 E-16	-	1.305 E-20	-	5.008 E-14	-	2.781 E-17	-	1.776 E-4	100.00
5	4.845 E-13	-	4.845 E-13	-	2.121 E-17	-	1.795 E-13	-	1.481 E-17	-	4.243 E-4	100.00
0	4.845 E-8	-	4.845 E-8	-	4.129 E-11	-	1.945 E-11	-	7.550 E-18	-	9.170 E-4	100.00

than the primary destruction term. The lifetime of ground-state oxygen is about 10^{-5} s based on the chemistry described above. The vertical profiles of atomic oxygen are presented in figure 32. The level of $O(^3p)$ is enhanced only slightly, about 10 percent at the surface for an albedo of 0.00. For an albedo of 0.25, the ground-state atomic oxygen concentration is increased by a factor of 1.5 compared to the Leighton approximation. An albedo of 0.50 approximately doubles the abundance of $O(^3p)$, while a factor of 2.7 increase is obtained at the surface for an albedo of 0.75. Finally, for a surface that is a perfect reflector, i.e., the albedo is 1.00, the surface concentration of ground-state oxygen is increased by a factor of 3.4. At the tropopause, a trend similar to that at the surface is noticed with the exception that the multiple scattering cases with low albedos are enhanced more than the corresponding factor at the surface. There are no measured troposphere values of $O(^3p)$ available to compare with the theoretical calculations.

Excited oxygen atom $O(^1D)$. -

Production	Destruction
J1: $O_3 + h\nu \rightarrow O(^1D) + O_2$	K37: $O(^1D) + M \rightarrow O(^3p) + M$
	K16: $O(^1D) + H_2O \rightarrow 2OH$
	K2 : $O(^1D) + CH_4 \rightarrow CH_3 + OH$
	K17: $O(^1D) + H_2 \rightarrow H + OH$
	K41: $O(^1D) + CH_4 \rightarrow CH_2O + H_2$
	K47: $O(^1D) + NH_3 \rightarrow NH_2 + OH$

The excited oxygen atom $[O(^1D)]$, which plays an important role in tropospheric photochemistry, is only produced when ozone is photolyzed in the spectral range from 300 to 320 nm (see earlier discussion under "Photolysis Rate Calculations"). The $O(^1D)$ atom derives its importance from the fact that it reacts with water vapor and produces hydroxyl radicals, which in turn determine the levels of many tropospheric gases.

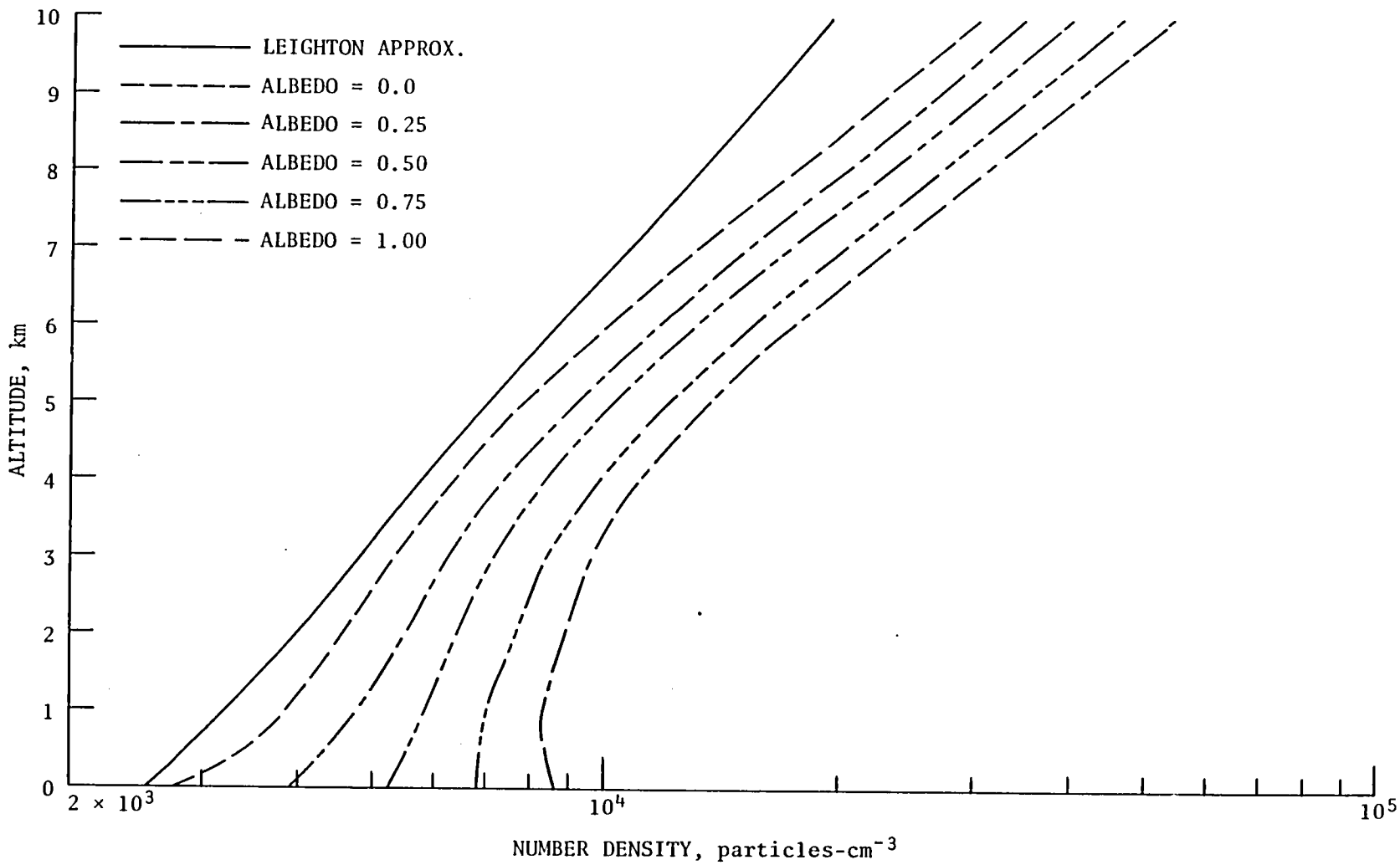

Figure 32. Vertical distributions of $O(^3P)$ for the multiple scattering cases with various albedos and the Leighton approximation.

The majority of the excited oxygen atoms are destroyed by quenching in the presence of a third body M (reaction 37). At the surface, approximately 88 percent is lost by quenching, and, in the mid and upper regions of the troposphere, about 97 percent is deactivated this way (see table 25). The very important reaction of $O(^1D)$ to H_2O (reaction 16) accounts for about 12 percent of the total loss of $O(^1D)$ at the surface. In the upper regions of the troposphere this reaction is responsible for approximately three percent of the total $O(^1D)$ loss. The reason that reaction 16 is proportionally much larger at the surface than at higher altitudes is a result of the relatively high number density of water vapor molecules close to the surface compared to higher altitudes. The amount of water vapor in the atmosphere is, of course, dependent on the temperature. With a rapidly decreasing temperature gradient, -6.5 K km^{-1}, the amount of water vapor decreases rapidly. The remaining four destruction mechanisms for $O(^1D)$ are between five and eight orders of magnitude less important than the primary loss mechanism. The calculated lifetime of excited oxygen is very short, about 10^{-9} s.

Larger differences between the Leighton approximation and the multiple scattering calculations are observed for $O(^1D)$ than for any other molecule. As mentioned previously, scattering is strongly wavelength dependent, i.e., the shorter the wavelength the more significant scattering becomes. The production of $O(^1D)$ occurs only at wavelengths between 300 to 320 nm, i.e., the ultraviolet end of the spectrum. Consequently, large differences in the vertical profiles of $O(^1D)$ will occur depending on the treatment of the radiation field. The number density of $O(^1D)$ at the surface is approximately doubled for the multiple scattering case with albedo of 0.00 compared to the Leighton approximation (see fig. 33). For an albedo of 0.25, this ratio is slightly more than tripled, and when the albedo is 0.50 the ratio is nearly 4.5. A factor of 6 increase results when the surface albedo is 0.75, and an albedo of 1.00 yields a factor of 8.5 increase. In the upper troposphere the vertical profiles calculated with the multiple scattering code are enhanced by factors varying from 4.3 for a 0.00 albedo to 5.6 when the albedo is 1.00. There are no measurements of tropospheric $O(^1D)$ for comparison with theoretical calculations.

Table 25. Production and destruction terms of $O(^1D)$ and percent of total production and destruction.

Production Rate (molecules-cm^{-3}-s^{-1}) and Percent of Total Production

Altitude, km	J1	%
10	9.713 E-6	100.00
5	7.109 E-6	100.00
0	4.736 E-6	100.00

Destruction Frequency (s^{-1}) and Percent of Total Destruction

Altitude, km	K37	%	K16	%	K2	%	K17	%	K41	%	K47	%	Total	%
10	2.752 E-8	97.24	7.820 E-6	2.76	1.077 E-3	-	4.257 E-2	-	1.806 E-2	-	1.118 E-0	-	2.830 E-8	100.00
5	4.896 E-8	96.64	1.702 E-7	3.36	2.984 E-3	-	7.574 E-2	-	3.213 E-2	-	2.110 E-0	-	5.066 E-8	100.00
0	8.160 E-8	87.65	1.150 E-8	12.35	4.973 E-3	-	1.262 E-3	-	5.355 E-2	-	7.970 E-0	-	7.970 E-8	100.00

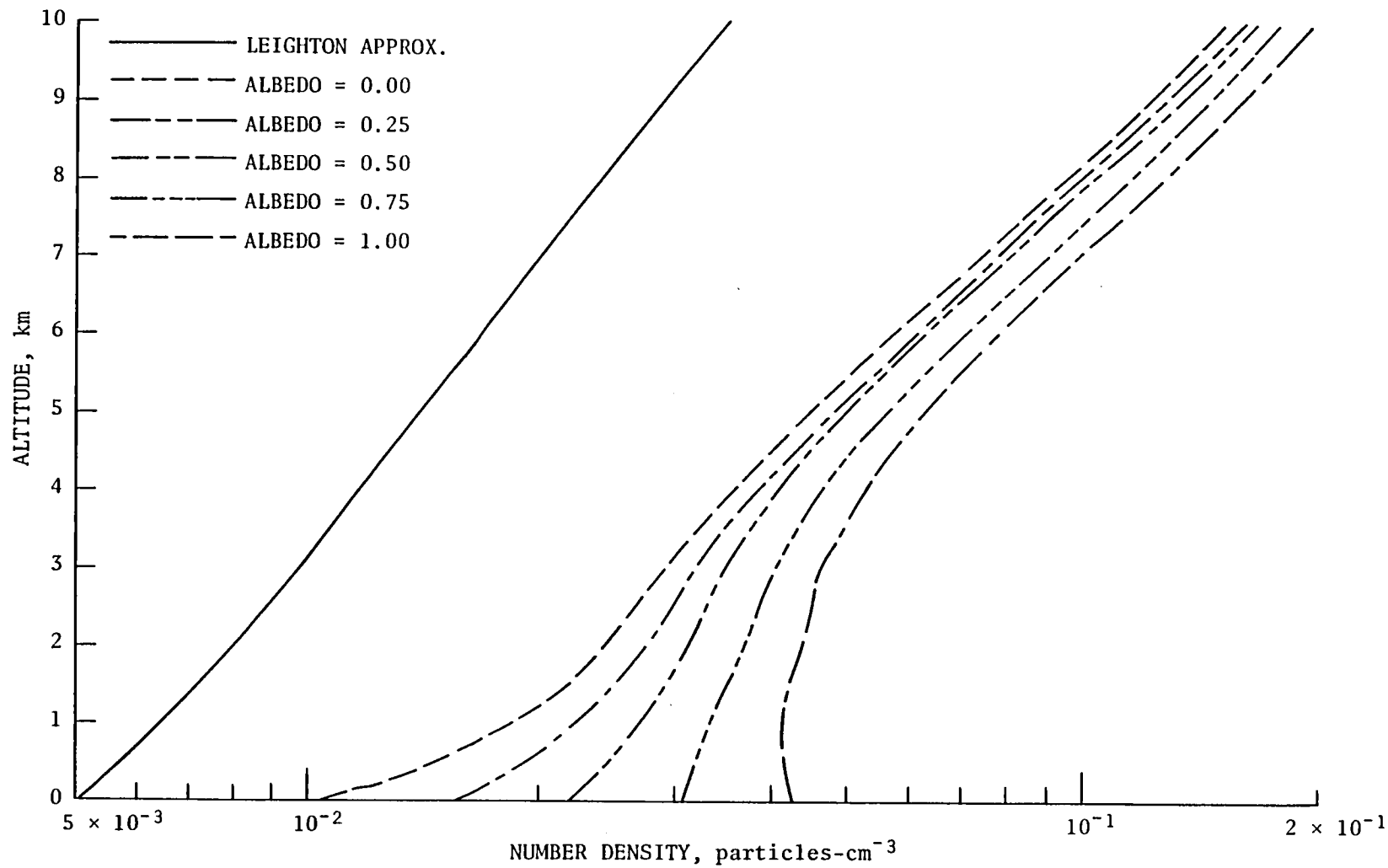

Figure 33. Vertical distributions of $O(^1D)$ for the multiple scattering cases with various albedos and the Leighton approximation.

Future perturbations to the oxygen budget. - As mentioned earlier, it appears that the most abundant species of this group, O_2, will not be altered significantly due to any potential perturbations in the future. However, the second most abundant oxygen species, ozone, could possibly undergo substantial modifications due to anthropogenic activity. Much of the early interest in stratospheric photochemistry centered around the issue of ozone depletion due to jet-engine emissions (ref. 117) and catalytic O_3 destruction initiated by the upward diffusion of chlorofluoromethanes commonly called "freons" (ref. 118). Although ozone is a so-called "trace gas," i.e., it is present in only minute quantities, it absorbs the potentially harmful radiation in the spectral range from 280 to 320 nm. This wavelength region is commonly referred to as the UV-B, where B stands for biological (ref. 119). Most biological processes, although not all, are very sensitive to the amount of radiation that is filtered through the UV-B part of the spectrum. Even relatively small changes in total radiative flux in this spectral region could have a significant impact on many ecological systems. This can easily be appreciated by comparing so-called "biological action spectra" to the amount of O_3 absorption in the UV-B. Many biological organisms and functions have action spectra that are virtual overlays to the ozone absorption. Examples of this are deoxyribonucleic acid (DNA) and erythema (sunburn). The fact that DNA molecules, the building blocks of life, are sensitive to radiation in the same region that ozone is a strong absorber has great implications for the development and evolution of life. In the primordial atmosphere oxygen and ozone were present in only very minute fractions and nearly all radiation in the UV-B region reached the surface of the Earth. As the atmospheric level of oxygen started to rise, so did the level of ozone, and consequently more of the UV-B radiation was shielded from the surface by O_3 absorption. It has been calculated that the present day ozone layer has a shielding effect equal to a water column of 10-m depth. Thus, life would have had to originate deep in water and migrate on to land as the ozone layer started to grow. It should be pointed out that some primitive organisms have a repair mechanism whereby they are able to repair damage caused by elevated levels of UV-B radiation (ref. 120). This would then offer an alternative path to biological evolution. It is very evident that the lessons

learned from atmospheric evolution must be kept in mind when anthropogenic modifications are discussed. Calculations have shown that a two percent increase in skin cancer would occur for each one percent reduction in total ozone (ref. 121). There is also evidence that this 2:1 ratio would not maintain its linearity if a sizeable fraction of the total ozone were depleted. Other radiative effects due to altered levels of ozone would occur as a result of the ozone absorption in the 9.6-μm region, which is in the so-called "atmospheric window region" of 8 to 12 μm. In addition to the radiative changes of O_3, the photochemistry would also be altered, since ozone photolysis produces the excited oxygen atom [$O(^1D)$], which subsequently reacts with water vapor to form hydroxyl radicals (OH). In a later subsection (see "Hydroxyl radical") it will be shown how the abundance of OH controls the level of many tropospheric gases.

The Hydrogen Group

Introduction. - This family of species consists of six gases with lifetimes ranging from 10^{-7} s for atomic hydrogen (H) to 10 yr for molecular hydrogen (H_2) and abundances varying from several percent for water vapor to a mixing ratio of 10^{-20} for atomic hydrogen. In addtion to water vapor, some other key tropospheric gases, such as the hydroxyl radical (OH) and hydrogen peroxide (H_2O_2), are members of this group. The importance of the hydroxyl radical on tropospheric photochemistry can easily be understood by realizing that 35 percent of all chemical reactions included in this model involve these species. Hydrogen peroxide is believed to contribute to acid rain and is, therefore, of considerable interest. A strong correlation between the concentration of hydrogen peroxide and acidity in rainwater has been observed. The reaction paths for the hydrogen species are shown in figure 34.

Water vapor (H_2O). - The tropospheric abundance of water vapor (H_2O) is highly variable. The concentration of H_2O is a strong function of latitude and season. In this study an average concentration of the values of January and July in the U.S. Standard Atmosphere Supplement (ref. 28) at 30°N latitude was used. Water vapor is somewhat of an anomaly. In general, the longer the life-

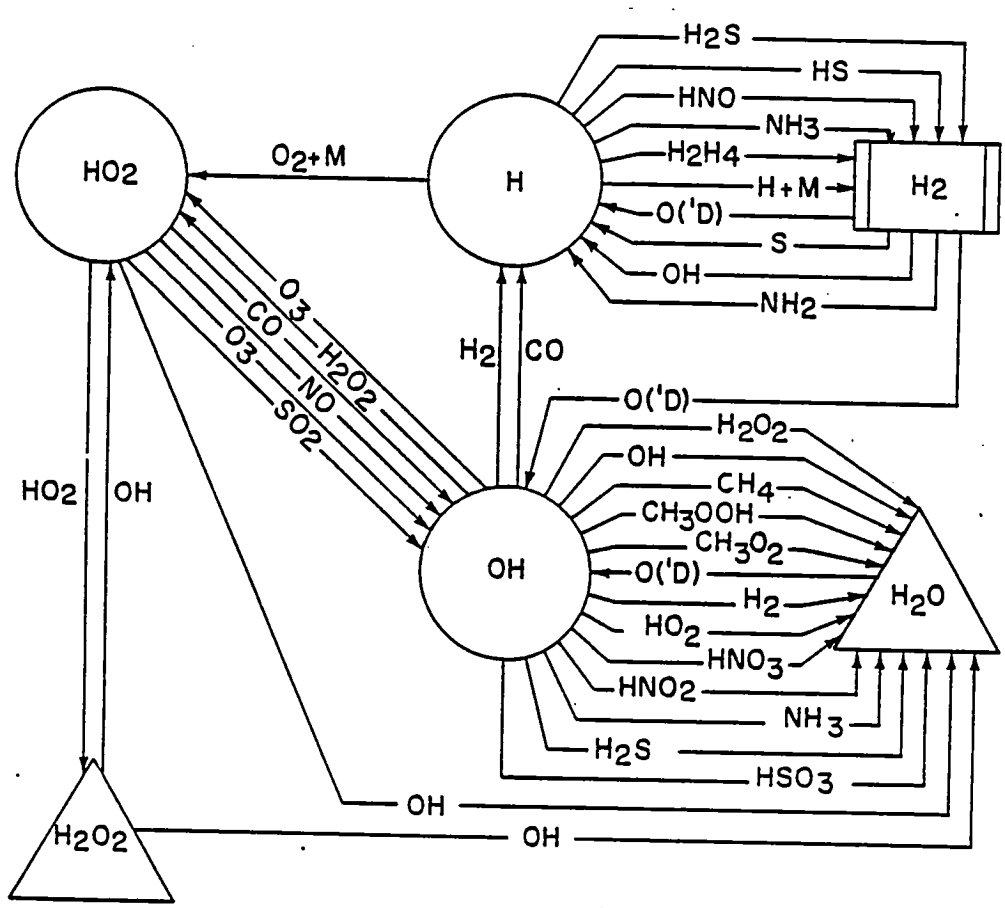

Figure 34. Reaction paths of the hydrogen family.

time of an atmospheric species, the more inert it is. Water vapor is a relatively abundant tropospheric species, yet it has only a moderately long lifetime. This is because water vapor is continuously emitted into the troposphere by evaporation. Water vapor, like other gases, exerts a vapor pressure. Sometimes the vapor pressure of water vapor is referred to as the partial pressure of H_2O. Under normal atmospheric conditions, the vapor pressure of H_2O is below the saturation vapor pressure. When the saturation vapor pressure is reached or exceeded, cloud droplets will form and precipitation may occur. In some cases supersaturation can occur and precipitation will not fall despite the fact that the vapor pressure of H_2O has exceeded the saturation vapor pressure. The saturation vapor pressure is a function of temperature only. Thus, the tropospheric distribution of water vapor should parallel that of temperature. Consequently, since the temperature profile is specified in one-dimensional models implicitly, so is the water vapor profile. The ratio of the partial pressure of water vapor to the saturation pressure is called "relative humidity," a quantity expressed in percent. Oddly enough, human comfort depends more on relative humidity than absolute humidity (ref. 122). Once the relative humidity exceeds 80 percent, the air starts to feel clammy, even though the absolute moisture content might be very low.

Photochemically, water vapor is of tremendous importance since it is the reaction of H_2O with the excited oxygen atom $[O(^1D)]$ that forms the hydroxyl radical (OH). The level of OH, the major tropospheric scavenger, determines the atmospheric abundances of many species. This will be discussed further under "Hydroxyl radical." Water vapor is also of significance due to its radiative properties. It has absorption bands in the 6-, 10-, and 20-μm regions and contributes significantly to the greenhouse effect.

Molecular hydrogen (H_2). - The second most abundant species of the hydrogen group is molecular hydrogen (H_2), which has a mixing ratio of 0.5 ppm in the troposphere (ref. 123). Molecular hydrogen is believed to be formed primarily by bacterial fermentation in the soil (ref. 123), as well as by photolysis of formaldehyde (photolytic process 4.12). Additional sources include

volcanic outgassing and outgassing from hot springs (ref. 124). In fact, on rare occasions a burning hydrogen flame has been observed in the Kilanea Volcano (ref. 125). The major removal mechanism for atmospheric hydrogen is exospheric escape (ref. 126). In the troposphere molecular hydrogen is lost primarily due to the reaction with the hydroxyl radical forming atomic hydrogen and water vapor. The tropospheric lifetime of molecular hydrogen is relatively long (10 years), a further indication of its chemical inertness.

Hydrogen peroxide (H_2O_2). - Certain tropospheric gases have thermodynamic properties rendering them highly water soluble (ref. 127). Hydrogen peroxide is among those species. Other examples are hydrogen chloride (HCl) and hydrogen bromide (HBr) (ref. 48). As discussed previously (see "Water vapor"), the amount of water vapor in the troposphere is a strong function of the temperature profile. Typically, the vertical distribution of H_2O shows a strong negative gradient. The calculated turnover time for tropospheric H_2O to cycle in and out of these various phases is about one day (ref. 127). Hence, if the photochemical lifetime of a species is longer than one day and it is highly water soluble, the vertical profile should closely resemble that of water vapor. Hydrogen peroxide has a lifetime of approximately two days and would therefore fall into the category of species that are controlled by water vapor. Consequently, for this study a vertical distribution of hydrogen peroxide of 5×10^{-8} times the H_2O distribution was specified, giving a mixing ratio at the surface of 1 ppb. This is in reasonably close agreement with recent measurements (ref. 128). The highly polluted Los Angeles basin exhibits values in the 4 to 15 ppb range on weekdays and 4 to 11 ppb on weekends. Both weekday and weekend measurements show diurnal variations with early afternoon peak and minimum values just prior to sunrise. The measurements in rural Colorado (ref. 129) are generally 1 to 3 ppb with diurnal maxima and minima occurring at the same times as in the Los Angeles study.

On a local scale, high abundances of H_2O_2 might cause photochemical smog. The photolysis of H_2O_2 causing two hydroxyl radicals is normally a relatively slow process, but if large amounts of hydrogen peroxide are present in the

morning at the commencement of photochemistry, the enhanced levels of OH can react with oxides of nitrogen (NO_x) and hydrocarbons to form smog. There is also increasing evidence that hydrogen peroxide might play a role in the formation of acid rain since there is a strong correlation between the concentration of H_2O_2 and acidity in rainwater (ref. 129).

Hydroperoxyl radical (HO_2). -

Production		Destruction	
K15:	$H + O_2 + M \rightarrow HO_2 + M$	K22 :	$HO_2 + NO \rightarrow OH + NO_2$
K9 :	$CH_3O + O_2 \rightarrow HO_2 + CH_2O$	K20 :	$HO_2 + HO_2 \rightarrow H_2O_2 + O_2$
K21:	$OH + H_2O_2 \rightarrow HO_2 + H_2O$	K39 :	$HO_2 + O_3 \rightarrow OH + 2O_2$
K11:	$HCO + O_2 \rightarrow HO_2 + CO$	K4 :	$HO_2 + CH_3O_2 \rightarrow CH_3OOH + O_2$
K38:	$OH + O_3 \rightarrow HO_2 + O_2$	K18 :	$HO_2 + OH \rightarrow H_2O + O_2$
K59:	$HNO + O_2 \rightarrow HO_2 + NO$	K112:	$HO_2 + NO \rightarrow HNO_3$
		K78 :	$HO_2 + SO_2 \rightarrow SO_3 + OH$
		K13 :	$HO_2 + CO \rightarrow OH + CO_2$

Of the six chemical terms producing the hydroperoxyl radical (HO_2), five account for at least one percent of the total HO_2 production at some altitude in the troposphere (see table 26). The primary source of HO_2 in the troposphere is oxidation of atomic hydrogen by molecular oxygen in the presence of a third body (reaction 15). At the surface, this reaction accounts for almost 65 percent of the total production, increasing to nearly 80 percent at the tropopause. Secondary reactions at the surface are the reaction of methoxy (CH_3O) with molecular oxygen (O_2) (reaction 9), which contributes about 14.5 percent to the total HO_2 production at the surface, and the reaction of the hydroxyl radical to hydrogen peroxide (reaction 21), which accounts for slightly less than 13 percent at the surface. At the tropopause, reaction 9 still accounts for a relatively large share (11.6 percent), but the contribution of

Table 26. Production and destruction terms of HO_2 and percent of total production and destruction.

Production Rate (molecules cm^{-3}-s^{-1}) and Percent of Total Production

Altitude, km	K15	%	K9	%	K21	%	K11	%	K38	%	K59	%	Total	%
10	2.382 E-5	79.25	3.548 E-4	11.80	5.690 E-2	0.19	1.150 E-4	3.83	1.483 E-4	4.93	2.257 E-2	-	3.006 E-5	100.00
5	7.805 E-5	75.66	1.422 E-5	13.78	2.333 E-4	2.26	5.374 E-4	5.21	3.183 E-4	3.09	5.241 E-3	-	1.032 E-6	100.00
0	2.258 E-5	64.94	5.027 E-5	14.46	4.481 E-5	12.89	2.166 E-5	6.23	5.149 E-4	1.48	6.156 E-1	-	3.477 E-6	100.00

Destruction Frequency (s^{-1}) and Percent of Total Destruction

Altitude, km	K22	%	K20	%	K39	%	K4	%	K18	%	K112	%	K78	%
10	1.210 E-3	44.03	5.940 E-4	21.81	8.205 E-4	29.86	5.527 E-5	2.01	5.208 E-5	1.90	1.630 E-5	0.59	2.158 E-9	-
5	1.342 E-3	33.00	1.335 E-3	32.82	1.014 E-3	24.93	2.792 E-4	6.86	7.624 E-5	1.87	2.079 E-5	0.52	1.130 E-8	-
0	2.853 E-3	36.69	2.523 E-3	35.84	1.102 E-3	15.65	6.905 E-4	9.81	9.684 E-5	1.37	4.466 E-5	0.64	2.550 E-7	-

Altitude, km	K13	%	Total	%
10	1.032 E-8	-	2.748 E-3	100.00
5	1.836 E-8	-	4.067 E-3	100.00
0	3.060 E-8	-	2.040 E-3	100.00

reaction 21 has decreased to less than 0.2 percent. Another reaction with intermediate importance is the oxidation of the formyl radical (HCO) by molecular oxygen (reaction 11). At the surface, this reaction is responsible for more than 6 percent, in the midtroposphere a little more than 5 percent, and at the tropopause about 3.8 percent. The reaction of ozone (O_3) with hydroxyl radical (OH) (reaction 38) contributes about 1.5 percent at the surface, increasing its share of the total HO_2 production to nearly 5 percent at the tropopause. The final production term, oxidation of the nitroxyl radical (HNO) by molecular oxygen (reaction 59), is anywhere from seven to eight orders of magnitude less important than the primary production term (reaction 15). Of the eight loss terms, five contribute more than one percent to the total destruction of HO_2. The major loss terms are the reactions of HO_2 to NO (reaction 22), to itself (reaction 20), and to ozone (reaction 39). At the surface reactions 22 and 20 each account for approximately 36 percent of the total HO_2 destruction; in the midtroposphere their shares are about 33 percent each, while at the tropopause reaction 22 contributes to 44 percent of the total HO_2 loss and reaction 20 accounts for 20.0 percent. The third major loss mechanism, reaction 39, is responsible for 15.7 percent at the surface, incresaing to slightly less than 30 percent at the tropopause. Reaction 4, hydroperoxy interacting with methylperoxy, provides almost 10 percent of the total loss at the surface. Its share decreases monotonically throughout the troposphere to about two percent at the tropopause. The interaction of HO_2 with OH (reaction 18) is responsible for 1.4 to 1.9 percent of the total HO_2 loss depending on altitude, while the combination of HO_2 with NO accounts for slightly more than 0.5 percent throughout the troposphere. The two remaining loss terms, reactions 78 and 13, are 5 to 7 orders of magnitude less important than the major destruction mechanisms.

Including the more realistic treatment of the radiation field in the calculations enhanced the levels of HO_2 at the surface from 30 percent for an albedo of 0.0 to 110 percent for an albedo of 1.00. Each time the albedo was increased by 0.25, the number density of HO_2 increased by about 20 percent. At the tropopause there was approximately a factor of two increase in the number

densities between the Leighton approximation and the cases including multiple scattering (see fig. 35). The increased levels are primarily due to enhanced levels of atomic hydrogen (H), methoxy (CH_3O), and hydroxyl (OH).

Hydroxyl radical (OH). -

Production		Destruction	
K16 :	$H_2O + O(^1D) \rightarrow 2OH$	K12 :	$CO + OH \rightarrow CO_2 + H$
K39 :	$HO_2 + O_3 \rightarrow OH + 2O_2$	K1 :	$CH_4 + OH \rightarrow CH_3 + H_2O$
J12 :	$CH_3OOH + h\nu \rightarrow OH + CH_3O$	K100:	$CH_3SCH_3 + OH \rightarrow$ Products
J9 :	$H_2O_2 + h\nu \rightarrow 2OH$	K14 :	$H_2 + OH \rightarrow H + H_2O$
K66 :	$HS + O_2 \rightarrow OH + SO$	K10 :	$CH_2O + OH \rightarrow HCO + H_2O$
J7 :	$HNO_3 + h\nu \rightarrow OH + NO_2$	K38 :	$O_3 + OH \rightarrow HO_2 + O_2$
J8 :	$HNO_2 + h\nu \rightarrow OH + NO$	K5 :	$CH_3OOH + OH \rightarrow CH_3O_2 + H_2O$
K22 :	$HO_2 + NO \rightarrow OH + NO_2$	K24 :	$NO_2 + OH + M \rightarrow HNO_3 + M$
K78 :	$HO_2 + SO_2 \rightarrow OH + SO_3$	K64 :	$H_2S + OH \rightarrow HS + H_2O$
K2 :	$CH_4 + O(^1D) \rightarrow OH + CH_3$	K18 :	$HO_2 + OH \rightarrow H_2O + O_2$
K13 :	$HO_2 + CO \rightarrow OH + CO_2$	K21 :	$H_2O_2 + OH \rightarrow HO_2 + H_2O$
K17 :	$H_2 + O(^1D) \rightarrow OH + H$	K77 :	$SO_2 + OH + M \rightarrow HSO_3 + M$
K102:	$O + H_2S \rightarrow OH + HS$	K48 :	$NH_3 + OH \rightarrow NH_2 + H_2O$
K113:	$H_2O + NO_3 \rightarrow OH + HNO_3$	K105:	$HSO_3 + OH \rightarrow SO_3 + H_2O$
K47 :	$NH_3 + O(^1D) \rightarrow OH + NH_2$	K26 :	$HNO_3 + OH \rightarrow NO_3 + H_2O$
K51 :	$NH_2 + O \rightarrow OH + NH$	K86 :	$COS + OH \rightarrow HS + CO_2$
K46 :	$NH_3 + O \rightarrow OH + NH_2$	K25 :	$NO + OH \rightarrow HNO_2$

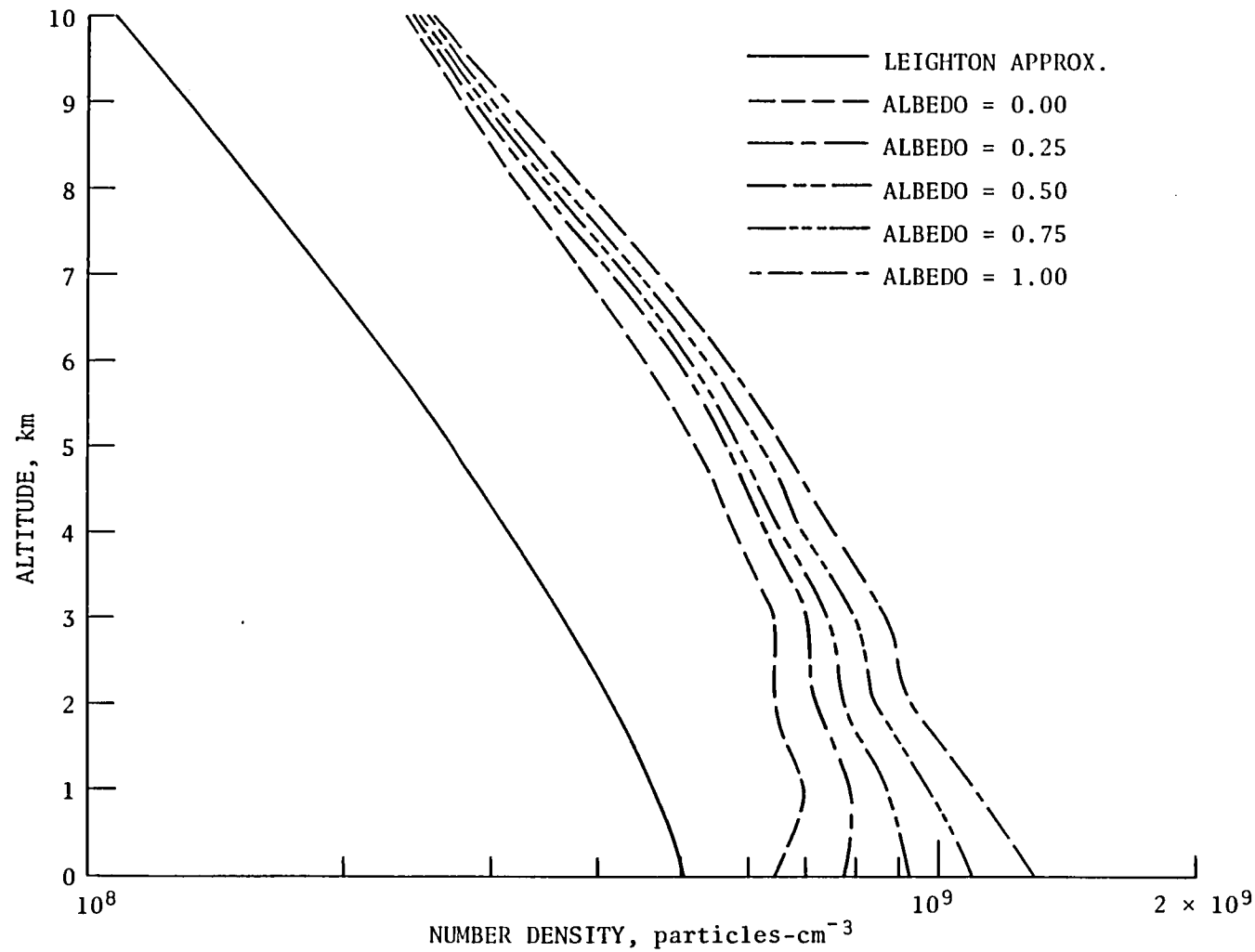

Figure 35. Vertical distributions of NO_2 for the multiple scattering cases with various albedos and the Leighton approximation.

Production (concl'd)	Destruction (concl'd)
K110: $HNO_3 + O \rightarrow OH + NO_3$	K87 : $CS_2 + OH \rightarrow HS + COS$
	K19 : $OH + OH \rightarrow H_2O + O$
	K40 : $HNO_2 + OH \rightarrow NO_2 + H_2O$
	K97 : $CH_3SH + OH \rightarrow$ Products
	K52 : $NH_2 + OH \rightarrow NH_3 + O$

Of the 114 chemical equations included in this model, 40 involve the hydroxyl radical. The fact that 35 percent of the total chemical processes involve this molecule is a testimony to its pivotal role in tropospheric photochemistry. The hydroxyl radical is formed primarily when water vapor (H_2O) reacts with the excited oxygen atom [$O(^1D)$] (reaction 16) and when the hydroperoxyl radical (HO_2) reacts with ozone (O_3) (reaction 39). These two reactions together account for approximately 85 percent of the total hydroxyl production at the surface (see table 27). Since ozone photolysis in the near-UV region ($\lambda < 320$ nm) produces the excited oxygen atom, it is very apparent that the abundance of ozone constitutes an important parameter, both explicitly and implicitly, in the formation of OH. Minor contributions are due to photolysis of the methylhydroperoxy radical (J12) and of hydrogen peroxide (J9) together with the oxidation of HS by molecular oxygen (O_2) (reaction 66). These processes account for 7.8, 3.9, and 3.2 percent of the total OH production, respectively. Very minor sources of OH are the photolysis of nitric acid (HNO_3) (J7), of nitrous acid (HNO_2) (J8), and the reaction of HO_2 with NO (reaction 22). These three processes provide only small fractions of the total OH production. They are responsible for 0.13, 0.08, and 0.05 percent, respectively. The remaining 10 reactions producing OH are between 4 and 9 orders of magnitude smaller than the predominating terms. In the higher regions of the troposphere, the reaction of water vapor (H_2O) with the excited oxygen atom [$O(^1D)$] is not as dominant as near the surface. Although the abundance of $O(^1D)$ increases with increased altitude, the rapid decrease of water vapor with altitude decreases the share of reaction 16 to some 25 percent at the tropopause.

Table 27. Production and destruction terms of OH and percent of total production and destruction.

Production Rate (molecules-cm^{-3}-s^{-1}) and Percent of Total Production

Altitude, km	K16	%	K39	%	J12	%	J9	%	K66	%	J7	%
10	4.050 E-4	25.49	9.702 E-4	61.07	1.997 E-4	12.57	4.993 E-2	0.31	5.628 E-1	0.04	4.398 E-2	0.28
5	2.975 E-5	46.23	2.706 E-5	42.05	6.519 E-4	10.13	8.377 E-3	1.30	3.588 E-2	0.06	7.648 E-2	0.12
0	1.170 E-6	57.53	5.561 E-6	27.34	1.578 E-5	7.76	7.980 E-4	3.92	6.494 E-4	3.19	2.560 E-3	0.13

Altitude, km	J8	%	K22	%	K78	%	K2	%	K13	%	K17	%
10	2.841 E-2	0.18	1.565 E-1	0.01	2.564 E-1	-	5.906 E-1	0.04	1.226 E-0	-	1.499 E-1	0.01
5	5.457 E-2	0.08	1.185 E-2	0.02	3.017 E-0	-	4.195 E-1	0.01	4.900 E-0	-	1.065 E-1	-
0	1.527 E-3	0.08	1.022 E-3	0.05	1.286 E-2	-	2.533 E-1	-	1.544 E-1	-	6.422 E-0	-

Altitude, km	K102	%	K113	%	K47	%	K51	%	K46	%	K110	%	Total	%
10	1.320 E-4	-	6.423 E-6	-	3.938 E-2	-	4.727 E-3	-	2.188 E-5	-	1.169 E-3	-	1.589 E-5	100.00
5	2.687 E-3	-	5.786 E-3	-	2.967 E-2	-	5.266 E-3	-	9.574 E-4	-	8.440 E-4	-	6.435 E-5	100.00
0	3.446 E-1	-	4.379 E-2	-	4.055 E-2	-	6.119 E-3	-	5.732 E-3	-	1.173 E-3	-	2.034 E-6	100.00

(continued)

Table 27. (Concluded.)

Destruction Frequency (s^{-1}) and Percent of Total Destruction

Altitude, km	K12	%	K1	%	K100	%	K14	%	K10	%	K38	%	K5	%
10	1.758 E-1	76.37	1.460 E-2	6.34	4.702 E-7	-	2.710 E-3	1.18	3.186 E-3	1.38	2.368 E-2	10.29	2.155 E-3	0.94
5	3.800 E-1	69.27	6.861 E-2	12.51	7.498 E-5	0.02	1.682 E-2	3.07	1.375 E-2	2.51	3.607 E-2	6.57	1.181 E-2	2.15
0	8.262 E-1	54.90	2.430 E-1	16.15	9.873 E-2	6.56	7.394 E-2	4.91	5.272 E-2	3.50	4.596 E-2	3.05	4.533 E-2	3.01

Altitude, km	K24	%	K64	%	K18	%	K21	%	K77	%	K48	%	K105	%
10	2.337 E-2	1.02	4.092 E-6	-	4.752 E-3	2.06	4.344 E-5	-	8.103 E-5	0.03	2.857 E-4	0.12	5.708 E-5	-
5	6.798 E-3	1.24	1.234 E-4	0.02	1.068 E-2	1.95	1.224 E-3	0.22	4.406 E-4	0.08	8.496 E-4	0.14	2.796 E-4	0.05
0	3.324 E-2	2.21	2.675 E-2	1.78	2.018 E-2	1.34	1.852 E-2	1.23	1.014 E-2	0.67	4.566 E-3	0.30	3.089 E-3	0.21

Altitude, km	K26	%	K86	%	K25	%	K87	%	K19	%	K40	%	K97	%
10	1.700 E-4	0.07	2.363 E-4	0.10	2.328 E-4	0.10	2.268 E-6	-	2.773 E-6	-	1.039 E-6	-	2.592 E-15	-
5	3.400 E-4	0.06	4.233 E-4	0.08	2.970 E-4	0.05	4.134 E-6	-	5.394 E-6	-	2.113 E-6	-	8.670 E-12	-
0	1.301 E-3	0.09	7.268 E-4	0.05	6.380 E-4	0.04	7.268 E-6	-	8.540 E-6	-	6.630 E-6	-	8.670 E-6	-

Altitude, km	K52	%	Total	%
10	1.348 E-8	-	2.303 E-1	100.00
5	4.160 E-8	-	5.486 E-1	100.00
0	1.341 E-7	-	1.505 E-0	100.00

The scale height of water vapor is only about two km, causing a very rapid "e-folding" of H_2O. The significance of a scale height is that, each time the vertical distance is increased by one scale height, the quantity under consideration has decreased by an amount that is equal to 1/e. Water vapor has, as mentioned earlier, a small-scale height of two km; other gases have scale heights that are larger. For example, the atmospheric pressure scale height is about eight km.

The second largest OH-producing term at the surface, reaction 39, dominates the production of hydroxyl radicals in the upper troposphere. At the tropopause, reaction 39 accounts for slightly more than 61 percent of the total OH production. Table 27 shows that reactions 16 and 39 reverse roles in the troposphere. The cumulative share of these 2 reactions to the total OH production is always between 85 and 88 percent, independent of altitude. Of the minor contributors, the photolysis of CH_3OOH increases with altitude as a source of OH, while photolysis of H_2O_2 and reaction 66 decrease. The remaining minor contributors account for approximately constant production of OH throughout the troposphere. In all, 22 reactions in this scheme destroy OH, and 11 of those are responsible for at least 1 percent at some tropospheric altitude. Another 6 reactions destroy between 0.01 and 1 percent, while 5 reactions can be neglected as OH sinks. The major destruction mechanism for the hydroxyl radical is the reaction of CO with OH (reaction 12). At the surface, this reaction deestroys about 55 percent of all hydroxyl molecules, in the midtroposphere 69.3 percent, and at the tropopause 76.4 percent. The second largest sink for hydroxyl is the reaction of OH with methane (CH_4) (reaction 1). This reaction accounts for shares varying from 16 percent at the surface to 6.3 percent at the tropopause. The third largest destruction mechanism at the surface is the reaction of dimethyl sulfide (DMS) (CH_3SCH_3) with OH (reaction 100). At the surface, DMS reacting with hydroxyl provides 6.6 percent of the total OH sink. In the midtroposphere it is a minute sink (0.02), and at the tropopause a negligible sink. The reason this reaction decreases its influence with altitude is the rapid decrease in DMS abundance with altitude. Of the remaining loss terms, five reactions (14, 10, 5, 24, and 18) account for any

where from one to five percent of the total OH destruction depending on altitude. Ozone interacting with OH (reaction 38) comprises 3 percent of the hydroxyl destruction at the surface, increasing to 10 percent at the tropopause. Of the remaining 13 chemical reactions destroying OH, 8 reactions (64, 21, 77, 48, 105, 26, 86, and 25) account for anywhere from 0.00 to 1.8 percent depending on altitude. The last 5 reactions (87, 19, 40, 97, and 52) are between 5 and 15 orders of magnitude less important as OH destruction mechanisms than the primary loss terms.

The photochemical lifetime of OH is on the order of one second. The importance of the hydroxyl radical as a sink for reduced species (such as CH_4, CH_3SCH_3, H_2, H_2S, NH_3, and CS_2), as well as partly oxidized species (e.g., CO, CH_2O, CH_3OOH, NO_2, HO_2, H_2O_2, SO_2, HSO_3, HNO_3, and COS), has long been recognized (ref. 3). Since OH plays such a central role in tropospheric photochemistry, it is absolutely essential to learn the distribution of this radical. Large differences exist in the vertical profiles calculated with the Anderson-Meier radiation code compared to the Leighton approximation (see fig. 36). At the surface and in the lowest few km, a strong dependence on the surface albedo is evident. At higher altitudes, this dependence is diminished and the multiple scattering calculations are closely grouped together. At the surface, the multiple scattering calculation with an albedo of 0.00 increases the OH number density by a factor of 1.4 compared to the Leighton approximation. When the albedo is 0.25, this difference is nearly doubled at the surface, and, for a = 0.50, OH is enhanced by a factor of 2.5. Using an albedo of 0.75 yields a factor of 3.4 increase in OH, and for the case of a = 1.00 the number density of OH at the surface is approximately quadrupled. In the upper parts of the troposphere the multiple scattering calculations increase the OH number densitites by a factor of three compared to the Leighton approximation. Enhanced levels of OH are obtained with the multiple scattering code because of the enhanced levels of $O(^1D)$ which have already been discussed (see "Atomic oxygen").

Measurements of the hydroxyl radical seem to confirm the enhanced levels obtained with the Anderson-Meier model. The first tropospheric measurement of OH was that by Wang et al. (ref. 130) in 1974. A value of 1.5×10^7 molecules

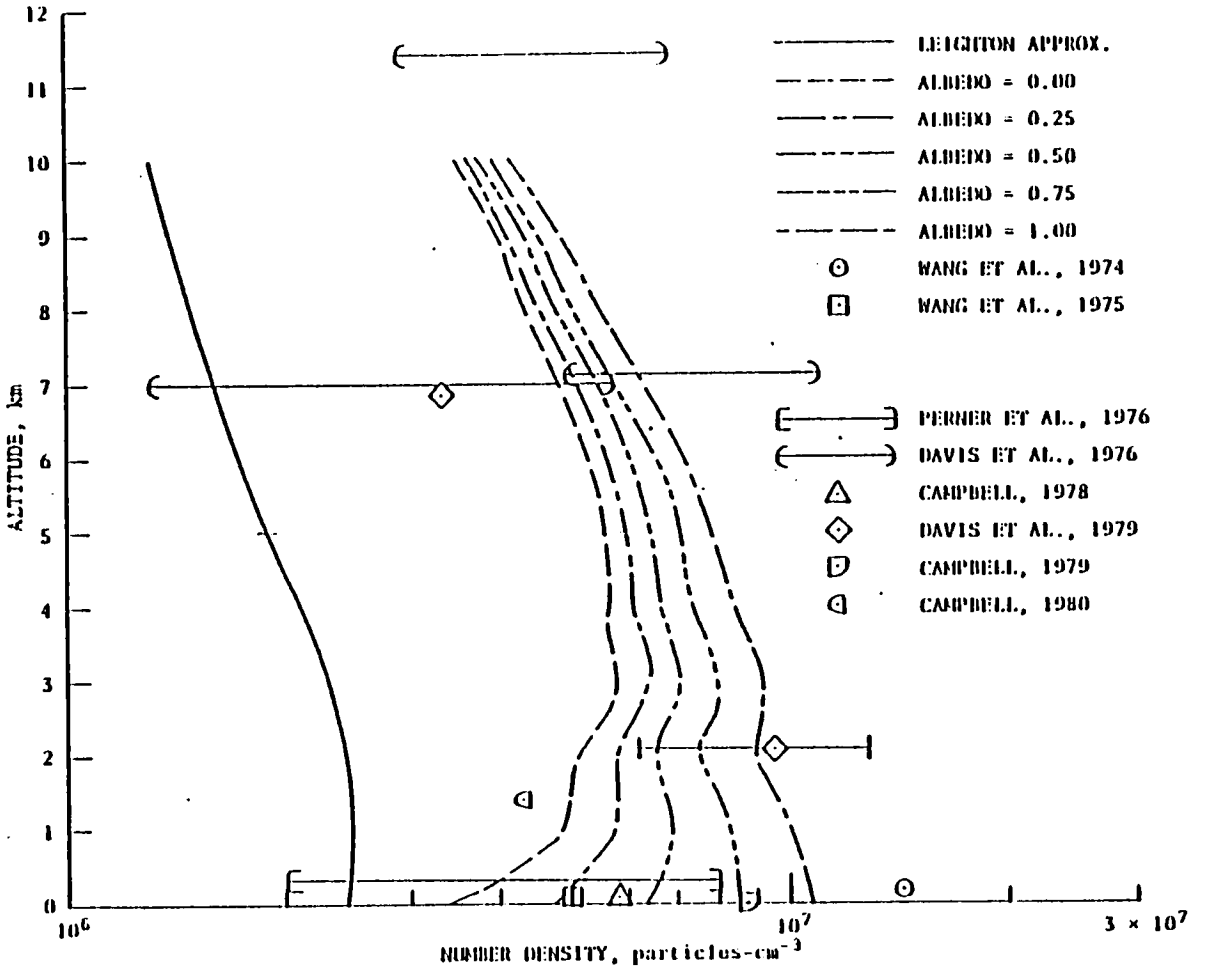

Figure 36. Vertical distributions of OH for the multiple scattering cases with various albedos and the Leighton approximation.

cm^{-3} was obtained; this is one of the highest values of tropospheric OH reported in the literature. Subsequent measurements by Wang et al. in 1975 (ref. 131) yielded a value of 5×10^6 molecules cm^{-3}. Perner et al. (ref. 132) measured hydroxyl at two different altitudes in 1976. The measured data near the surface had values ranging from 2 to 8×10^6 molecules cm^{-3} while the data at 2 km ranged from 6.4×10^6 to 1.3×10^7 molecules cm^{-3}. Davis et al. (ref. 133) also measured the hydroxyl radical in 1976, but at higher altitudes than Perner et al. The measurements at 7 km ranged from 1.3×10^6 to 1.1×10^7 depending on altitude, while the measurements at 11.5 km varied between 2.9 to 6.8×10^6 molecules cm^{-3}. More recent data by Campbell and Blankenship (ref. 134) yielded OH number densities of 5.8×10^6 molecules cm^{-3} in 1978 and 8.7×10^6 molecules cm^{-3} in 1979 (ref. 135). Davis et al. (ref. 136) measured OH at two altitudes in 1979. At 2 km, values ranged from 6.4×10^6 to 1.3×10^7 molecules cm^{-3}. At 7 km, a value of 3.3×10^6 molecules cm^{-3} was obtained. The most recent measurement is that of Campbell et al. (ref. 137) during the CHON-experiment on the Pawnee Grasslands in northern Colorado during the summer of 1980. A value of 4.3×10^6 molecules cm^{-3} was measured. All the above data have been transposed to figure 36 for comparison with the model calculated values. Clearly, a realistic treatment of the radiation field is necessary to obtain the higher value indicated by the measurements of several investigators.

Atomic hydrogen (H). -

Production		Destruction	
K12:	$CO + OH \rightarrow CO_2 + H$	K15 :	$O_2 + H + M \rightarrow HO_2 + M$
K14:	$H_2 + OH \rightarrow H_2O + H$	K84 :	$H_2S + H \rightarrow HS + H_2$
J10:	$CH_2O + h\nu \rightarrow HCO + H$	K114:	$HNO_3 + H \rightarrow$ Products
K17:	$O(^1D) + H_2 \rightarrow OH + H$	K85 :	$COS + H \rightarrow HS + CO$
K50:	$NH_2 + O \rightarrow HNO + H$	K42 :	$N_2H_4 + H \rightarrow N_2H_3 + H_2$
K56:	$NH + NO \rightarrow N_2 + O + H$	K49 :	$NH_3 + H \rightarrow NH_2 + H_2$

Production (concl'd)	Destruction (concl'd)
K95: $CH_3SH + O \rightarrow CH_3SO + H$	K82 : $HS + H \rightarrow H_2 + S$
K65: $HS + O \rightarrow SO + H$	K63 : $H + H + M \rightarrow H_2 + M$
K83: $S + H_2 \rightarrow HS + H$	K45 : $N_2H_3 + H \rightarrow 2NH_2$
K60: $HNO + M \rightarrow NO + H + M$	K61 : $HNO + H \rightarrow NO + H_2$

Atomic hydrogen (H) is involved in a total of 20 reactions: 10 produce it and 10 destroy it. Of the 10 terms producing H, only 3 are significant contributors. The primary path of H formation occurs as a result of carbon monoxide reacting with the hydroxyl radical (reaction 12). At the surface, 88 percent of all H atoms are formed this way, decreasing to slightly less than 75 percent at 10 km. Two secondary sources of hydrogen atoms in the troposphere are the reaction of molecular hydrogen (H_2) with the hydroxyl radical (OH) (reaction 14) and the photolysis of formaldehyde (CH_2O). At the surface, reaction 14 produces almost 8 percent of the total amount of hydrogen atoms, decreasing to about 1 percent at the tropopause. Photolysis of formaldehyde accounts for nearly 4 percent of all hydrogen atoms that are produced near the surface and increases to about 24 percent at the tropopause. The remaining 7 reactions that produce H atoms are of little or no significance, being between 4 to 42 orders of magnitude smaller than the primary source of hydrogen (see table 28). Atomic hydrogen is destroyed almost entirely by the oxidation with molecular oxygen (O_2) in the presence of a third body M (reaction 15). The other 9 reactions destroying atomic hydrogen are anywhere from 5 to 21 orders of magnitude less important than the primary source depending on altitude (see table 28). The chemical lifetime of atomic hydrogen is very short, approximately 10^{-7} s. The vertical profiles of H are altered significantly when the Anderson-Meier radiation model is coupled to the photochemical model (see fig. 37). The differences between the Leighton approximation and the multiple scattering calculations are very similar in magnitude to those calculated for OH. In fact, the vertical profiles of atomic hydrogen form a nearly perfect overlay to the vertical profiles of OH. This is readily understood from inspection of

Table 28. Production and destruction terms of H and percent of total production and destruction.

Production Rate (molecules-cm^{-3}-s^{-1}) and Percent of Total Production

Altitude, km	K12	%	K14	%	J10	%	K17	%	K50	%	K56	%
10	2.289 E-5	74.66	3.528 E-3	1.15	7.416 E-4	24.19	1.499 E-1	-	4.727 E-3	-	5.016 E-3	-
5	7.242 E-5	85.64	3.207 E-4	3.79	8.932 E-4	10.57	1.183 E-1	-	5.266 E-3	-	5.421 E-3	-
0	2.000 E-6	88.16	1.790 E-5	7.89	8.955 E-4	3.95	6.422 E-0	-	6.189 E-3	-	6.188 E-3	-

Altitude, km	K95	%	K65	%	K83	%	K60	%	Total	%
10	2.821 E-12	-	9.759 E-10	-	1.197 E-18	-	1.171 E-37	-	3.066 E-5	100.00
5	3.410 E-9	-	1.263 E-9	-	1.133 E-18	-	1.448 E-31	-	8.456 E-5	100.00
0	1.242 E-4	-	4.984 E-8	-	9.630 E-19	-	8.321 E-27	-	2.269 E-5	100.00

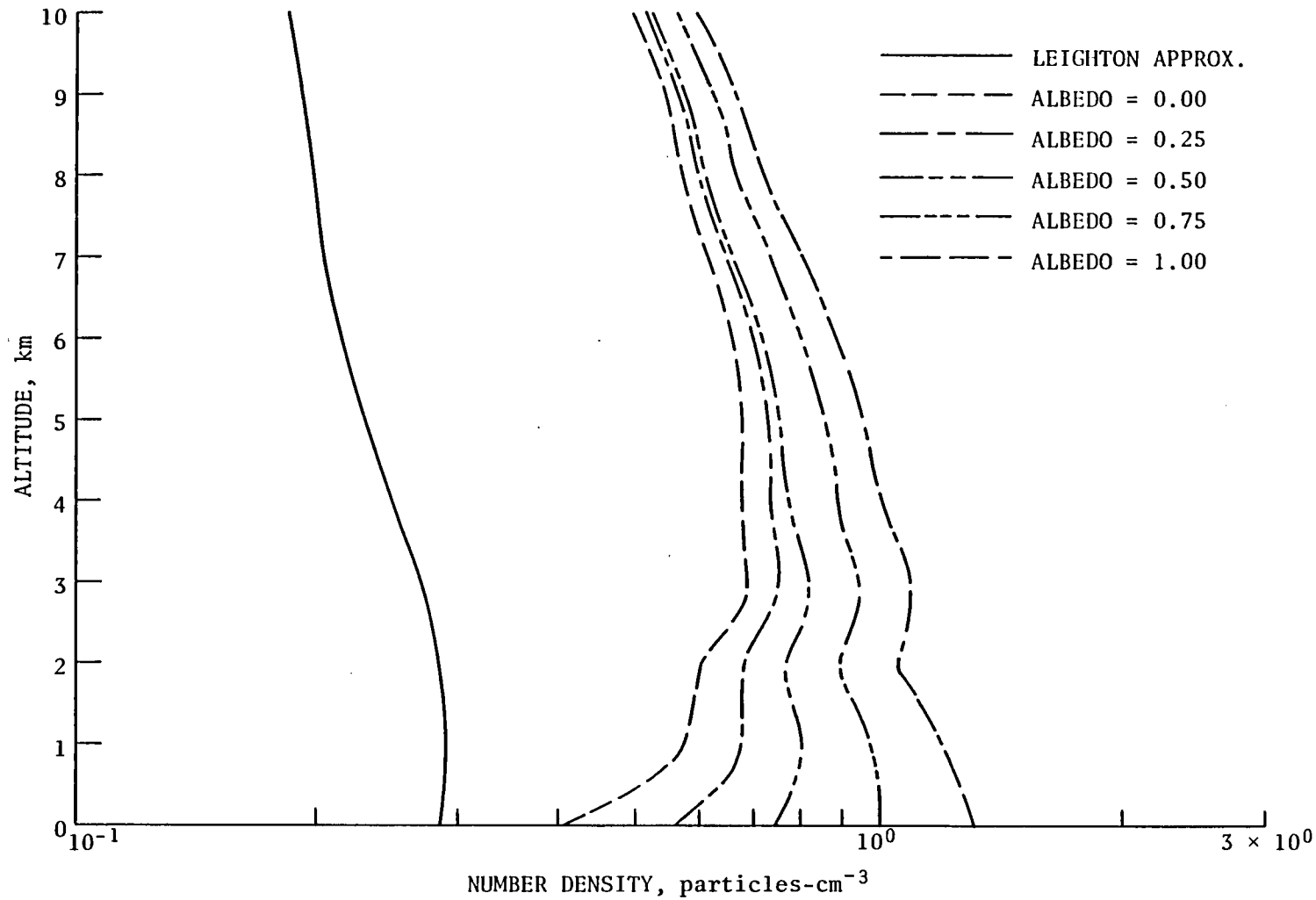

Figure 37. Vertical distributions of H for the multiple scattering cases with various albedos and the Leighton approximation.

the list of reactions producing atomic hydrogen as well as table 27. Reactions 12 and 14, which both depend on OH for production of H, together account for about 76 percent of the total production at the surface, decreasing to 66 percent at the tropopause. Consequently, it is not surprising to find large similarities in the vertical profiles of hydrogen and hydroxyl. Thus, the discussion concerning the enhanced intensity factor in the ratio of multiple scattering calculations to the Leighton approximation in the previous section on OH also applies to H. There are no atmospheric measurements of H available.

Future perturbations to the hydrogen budget. - The two most abundant hydrogen species, water vapor and molecular hydrogen, appear to be stable enough that anthropogenic perturbations will not significantly alter their distributions. A systematic, global-scale temperature increase from the CO_2 greenhouse effect may increase the water vapor content in the atmosphere slightly. Hydrogen peroxide (H_2O_2) is believed to act as a precursor for photochemical production of smog, as well as being involved in the formation of acid rain (ref. 128). Photochemical smog is a severe problem on a local scale in many metropolitan areas. Smog is usually formed when hydroxyl radicals react with odd nitrogen (NO_x) and hydrocarbons (HC) during certain meteorological conditions, such as temperature inversion, low windspeeds, and high atmospheric pressure. Acid rain is an ever-increasing problem on a regional scale. The industrialized parts of the world, in particular the northeastern part of the United States and Atlantic provinces of Canada, parts of California, and a large portion of western Europe, especially Scandinavia, have been plagued by this problem over the last couple of decades. Acid rain decreases crop yields and tree growth. The acidification of many lakes and streams decreases the fish population and consequently affects the sizes of fish catches. In addition to these basic issues of perturbations in the food supply, many esthetic art works are also threatened. For example, some of the exposed art works of marble in Venice, Italy are etched away at a staggering rate of six percent per year due to acid rain and air pollution (ref. 138). The problem of acidic precipitation will be discussed further in the section dealing with sulfur species [see, for example, "Sulfuric acid (H_2SO_4)"].

The most significant perturbations in tropospheric composition would occur if the abundance of the hydroxyl radical were altered. Ozone initiates a great deal of tropospheric chemistry (see discussion of "Ozone" under "The Oxygen Group"). Photolysis of ozone in the region from 300 to 320 nm results in the excited, metastable oxygen atom [$O(^1D)$], which very rapidly combines with water vapor to form two hydroxyl molecules. Thus, a change in ozone concentration would affect tropospheric photochemistry in two ways. By changing the tropospheric radiation field and by altering the abundance of $O(^1D)$. Both of these changes would significantly affect the distribution of hydroxyl. As already shown (see "Hydroxyl radical"), the number density of the hydroxyl radical is the rate-limiting factor for many tropospheric species. Due to the short lifetime of OH, any change in its abundance would necessarily be due to in situ photochemistry. Not only ozone, but also oxides of nitrogen can alter the level of hydroxyl. The reaction of HO_2 with NO (reaction 22) can produce OH (ref. 112). However, the magnitude of this source term is very uncertain since the measurements of background levels of tropospheric NO_x are highly variable. The most recent measurements of nitric oxide in pristine air have yielded relatively small concentrations which would tend to diminish the importance of reaction 22 as a source of OH (refs. 87-89). Presently, the strength of global NO_x emission is not very well known, although it is believed that the anthropogenic portion of NO_x emission may have increased at a five percent rate per year until catalytic convertors were made mandatory to decrease the pollution due to automobile exhaust (ref. 139). The interactions of the O_3-OH-NO_x system are in need of further study.

The Carbon Group

Introduction. - The eight carbon species included in this model are products of the oxidation of methane by the hydroxyl radical. Consequently, this sequence of reactions is known as the methane oxidation chain and is depicted in figure 38. Ultimately the oxidation of methane results in carbon monoxide (CO) and carbon dioxide (CO_2). Carbon dioxide is not included in the present model, as is customary with most photochemical models. Carbon dioxide is chem-

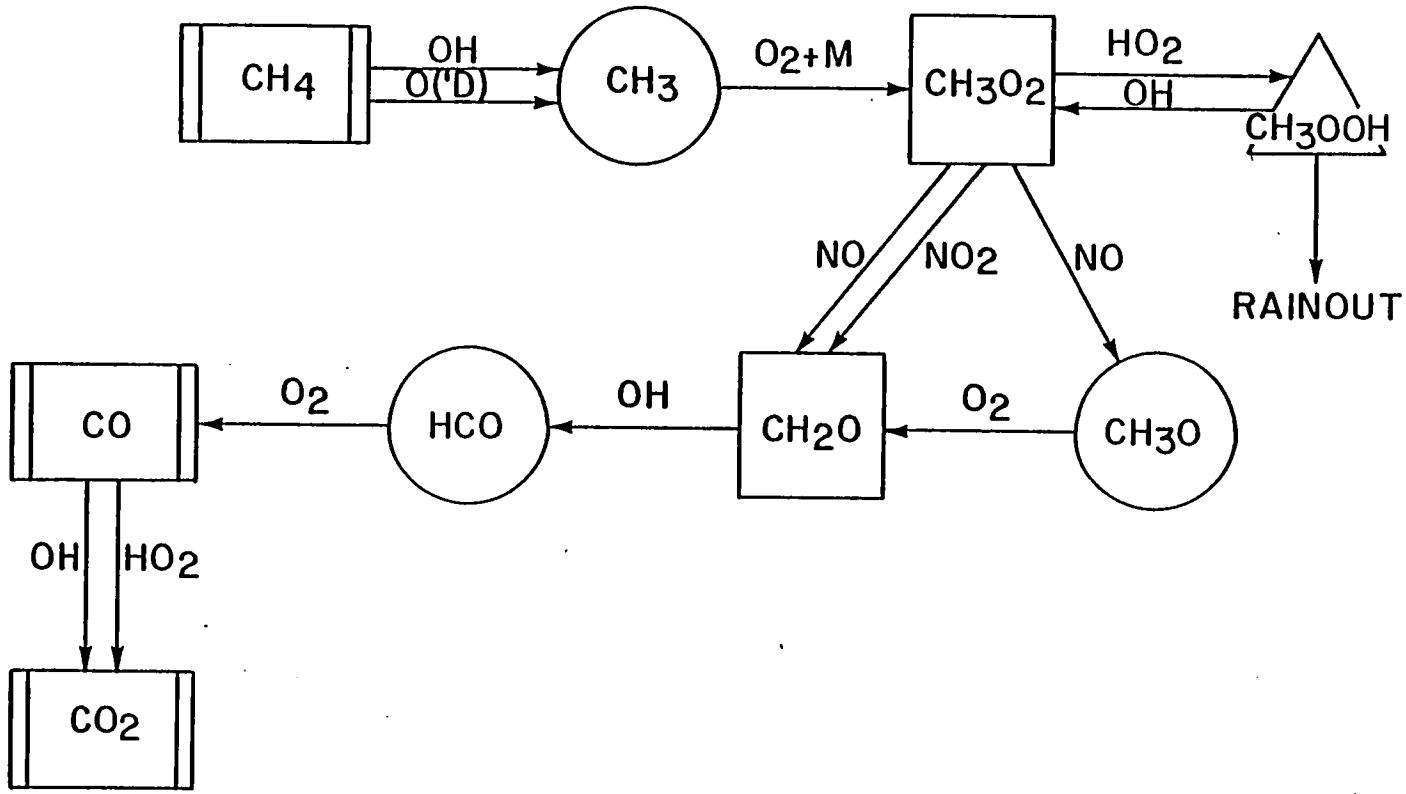

Figure 38. Reaction paths of the carbon family.

ically very inert and has a long lifetime of about five years. Hence, from a photochemical point of view, no accuracy is lost by omitting CO_2. Most of the atmospheric studies concerning CO_2 have centered on its thermal properties. This will be addressed further in the subsection titled "Future perturbations to the carbon budget."

Carbon monoxide is of great importance in tropospheric photochemistry since it is the main sink for hydroxyl. The abundance of carbon monoxide from the oxidation of methane could possibly be affected by the removal of intermediate species in the methane oxidation chain, namely methylhydroperoxy (CH_3OOH) and formaldehyde (CH_2O). These two species are believed to undergo heterogeneous removal, but the mechanisms for this removal are very uncertain.

Methane (CH_4). - Methane is a relatively long-lived species in the troposphere. Its mean tropospheric lifetime is on the order of four years. It is formed primarily by anaerobic decomposition in swamps, tidal flats, rice paddies, and estuaries. An average acre in a wetland might produce as much CH_4 as 1,361 kg/yr (3,000 lb/yr). Even domesticated animals produce large amounts of methane. Flatulence from the ruminants is accountable for an estimated 85×10^6 tons of CH_4 per year (ref. 140). In addition to the large natural sources of methane, there are also anthropogenic sources. Coal mining activities and oil drilling release methane into the atmosphere. The manmade activities are thought to account for 9 percent of the total amount of CH_4 with the remaining 91 percent from natural sources (ref. 141). There are no known chemical reactions in the atmosphere that produce CH_4. Hence, methane is released at the surface and diffuses upward, where it initiates a very important chemical cycle known as the methane oxidation chain (ref. 142).

The chemical cycle is graphically depicted in figure 38. Methane, together with carbon monoxide, is an important sink for hydroxyl. It is the reaction of methane with hydroxyl that initiates the methane oxidation chain that eventually produces carbon monoxide (CO) and carbon dioxide (CO_2). Carbon dioxide is not included in the present model, as is customary with most photochemical

models. Because carbon dioxide is chemically very inert and has a long lifetime of about five years, from a photochemical point of view no accuracy is lost by omitting CO_2. Most of the atmospheric studies concerning CO_2 have centered on its thermal properties. This will be addressed further under "Formyl radical."

Carbon monoxide (CO). - Carbon monoxide is a relatively unreactive species in the troposphere with a mean lifetime of approximately four months. It is well mixed in the vertical direction, but shows a large latitudinal gradient. The Northern Hemisphere has a mean concentration of approximately 0.20 parts per million by volume (ppmv), while the Southern Hemisphere has a mean concentration of about 0.05 ppmv (ref. 143). This large hemispherical asymmetry has been interpreted as evidence of large-scale anthropogenic modifications. The majority of the Earth's population lives in the Northern Hemisphere, where most anthropogenic activities occur. Manmade activities believed to cause increases in the carbon monoxide concentration include automobile emissions and emissions from industrial plants. As much as 82 percent of all surface emissions of CO are believed to be industrial in origin (ref. 141). Any combustion process that is insufficiently oxidized leads to CO production. In high concentrations CO is very toxic.

On the local scale, CO is clearly a pollutant of considerable concern. An exposure to a concentration of 120 ppm for an hour is serious enough to severely restrict a person's ability to pursue activities that require coordination, such as driving an automobile, yet the average CO concentration in many tunnels, garages, and even the streets of metropolitan areas frequently exceeds 100 ppm (ref. 138). On the global scale, however, CO derives most of its importance as the sink for the hydroxyl radical

$$CO + OH \rightarrow CO_2 + H$$

In the present model carbon monoxide is treated as input with a globally averaged concentration of 0.125 ppm.

Methylhydroperoxy (CH_3OOH). -

Production	Destruction
K4: $CH_3O_2 + HO_2 \rightarrow CH_3OOH + O_2$	J12: $CH_3OOH + h\nu \rightarrow CH_3O + OH$
	K5 : $CH_3OOH + OH \rightarrow CH_3O_2 + H_2O$

The methylhydroperoxy radical (CH_3OOH) is formed as an intermediate species in the methane oxidation chain. It is formed when the methylperoxy radical (CH_3O_2) combines with the hydroperoxyl radical (HO_2). Chemical destruction terms include oxidation with OH (reaction 5), yielding the methylperoxy radical and water vapor, and photolysis (J12), resulting in the formation of the methoxy radical and hydroxyl radical. Methylhydroperoxy is also believed to undergo heterogeneous losses. Chemically, the primary loss mechanism at all altitudes is photolysis (J12) (see table 29). At the surface, photodissociation destroys about 59 percent of the CH_3OOH molecules, while 41 percent of the destruction occurs via the path provided by reaction 5. Photolysis increases its importance with altitude such that, at the tropopause, more than 87 percent is lost by photolysis and approximately 12 percent is lost by reaction 5.

The chemical lifetime of CH_3OOH based on these calculations is slightly more than four days, hence it is necessary to use the continuity equation to calculate its vertical distribution. There are no tropospheric measurements available to use as a guide for boundary conditions. A condition of zero flux was used at both the upper and lower boundaries yielding the vertical profiles in figure 39. Inclusion of multiple scattering and surface albedo increases the number densities at the surface about 50 percent compared to the Leighton approximation. This enhancement is due primarily to the increased level of HO_2. The photolysis frequency at the surface is only increased by six percent (see "Comparison of Calculated Photodissociation Frequencies Using the Leighton Approximation and the Matrix Inversion Technique"). Consequently, the loss terms at the surface are not altered significantly between the Leighton approximation and the calculations with multiple scattering included. Thus, the net effect is to increase number densities in the lower regions of the troposphere.

Table 29. Production and destruction terms for CH_3OOH and percent of total production and destruction.

Production Rate (molecules-cm^{-3}-s^{-1}) and Percent of Total Production

Altitude, km	K4	%
10	6.566 E-3	100.00
5	7.452 E-4	100.00
0	3.483 E-5	100.00

Destruction Frequency (s^{-1}) and Percent of Total Destruction

Altitude, km	J12	%	K5	%	Total	%
10	1.997 E-6	87.62	2.882 E-7	12.38	2.279 E-6	100.00
5	1.821 E-6	74.33	6.289 E-7	25.67	2.450 E-6	100.00
0	1.596 E-6	58.94	1.112 E-6	41.06	2.708 E-6	100.00

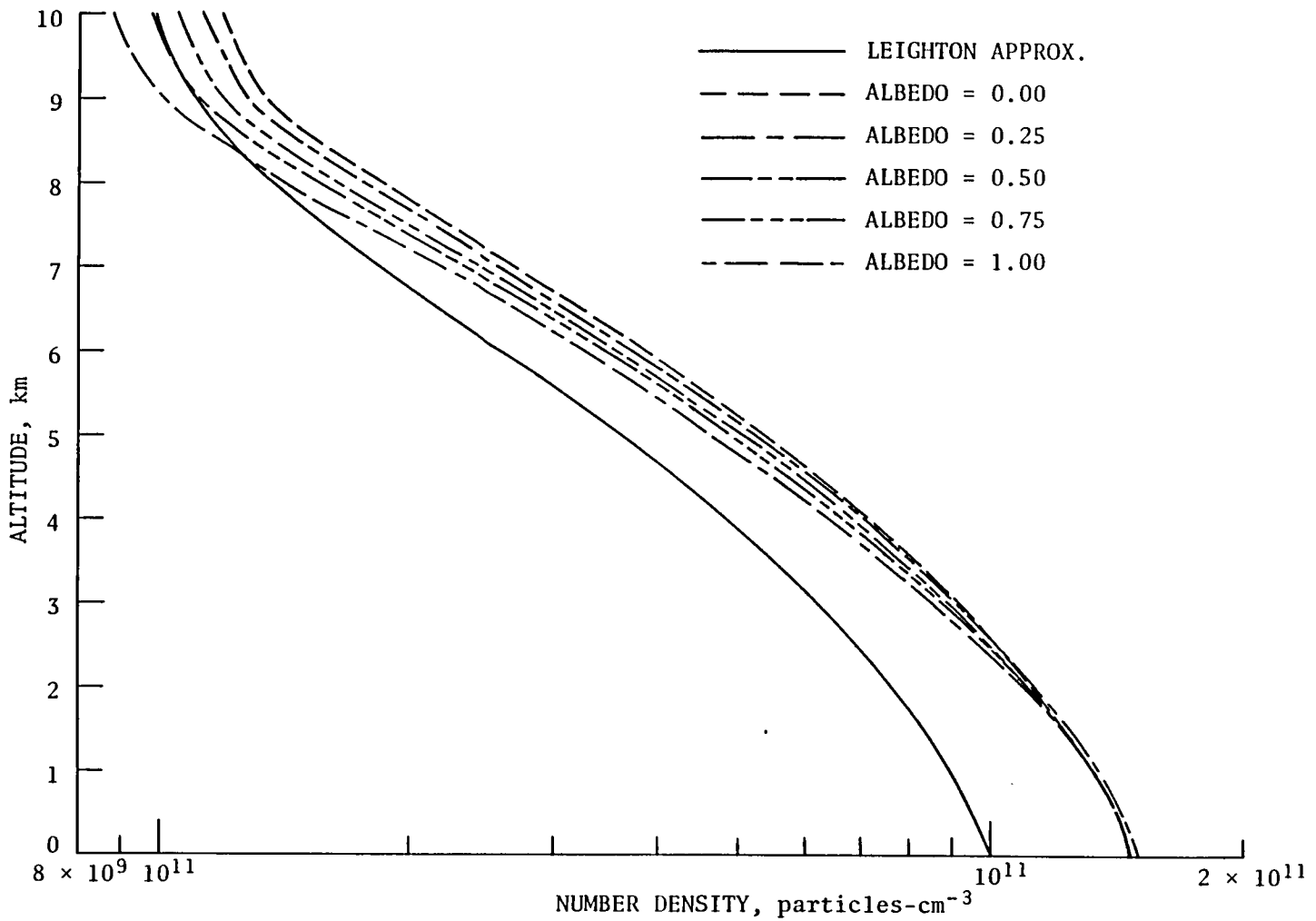

Figure 39. Vertical distributions of CH_3OOH for the multiple scattering cases with various albedos and the Leighton approximation.

Near the tropopause photolysis is more than doubled when the multiple scattering code is used. In addition, photodissociation is the predominant loss mechanism at high altitudes, with the net effect of decreasing the number densities for the multiple scattering calculations compared to the Leighton approximation.

Formaldehyde (CH_2O). -

Production	Destruction
K9 : $CH_3O + O_2 \rightarrow CH_2O + HO_2$	J11: $CH_2O + h\nu \rightarrow H_2 + CO$
K41: $CH_4 + O(^1D) \rightarrow CH_2O + H_2$	K10: $CH_2O + OH \rightarrow HCO + H_2O$
	J10: $CH_2O + h\nu \rightarrow HCO + H$

Formaldehyde (CH_2O) is formed chemically from the methane oxidation chain by the reaction of the methoxy radical with molecular oxygen (reaction 9) and also, but less significantly, by the reaction of methane and the excited oxgen atom (reaction 41). Formaldehyde is also emitted anthropogenically as a result of incomplete combustion by automobiles and diesel engines (ref. 144). It has also been suggested that aldehydes are emitted biogenically through plants (ref. 145). The chemical losses are due to photolysis with two different paths (J10 and J11), as well as reaction with OH (reaction 10) (see table 30). The photodissociation leading to H_2 and CO (J11) dominates throughout the troposphere with values ranging from 57 percent at the surface to 67 percent at the tropopause. Secondary losses are due to the reaction with OH (reaction 10), which is responsible for 25 percent of the total loss of CH_2O at the surface, and to the photolysis leading to HCO + H_2O (J10) (approximately 18%). In the midtroposphere, these two loss mechanisms are of equal importance, while in the higher regions of the troposphere photolytic reaction J10 becomes the secondary loss mechanism (21%) and reation 10 is tertiary (nearly 12%). The chemical lifetime of CH_2O based on the reactions above is approximately two hours, but it has been postulated that formaldehyde undergoes a significant amount of

Table 30. Production and destruction terms for CH_2O and percent of total production and destruction.

Production Rate (molecules-cm^{-3}-s^{-1}) and Percent of Total Production

Altitude, km	K9	%	K41	%	Total	%
10	3.548 E-4	99.98	6.361 E-0	0.02	3.549 E-4	100.00
5	1.423 E-5	100.00	4.517 E-0	-	1.423 E-5	100.00
0	5.035 E-5	100.00	2.725 E-0	-	5.035 E-5	100.00

Destruction Frequency (s^{-1}) and Percent of Total Destruction

Altitude, km	J11	%	K10	%	J10	%	Total	%
10	8.030 E-5	67.07	1.414 E-5	11.81	2.528 E-5	21.12	1.197 E-4	100.00
5	7.468 E-5	62.32	2.191 E-5	18.29	2.324 E-5	19.39	1.198 E-4	100.00
0	6.632 E-5	57.22	2.909 E-5	25.10	2.050 E-5	17.68	1.159 E-4	100.00

heterogeneous loss which would act to further decrease its lifetime. The extent to which heterogeneous losses contribute to the overall loss of CH_2O is presently not very well known.

Formaldehyde has been measured extensively in urban air (ref. 146), as well as in more pristine rural settings (ref. 147) and over the ocean (ref. 148). The most recent masurements of background concentrations of formaldehyde indicate levels of less than 0.3 ppbv (ref. 85), 0.4 ppbv (ref. 148), and 0.0 to 2.0 ppbv (ref. 147) respectively. These measurements have been transposed to figure 40 and generally show a good agreement with the calculated profiles of CH_2O. The effects of albedo and multiple scattering increase the number density for low values of the albedo. This is easily understood by inspection of tables 10 and 11. Initially, at the surface, there is no appreciable effect for the photolytic reaction J10 compared to the Leighton approximation, and for reaction J11 there is a five percent decrease in the photodissociation frequency. This insensitivity to photodissociation coupled with enhanced values for CH_3O and $O(^1D)$ has the effect of increasing the surface concentration of CH_2O. As one ascends through the troposphere and simultaneously considers higher values for albedos, the increase is diminished. For an albedo of 1.00 above 8 km, formaldehyde is decreased below the level obtained using the Leighton approximation. This can also be explained for the values in tables 10 and 11. For high albedos and high altitudes, there is more than a factor of three increase in the photodissociation frequencies J10 and J11. Hence, the destruction mechanism for formaldehyde is enhanced, resulting in decreased levels of CH_2O.

Methylperoxy radical (CH_3O_2). -

Production		Destruction	
K3:	$CH_3 + O_2 + M \rightarrow CH_3O_2 + M$	K4:	$CH_3O_2 + HO_2 \rightarrow CH_3OOH + O_2$
K5:	$CH_3OOH + OH \rightarrow CH_3O_2 + H_2O$	K109:	$CH_3O_2 + CH_3O_2 \rightarrow 2CH_3O + O_2$
		K79 :	$CH_3O_2 + SO_2 \rightarrow CH_3O + SO_3$
		K7:	$CH_3O_2 + NO_2 \rightarrow CH_2O + HNO_3$

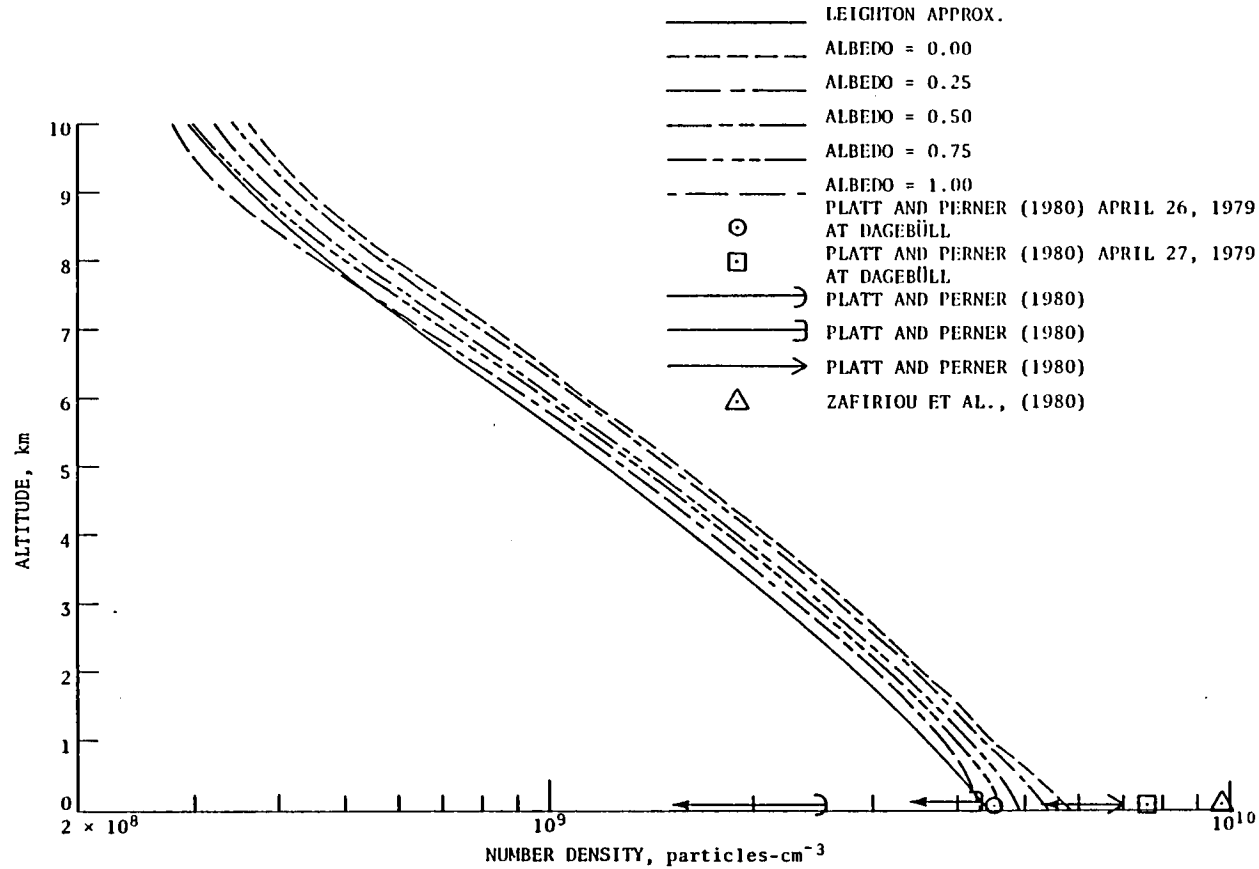

Figure 40. Vertical distributions of CH_2O for the multiple scattering cases with various albedos and the Leighton approximation.

The methylperoxy radical (CH_3O_2) is formed primarily as a result of the reaction of molecular oxygen with the methyl radical in the presence of a third body (reaction 3). A secondary contributor is the reaction of CH_3OOH with OH (reaction 5). An inspection of table 31 reveals that reaction 3 accounts for approximately 85 percent of the CH_3O_2 production, regardless of altitude. The remaining 15 percent is due to reaction 5.

Chemical destruction of CH_3O_2 is due to four different reactions. The primary loss mechanism is reaction 4, which results in between 95 and 97 percent of the total tropospheric loss, depending on altitude. Methylperoxy radical with itself (reaction 109) accounts for approximately 2.5 percent, while the reaction of CH_3O_2 with NO_2 (reaction 7) is responsible for about 0.5 percent of the total loss. Reaction 79, SO_2 with CH_3O_2, is somewhat altitude dependent with 1.5 percent of the total loss at the surface proceeding through this path, diminishing in importance to 0.1 percent at the tropopause. The chemical lifetime of the methylperoxy radical at the surface, based on the chemistry described above, is about six minutes. The effect of multiple scattering and surface albedo on CH_3O_2 is shown in figure 41. The number densities of CH_3O_2 are slightly more than doubled for the multiple scattering calculations compared to the Leighton approximation. The choice of albedo makes approximately a 20 percent difference at the surface for each successive run, i.e., the number density of CH_3O_2 at the surface for the case of an albedo of 0.50 is about 20 percent greater than the case of an albedo of 0.25, which in turn is 20 percent greater than the case of a = 0.00. At higher altitudes, however, these differences are not as large. There are no measurements of CH_3O_2 available with which to compare the model calculated results.

Methoxy radical (CH_3O).

Production	Destruction
K8 : $CH_3O_2 + NO \rightarrow CH_3O + NO_2$	K9: $CH_3O + O_2 \rightarrow CH_2O + HO_2$
J12 : $CH_3OOH + h\nu \rightarrow CH_3O + OH$	

Table 31. Production and destruction terms of CH_3O_2 and percent of total production and destruction.

Altitude, km	K3	%	K5	%	Total	%
10	1.888 E-4	87.00	2.882 E-3	13.00	2.170 E-4	100.00
5	1.302 E-5	85.26	2.251 E-4	14.74	1.527 E-5	100.00
0	5.868 E-5	84.24	1.098 E-5	15.76	6.966 E-5	100.00

Destruction Frequency (s^{-1}) and Percent of Total Destruction

Altitude, km	K4	%	K109	%	K79	%	K7	%	Total	%
10	3.811 E-4	97.08	8.960 E-6	2.28	3.561 E-7	0.10	2.129 E-6	0.54	3.925 E-4	100.00
5	1.133 E-3	96.49	3.421 E-5	2.91	1.865 E-6	0.16	5.160 E-6	0.44	1.173 E-3	100.00
0	2.669 E-3	95.31	6.706 E-5	2.42	4.208 E-5	1.51	2.141 E-5	0.76	2.800 E-3	100.00

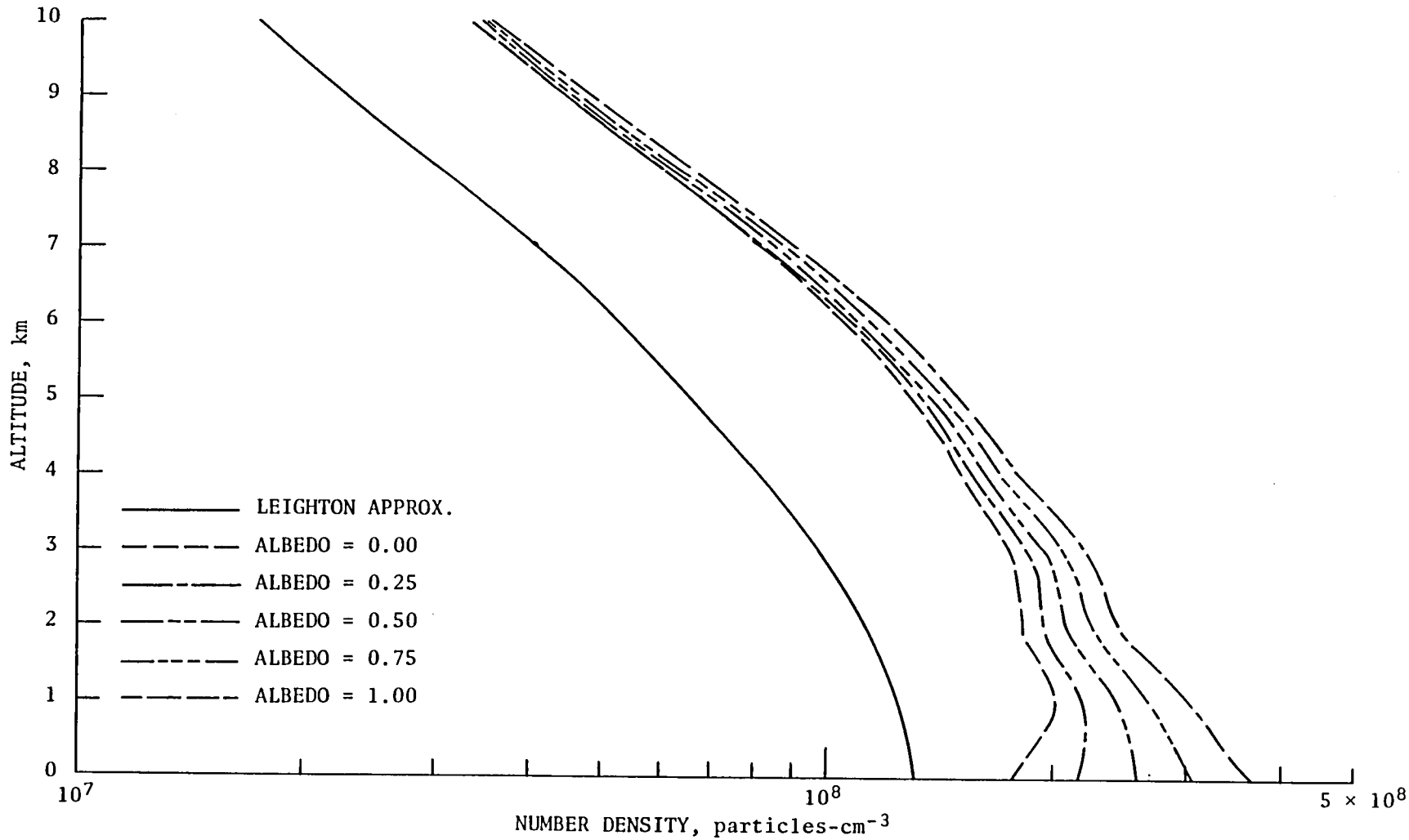

Figure 41. Vertical distributions of CH_3O_2 for the multiple scattering cases with various albedos and the Leighton approximation.

Production (concl'd)

K109: $CH_3O_2 + CH_3O_2 \rightarrow 2CH_3O + O_2$

K79 : $CH_3O_2 + SO_2 \rightarrow CH_3O + SO_3$

K99 : $CH_3SCH_3 + O \rightarrow CH_3O + CH_2S$

Of the five chemical reactions producing the methoxy radical, only two are of real significance. Reaction 8 accounts for almost two-thirds of the total loss at the surface (65.7%) while photolysis of methylhydroperoxy (J12) accounts for 31.1 percent. The remaining 3 percent is shared by reaction 109 (1.8 percent), reaction 79 (1.1 percent), and reaction 99 (0.3 percent) (see table 32). In higher regions of the troposphere, reactions 8 and J12 reverse roles with photolysis becoming the dominant production mechanism (55.2%). Reaction 8 provides 44.3 percent of the total production at the tropopause, and reaction 109 accounts for 0.5 percent. Reactions 79 and 99 that were minor pathways for methoxy production at the surface are of no importance at the tropopause. The only known chemical loss mechanism for CH_3O is the oxidation with O_2 (reaction 9). The chemical lifetime of methoxy is very short, on the order of 10^{-4} s, well justifying the PCE assumption.

The choice of surface albedo significantly alters the vertical profile of CH_3O (see fig. 42). For a surface albedo of 0.00, more than a 40 percent enhancement results compared to the Leighton approximation. For the case close to globally averaged conditions (albedo = 0.25), nearly a doubling in the CH_3O number density at the surface results. The extreme case of a surface albedo of 1.00 yields slightly more than a quadrupling in number densities in the low troposphere. Near the tropopause the multiple scattering cases are more closely grouped together and, on the average, are a factor of 2.5 larger than the Leighton approximation. The methoxy radical is so dependent on surface albedo partly because of its dependence on CH_3O_2 and CH_3OOH for its production. As seen in the previous subsection, CH_3O_2 varies a great deal with albedo, and this effect cascades into the production of CH_3O. Also, the multiple scattering calculations for CH_3OOH are enhanced 50 percent over the Leighton approxi-

Table 32. Production and destruction terms of CH_3O and percent of total production and destruction.

Production Rate (molecules-cm^{-3}-s^{-1}) and Percent of Total Production

Altitude, km	K8	%	J12	%	K109	%	K79	%	K99	%	Total	%
10	1.604 E-4	44.34	1.997 E-4	55.21	1.544 E-2	0.45	6.135 E-0	-	5.207 E-2	-	3.617 E-4	100.00
5	7.815 E-4	53.63	6.519 E-4	44.74	2.250 E-3	1.54	1.227 E-2	0.09	3.234 E-0	-	1.457 E-5	100.00
0	3.330 E-5	65.73	1.576 E-5	31.11	8.856 E-3	1.75	5.491 E-3	1.08	1.648 E-3	0.33	5.066 E-5	100.00

Destruction Frequency (s^{-1}) and Percent of Total Destruction

Altitude, km	K9	%
10	1.175 E-2	100.00
5	6.407 E-2	100.00
0	2.578 E-3	100.00

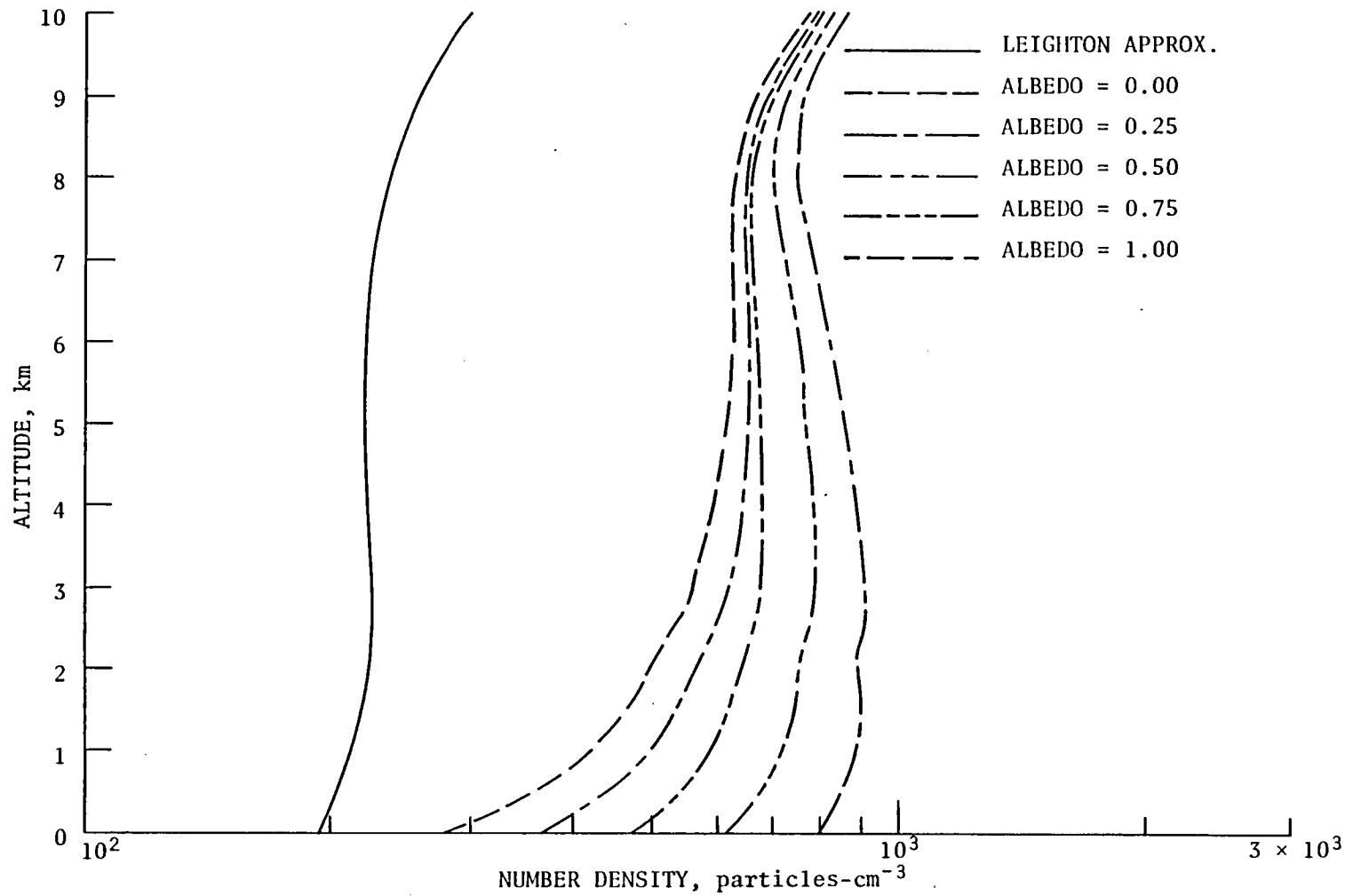

Figure 42. Vertical distributions of CH_3O for the multiple scattering cases with various albedos and the Leighton approximation.

mation. At higher altitudes the differences between the multiple scattering calculations and the Leighton approximation for CH_3O_2 and CH_3OOH are not as pronounced (see figs. 41 and 39, respectively). Hence, smaller effects of multiple scattering on the vertical distributions of CH_3O would be expected in the higher regions of the troposphere. The methoxy radical has not been measured; hence, a comparison with model calculated values is not possible.

Methyl radical (CH_3). -

Production	Destruction
K1 : $CH_4 + OH \rightarrow CH_3 + H_2O$	K3 : $CH_3 + O_2 + M \rightarrow CH_3O_2 + M$
K98: $CH_3SCH_3 + O \rightarrow CH_3 + CH_3SO$	K92: $CH_3 + SO_2\ (+M) \rightarrow CH_3SO_2\ (+M)$
K2 : $CH_4 + O(^1D) \rightarrow CH_3 + OH$	
K94: $CH_3SH + O \rightarrow CH_3 + HSO$	

The methyl radical (CH_3) is formed almost exclusively as a result of methane reacting with hydroxyl (reaction 1). The other three production terms are either very small contributors (reactions 98 and 2) or insignificant (reaction 94). Reaction 11 provides almost 100 percent of the production of the CH_3 at all altitudes (see table 33). At the surface, reaction 98 is responsible for 0.21 percent of the total methyl production and reaction 2 for a scant 0.01 percent. At the tropopause, reation 2 has a 0.31 percent share of the total methyl production, while reactions 98 and 94 are negligible. The destruction of CH_3 occurs nearly always as a result of oxidation by O_2 in the presence of a third body (reaction 3). This loss mechanism is 10 to 11 orders of magnitude more important than the only other identified loss of CH_3 (reaction 92). The chemical lifetime of the methyl radical is extremely short, about 10^{-8} s. The vertical profiles of CH_3 show a large dependence on surface albedo, similar to the CH_3O and CH_3O_2 profiles. This is due to its strong dependence on the hydroxyl radical. As seen in table 33, more than 99 percent of the CH_3 molecules are formed by OH reacting with CH_4. Since methane is specified, varia-

Table 33. Production and destruction terms of CH_3 and percent of total production and destruction.

Production Rate (molecules-cm^{-3}-s^{-1}) and Percent of Total Production

Altitude, km	K1	%	K98	%	K2	%	K94	%	Total	%
10	1.927 E-4	99.69	3.967 E-2	-	5.906 E-1	0.31	2.821 E-12	-	1.933 E-4	100.00
5	1.308 E-5	99.97	2.465 E-0	-	4.195 E-1	0.03	3.407 E-9	-	1.308 E-5	100.00
0	5.882 E-5	99.78	1.255 E-3	0.21	2.530 E-1	0.01	1.242 E-4	-	5.895 E-5	100.00

Destruction Frequency (s^{-1}) and Percent of Total Destruction

Altitude, km	K3	%	K92	%	Total	%
10	6.489 E-6	100.00	3.237 E-5	-	6.489 E-6	100.00
5	1.530 E-7	100.00	1.695 E-4	-	1.530 E-7	100.00
0	3.267 E-7	100.00	3.825 E-3	-	3.267 E-7	100.00

tions in the production terms are directly proportional to the changes in the levels of OH. Similarly, the loss mechanism of CH_3 is dominated by oxidation with O_2, which is also a specified input (see "Molecular oxygen"). Hence, the changes in the vertical profiles of CH_3 as a function of albedo are due entirely to altered levels of OH. In fact, so strong is this dependence that the graph showing the vertical profiles of CH_3 (fig. 43) can be overlaid with an almost perfect fit to the graph of the OH distributions (fig. 36). No measurements of the methyl radical exist.

Formyl radical (HCO). -

Production	Destruction
K10: $CH_2O + OH \rightarrow HCO + H_2O$	K11: $HCO + O_2 \rightarrow CO + HO_2$
J10: $CH_2O + h\nu \rightarrow HCO + H$	

The formyl radical (HCO) is formed two ways: by reaction of formaldehyde (CH_2O) with hydroxyl (OH) (reaction 10) and by photodissociation of CH_2O (J10). Of these two production terms, reaction 10 is 7 to 10 orders of magnitude more important than the photolytic production (J10) (see table 34). The only identified chemical destruction is due to oxidation by molecular oxygen (O_2) (reaction 11). The chemical lifetime of the formyl radical in the troposphere is very short, on the order of 10^{-8} s. The inclusion of multiple scattering and surface albedo creates large differences from the Leighton approximation in the low troposphere, similar to results for other rapidly reacting hydrocarbon species (see fig. 44). Again, this is due to a very strong dependence on OH. The vertical profiles of HCO resemble those of OH but are smoother. This smoothing is a result of the reaction of OH to CH_2O. Formaldehyde depends inversely on surface albedo, i.e., an albedo of 0.00 shows the greatest enhancement at the surface. Consequently, the vertical profiles of HCO are governed by the combined effects of CH_2O and OH. No measurements of HCO exist.

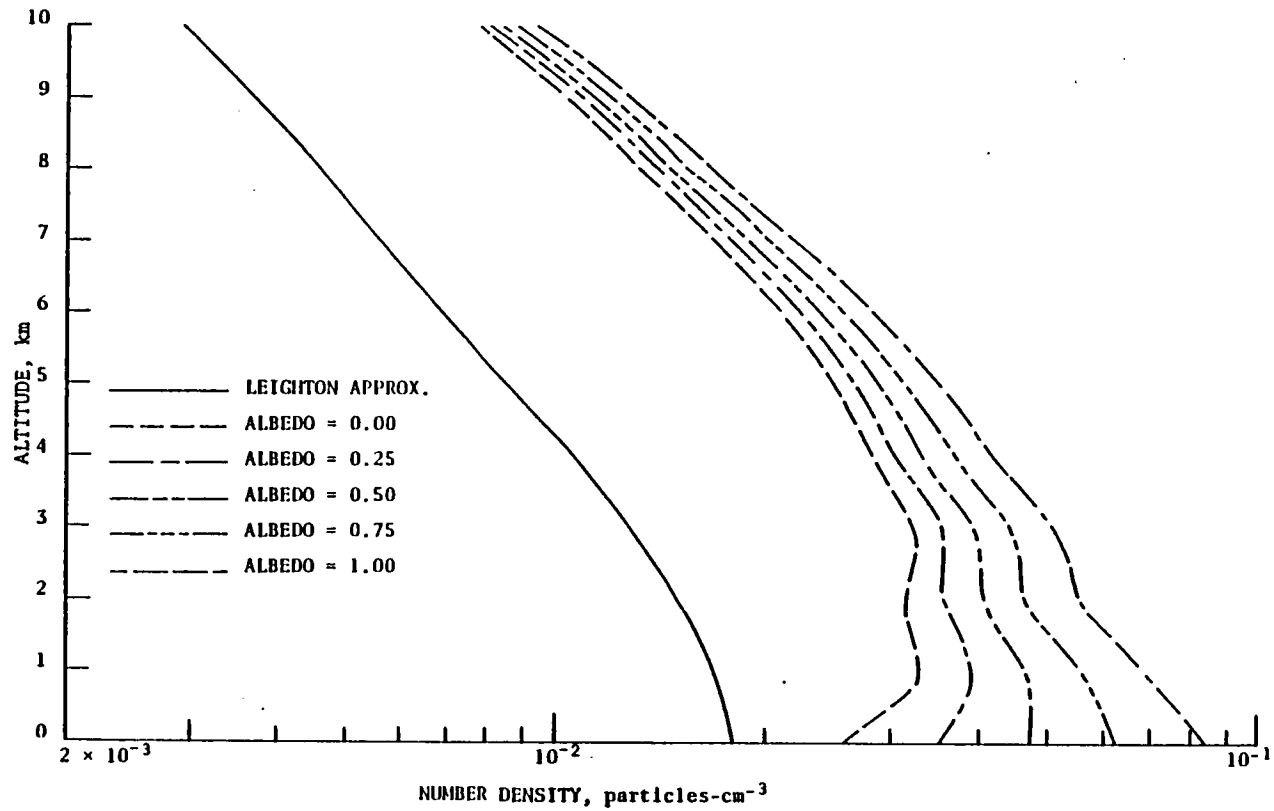

Figure 43. Vertical distributions of CH_3 for the multiple scattering cases with various albedos and the Leighton approximation.

Table 34. Production and destruction terms for HCO and percent of total production and destruction.

Production Rate (molecules-cm^{-3}-s^{-1}) and Percent of Total Production

Altitude, km	K10	%	J10	%	Total	%
10	4.151 E-3	100.00	2.528 E-4	-	4.151 E-3	100.00
5	2.621 E-4	100.00	2.324 E-5	-	2.621 E-4	100.00
0	1.276 E-5	100.00	2.050 E-5	-	1.276 E-5	100.00

Destruction Frequency (s^{-1}) and Percent of Total Destruction

Altitude, km	K10	%
10	8.987 E-6	100.00
5	1.599 E-7	100.00
0	2.665 E-7	100.00

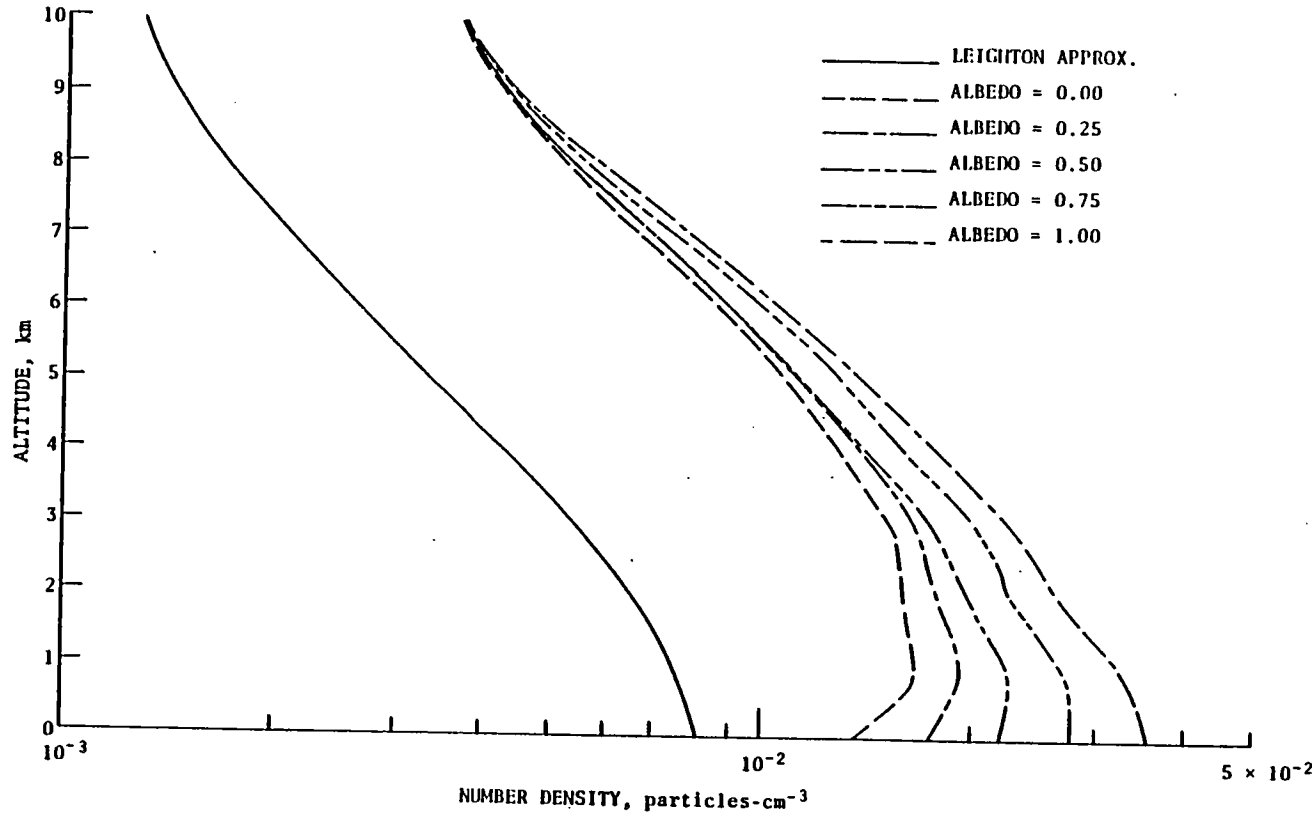

Figure 44. Vertical distributions of HCO for the multiple scattering cases with various albedos and the Leighton approximation.

Future perturbations to the carbon budget. - Most of the early work in atmospheric radiation and chemistry concerned itself with CO_2. In fact scientists were already concerned with this problem at the end of the last century (ref. 1). The mere fact that this problem still exists today, some 80 years later, is a testimonial to its significance. The global increase of CO_2 as a function of time is well documented (ref. 149). The atmospheric level of CO_2 is approximately 330 ppmv with a current yearly increase of about 1 ppmv. Due to the nonlinearity of the atmosphere-hydrosphere-biosphere-lithosphere system, a doubling in the CO_2 level would not necessarily take 330 years. The models of Keeling (ref. 149) and Hoffert (ref. 150) predict a doubling in the CO_2 concentration in 50 years. The quantitative long-term increase in CO_2 is somewhat difficult to predict, since the roles of the oceans and the biosphere as sinks in the carbon cycling are not fully understood. In particular, the deep-ocean uptake of CO_2 needs to be clarified.

Recently it has been suggested that alterations in the land biota, such as deforestation and biomass burning, might enhance the atmospheric level of CO_2 (ref. 151). The natural level of CO_2 is determined by photosynthesis, the process by which plants use CO_2 to synthesize organic compounds. Carbon dioxide is returned to the atmosphere by oxidation of dead organic matter. Obviously, any large-scale perturbation in the biota due to human activities is bound to enhance the level of CO_2 in the atmosphere. Biomass burning directly emits carbon dioxide into the atmosphere.

The second part of the CO_2 climate problem deals with the potential of a global temperature increase due to the greenhouse effect as the level of CO_2 rises. The thermal properties of CO_2 have been the subject of intense studies and are well understood (ref. 152). One-dimensional, radiative-convective models have been used extensively to calculate temperature enhancements (ref. 153). At this time, the most complete radiative-convective model used to study the CO_2 climate problem is that of Augustsson and Ramanathan (ref. 154). This model includes the fundamental bands of 4 isotopes of CO_2 in addition to the 6 "hot bands" in the 15-μm region. Furthermore, several of the weak bands in the 7 to 8 μm, 9 to 10 μm, and 12 to 18 μm regions were also included. The

Augustsson-Ramanathan model predicted an increase in the global surface temperature of approximately 2.0 K for a doubling of the CO_2 level. It is important to note that the temperature increase represents a globally averaged value and that the increase in the high latitudes would be much greater, perhaps by a factor of 3 to 4, due to certain feedback mechanisms such as a decrease in the albedo and a greater thermal stability of the troposphere. It therefore appears as though a simple doubling of the CO_2 level in the atmosphere would pose a very serious problem, indeed, on the global scale.

Another potentially threatening problem involving species of the carbon group deals with the increasing flux of CO due to anthropogenic activities (ref. 155). A recent study has predicted that the level of methane will increase to 2.45 ppm in the next 50 years due to an increase in CO flux. Methane increases as a result of the reaction between CO_2 and OH, which initiates the methane oxidation chain. Hence, CO and CH_4 compete with each other for the available hydroxyl radicals. Since CO reacts more rapidly with OH than does CH_4 (see "Hydroxyl radical"), an increase in CO emission would enhance the level of CH_4. A doubling of the level of methane would result in an increased surface temperature of 0.3 to 0.4 K, depending on the absorption data used (ref. 156). This is less than the CO_2 doubling would yield, but it is nevertheless significant. The combined effects of CO_2 and CH_4 doubling simultaneously is especially disturbing. The CO_2 doubling constitutes a problem with runaway effects; and by the time mankind is ready to rectify this threat it could be too late.

The Sulfur Group

Introduction. - Of the five major chemical families in the troposphere, sulfur is perhaps the least studied and understood. The sulfur species family consists of species in various states of oxidation (from highly reduced to highly oxidized) with a wide range of lifetimes (from 10^{-7} s to several years). Most sulfur reactions have a common feature: a trend toward further oxidation. The oxidation chain for the sulfur family is shown in figure 45.

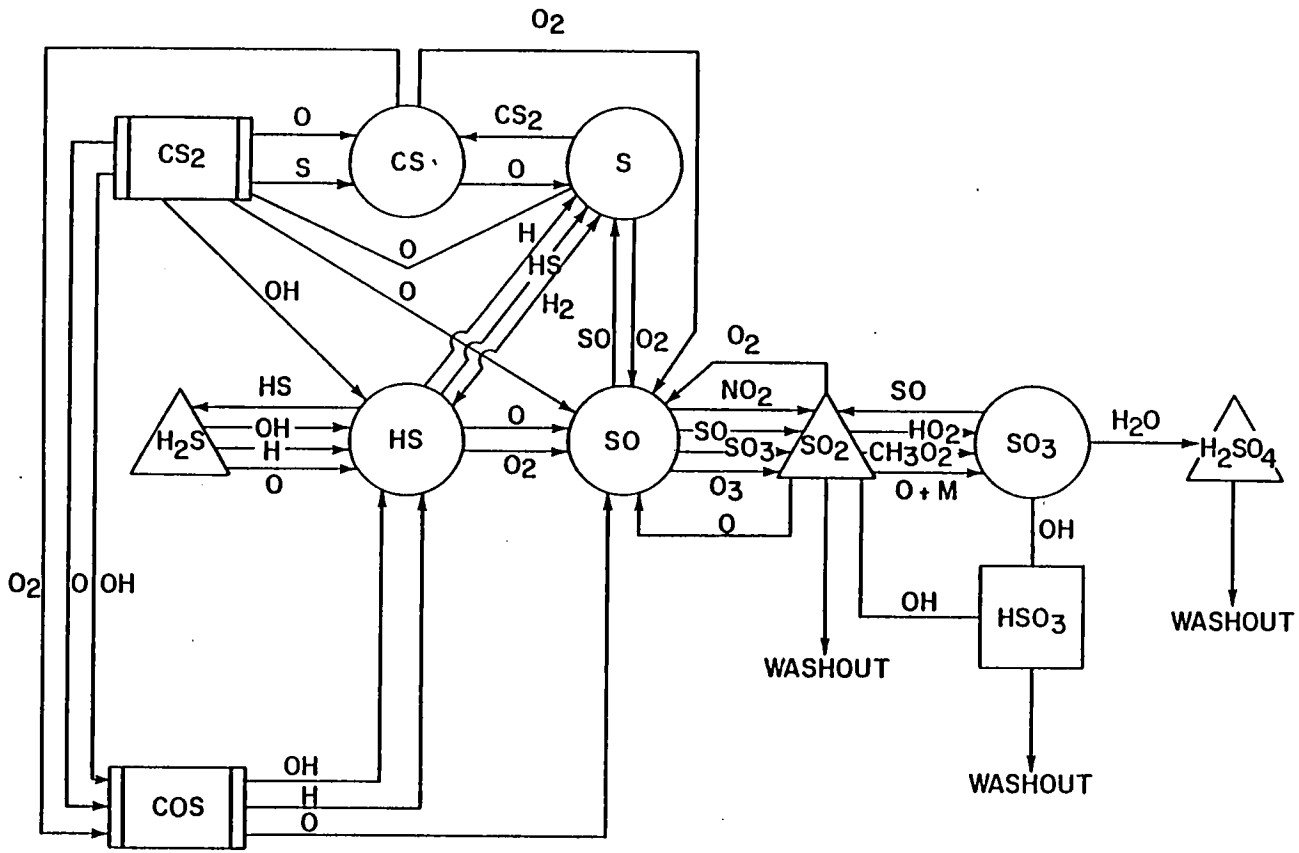

Figure 45. Reaction paths of the sulfur family.

It has been known for a long time that species of the sulfur family adversely affect the air quality on the local and regional scales. This is due mainly to antropogenic emissions in large metropolitan areas. It has also been known for about two decades that species of the sulfur family diffuse upward into the stratosphere where they form sulfur particulates that constitute the stratospheric "aerosol layer" usually found around 20 km (refs. 157, 158). Natural emissions of particulates from volcanoes also contribute to the aerosol layer.

In this section, the sources and sinks of the sulfur compounds are examined. Some sulfur species are produced chemically as well as emitted anthropogenically. Loss mechanisms include chemical reactions and heterogeneous losses, i.e., rainout, washout, and dry deposition. The chemical production and loss terms for each species listed below are arranged in order of importance.

Sulfur dioxide (SO_2). - The chemical reactions that affect sulfur dioxide in this model are (in order of importance):

Production		Destruction	
K68 :	$SO + O_2 \rightarrow SO_2 + O$	K77 :	$SO_2 + OH\ (+M) \rightarrow HSO_3\ (+M)$
K69 :	$SO + NO_2 \rightarrow SO_2 + NO$	K79 :	$SO_2 + CH_3O_2 \rightarrow SO_3 + CH_3O$
K103:	$SO + O_3 \rightarrow SO_2 + O_2$	K78 :	$SO_2 + HO_2 \rightarrow SO_3 + OH$
K90 :	$SO + SO \rightarrow SO_2 + S$	K104:	$SO_2 + O + M \rightarrow SO_3 + M$
K91 :	$SO + SO_3 \rightarrow 2SO_2$	K92 :	$SO_2 + CH_3\ (+M) \rightarrow CH_3SO_2\ (+M)$
		K81 :	$SO_2 + O \rightarrow SO + O_2$

The chemical production of SO_2 always involves SO (reactions 68, 69, 103, 90, and 91). Of these reactions, only the recombination of sulfoxy (SO) with molecular oxygen (O_2) (reaction 68) and sulfoxy with nitrogen dioxide (NO_2) (reaction 69) are of major importance. Sulfoxy reacting with ozone (O_3) (reaction 103) is of minor importance, while the reactions of SO with itself (reac-

tion 90) and with sulfur trioxide (SO_3) (reaction 91) are negligible. The most importance gas phase loss is due to the reaction with OH (reaction 77). A minor loss mechanism is due to reaction with the methylperoxy radical (CH_3O_2) (reaction 79). Reactions with the hydroperoxy radical (HO_2) (reaction 78), with atomic oxygen (O) in the presence of a third body (reaction 104), with the methyl radical (CH_3) (reaction 92), and with atomic oxygen (O) (reaction 81) are all negligible. The lifetime of SO_2 based solely on gas phase chemistry is about 2.5 days. Table 35 lists the production rates and the loss frequencies for the chemical reactions that involve SO_2. The destruction term is given as a frequency (s^{-1}) rather than as a rate (molecules $cm^3 s^{-1}$) so that the chemical lifetime can more readily be computed. The chemical lifetime (τ) of a species is related to the loss frequency (L) as:

$$\tau = L^{-1}$$

In addition to chemical production and loss terms, SO_2 is emitted anthropogenically as well as naturally. It is known as a product of fuel combustion (ref. 159) and has also been detected in the exhaust of turbines (ref. 160) and of diesel engines (ref. 161). The application of certain types of fertilizers also emits SO_2 (ref. 162), and sulfur dioxide has been found in the smoke from erupting volcanoes (refs. 163, 164).

In addition to its chemical destruction, SO_2 is also lost via heterogeneous processes. The heterogeneous loss of SO_2 has been estimated to be about 50 percent of the total loss and is modeled following the procedure of Turco et al. (ref. 52) with the exception that the present model has the tropopause at 10 km while the model of Turco et al. uses 13 km for tropopause altitude. Inclusion of the heterogeneous loss of SO_2 lowers its lifetime to slightly less than two days. At the lower boundary, a flux of 1.275×10^{10} molecules $cm^{-2} s^{-1}$ was used together with a depositional velocity of 1.0 cm s^{-1}. This results in a surface mixing ratio of 0.5 ppb. The resulting vertical profile is shown in figure 46. The solid line represents the Leighton approximation, while the various broken and dotted lines represents the vertical profiles of SO_2 as

Table 35. Production and destruction terms of SO_2 and percent of total production and destruction.

Production Rate (molecules-cm^{-3}-s^{-1}) and Percent of Total Production

Altitude, km	K68	%	K69	%	K103	%	K90	%	K91	%	Total	%
10	7.855 E-0	96.50	8.144 E-3	0.10	2.767 E-1	3.40	4.495 E-13	-	1.083 E-15	-	8.140 E-0	100.00
5	4.207 E-2	99.42	9.376 E-2	0.03	2.131 E-0	0.50	1.014 E-11	-	6.714 E-15	-	4.229 E-2	100.00
0	6.472 E-4	99.99	8.572 E-0	0.01	1.922 E-2	-	4.925 E-9	-	1.480 E-13	-	6.473 E-4	100.00

Destruction Frequency (s^{-1}) and Percent of Total Destruction

Altitude, km	K77	%	K79	%	K78	%	K104	%	K92	%	K81	%	Total	%
10	9.778 E-7	94.29	5.686 E-8	5.48	2.337 E-9	0.27	3.608 E-11	-	8.740 E-16	-	2.384 E-24	-	1.037 E-6	100.00
5	1.486 E-6	86.98	2.171 E-7	12.71	5.338 E-9	0.31	4.405 E-11	-	2.554 E-15	-	2.638 E-22	-	1.708 E-6	100.00
0	1.926 E-6	81.37	4.307 E-7	18.20	1.011 E-8	0.43	4.404 E-11	-	5.388 E-15	-	8.304 E-21	-	2.376 E-6	100.00

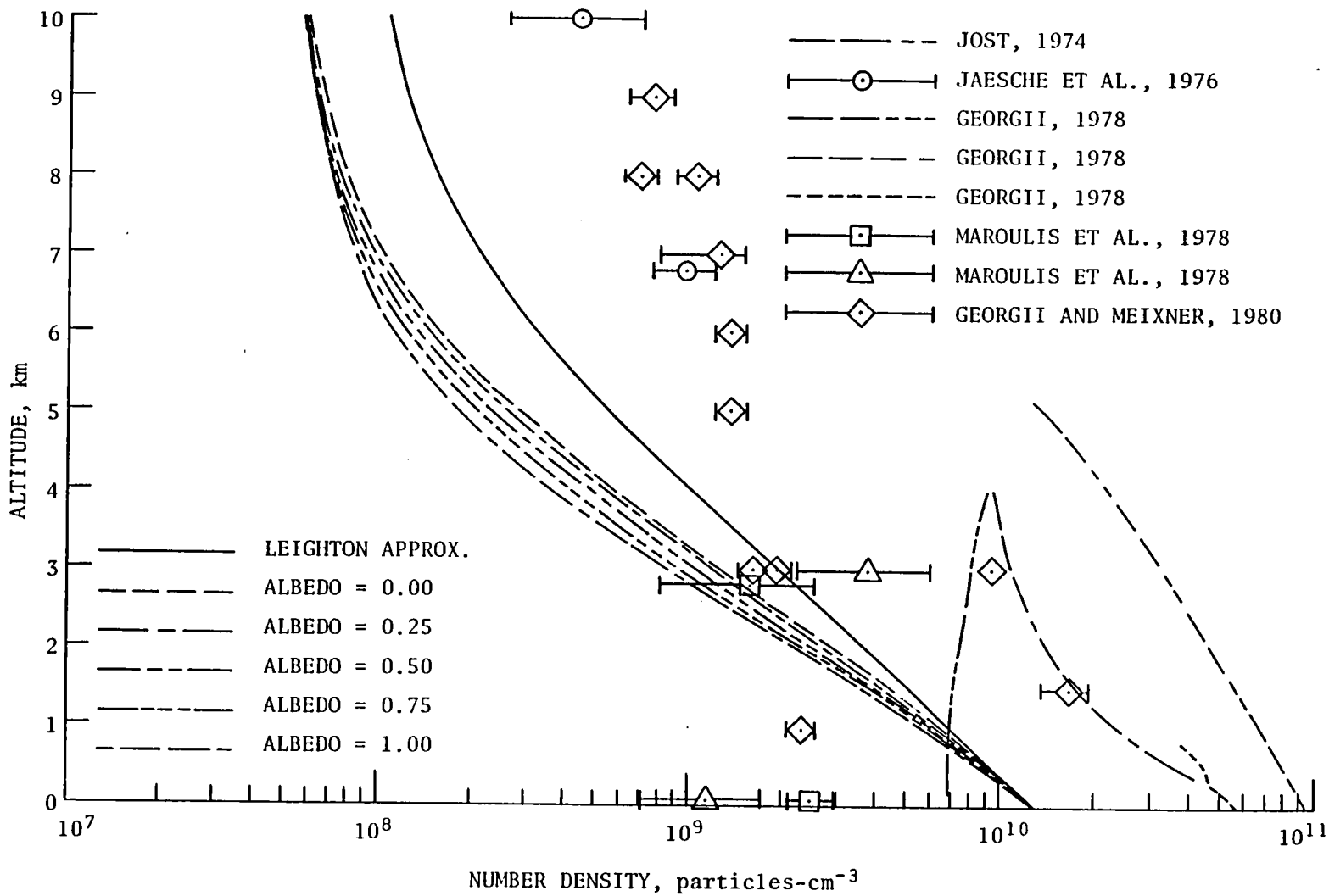

Figure 46. Vertical distributions of SO_2 for the multiple scattering cases with various albedos and the Leighton approximation.

calculated with the multiple scattering routine for varying albedos. In all calculations, a zero flux condition was imposed at the upper boundary. Inclusion of multiple scattering and ground albedo results in a decrease of SO_2 compared to the Leighton approximation. This is not very surprising, since the major loss mechanism for SO_2 is the reaction with the hydroxyl radical (OH). In fact, 80 to 90 percent of the time, depending on altitude, SO_2 is lost by reaction 77. The vertical profiles of OH were drastically enhanced, as seen previously, when multiple scattering and ground albedo were accounted for.

Vertical profiles have been measured by Jost (ref. 165), Georgii (ref. 166), and Georgii and Meixner (ref. 167). In general, these measurements show a decreasing mixing ratio with altitude similar to the calculations with the present model. One notable exception is a profile by Georgii (ref. 166) over the Atlantic Ocean (indicated by diamonds in fig. 46). In this case, there is an increase in mixing ratio with altitude. This would be consistent with the theory that the oceans act as a sink for SO_2 (ref. 168). Also included are some measurements by Maroulis et al. (ref. 169) and by Jaeschke et al. (ref. 170). The surface mixing ratio of the vertical profiles by Georgii (ref. 166) and Jost (ref. 165) are about an order of magnitude higher than those calculated by the present model. This is not very surprising since Georgii's and Jost's measurements were made over western Europe, an area which is known to have a high background concentration of SO_2.

Depositional velocities at the surface have a range of 0.1 to 2.5 cm s^{-1} (ref. 171). A value of 1.0 cm s^{-1} has been suggested as an average depositional velocity (ref. 172) and was used in this study. With a slow depositional velocity, a very rapid increase in mixing ratio with altitude results. Conversely, with a high depositional velocity, the mixing ratio increases slowly with altitude. In all calculations, the flux of SO_2 was kept constant at 1.275×10^{10} molecules cm^{-2} s^{-1}. There are numerous estimates of global SO_2 emission. For example, Katz (ref. 173) estimated that 77×10^6 metric tons (77 Mt) were emitted. Subsequent estimates by Robinson and Robbins (ref. 174) indicate that the annual global SO_2 emission strength is 146 Mt. Of this amount, 70 percent comes from coal combustion, 16 percent from petroleum fuel

combustion, and the rest from various processes such as petroleum refining and smelting. Approximately 95 percent of all the anthropogenically emitted sulfur compounds are in the form of SO_2 (ref. 175). A recent estimate of global, land, sulfur dioxide emission was made by Shinn and Lynn (ref. 162). They estimated anthropogenic emissions to be 183 Mt, with 33 Mt of that amount in the form of fertilizers. Natural emissions (biogenic and volcanic) were found to be 210 Mt. Hence, man's activities account for nearly 50 percent of all SO_2 that is emitted into the atmosphere. Since the bulk of this figure involves coal combustion, a switch to greater use of coal, as recently suggested, is likely to rapidly increase man's contribution to the total sulfur budget. In large concentrations, SO_2 is very toxic to animals and plants. It is an important precursor to formation of particulates. This affects the aerosol loading, which has climatic implications in addition to the very obvious problem of reduced visibility. The climatic aspect to consider is related to the infrared absorption bands of SO_2 at 8.7 μm and 7.3 μm (ref. 156).

Carbonyl sulfide (COS). -

Production	Destruction
K75: $CS + O_2 \rightarrow COS + O$	K86 : $COS + OH \rightarrow HS + CO_2$
K87: $CS_2 + OH \rightarrow COS + HS$	K101: $COS + O \rightarrow SO + CO$
K71: $CS_2 + O \rightarrow COS + S$	K85 : $COS + H \rightarrow HS + CO$
	K89 : $COS + S \rightarrow CO + S_2$

The chemical sources of carbonyl sulfide (COS) are the reactions of carbon sulfide (CS) with molecular oxygen (O_2) (reaction 75) and the reactions of carbon disulfide (CS_2) with the hydroxyl radical (OH) (reaction 87) and with atomic oxygen (reaction 71). At the surface, reactions 75 and 87 are of equal importance as a chemical source term for COS, with reaction 71 providing a minor path (see table 36). With increasing altitude, reaction 75 becomes the

Table 36. Production and destruction terms of COS and percent of total production and destruction.

Production Rate (molecules-cm^{-3}-s^{-1}) and Percent of Total Production

Altitude, km	K75	%	K87	%	K71	%	Total	%
10	2.082 E-1	73.31	2.952 E-0	10.25	5.026 E-0	17.44	2.880 E-1	100.00
5	1.972 E-1	60.94	7.879 E-0	24.35	4.759 E-0	14.71	3.236 E-1	100.00
0	1.677 E-1	43.67	1.759 E-1	45.81	4.037 E-0	10.52	3.840 E-1	100.00

Destruction Frequency (s^{-1}) and Percent of Total Destruction

Altitude, km	K86	%	K101	%	K85	%	K89	%	Total	%
10	1.172 E-8	99.82	2.148 E-11	0.18	4.086 E-15	-	3.637 E-22	-	1.174 E-8	100.00
5	1.175 E-8	99.84	2.707 E-11	0.16	5.101 E-15	-	6.210 E-22	-	1.718 E-8	100.00
0	2.179 E-8	99.88	2.609 E-11	0.12	6.281 E-15	-	7.817 E-22	-	2.182 E-8	100.00

dominant term while reaction 87 continuously diminishes its influence and, in fact, at the tropopause is of even less importance than reaction 71. The loss mechanisms of COS are totally dominated by the reaction of COS to OH (reaction 86). All other chemical losses of COS, i.e., reaction with atomic oxygen (reaction 101), reaction with atomic hydrogen (H) (reaction 85), and reaction with atomic sulfur [$S(^3P)$] (reaction 89) can virtually be neglected. The calculated lifetime of COS based on the loss mechanisms mentioned above is about 500 days.

In addition to the chemical production terms mentioned above, COS is also emitted anthropogenically and naturally. Some of the natural processes emitting COS include erupting volcanoes (ref. 164) and forest fires (ref. 176). Some of the industrial processes forming COS include the manufacturing of petroleum (ref. 177) and of synthetic fiber (ref. 178). Carbonyl sulfide is a very stable molecule and, consequently, should be very well mixed in the troposphere. In the model calculations, a surface boundary value of 0.5 ppbv was used together with a condition of zero flux at the tropopause. The resulting vertical profile is shown in figure 47.

The measurements of COS have mostly been made at the surface and indicate that it is very well mixed. Sandalls and Penkett (ref. 179) obtained a value of 0.51 ppb. Torres et al. (ref. 180) measured an average value of 0.512 ppb over a wide range of latitudes, while Maroulis et al. (ref. 181) found an average value of 0.467 ppb over 3 different locations in the United States. Some early data by Hanst et al. (ref. 182) indicated a value of 0.2 ppb at the surface, but these measurements were associated with large experimental uncertainties. The vertical profiles calculated by the model show a nearly constant mixing ratio in the troposphere as would be expected from its long lifetime. Carbonyl sulfide diffuses into the stratosphere, where it undergoes photolysis forming SO (ref. 158). Hence, COS would be an important precursor to the formation of the particulates that constitute the aerosol layer. As shown in figure 47, there are only slight differences between the Leighton approximation and the multiple scattering cases. This is not unexpected: since COS is a relatively unreactive molecule, its vertical distribution will closely resemble the distribution obtained from a pure transport solution (neglecting chemical terms).

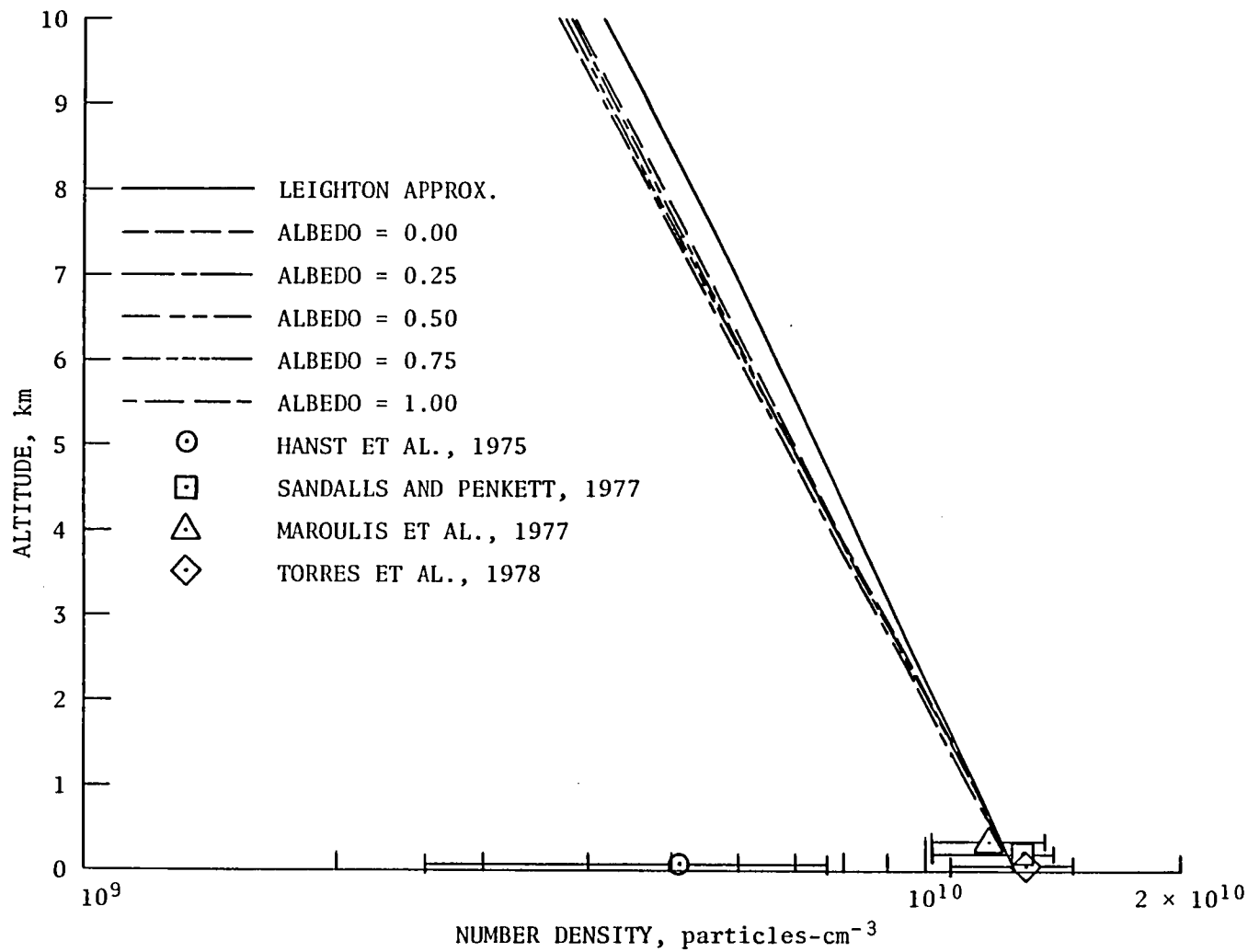

Figure 47. Vertical distributions of COS for the multiple scattering cases with various albedos and the Leighton approximation.

Hydrogen sulfide (H_2S). -

Production	Destruction
K93: $HS + HS \rightarrow H_2S + H$	K64 : $H_2S + OH \rightarrow HS + H_2O$
	K84 : $H_2S + H \rightarrow HS + H_2$
	K102: $H_2S + O \rightarrow HS + OH$

The only known chemical production of hydrogen sulfide (H_2S) in the atmosphere is due to the reaction of the thiohydroxyl radical (HS) with itself (reaction 93). This is only of very minor importance when the total budget of H_2S is considered. The primary loss mechanism for H_2S is its reaction with OH (reaction 64). The losses due to reactions with atomic hydrogen (reaction 84) and with atomic oxygen (reaction 102) are nearly negligible (see table 37). It is only at the tropopause where reaction 64 does not contribute to 100 percent of the total loss of H_2S (to the accuracy of 2 decimal places). At this altitude reaction 84 contributes a minute 0.01 percent of the overall destruction.

The calculated lifetime of H_2S based on these three chemical losses is nearly one day. Some of the industrial activities that have been identified as emitting H_2S include wood pulping (ref. 183) and sewage treatment (ref. 184). Hydrogen sulfide is formed primarily by microbial activity (ref. 185). Volcanoes also emit H_2S (ref. 186) as does animal waste (ref. 187). Only few measurements of H_2S exist (refs. 167, 188). The measurements by Georgii (ref. 167) are the only measurements with a vertical distribution. Most of Georgii's measurements indicate a surface mixing ratio of 1.5 to 3.0 ppb. It should be kept in mind, however, that these measurements were obtained in the tidal flats of northwestern Germany, an area that emits higher fluxes than the globally averaged surface. Robinson and Robbins (ref. 174) estimated the globally averaged surface mixing ratio to be 0.2 ppb. Using this value as the lower boundary condition and zero flux at the tropopause, the model-calculated profiles are shown in figure 48. The model shows a very rapid decrease in the vertical distributions similar to Georgii's measurements. In the case of H_2S,

Table 37. Production and destruction terms of H_2S and percent of total production and destruction.

Production Rate (molecules-cm^{-3}-s^{-1}) and Percent of Total Production

Altitude, km	K93	%
10	1.177 E-18	100.00
5	1.511 E-17	100.00
0	1.771 E-13	100.00

Destruction Frequency (s^{-1}) and Percent of Total Destruction

Altitude, km	K64	%	K84	%	K102	%	Total	%
10	5.583 E-6	99.99	6.075 E-10	0.01	1.383 E-10	-	5.584 E-6	100.00
5	9.154 E-6	100.00	8.641 E-11	-	1.045 E-10	-	9.154 E-6	100.00
0	1.270 E-5	100.00	7.284 E-11	-	6.758 E-11	-	1.270 E-5	100.00

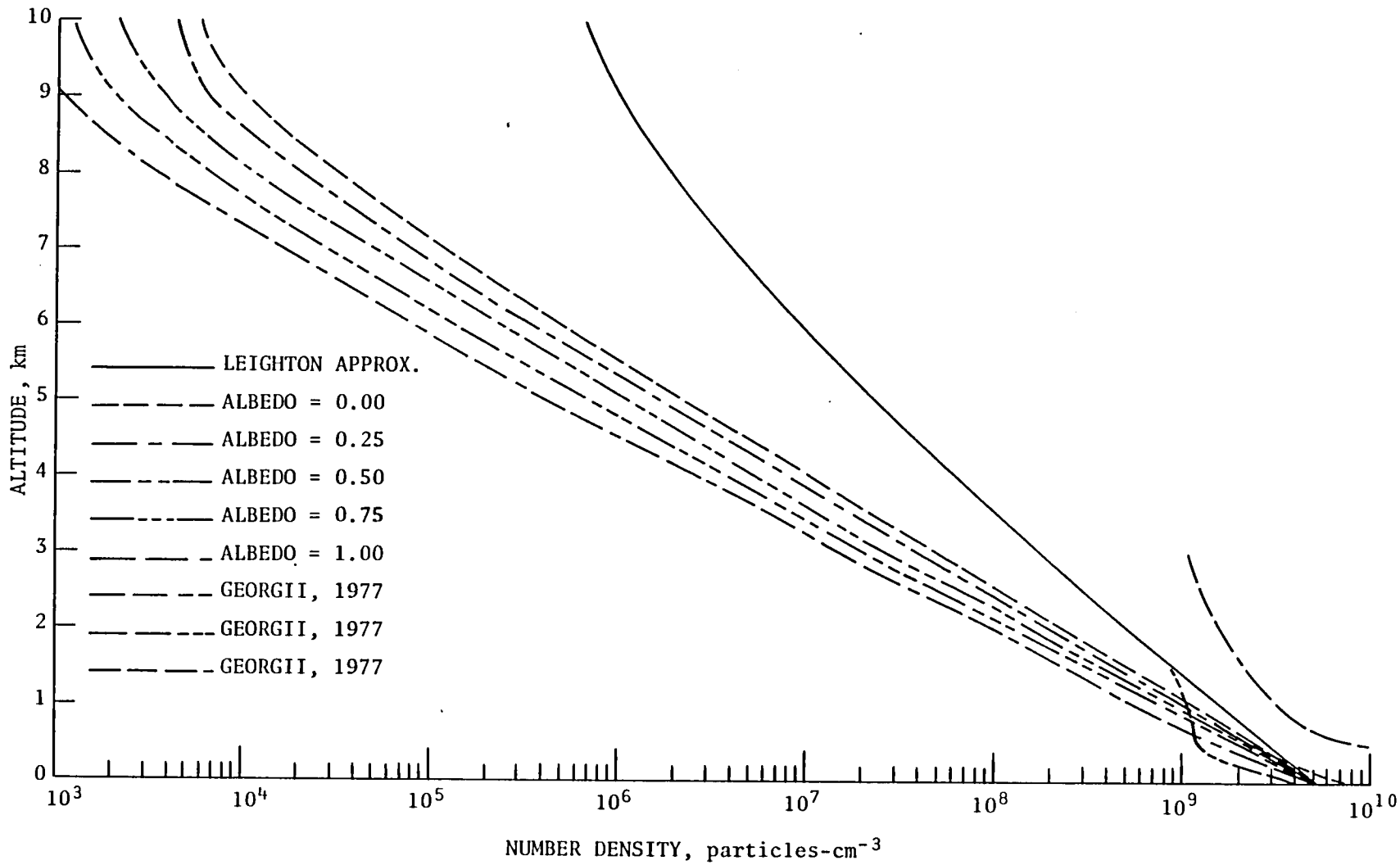

Figure 48. Vertical distributions of H_2S for the multiple scattering cases with various albedos and the Leighton approximation.

there are greater differences between the Leighton approximation and the results from the multiple scattering calculations than was the case for COS. Since H_2S is fairly reactive, it responds noticeably to the enhanced OH levels. In the midtroposphere, H_2S decreases by an order of magnitude for an albedo of 0.25 compared to the Leighton approximation, and at the tropopause level the decrease if about two orders of magnitude.

Carbon disulfide (CS_2). -

Production	Destruction
	K70 : $CS_2 + O \rightarrow SO + CS$
	K87 : $CS_2 + OH \rightarrow HS + COS$
	K71 : $CS_2 + O \rightarrow S + COS$
	K72 : $CS_2 + O \rightarrow S_2 + CO$
	K88 : $CS_2 + S \rightarrow S_2 + CS$

There are no known chemical reactions in the atmosphere that produce carbon disulfide (CS_2), although CS_2 is formed both naturally by volcanic emissions (ref. 164) and by anthropogenic emissions such as the manufacture of petroleum (ref. 177) and of synthetic fiber (ref. 161). Carbon disulfide has also been measured in seawater (ref. 189), giving an almost constant value of 5.2×10^{-13} g/ml water over a wide range of latitudes. This would indicate a natural source for CS_2.

The primary loss mechanism for CS_2 is the reaction with atomic oxygen, yielding sulfoxy (SO) and carbon sulfide (CS) (reaction 70). At the surface this reaction accounts for more than 50 percent of the total loss of CS_2 (see table 38). Similarly, at the surface, reaction 87 is responsible for about 30 percent of the loss and reactions 71 and 72 each contribute nearly 7 percent. In the midtropospheric region, reaction 70 has increased its share to almost 70 percent, while reaction 87 has decreased its influence to less than 15 percent. Reactions 71 and 72 have increased slightly in importance, with each reaction

Table 38. Production and destruction terms of CS_2 and percent of total production and destruction. (No chemical production terms are known.)

	Destruction Frequency (s^{-1}) and Percent of Total Destruction											
Altitude, km	K70	%	K87	%	K71	%	K72	%	K88	%	Total	%
10	2.770 E-8	76.31	1.953 E-9	5.37	3.324 E-9	9.16	3.324 E-9	9.16	8.219 E-19	-	3.630 E-8	100.00
5	1.439 E-8	69.51	2.859 E-9	13.81	1.727 E-9	8.34	1.727 E-9	8.34	4.374 E-19	-	2.070 E-8	100.00
0	6.956 E-9	56.75	3.632 E-9	29.63	8.345 E-10	6.81	8.345 E-10	6.81	2.231 E-19	-	1.226 E-8	100.00

contributing about 8 percent to the total loss of CS_2. At the tropopause, reaction 70 acounts for more than 75 percent of the loss, reactions 71 and 72 for almost 10 percent each, and reaction 87 for a scant 5 percent. Throughout the troposphere the reaction of CS_2 with atomic sulfur [$S(^3p)$] is of negligible importance. The lifetime of CS_2 based on these reactions is about 2.5 years.

Measurements of CS_2 are very sparse and until recently confined to a single location in England (ref. 179). The average surface value obtained was 0.19 ppb. No vertical measurements are available. Using the value of 0.19 ppb as the lower boundary condition and zero flux at the tropopause, the model-calculated profiles are shown in figure 49. Carbon disulfide decreases relatively slowly with altitude as would be expected from its long lifetime. The recent measurements of CS_2 (ref. 190) seem to indicate much lower values than yielded by the earlier measurements. The more realistic treatment of the radiation field has very little influence on CS_2 due to its long lifetime.

Sulfuric acid (H_2SO_4). -

Production	Destruction
K80 : $SO_3 + H_2O \rightarrow H_2SO_4$	Heterogeneous losses

Sulfuric acid is formed chemically by the reaction of sulfur trioxide (SO_3) with water vapor (H_2O) (reaction 80), naturally by volcanic emissions (ref. 163), and anthropogenically in the exhaust of automobiles (ref. 161) and in the manufacturing process of H_2SO_4 (ref. 191). Sulfuric acid occurs both in liquid and solid forms. It forms the solid form (sulfate, $SO_4^{=}$) when it combines with cations other than hydrogen. Hence, H_2SO_4 affects the environment in two ways:

(1) by formation of aerosol particulates which reduce incoming radiation and also visibility, and

(2) by lowering the pH in rainwater.

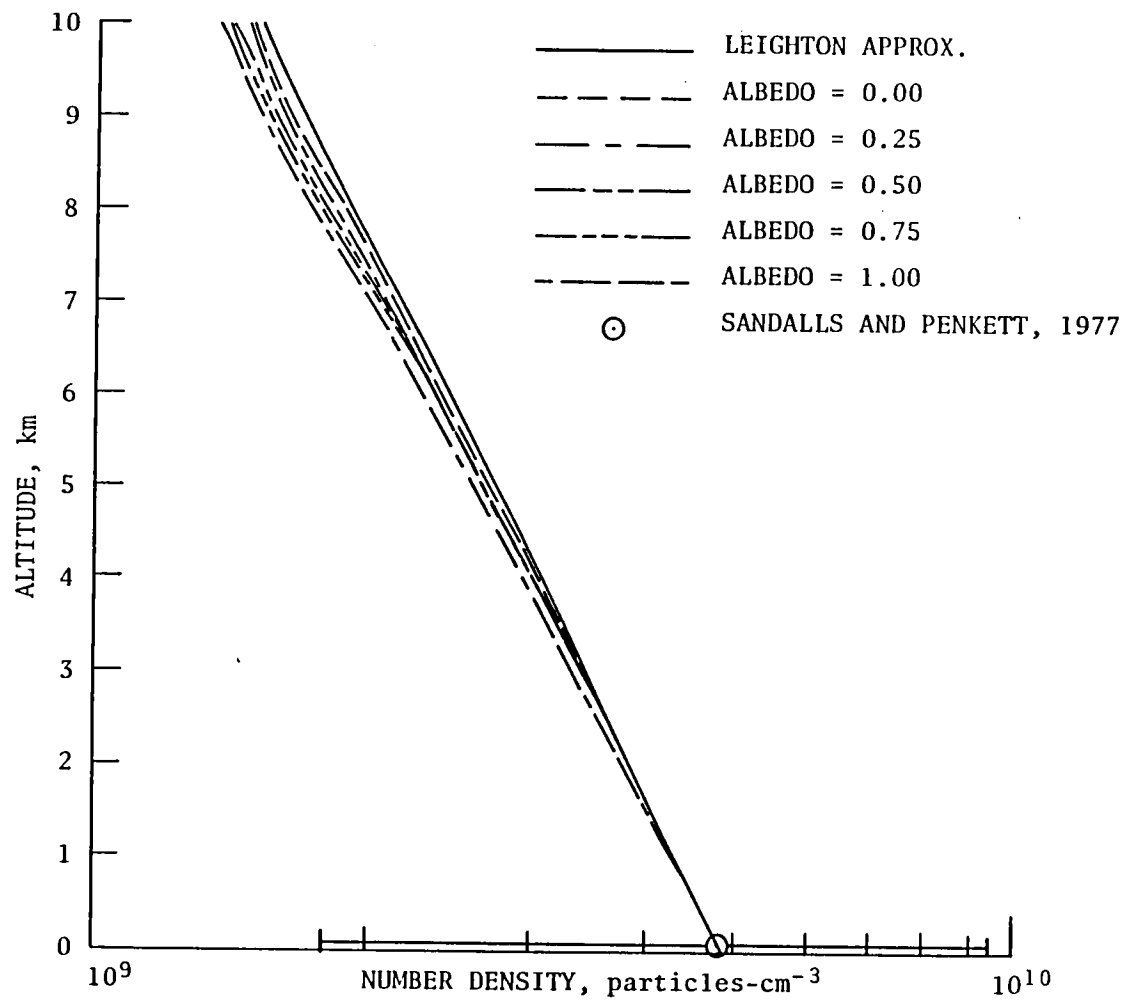

Figure 49. Vertical distributions of CS_2 for the multiple scattering cases with various albedos and the Leighton approximation.

In Scandinavia, which is downwind from the large industrial areas in Germany and Great Britain, a gradual lowering of pH in rainwater with time has been measured. The average rate of decrease has been 0.3 to 0.4 units of pH per decade (ref. 192). Similar acidic rainfalls have been observed in the Atlantic provinces of Canada, downwind of the highly industrialized metropolitan northeast corridor (ref. 193). Acid precipitation is known to have an adverse effect on soils and vegetation. If a soil becomes more acidic, leaching of nutrients in the top soil layer (humus) is accelerated (ref. 194). This leaching affects, among other things, the rate-of-growth of trees. For example, forest productivity in Scandinavia has decreased by one percent per year during the last few decades due to the high incidence of acidic precipitation (ref. 193). Ammonia (NH_3) plays an important role in neutralizing acidic sulfur species. Consequently, if the global sulfur budget increases more rapidly than the global ammonia budget, a further increase in acid precipitation would be expected.

The only known loss mechanism for H_2SO_4 is heterogeneous loss. In the present model, a heterogeneous loss rate similar to that of Turco et al. (ref. 52) was used, again with the exception of a lower tropopause altitude (10 km vs. 13 km). The lifetime of H_2SO_4 at the surface based on the heterogeneous loss rate is about 0.5 day (see table 39).

It is of great importance to understand the fate of the H_2SO_4 molecules. Sulfuric acid can occur in liquid form and rainout in the form of acid rain, which affects the environment adversely, or it can occur in solid form, which affects the growth of the aerosol layer and, hence, ultimately will affect the climate. In the model, a zero flux condition was imposed at both boundaries. The resulting vertical profiles are shown in figure 50. There are no tropospheric measurements of H_2SO_4 with which to compare the calculated values. Sulfuric acid concentration is more than doubled for an albedo of 0.25 compared to the Leighton approximation. This increase in concentration is due to an enhanced level of sulfur trioxide (SO_3) which reacts with water vapor to form H_2SO_4. The level of SO_3 was increased as a result of an increase in the OH level when the multiple scattering code was used.

Table 39. Production and destruction of H_2SO_4 and percent of total production and destruction.

Production Rate (molecules-cm^{-3}-s^{-1}) and Percent of Total Production

Altitude, km	K80	%
10	8.031 E-1	100.00
5	6.610 E-2	100.00
0	1.314 E-4	100.00

Destruction Frequency (s^{-1}) and Percent of Total Destruction

Altitude, km	Heterog. loss	%
10	5.31 E-6	100.00
5	1.42 E-5	100.00
0	2.30 E-5	100.00

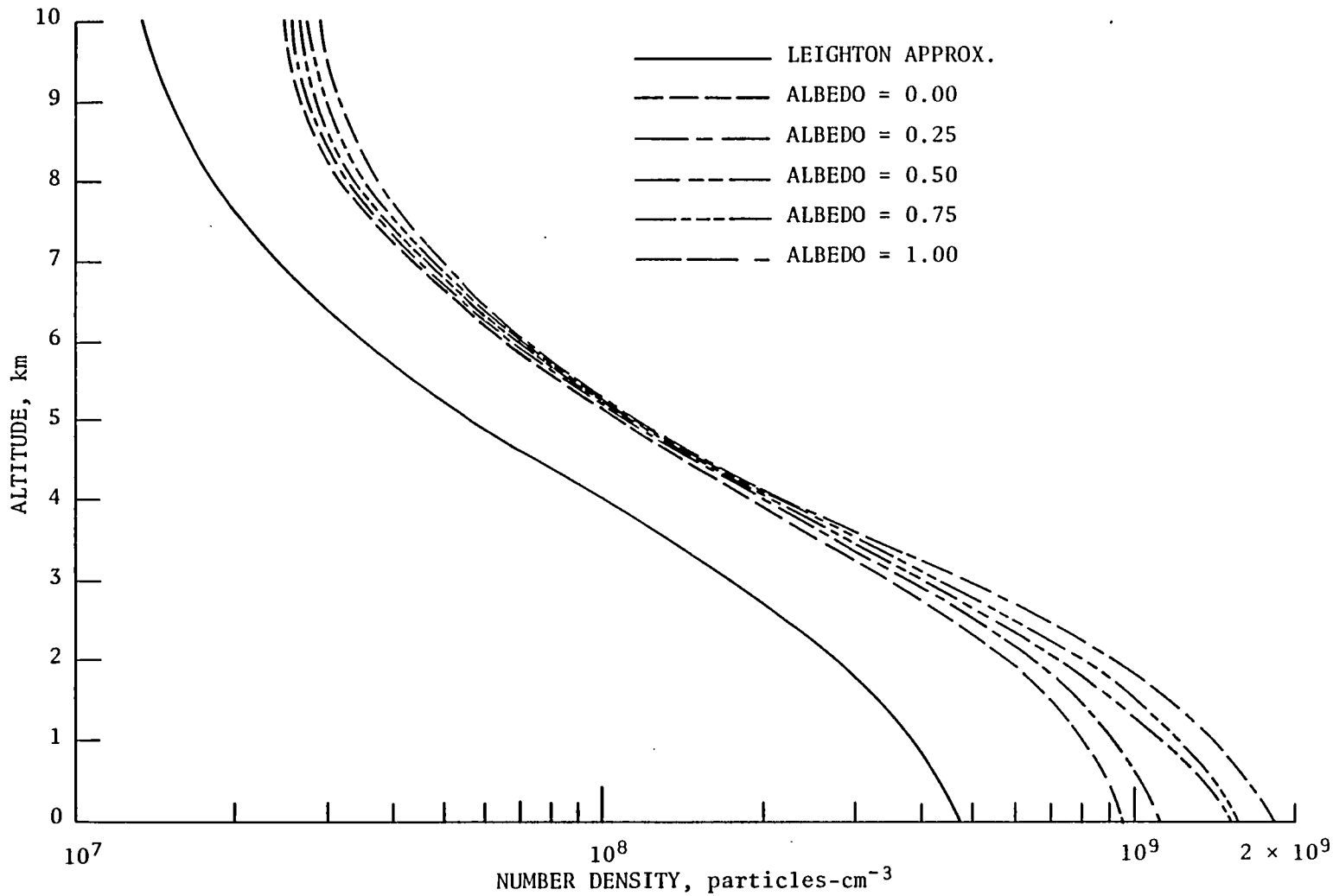

Figure 50. Vertical distributions of H_2SO_4 for the multiple scattering cases with various albedos and the Leighton approximation.

Sulfuric acid radical (HSO_3). -

Production	Destruction
K77 : $SO_2 + OH \rightarrow HSO_3$	K105: $HSO_3 + OH \rightarrow SO_3 + H_2O$
	Heterogenous losses

The only known chemical reaction producing the sulfuric acid radical (HSO_3) is the reaction of SO_2 with OH. It is important to learn how gaaseous sulfur is eventually converted into aerosol particulates. One reaction scheme that eventually produces H_2SO_4 is via the HSO_3 radical. The HSO_3 to H_2SO_4 conversion is not immediate, however. It is therefore of considerable interest to discover the ultimate fate of the HSO_3 radical. Some complex reaction schemes for HSO_3 have been suggested (refs. 195-197), but none is supported by rate constants. Gas phase loss occurs as a result of reaction of HSO_3 with OH (reaction 105). The homogeneous lifetime of HSO_3 is approximately 12 hr at the surface (see table 40). The heterogeneous loss term is modeled similar to H_2SO_4 (ref. 52). The combined lifetime due to both homogeneous and heterogeneous chemistry is about six hours at the surface.

It is of interest to find out the details of the fate of the HSO_3 radical because it offers a loss mechanism for sulfur before oxidation to H_2SO_4 occurs. As is the case of H_2SO_4, no tropospheric measurements of HSO_3 exist. The free acid H_2SO_3 is not believed to exist, while the bisulfites containing HSO_3 are known (ref. 198). The boundary conditions chosen for HSO_3 are similar to those for H_2SO_4. The resulting profiles are shown in figure 51. At the surface HSO_3 is lost by almost equal amounts due to gas-phase reaction and heterogeneous loss. With increasing altitude, the gas-phase loss starts to predominate over the heterogeneous loss such that, at the tropopause, approximately 70 percent of the HSO_3 molecules are destroyed due to reaction 77 and the remaining 30 percent are lost heterogeneously. The model-calculated vertical profiles of HSO_3, shown in figure 51, have an interesting crossover point at two km. Ini-

Table 40. Production and destruction terms of HSO_3 and percent of total production and destruction.

Production Rate (molecules-cm^{-3}-s^{-1}) and Percent of Total Production

Altitude, km	K77	%
10	1.055 E-2	100.00
5	5.179 E-2	100.00
0	2.454 E-4	100.00

Destruction Frequency (s^{-1}) and Percent of Total Destruction

Altitude, km	K105	%	Heterog. loss	%	Total	%
10	1.302 E-5	71.04	5.310 E-6	28.96	1.833 E-5	100.00
5	1.906 E-5	57.31	1.420 E-6	42.69	3.326 E-6	100.00
0	2.420 E-5	51.77	2.300 E-5	48.73	4.720 E-5	100.00

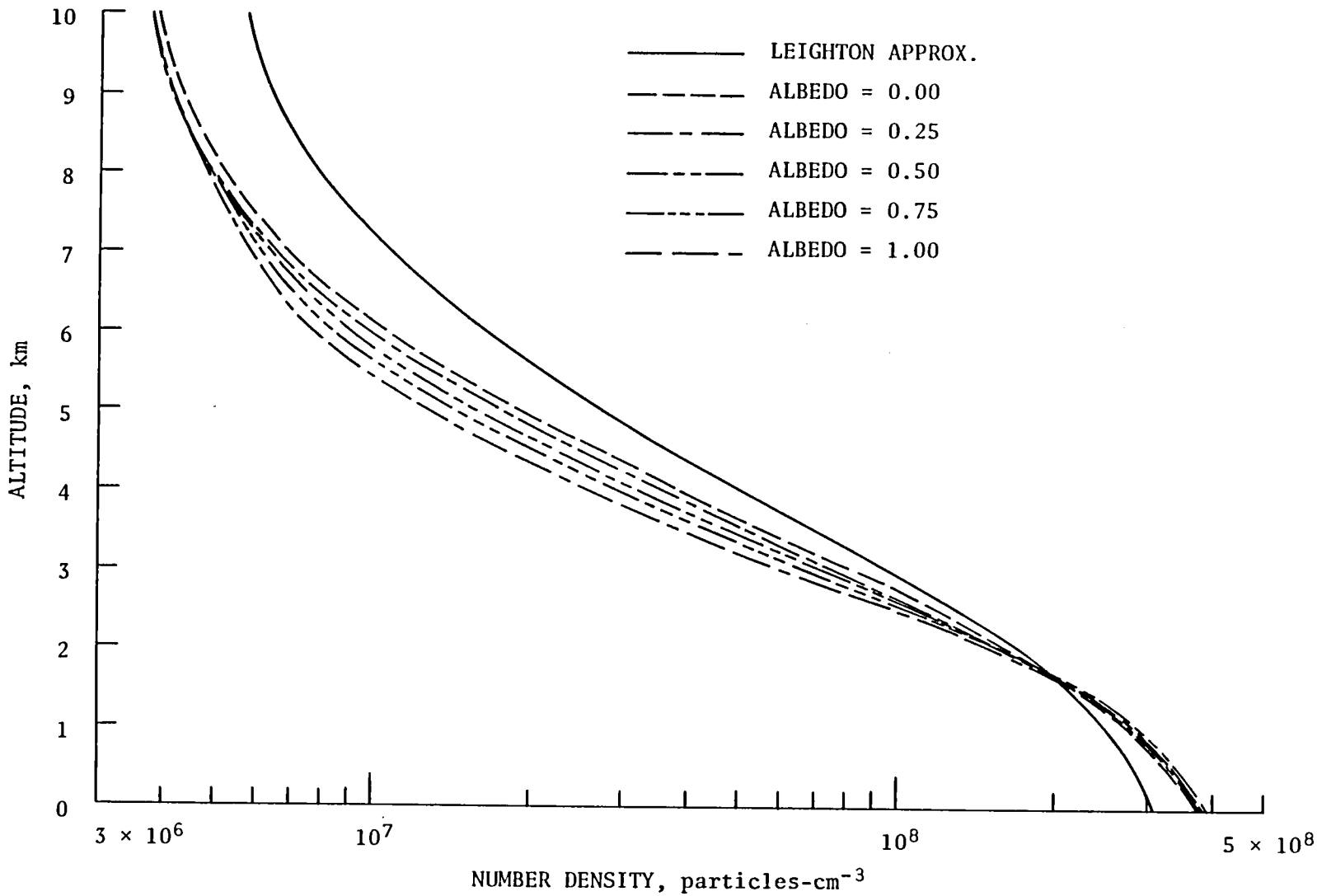

Figure 51. Vertical distributions of HSO_3 for the multiple scattering cases with various albedos and the Leighton approximation.

tially, the multiple scattering calculations show slightly enhanced levels of HSO_3 compared to the Leighton approximation. At 2 km, nearly all calculations have similar values, and between 2 and 10 km inclusion of the multiple scattering code causes decreased levels of HSO_3. This crossover point is due to the fact that both the production and loss terms are dependent on the OH level. In the mid to upper regions of the troposphere, the levels of SO_2 are decreased when the multiple scattering code is used. Hence, these decreased SO_2 levels combine with enhanced levels of OH and produce vertical profiles of HSO_3 that are smaller in magnitude than the vertical profile calculated using the Leighton approximation.

Sulfoxy (SO). -

Production		Destruction	
K66 :	$HS + O_2 \rightarrow SO + OH$	K68 :	$SO + O_2 \rightarrow SO_2 + O$
K70 :	$CS_2 + O \rightarrow SO + CS$	K103:	$SO + O_3 \rightarrow SO_2 + O_2$
K74 :	$CS + O_2 \rightarrow SO + CO$	K69 :	$SO + NO_2 \rightarrow SO_2 + NO$
K76 :	$S + O_2 \rightarrow SO + O$	K90 :	$SO + SO \rightarrow SO_2 + S$
K101:	$COS + O \rightarrow SO + CO$	K91 :	$SO + SO_3 \rightarrow 2SO_2$
K65 :	$HS + O \rightarrow SO + H$		
K81 :	$SO_2 + O \rightarrow SO + O_2$		

At the surface, sulfoxy (SO) is formed almost exclusively (more than 99.9 percent of the time) by oxidation of the thiohydroxyl radical (HS) with molecular oxygen (O_2) (reaction 66). Of very minor importance are the oxidation of CS_2 with O (reaction 70) and the oxidation of CS with O_2 (reaction 74). The remaining four reactions producing SO at the surface are negligible (see table 41). In the midtroposphere, reaction 66 is still by far the dominant production mechanism for SO (85 percent), but reaction 70 now provides 10 percent of the total SO production. Reaction 74 is contributing slightly less than 5

Table 41. Production and destruction terms of SO and percent of total production and destruction.

Production Rate (molecules-cm^{-3}-s^{-1}) and Percent of Total Production

Altitude, km	K66	%	K70	%	K74	%	K76	%	K101	%	K65	%	K81	%	Total	%
10	5.628 E-1	47.01	4.210 E-1	35.17	2.083 E-1	17.40	4.998 E-1	0.41	9.065 E-2	0.01	9.759 E-10	-	1.842 E-17	-	1.198 E-2	100.00
5	3.588 E-2	85.71	3.965 E-1	9.47	1.972 E-1	4.71	4.735 E-1	0.11	2.010 E-1	-	1.263 E-9	-	9.324 E-15	-	4.186 E-2	100.00
0	6.475 E-4	99.92	3.369 E-1	0.05	1.677 E-1	0.03	4.025 E-1	-	3.318 E-1	-	4.984 E-8	-	1.059 E-10	-	6.480 E-4	100.00

Destruction Frequency (s^{-1}) and Percent of Total Destruction

Altitude, km	K68	%	K103	%	K69	%	K90	%	K91	%	Total	%
10	6.587 E-1	96.56	2.280 E-2	3.34	6.654 E-4	0.10	1.118 E-13	-	7.058 E-17	-	6.822 E-1	100.00
5	7.236 E-0	99.47	3.666 E-2	0.50	1.613 E-3	0.03	3.488 E-13	-	3.158 E-17	-	7.274 E-0	100.00
0	5.051 E-1	99.89	4.903 E-2	0.10	6.690 E-3	0.01	7.686 E-12	-	5.774 E-17	-	5.057 E-1	100.00

percent, and reaction 76 a scant 0.1 percent. At the tropopause (10 km), reaction 66 is still the largest producer of SO, but its share has decreased to 47 percent compared to the increase of reaction 70 to 35 percent and reaction 74 to almost 17.5 percent. Even reaction 76 shows a modest gain to 0.4 percent, and reaction 101 now contributes a miniscule 0.01 percent to the total SO production. The oxidation of the HS with O (reaction 65) and the oxidation of SO_2 with O (reaction 81) are negligible when compared to the other reactions producing SO.

Losses are primarily due to oxidation of SO with O_2 (reaction 68). More than 99 percent of the destruction of SO at the surface occurs as a result of reaction 68. This predominance is evident even in higher regions of the troposphere. At 5 km, reaction 68 accounts for about 99.5 percent and, at 10 km, for approximately 96.5 percent of the total loss. The remaining portion of the SO destruction is due to reaction 103, which provides 0.1 percent of the loss at the surface, 0.5 percent at 5 km, and about 3.5 percent at the tropopause. Reaction 69 offers a minor pathway to loss of sulfoxy (see table 41). Negligible loss mechanisms include the reaction of sulfoxy with itself (reaction 90) and of SO reacting with SO_3 (reaction 91). Hence, the five loss mechanisms for SO always produce SO_2, which is an important SO_2 precursor. The calculated lifetime of SO based on the reactions above is on the order of 10^{-2} s.

Due to its short lifetime and high reactivity, measurements of SO cannot be made, as is the case for most reactive, short-lived, photochemical equilibrium species. The vertical profiles of SO are plotted in figure 52. At the surface there are large differences in the values of number densities of SO due to the various albedos. There is almost a logarithmic increase from the Leighton approximation to the multiple scattering case with an albedo of 1.00. Between 2 and 4 km the roles are reversed, with the Leighton approximation yielding the highest number densities and the multiple scattering case, with an albedo of 1.00, the lowest. Near the tropopause the roles are reversed again, resembling the distribution at the surface. This peculiar behavior in the vertical distribution of SO is due to its strong dependence on HS for its formation. Hence, the vertical profiles of SO closely resemble those of the thiohydroxyl radical (HS) which is discussed in the next subsection.

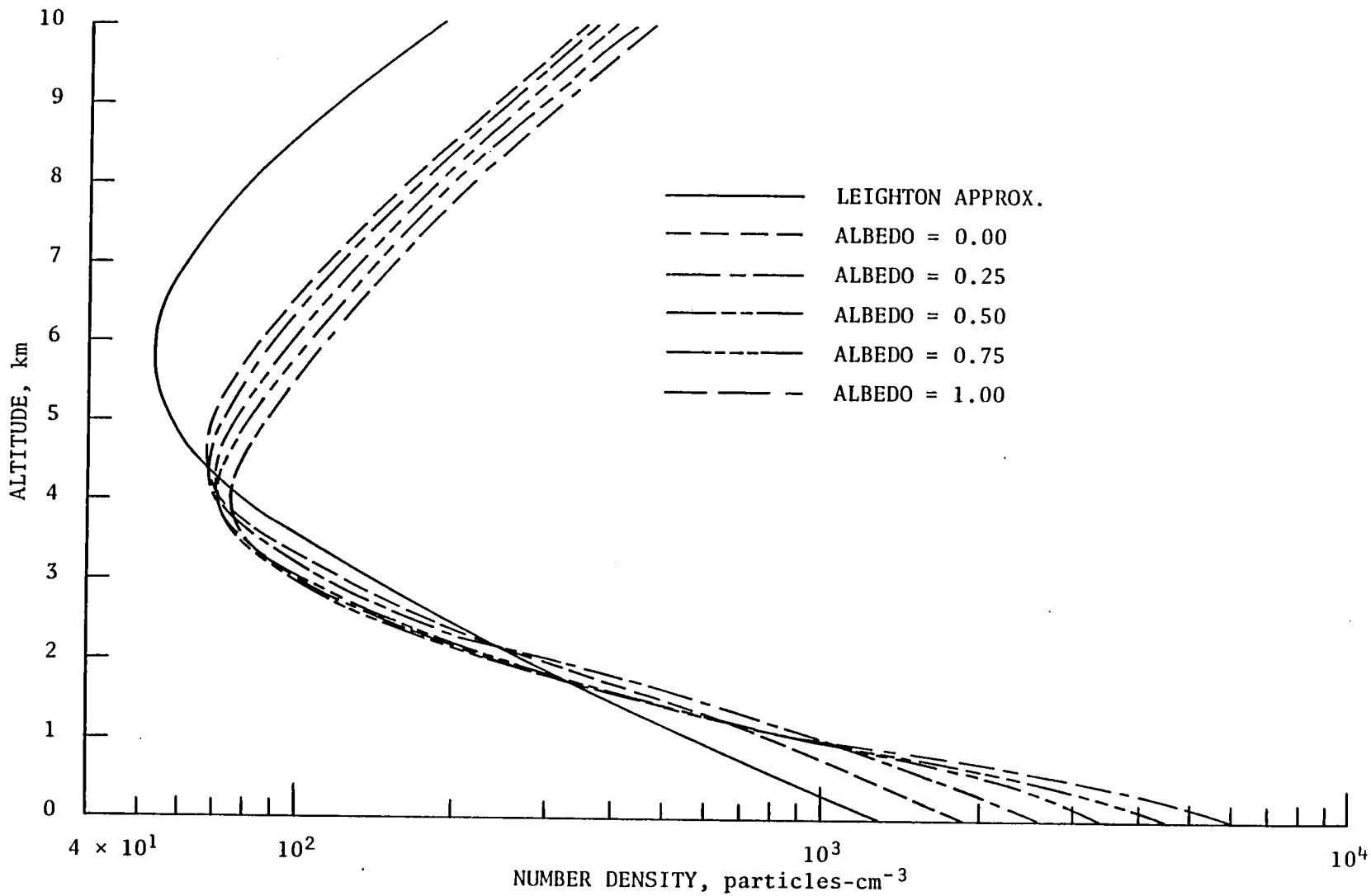

Figure 52. Vertical distributions of SO for the multiple scattering cases with various albedos and the Leighton approximation.

Thiohydroxyl radical (HS). -

Production		Destruction	
K64 :	$H_2S + OH \rightarrow HS + H_2O$	K66 :	$HS + O_2 \rightarrow SO + OH$
K86 :	$COS + OH \rightarrow HS + CO_2$	K67 :	$HS + NO \rightarrow$ products
K87 :	$CS_2 + OH \rightarrow HS + COS$	K65 :	$HS + O \rightarrow SO + H$
K102:	$H_2S + O \rightarrow HS + OH$	K82 :	$HS + H \rightarrow S + H_2$
K84 :	$H_2S + H \rightarrow HS + H_2$	K93 :	$HS + HS \rightarrow H_2S + S$
K85 :	$COS + H \rightarrow HS + CO$		
K83 :	$S + H_2 \rightarrow HS + H$		

The thiohydroxyl radical (HS) is a highly reactive species formed by seven reactions and destroyed by five. Only two of the seven reactions forming HS are of significance. At the surface, reaction of H_2S with OH (reaction 64) provides more than 99.5 percent of the thiohydroxyl radicals that are produced (see table 42). Reaction of COS with OH (reaction 86) contributes about 0.4 percent, while the reaction of H_2S with H (reaction 87) is responsible for a scant 0.02 percent. At 5 km, 64 percent of the HS produced is due to reaction 64, and about 34.4 percent to reaction 86. Again reaction 87 is a minor contributor (2.1%). At the tropopause, reaction 86 dominates over reaction 64 with 86.6 percent and 9.4 percent production, respectively. At this altitude reaction 87 contributes to 5 percent of the HS formation.

Losses of HS are due almost entirely to the oxidation of O_2 (reaction 66). Of negligible importance are the remaining four loss mechanisms: HS reacting with NO (reaction 67), HS oxidized by O (reaction 65), HS reacting with H (reaction 82), and HS reacting with itself (reaction 93). In fact, reaction 66 dominates by more than nine orders of magnitude over any of the other loss mechanisms for HS.

Table 42. Production and destruction terms of HS and percent of total production and destruction.

Production Rate (molecules-cm^{-3}-s^{-1}) and Percent of Total Production

Altitude, km	K64	%	K86	%	K87	%	K102	%	K84	%	K85	%	K83	%	Total	%
10	5.336 E-0	9.38	4.858 E-1	85.60	2.953 E-0	5.02	1.334 E-4	-	1.069 E-4	-	1.694 E-5	-	1.196 E-18	-	5.687 E-1	100.00
5	2.353 E-2	63.50	1.274 E-2	34.38	7.879 E-0	2.12	2.687 E-3	-	2.222 E-3	-	3.789 E-5	-	1.133 E-18	-	3.706 E-2	100.00
0	6.476 E-4	99.55	2.778 E-2	0.43	1.759 E-1	0.02	3.446 E-1	-	3.715 E-1	-	8.008 E-5	-	9.630 E-19	-	6.506 E-4	100.00

Destruction Frequency (s^{-1}) and Percent of Total Destruction

Altitude, km	K66	%	K67	%	K65	%	K82	%	K93	%	Total	%
10	1.797 E-5	100.00	1.164 E-4	-	3.117 E-6	-	4.643 E-12	-	7.514 E-15	-	1.797 E-5	100.00
5	3.198 E-5	100.00	1.485 E-4	-	1.125 E-6	-	5.789 E-12	-	2.693 E-14	-	3.198 E-5	100.00
0	5.330 E-5	100.00	3.190 E-4	-	4.102 E-7	-	7.138 E-12	-	2.916 E-12	-	5.330 E-5	100.00

The resulting lifetime of HS is very short, on the order of 10^{-6} s. Its calculated vertical profiles are shown in figure 53. The vertical distributions of HS are very similar to those of SO, except in the upper troposphere, where HS decreases continuously while SO exhibits increases. This difference is due to the fact that SO is very dependent on CS_2 for its formation in the upper troposphere. Carbon disulfide is a very stable and well-mixed molecule; consequently, there is nearly as great of an abundance of it at the tropopause as there is at the surface.

Carbon sulfide (CS). -

Production	Destruction
K70 : $CS_2 + O \rightarrow CS + SO$	K74 : $CS + O_2 \rightarrow SO + CO$
K88 : $CS_2 + S \rightarrow CS + S_2$	K75 : $CS + O_2 \rightarrow COS + O$
	K73 : $CS + O \rightarrow S + CO$

Carbon sulfide (CS) is formed primarily when CS_2 is oxidized by O (reaction 70) and, of negligible importance, when S reacts with CS_2 (reaction 88). Table 43 shows more than 10 orders of magnitude difference between these 2 reactions. The two primary loss mechanisms are oxidation of CS with O_2 (reactions 74 and 75). The reaction of CS with O_2 takes two paths with equal preference. A negligible loss for CS is the oxidation with O (reaction 73). The lifetime of CS based on these reactions is on the order of 10^{-2} s, well justifying the PCE assumption. The vertical profiles shown in figure 54 generally increase with altitude. The multiple scattering calculation with an albedo of 0.00 shows small differences in the low and midtroposphere compared to the Leighton approximation. Near the tropopause, however, there is almost a 50 percent increase in the CS number density. An increase in the surface albedo has the effect of increasing the values of the vertical profiles of CS. For an albedo of 0.25, approximately a 60 percent increase in the CS number density at the surface results. In the midtroposphere, the increase is on the order of 25 percent, while at 10 km the increase is nearly 75 percent.

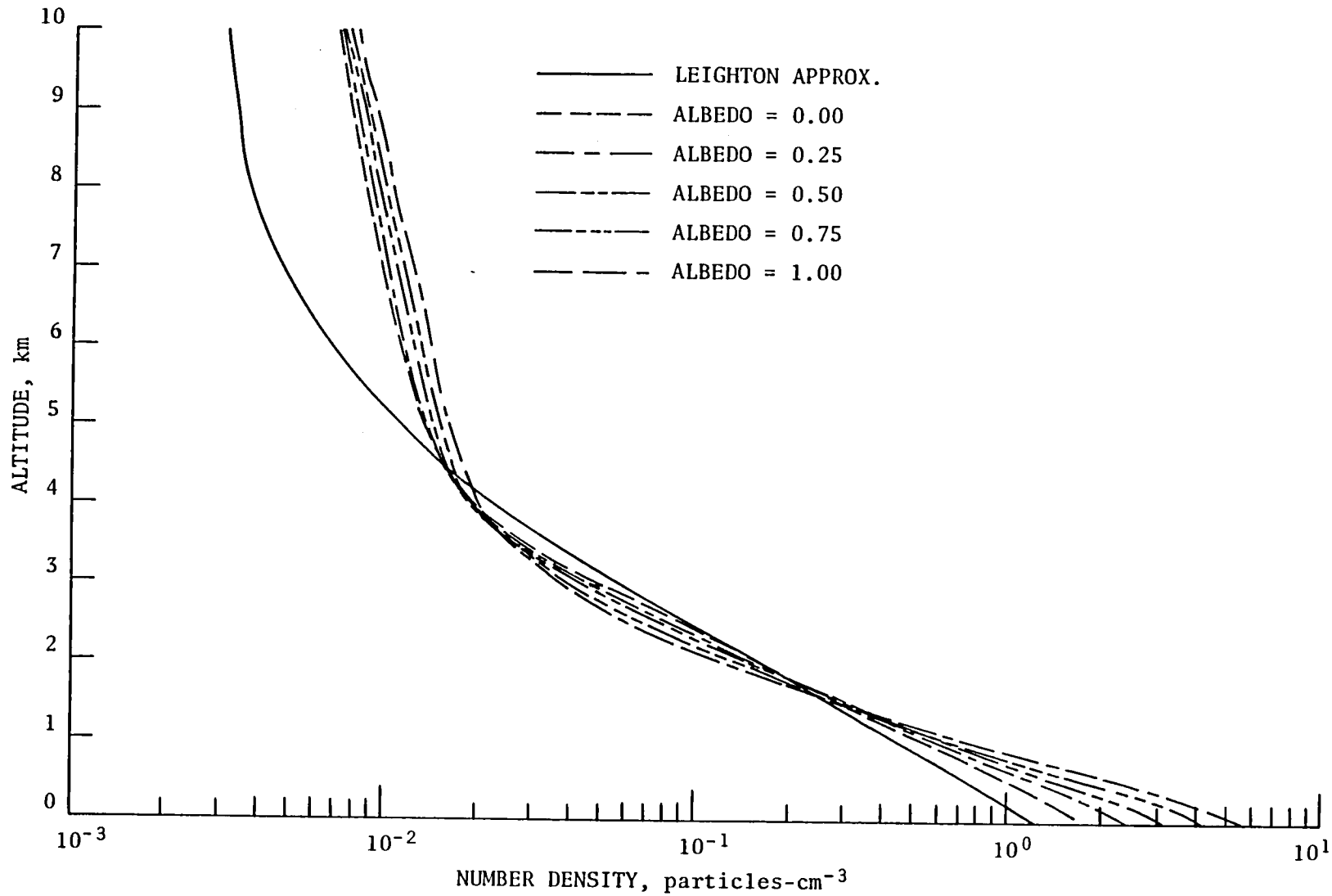

Figure 53. Vertical distributions of HS for the multiple scattering cases with various albedos and the Leighton approximation.

Table 43. Production and destruction terms of CS and percent of total production and destruction.

Production Rate (molecules-cm^{-3}-s^{-1}) and Percent of Total Production

Altitude, km	K70	%	K88	%	Total	%
10	4.188 E-1	100.00	1.242 E-9	-	4.188 E-1	100.00
5	3.965 E-1	100.00	1.206 E-9	-	3.964 E-1	100.00
0	3.369 E-1	100.00	1.081 E-9	-	3.369 E-1	100.00

Destruction Frequency (s^{-1}) and Percent of Total Destruction

Altitude, km	K74	%	K75	%	K73	%	Total	%
10	5.392 E-0	50.00	5.392 E-0	50.00	4.285 E-8	-	1.078 E-1	100.00
5	9.593 E-0	50.00	9.593 E-0	50.00	1.547 E-8	-	1.919 E-1	100.00
0	1.599 E-1	50.00	1.599 E-1	50.00	5.632 E-8	-	3.198 E-1	100.00

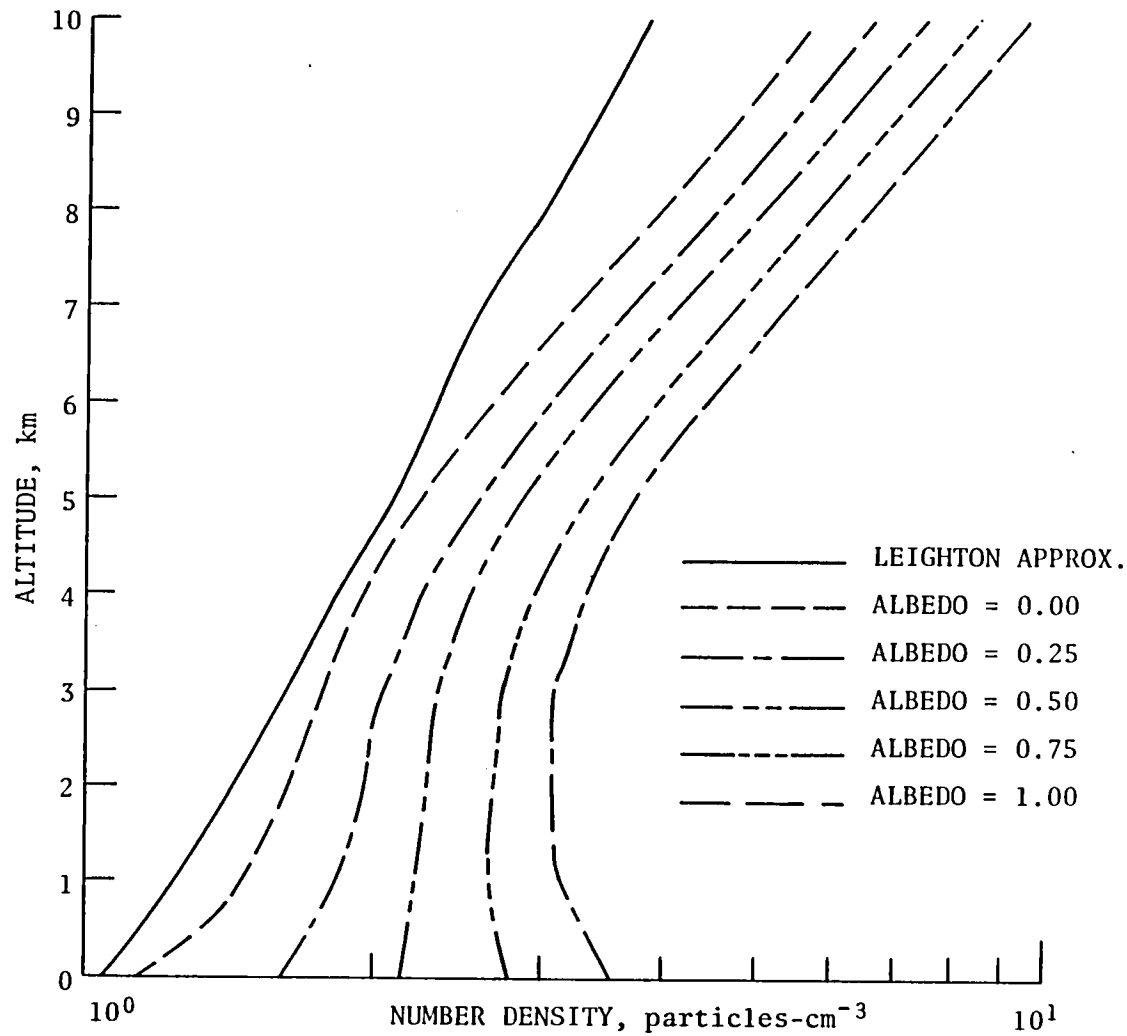

Figure 54. Vertical distributions of CS for the multiple scattering cases with various albedos and the Leighton approximation.

Sulfur trioxide (SO_3). -

Production	Destruction
K105: $HSO_3 + OH \rightarrow SO_3 + H_2O$	K80 : $SO_3 + H_2O \rightarrow H_2SO_4$
K79 : $SO_2 + CH_3O_2 \rightarrow SO_3 + CH_3O$	K91 : $SO_3 + SO \rightarrow 2SO_2$
K78 : $SO_2 + HO_2 \rightarrow SO_3 + OH$	
K104: $SO_2 + O + M \rightarrow SO_3 + M$	

Sulfur trioxide (SO_3) is the only intermediate sulfur species that is known to have nonchemical production terms. The relative importance of chemical versus nonchemical contributions to the total SO_3 budget is poorly understood. Chemically, SO_3 is produced primarily by the reaction of HSO_3 with OH (reaction 105) and by SO_2 reacting with the methylperoxy radical (CH_3O_2) (reaction 79). Reaction 105 acounts for 57 percent of the total SO_3 production at the surface, while reaction 79 accounts for 42 percent. Approximately 1 percent of the SO_3 production comes from the interaction of SO_2 and HO_2 (reaction 78), while a negligible 0.01 percent is due to reaction 104 (see table 44). In the midtroposphere the predominance of reaction 105 is increased to 81 percent, while reaction 79 decreases in its production to approximately 18.5 percent. Reaction 78 accounts for slightly less than 0.5 percent of the SO_3 production in this region, while reaction 104 can be neglected. At the tropopause (10 km) reaction 105 produces about 92 percent of all the SO_3 molecules. Reaction 78 accounts for 7.5 percent and reaction 78 is a minor contributor with 0.3 percent. Again the reaction of SO_2 with O in the presence of a third body M (reaction 104) can be neglected. Minor contributors to SO_3 production are SO_2 reacting with HO_2 (reaction 78) and SO_2 being oxidized by O in the presence of a third body (reaction 104). The main path for SO_3 destruction is the reaction with water vapor (H_2O) (reaction 80). Of negligible importance is the reaction of SO_3 with SO (reaction 91). Sulfur trioxide is very short-lived. Its lifetime is on the order of 10^{-6} s.

Table 44. Production and destruction terms of SO_3 and percent of total production and destruction.

Production Rate (molecules-cm^{-3}-s^{-1}) and Percent of Total Production

Altitude, km	K105	%	K79	%	K78	%	K104	%	Total	%
10	7.432 E-1	92.08	6.135 E-0	7.60	2.564 E-1	0.32	3.929 E-3	-	8.072 E-1	100.00
5	5.329 E-2	80.91	1.227 E-2	18.63	3.017 E-0	0.46	2.489 E-2	-	6.586 E-2	100.00
0	7.478 E-3	57.09	5.491 E-3	41.92	1.286 E-2	0.98	5.615 E-1	0.01	1.310 E-4	100.00

Destruction Frequency (s^{-1}) and Percent of Total Destruction

Altitude, km	K80	%	K91	%	Total	%
10	2.275 E-3	100.00	3.726 E-13	-	2.275 E-3	100.00
5	4.186 E-4	100.00	1.163 E-13	-	4.186 E-4	100.00
0	4.550 E-5	100.00	2.562 E-12	-	4.550 E-5	100.00

The vertical profiles due to the chemistry described above and due to the multiple scattering calculations with various albedos are shown in figure 55. Sulfur trioxide varies strongly as a function of ground albedo. The number density at the surface is more thhan doubled for the case of 0.25 albedo compared to the Leighton approximation, and more than quadrupled for an albedo of 1.00. Above 3 km the effect of albedo is diminished as the major loss term (reaction 80) becomes increasingly predominant. This reaction involves the recombination of SO_3 with water vapor. Since water vapor has a specified vertical profile (discussed under "Water vapor"), only small variations would be expected once the reflecting properties of the surface albedo are accounted for.

Atomic sulfur [$S(^3p)$]. -

Production	Destruction
K71 : $CS_2 + O \rightarrow S + COS$	K76 : $S + O_2 \rightarrow SO + O$
K73 : $CS + O \rightarrow S + CO$	K88 : $S + CS_2 \rightarrow S_2 + CS$
K90 : $SO + SO \rightarrow S + SO_2$	K89 : $S + COS \rightarrow S_2 + CO$
K82 : $HS + H \rightarrow S + H_2$	K83 : $S + H_2 \rightarrow HS + H$
K93 : $HS + HS \rightarrow S + H_2S$	

The production of atomic sulfur [$S(^3P)$] in the atmosphere is due almost entirely to the reaction of CS_2 with O (reaction 71). Of negligible importance are the four reactions: CS with O (reaction 73), SO with itself (reaction 90), HS with H (reaction 83), and HS with itself (reaction 93). Depending on altitude, these four reactions are anywhere from 8 to 17 orders of magnitude less important than reaction 71. Loss of S is primarily by oxidation with molecular oxygen (reaction 76). The reactions of $S(^3p)$ with CS_2 (reaction 88), with COS (reaction 89), and with H_2 (reaction 83) are virtually negligible as losses for $S(^3p)$ (see table 45). The lifetime of $S(^3p)$ is extremely short, aout 10^{-7} s.

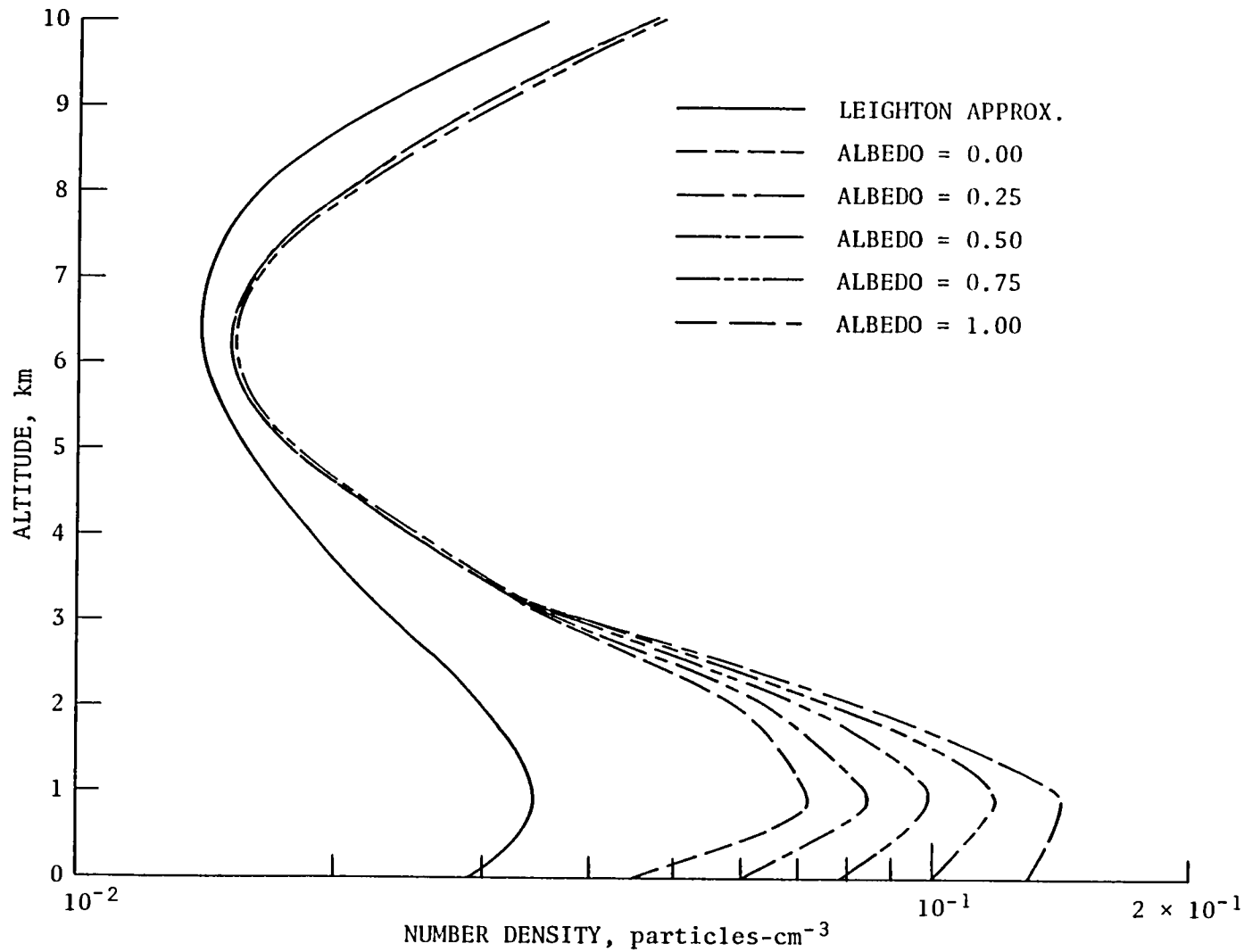

Figure 55. Vertical distributions of SO_3 for the multiple scattering cases with various albedos and the Leighton approximation.

Table 45. Production and destruction terms of $S(^2P)$ and percent of total production and destruction.

Production Rate (molecules-cm^{-3}-s^{-1}) and Percent of Total Production

Altitude, km	K71	%	K73	%	K90	%	K82	%	K93	%	Total	%
10	5.051 E-0	100.00	1.656 E-6	-	1.041 E-10	-	1.454 E-15	-	1.176 E-18	-	5.051 E-0	100.00
5	4.758 E-0	100.00	3.181 E-7	-	1.014 E-11	-	6.505 E-15	-	1.511 E-17	-	4.785 E-0	100.00
0	4.043 E-0	100.00	5.916 E-8	-	4.923 E-9	-	8.672 E-13	-	1.771 E-13	-	4.043 E-0	100.00

Destruction Frequency (s^{-1}) and Percent of Total Destruction

Altitude, km	K76	%	K88	%	K89	%	K83	%	Total	%
10	3.954 E-6	100.00	9.828 E-4	-	1.213 E-6	-	9.460 E-13	-	3.954 E-6	100.00
5	7.035 E-6	100.00	1.791 E-3	-	6.853 E-6	-	1.683 E-12	-	7.035 E-6	100.00
0	1.172 E-7	100.00	3.149 E-3	-	2.904 E-5	-	2.805 E-12	-	1.172 E-7	100.00

The vertical profiles of $S(^3p)$ are shown in figure 56. Inspection of this figure shows that the influence of radiation and chemistry must be very similar to that for carbon sulfide, since the vertical profiles of $S(^3p)$ can be laid over those of CS (with the horizontal scale shifted). This is not unexpected since both $S(^3p)$ and CS are formed and destroyed by similar reactions with identical rate constants. Both $S(^3p)$ and CS are formed when CS_2 reacts with O and, similarly, both are destroyed by oxidation with O_2. Consequently, their vertical profiles should be identical in their shapes for the various albedos.

Methanethiol (CH_3SH). -

Production	Destruction
	K97 : $CH_3SH + OH \rightarrow$ products
	K94 : $CH_3SH + O \rightarrow CH_3 + HSO$
	K95 : $CH_3SH + O \rightarrow CH_3SO + H$
	K96 : $CH_3SH + O \rightarrow CH_3SOH$

No chemical source in the atmosphere is known to exist for methanethiol (CH_3SH), but both natural and anthropogenic sources are known. Some of the natural processes emitting CH_3SH include microbes (ref. 185) and animal waste (ref. 199). Anthropogenically, CH_3SH is emitted due to petroleum manufacturing (ref. 177), sewage treatment (ref. 200) and wood pulping (ref. 183). Destruction of CH_3SH at the surface proceeds almost exclusively (99.9%) through reaction 97. Reactions 94, 95, and 96 each account for a minute 0.01 percent. Even in the mid and upper regions of the troposphere, these percentages remain almost constant (see table 46). The vertical profiles of CH_3SH (see fig. 57) decrease very rapidly with altitude. This is due to the efficient reaction with OH. The lower boundary condition is held constant at 0.001 parts per trillion by volume (pptv). The calculated lifetime based on the four destruction terms above is slightly more than three hours. The combination of short

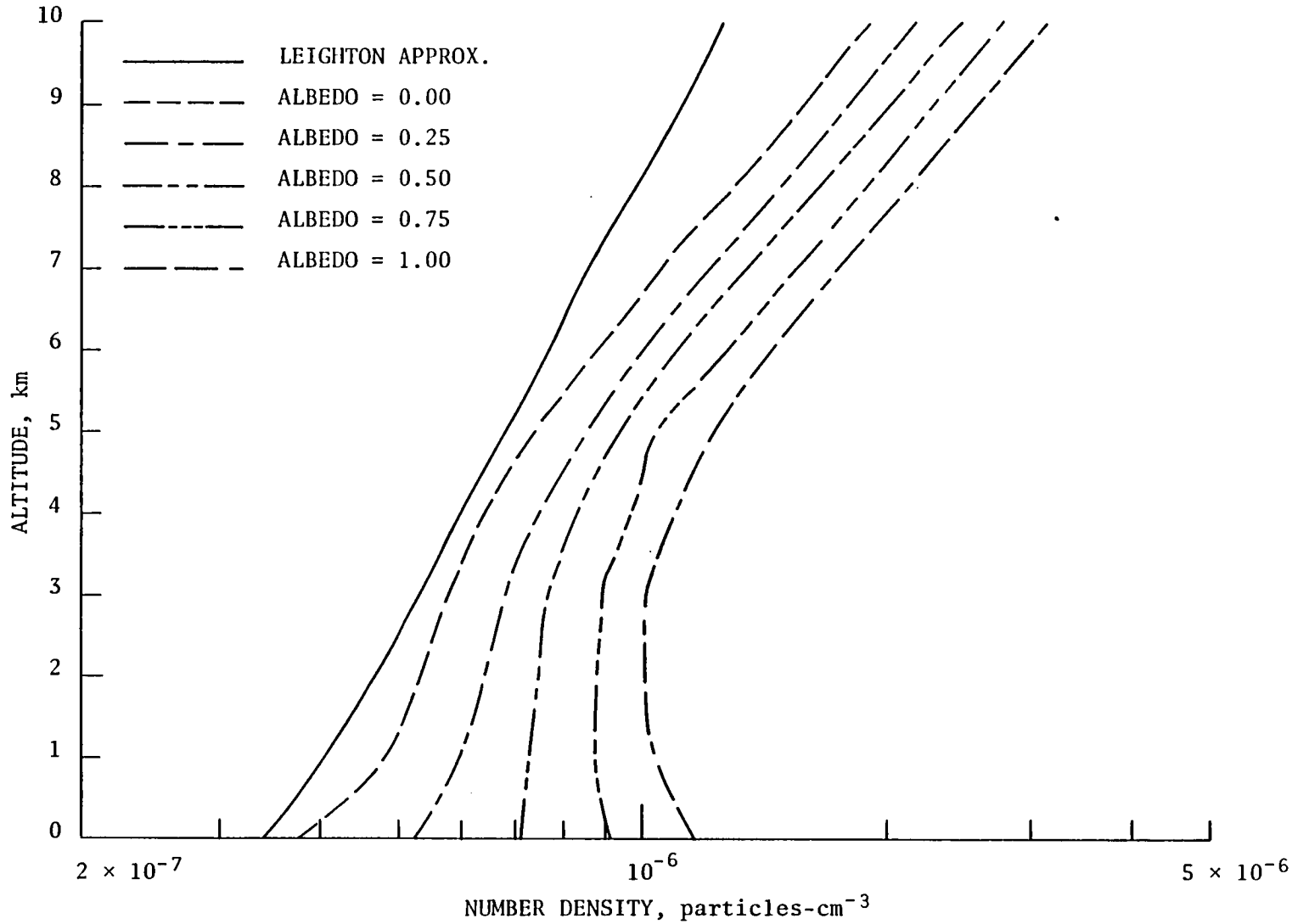

Figure 56. Vertical distributions of $S(^3p)$ for the multiple scattering cases with various albedos and the Leighton approximation.

Table 46. Destruction terms of CH_3SH and percent of total destruction. (No chemical production terms are known.)

	Destruction Frequency (s^{-1}) and Percent of Total Destruction									
Altitude, km	K97	%	K94	%	K95	%	K96	%	Total	%
10	4.428 E-5	99.76	3.701 E-8	0.08	3.701 E-8	0.08	3.701 E-8	0.08	4.439 E-5	100.00
5	6.480 E-5	99.94	1.336 E-8	0.02	1.336 E-8	0.02	1.336 E-8	0.02	6.484 E-5	100.00
0	8.230 E-5	99.97	4.872 E-9	0.01	4.872 E-9	0.01	4.872 E-9	0.01	4.439 E-5	100.00

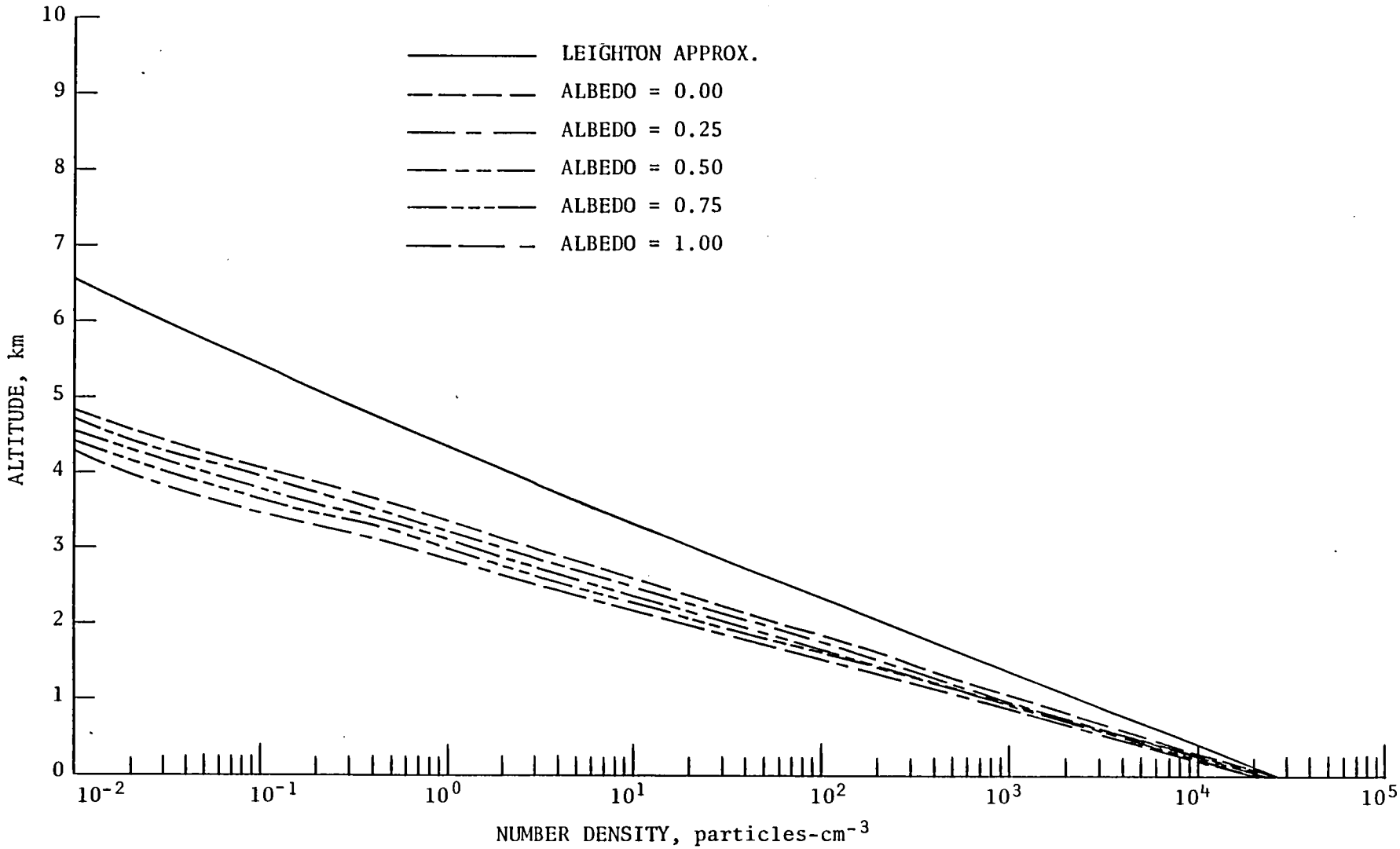

Figure 57. Vertical distributions of CH_3SH for the multiple scattering cases wtih various albedos and the Leighton approximation.

lifetime, strong dependence on OH, and an absence of a chemical source term produces the rapidly decreasing vertical profiles. Methanethiol has a strong dependence on albedo which is to be expected since the destruction term is dominated by the reaction with OH (reaction 97). The hydroxyl radical in turn has a very strong dependence on surface albedo, as seen in the subsection titled "Hydroxyl radical."

Dimethyl sulfide (CH_3SCH_3). -

Production	Destruction
	K100: $CH_3SCH_3 + OH \rightarrow$ products
	K99 : $CH_3SCH_3 + O \rightarrow CH_2S + CH_3O$
	K98 : $CH_3SCH_3 + O \rightarrow CH_3SO + CH_3$

Dimethyl sulfide (CH_3SCH_3), sometimes also written as $(CH_3)_2S$, like CH_3SH has no known chemical source terms in the atmosphere. The same natural and anthropogenic sources that emit CH_3SH have also been identified as emitting CH_3SCH_3. Hence, the natural sources are microbial activity (ref. 185) and animal waste (ref. 199), while the manmade sources are sewage treatment (ref. 200), wood pulping (ref. 183), and the manufacturing of petroleum products (ref. 177). Chemical destruction at the ground occurs primarily as a result of reaction 100. Minor contributions are due to reactions 99 and 98. In the upper region of the troposphere, reaction 100 still dominates with approximately 87 percent, 7.5 percent of the production is due to reaction 99, and 5.5 percent is due to reaction 98 (see table 47). The chemical lifetime based on the three destruction terms is approximately 12 hr. The vertical profiles of CH_3SCH_3 (see fig. 58) exhibit very similar characteristics to those of CH_3SH. This is to be expected since the same arguments that applied to CH_3SH are pertinent to CH_3SCH_3.

Table 47. Destruction terms of CH_3SCH_3 and percent of total destruction. (No chemical production terms are known.)

Destruction Frequency (s^{-1}) and Percent of Total Destruction

Altitude, km	K100	%	K99	%	K98	%	Total	%
10	1.443 E-5	86.97	1.227 E-6	7.40	9.349 E-7	5.63	1.359 E-5	100.00
5	1.957 E-5	96.16	4.431 E-7	2.18	3.376 E-7	1.66	2.035 E-5	100.00
0	2.345 E-5	98.82	1.616 E-7	0.68	1.231 E-7	0.50	2.371 E-5	100.00

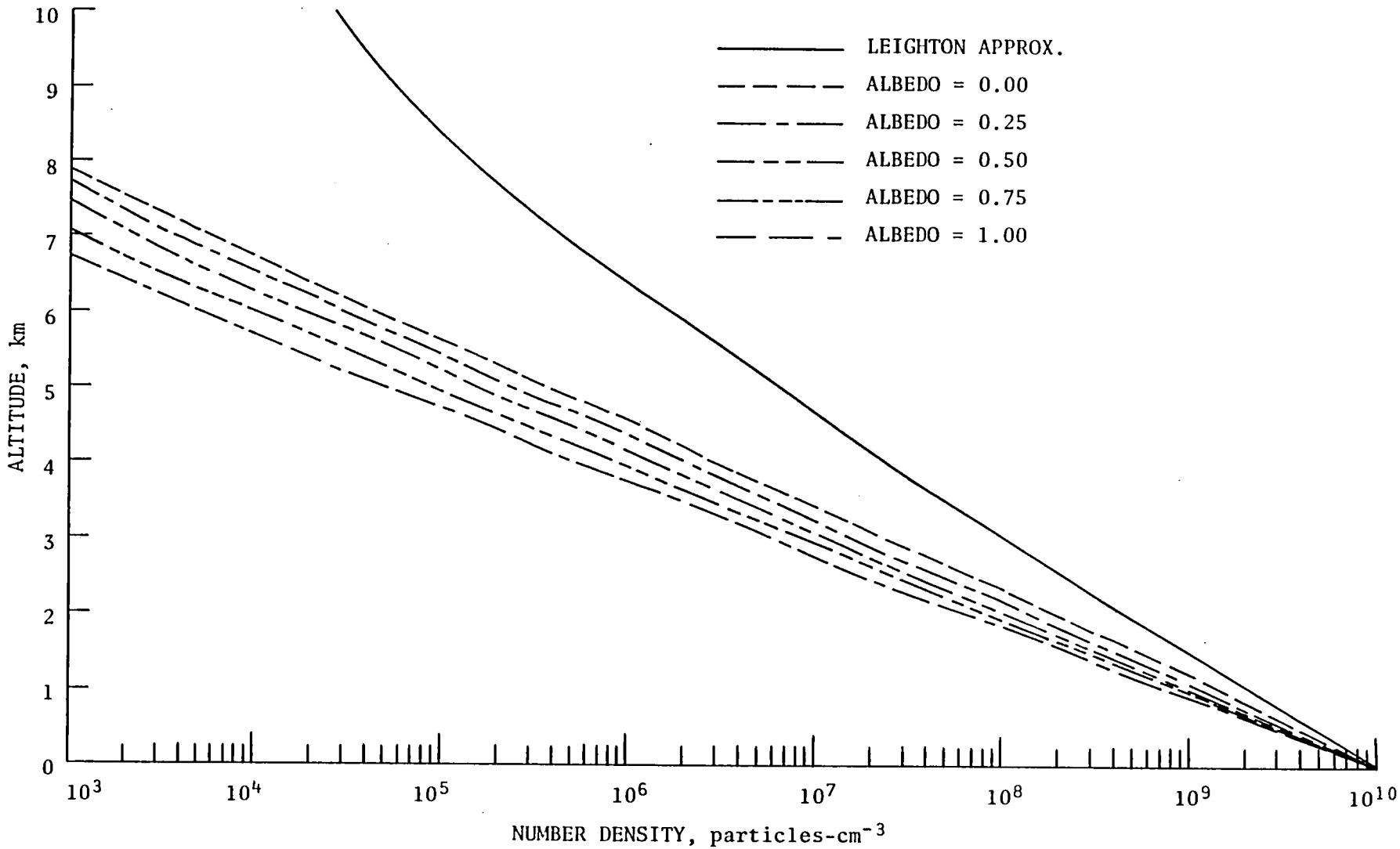

Figure 58. Vertical distributions of CH_3SCH_3 for the multiple scattering cases with various albedos and the Leighton approximation.

Future perturbations to the sulfur budget. - A couple of decades ago the only global scale consequences of the sulfur species was thought to be the formation of stratospheric particulates (refs. 157, 158). This argument was based on the relatively moderate lifetimes of most sulfur species. Lifetimes on the order of a few days to a week were thought to preclude any important contributions to global tropospheric chemistry. We now know that sulfur species play an integral part in the highly coupled and complex chemical system that constitutes the troposphere. Sulfur dioxide emissions have exhibited an upward trend during the 1960's. This trend was partially reversed during the 1970's. Some actions responsible for this decrease were a greater use of clean-burning natural gas and of crude oil with low sulfur content. Also, a slower economic growth coupled with energy conservation contributed to a decrease in SO_2 emissions. Recently, this trend has started upward again. The global concentrations of sulfur compounds are very likely to see a rapid increase in years to come due to energy policies. Already emission standards for many oil-burning power plants and industrial plants have been relaxed to allow for usage of lower grade crude oil containing more sulfur. Anthropogenic emissions are currently responsible for approximately half as much of the atmospheric sulfur concentrations as the natural emissions, but some 20 to 25 years from now manmade emissions may equal those of nature and may, at the turn of the century, surpass natural emissions in the Northern Hemisphere (ref. 175).

The estimates of global emission of sulfur are widely varying. Katz (ref. 173) made some early estimates and calculated that 77×10^6 metric tons of SO_2 were emitted in 1943. The Study of Critical Environmental Problems (ref. 201) established a global emission of 93×10^6 metric tons per year in 1967-68. Robinson and Robbins (ref. 174) estimated the annual total SO_2 emission in the mid-1960's to be 146×10^6 metric tons. A more recent estimate (ref. 162) suggests global manmade emissions of SO_2 of 183×10^6 metric tons. It is significant to note that, of the total global emissions of SO_2, 93.5 percent occurs in the Northern Hemisphere and only 6.5 percent in the Southern Hemisphere (ref. 201). The most recent estimate (ref. 162) of global bacterio-

genic production of SO_2 is 210×10^6 metric tons. Fertilizers are thought to acount for 33×10^6 metric tons. This portion of the sulfur budget is very likely to increase further.

In the SCEP report (ref. 201) some predictions for the future were made. An annual growth in fossil fuel usage of 4 percent between 1970 and 1980 was assumed, with a 3.5 percent growth rate expected from 1980 to 2000. By the year 2000 A.D., a global anthropogenic emission of 275×10^6 metric tons per year would occur (ref. 201). However, at the present time it seems that any predictions of future crude oil usage are risky at best.

It is evident that future sulfur levels in the atmosphere will be a strong function of man's activities. Many questions concerning sulfur species remain to be answered: for example, the exact amounts of naturally vs. anthropogenically produced sulfur need to be ascertained. Also, the global concentration of SO_2 needs to be calculated. Present measurements are too inconclusive and, in part, contradictory. Furthermore, short-term and long-term impacts of SO_2 emissions on the sulfur budget must be better understood. The primary chemical loss for SO_2 is OH. The hydroxyl radical is very reactive and acts somewhat like a tropospheric vaccuum cleaner. Sulfur dioxide competes with many other species for the OH radical. The budgets of these competing trace gases need to be addressed. The importance of homogeneous vs. heterogeneous loss for SO_2 needs further research. Presently, it is believed that 50 percent of SO_2 is lost homogeneously and 50 percent is lost heterogeneously, but this breakdown is only a very crude estimate. The depositional velocity of SO_2 needs further defining. Estimates vary from 0.1 to 2.5 cm s^{-1} with 1.0 cm s^{-1} as an average. The vertical profiles of SO_2 are very dependent on this quantity. It is also most important to find the mechanism that controls the sulfur dioxide-to-sulfate (gas-to-particle) conversion. From figure 45 it can be seen that SO_2 is converted to H_2SO_4 via the intermediate species SO_3. A possible alternate reaction path involves the HSO_3 radical. The fate of this molecule is virtually unknown. Also, the kinetic data concerning the reactions that convert SO_2 to SO_4^{-2} need to be improved. Finally, the role of ammonia (NH_3) in aerosol formation needs to be addressed. Ammonia is largely responsible for neutraliz-

ing the acidic sulfur species. Hence, if the sulfur budget increases more rapidly than the ammonia budget, an increase in acidic precipitation over the already high levels would result.

In conclusion, we have seen that the sulfur family, because it is largely so anthropogenic, will play an increasingly important role in tropospheric chemistry. Additional research is needed to answer many of the questions related to the tropospheric sulfur budget. The answers to these questions will have an impact on many fields of scientific study, e.g., radiative transfer, climatology, meteorology, agronomy, ecology, and limnology, just to mention a few.

CONCLUSIONS

A one-dimensional radiative transfer/photochemical model that includes detailed radiative transfer processes which control the levels of incoming solar radiation in the troposphere, e.g. Rayleigh and Mie scattering and surface albedo, and a detailed chemistry package that includes 114 chemical reactions, 12 photolytic processes, and eddy transport have been described. Thirty-eight tropospheric gases were investigated with respect to the processes that govern their distributions, i.e., transport, radiation, and chemistry. The radiative transfer model makes use of a matrix inversion code that calculates the source function accurately and with a high degree of computational precision and efficiency. It was found that inclusion of multiple scattering and surface albedo significantly alters the vertical profiles of most species compared to the Leighton approximation, a one-stream radiation approximation widely used in most tropospheric models. In particular, large differences are calculated for species that are dependent on processes in the near ultraviolet region (300 to 320 nm). The frequencies for ozone photolysis yielding excited oxygen [$O(^1D)$] are enhanced between factors of two to eight, depending on altitude and surface albedo. The increased levels of $O(^1D)$ cause enhanced levels of the hydroxyl radical (OH), which is formed when water vapor (H_2O) reacts with the excited oxygen atom [$O(^1D)$]. Since reaction with OH is major chemical loss mechanism for many tropospheric gases, it is essential

to know the distribution of this radical with high accuracy. At the surface, the OH number densities are increased from a factor of 1.4 to a factor of 4.0, depending on the assumed surface albedo. In the upper troposphere, the OH number densities are enhanced by a factor of 3.0. The theoretical results have been compared to measured values when such measurements are available. Measurements of many species and photolytic processes, in general, agree very well with the distributions obtained with the multiple scattering radiative transfer model coupled to the tropospheric photochemical model.

Future studies should include a description of the photochemical production, transformation and removal of tropospheric aerosols, and the sensitivity of aerosol production to concentrations of sulfur dioxide (SO_2), odd nitrogen (NO_x), and ammonia (NH_3). In addition, the photochemical production of acid rain needs to be addressed. Furthermore, the rainout parameterization of water-soluble gases needs to be improved.

A vast improvement in the calculations of the radiation field would be the inclusion of clouds. The amount of incoming radiation in the troposphere is altered significantly when clouds are present compared to a cloudless sky. Since the Earth has approximately a 50 percent cloudcover on the average, the need to include clouds in the radiative transfer calculations is obviously great.

REFERENCES

1. Chamberlain, T.C.: An Attempt to Frame a Working Hypothesis of the Cause of Glacial Periods on an Atmospheric Basis. J. Geol., Vol. 7, 1899, pp. 575, 667, 751.

2. Cunnold, D.F.; Aleya, F.; Phillips, N.; and Prinn, R.: A Three-Dimensional Dynamic-Chemical Model of Atmospheric Ozone. J. Atmos. Sci., Vol. 32, No. 1, Jan. 1975, pp. 170-194.

3. Levy, H., II: Normal Atmosphere: Large Radical and Formaldehyde Concentrations Predicted. Science, Vol. 173, No. 3992, July 1971, pp. 141-143.

4. Levy, H., II: Photochemistry of the Lower Troposphere. Planetary and Space Sci., Vol. 20, No. 6, June 1972, pp. 919-935.

5. Levy, H., II: Photochemistry of Minor Constituents in the Troposphere. Planetary and Space Sci., Vol. 21, No. 4, Apr. 1973, pp. 575-591.

6. Chameides, W.L.; and Walker, J.C.G.: A Photochemical Theory of Tropospheric Ozone. J. Geophys. Res., Vol. 78, No. 36, Dec. 1973, pp. 8751-8760.

7. Stewart, R.W.; Hameed, S.; and Pinto, J.P.: Photochemistry of Tropospheric Ozone. J. Geophys. Res., Vol. 82, No. 21, July 1977, pp. 3134-3140.

8 Liu, S.C.: Possible Effects on Tropospheric O_3 and OH Due to NO Emissions. Geophys. Res. Lett., Vol. 4, No. 8, Aug. 1977, pp. 325-328.

9. Fishman, J.; and Crutzen, P.J.: A Numerical Study of Tropospheric Photochemistry Using a One-Dimensional Model. J. Geophys. Res., Vol. 82, No. 37, Dec. 1977, pp. 5897-5906.

10. Man's Impact on the Troposphere. Edited by Levine, J.S.; and Schryer, D.R.: NASA Reference Publication 1022, 1978, 372 pp.

11. Levine, J.S.; Augustsson, T.R.; and Hoell, J.M.: The Vertical Distribution of Atmospheric Ammonia. Geophys. Res. Lett., Vol. 7, No. 5, May 1980, pp. 317-320.

12. Augustsson, T.R.; Levine, J.S.; and Tiwari, S.N.: The Sulfur Budget of the Troposphere. EOS, Vol. 61, No. 17, Apr. 1980, p. 239.

13. Anderson, D.E., Jr.; and Meier, R.R.: Effects of Anisotropic Multiple Scattering on Solar Radiation in the Troposphere and Stratosphere. Appl. Opt., Vol. 18, No. 12, June 1979, pp. 1955-1960.

14. Luther, F.M.; and Gelinas, R.J.: Effect of Molecular Multiple Scattering and Surface Albedo on Atmospheric Photodissociation Rates. J. Geophys. Res., Vol. 81, No. 6, Feb. 1976, pp. 1125-1132.

15. Luther, F.M.; Wuebbles, D.J.; Duewer, W.H.; and Chang, J.S.: Effect of Multiple Scattering on Species Concentration and Model Sensitivity. J. Geophys. Res., Vol. 83, No. C7, July 1978, pp. 3563-3570.

16. Crutzen, P.J.; Isaksen, I.S.A.; and McAfee, J.R.: The Impact of the Chlorocarbon Industry on the Ozone Layer. J. Geophys. Res., Vol. 83, No. C1, Jan. 1978, pp. 345-363.

17. Callis, L.B.; Ramanathan, V.; Boughner, R.E.; and Barkstrom, B.R.: The Stratosphere: Scattering Effects, a Coupled 1-D Model and Thermal Balance Effects. Proc. of the Fourth CIAP Conf., Rep. DOT-TSC-OST-75-38, 1975, U.S. Department of Transportation (Washington, D.C.), pp. 224-233.

18. Lettau, H.: Compendium on Meteorology. Edited by Malone, T.F., Am. Meteor. Soc., 1951, pp. 320-333.

19. U.S. Standard Atmosphere. U.S. Government Printing Office (Washington, D.C.), 1962.

20. Chameides, W.L.; and Walker, J.C.G.: A Time-Dependent Photochemical for Ozone Near the Ground. J. Geophys. Res., Vol. 81, No. 3, Jan. 1976, pp. 413-420.

21. McConnell, J.C.: Atmospheric Ammonia. J. Geophys. Res., Vol. 78, No. 33, Nov. 1973, pp. 7812-7821.

22. McElroy, M.B.; Wofsy, S.C.; and Daksze, N.: Photochemical Sources for Atmospheric H_2S. Atmospheric Environment, Vol. 14, No. 1, Jan. 1979, pp. 159-163.

23. Johnston, H.S.; Kattenhorn, D.; and Whitten, G.: Use of Excess Carbon 14 Data to Calibrate Models of Stratospheric Ozone Depletion by Supersonic Trnsports. J. Geophys. Res., Vol. 81, No. 3, Jan. 1976, pp. 368-380.

24. Hunten, D.M.: The Philosophy of One-Dimensional Modeling. Fourth Conf. on CIAP, Feb. 1975.

25. Leighton, P.A.: Photochemistry of Air Pollution. Academic Press (N.Y.), 1961.

26. Ackerman, M.: Ultraviolet Solar Radiation Related to Mesospheric Processes. Inst. Aeronautic Spatiale Belgique (Brussels, Belgium) A-77, 1970, pp. 149-159.

27. Elterman, L.: UV, Visible, and IR Attenuation for Altitudes to 50 km. Environmental Research Paper 285, U.S. Air Force Cambridge Research Laboratory (Bedford, Mass.), 1968, pp. 1-48.

28. U.S. Standard Atmosphere Supplements. U.S. Government Printing Office (Washington D.C.), 1966.

29. The Stratosphere: Present and Future: NASA Reference Publication 1049, edited by Hudson, R.D., and Reed, E.I., 1979.

30. Lin, C.L.; and DeMore, W.E.: $O(^1D)$ Production in Ozone Photolysis Near 3100 A. J. Photochem., Vol. 2, 1973, pp. 161-164.

31. Moortgat, G.K.; and Warneck, P.: Relative $O(^1D)$ Quantum Yields in the Near UV Photolysis of Ozone at 298 K. Zeitung Naturforschung, Vol. A 30, 1975, pp. 835-844.

32. Moortgat, G.K.; Kudszus, E.; and Warneck, P.: Temperature Dependence of $O(^1D)$ Formation in the Near UV. Photolysis of Ozone. J. Chem. Soc., Faraday Transactions, II, Vol. 73, 1977, pp. 1216-1221.

33. Moortgat, G.K.; and Kudszus, E.: Mathematical Expression for the $O(^1D)$ Quantum Yields From the O_3 Photolysis as a Function of Temperature (230-320 K) and Wavelength (295-320 nm). Geophys. Res. Lett., Vol. 5, No. 3, Mar. 1978, pp. 191-194.

34. Amimoto, S.T.; Force, A.P.; and Wiesenfeld, J.R.: Ozone Photochemistry: Production and Deactivation of $O(^1D_2)$ Following Photolysis at 248 nm. Chem. Phys. Lett., Vol. 60, No. 1, Dec. 1978, pp. 40-43.

35. Kajimoto, O.; and Cvetanovic, R.J.: Absolute Quantum Yield of $O(^1D_2)$ in the Photolysis of Ozone in the Hartley Band. Int. J. Chem. Kinetics, Vol. 11, No. 6, June 1979, pp. 605-612.

36. Fairchild, C.E.; Stone, E.J.; and Lawrence, G.M.: Photofragment Spectroscopy of Ozone in the UV Region 270-310 nm and at 600 nm. J. Chem. Phys., Vol. 69, No. 8, Apr. 1978, pp. 3632-3638.

37. Sparks, R.S.; Carson, L.; Shobatake, K.; Kowalczyk, M.L.; and Lee, Y.T.: Dynamics of Photodissociation of O_3. Paper presented at the 7th Internat'l. Symp. on Molecular Beams (Riva Del Garda, Italy), May 28-June 1, 1979.

38. Harker, A.B.; and Johnston, H.S.: Photolysis of Nitrogen Dioxide to Produce Transient O, NO_3 and N_2O_5. J. Phys. Chem., Vol. 77 No. 9, Apr. 1973, pp. 1153-1156.

39. Bass, A.M.; Ledford, A.E., Jr.; and Laufer, A.H.: Extinction Coefficients of NO_2 and N_2O_4. J. Res. Nat'l. Bureau of Standards, Section A 80, 1976, pp. 143-166.

40. Moortgat, G.K.; and Warneck, P.: CO_2 and H_2 Quantum Yields in the Photodecomposition of Formaldehyde in Air. J. Chem. Phys., Vol. 70, No. 8, Apr. 1979, pp. 3639-3651.

41. Graham, R.A.; and Johnston, H.S.: The Photochemisry of NO_3 and the Kinetics of the N_2O_5-O_3 System. J. Phys. Chem., Vol. 82, No. 3, Feb. 1978, pp. 254-268.

42. Johnston, H.S.; and Graham, R.A.: Gas Phase Ultraviolet Absorption Spectrum of Nitric Acid Vapor. J. Phys. Chem., Vol. 77, No. 1, Jan. 1973, pp. 62-63.

43. Johnston, H.S.; Chang, S.-G.; and Whitten, G.: Photolysis of Nitric Acid Vapor. J. Phys. Chem., Vol. 78, No. 1, Jan. 1974, pp. 1-7.

44. Stockwell, W.R.; and Calvert, J.G.: The Near Ultraviolet Absorption Spectrum of Gaseous HONO and N_2O_3. J. Photochem., Vol. 8, 1978, pp. 193-203.

45. Molina, L.T.; Schinke, S.D.; and Molina, M.J.: Ultraviolet Absorption Spectrum of Hydrogen Peroxide Vapor. Geophys. Res. Lett., Vol. 4, No. 12, Dec. 1977, pp. 580-582.

46. Lin, C.L.; Rohagi, N.K.; and DeMore, W.E.: Ultraviolet Absorption Cross Sections of Hydrogen Peroxide. Geophys. Res. Lett., Vol. 5, No. 2, Feb. 1978, pp. 113-115.

47. Arguello, G.; and Molina, M.J.: Ultraviolet Absorption Spectrum of CH_3OOH Vapor. Geophys. Res. Lett., Vol. 6, No. 12, Dec. 1979, pp. 953-955.

48. Stedman, D.H.; Chameides, W.L.; and Cicerone, R.J.: The Vertical Distribution of Soluble Gases in the Troposphere. Geophys. Res. Lett., Vol. 2, No. 8, Aug. 1975, pp. 333-336.

49. Boughner, R.E.; and Nealy, J.E.: A Coupled Radiative-Convective-Photochemical Model of the Stratosphere. NASA Technical Paper No. 1418, Apr. 1979.

50. Palmen, E.; and Newton, C.W.: Atmospheric Circulation Systems - Their Structure and Physical Interpretation. Academic Press (N.Y.), 1969.

51. Wofsy, S.C.; McConnell, J.C.; and McElroy, M.B.: Atmospheric CH_4, CO and CO_2. J. Geophys. Res., Vol. 77, No. 24, Aug. 1972, pp. 4477-4493.

52. Turco, R.P., Hamill, P.; Toon, O.B.; Whitten, R.C.; and Kiang, C.S.: A One-Dimensional Model Describing Aerosol Formation and Evolution in the Stratosphere :I. Physical Processes and Mathematical Analogs. J. Atmos. Sci., Vol. 36, No. 4, Apr. 1979, pp. 669-717.

53. Dickerson, R.R.; Stedman, D.H.; Chameides, W.L.; Crutzen, P.J.; and Fishman, J.: Actionometric Measurements and Theoretical Calculations of $J(O_3)$, the Rate of Photolysis of Ozone to $O(^1D)$. Geophys. Res. Lett., Vol. 6, No. 11, Nov. 1979, pp. 833-836. (Also correction, Geophys. Res. Lett., Vol. 7, No. 1, Jan. 1980, p. 112).

54. Hanser, F.A.; and Sellers, B.: Variations of $O(^1D)$ Photoproduction Rate for the 1977 Gametag Flights. J. Geophys. Res., Vol. 85, No. C12, Dec. 1980, pp. 7377-7382.

55. Stedman, D.H.; Chameides, W.L.; and Jackson, J.O.: Comparison of Experimental and Computed Values of $J(NO_2)$. Geophys. Res. Lett., Vol. 2, No. 1, Jan. 1975, pp. 22-25.

56. Harvey, R.B.; Stedman, D.H.; and Chameides, W.L.: Determination of the Absolute Rate of Solar Photolysis of NO_2. J. Air Pollution Control Assoc., Vol 27, 1977, pp. 663-668.

57. Stedman, D.H.; and Smith, J.: A Qualitative Understanding of Ozone Observations. The CHON Photochemistry of the Troposphere, Nat'l. Center for Atmospheric Res. (Boulder, Colo.), 1980, pp. 21-27. (Available as NCAR/CQ-7+1980-ASP).

58. Graham, R.A.; and Johnston, H.S.: The Photochemistry of NO_3 and the Kinetics of the N_2O_5-O_3 System. J. Phys. Chem., Vol. 82, No. 3, Feb. 1978, pp. 254-268.

59. Magnotta, F.; and Johnston, H.S.: Photodissociation Quantum Yields for the NO_3 Free Radical. Geophys. Res. Lett., Vol. 7, No. 10, Oct. 1980, pp. 769-772.

60. Hoell, J.M.; Harward, C.N.; and Williams, B.S.: Remote Infrared Heterodyne Radiometer Measurements of Atmospheric Ammonia. Geophys. Res. Lett., Vol. 7, No. 5, May 1980, pp. 313-316.

61. Erikson, E.: Composition of Atmospheric Precipitation: I. Nitrogen Compounds. Tellus, Vol. 4, 1952, pp. 215-232.

62. Health and Environmental Effects of Coal Gasification and Liquefaction Technologies. Edited by Antizzo, J., Mitre Corporation M78-58, 1978.

63. Dawson, G.A.: Atmospheric Ammonia from Undisturbed Land. J. Geophys. Res., Vol. 82, No. 21, July 1977, pp. 3125-3133.

64. Healy, T.V.; McKay, H.A.C.; Pilbeam, A.; and Scargill, D.: Ammonia and Ammonium Sulfate in the Troposphere over the United Kingdom. J. Geophys. Res., Vol. 75, No. 12, Apr. 1970, pp. 2317-2321.

65. Georgii, H.W.; and Muller, W.J.: On the Distribution of Ammonia in the Middle and Lower Troposphere. Tellus, Vol. 26, 1974, pp. 180-184.

66. Hoell, J.M.; Harward, C.N.; and McClenny, W.A.: Comparison of Remote Infrared Heterodyne Radiometer and In Situ Measurements of Atmospheric Ammonia. Paper presented at the Conf. on Lasers and Electro-Optical Systems (San Diego, Calif.), Feb. 26-28, 1980.

67. Hoell, J.M.; Levine, J.S.; Augustsson, T.R.; and Harward, C.N.: Atmospheric Ammonia: Measurements and Modeling. AIAA Paper No. 81-0376, Jan. 1981.

68. Kelly, T.J.; Stedman, D.H.; Ritter, J.A.; and Harvey, R.B.: Measurements of Oxides of Nitrogen and Nitric Acid in Clean Air. J. Geophys. Res., Vol. 85, No. C12, Dec. 1980, pp. 7417-7425.

69. Liu, S.C.: Possible Nonurban Environmental Effects Due to Carbon Monoxide and Nitrogen Oxides Emission. In: Man's Impact on the Troposphere. Edited by Levine, J.S.; and Schryer, D.R., NASA Reference Publication 1022, 1978, pp. 65-79.

70. Effect on Increased Nitrogen Fixation on Stratospheric Ozone. Report No. 53, Council on Agricultural Science and Technology, Jan. 1976.

71. Noxon, J.F.: Atmospheric Nitrogen Fixation by Lightning. Geophys. Res. Lett., Vol. 3, No. 8, Aug. 1977, pp. 463-465.

72. Griffing, G.W.: Ozone and Oxides of Nitrogen Production During Thunderstorms. J. Geophys. Res., Vol. 82, No. 6, Feb. 1977, pp. 943-950.

73. Chameides, W.L.; Stedman, D.H.; Dickerson, R.R.; Rusch, D.W.; and Cicerone, R.J.: No_x Production in Lightning. J. Atmos. Sci., Vol. 34, No. 1, Jan. 1977, pp. 143-149.

74. Tuck, A.F.: Production of Nitrogen Oxides by Lightning Discharges. Quart. J. Roy. Meteor. Soc., Vol. 102, No. 434, Oct. 1976, pp. 749-755.

75. Hill, R.D.; Rinker, R.G.; and Wilson, H.D.: Atmospheric Nitrogen Fixation by Lightning. J. Atmos. Sci., Vol. 37, No. 1, Jan. 1980, pp. 179-192.

76. Levine, J.S.; Rogowski, R.S.; Gregory, G.L.; Howell, W.E.; and Fishman, J.: Simultaneous Measurements of NO_x, NO and O_3 Production in a Laboratory Electric Discharge: Atmospheric Implications. Geophys. Res. Lett., Vol. 8, No. 4, Apr. 1981, pp. 357-360.

77. Dawson, G.A.: Nitrogen Fixation by Lightning. J. Atmos. Sci., Vol. 37, No. 1, Jan. 1980, pp. 174-178.

78. Junge, C.E.: Air Chemistry and Radioactivity. Academic Press (N.Y.), 1963.

79. Ripperton, L.A.; Worth, J.J.B.; and Kornreich, L.: Nitrogen Dioxide and Nitric Oxide in Non-Urban Air. Presented at the 61st Annual Meeting of the Air Pollution Control Assoc., June 1968.

80. Breeding, R.J.; Lodge, J.P., Jr.,; Pate, J.B.; Sheesley, D.C.; Klonis, H.B.; Fogle, B.; Anderson, J.A.; Englert, T.R.; Haagenson, P.L.; McBeth, R.B.; Morris, A.L.; Pogue, R.; and Wartburg, A.F.: Background Concentrations of Trace Gases in the Central United States. J. Geophys. Res., Vol. 78, No. 30, Oct. 1973, pp. 7057-7064.

81. Moore, H.: Isotopic Measurements of Atmospheric Nitrogen Compounds. Tellus, Vol. 26, Nos. 1-2, Jan.-Apr. 1974, pp. 169-174.

82. Lodge, J.P., Jr.; Machado, P.A.; Pate, J.B.; Sheesly, D.C.; and Wartburg, A.F.: Atmospheric Trace Chemistry in the American Humid Tropics. Tellus, Vol. 26, Nos. 1-2, Jan.-Apr. 1974, pp. 250-253.

83. Noxon, J.F.: Nitrogen Dioxide in the Stratosphere and Troposphere Measured by Ground-Based Absorption Spectroscopy. Science, Vol. 189, No. 4202, Aug. 1975, pp. 547-549.

84. Noxon, J.F.: Tropospheric NO_2. J. Geophys. Res., Vol. 83, No. C6, June 1978, pp. 3051-3057.

85. Platt, U.; and Perner, D.: Direct Measurements of Atmospheric CH_2O, HNO_2, O_3, NO_2, and SO_2 by Differential Optical Absorption in the Near UV. J. Geophys. Res., Vol. 85, No. C12, Dec. 1980, pp. 7453-7458.

86. Briehl, D.C.; Hilsenrath, E.; Ridley, B.A.; and Schiff, H.I.: In Situ Measurements of Nitric Oxide, Water Vapor and Ozone From an Aircraft. Second Internat'l. Conf. on the Environmental Impact of Aerospace Operations in the High Atmosphere - Preprints, Am. Meteor. Soc., July 1974, pp. 11-15.

87. Drummond, J.W.: Atmospheric Measurements of Nitric Oxide Using a Chemiluminescent Detector. Ph.D. Thesis, University of Wyoming (Laramie), 1977.

88. Torres, A.L.: (Personal communication), 1981.

89. McFarland, M.; Kley, D.; Drummond, J.W.; Schmeltekopf, A.L.; and Winkler, R.H.: Nitric Oxide Measurements in the Equatorial Pacific Region. Geophys. Res. Lett., Vol. 6, No. 7, July 1979, pp. 605-608.

90. Chameides, W.L.: The Photochemical Role of Tropospheric Nitrogen Oxides. Geophys. Res. Lett., Vol. 5, No. 1, Jan. 1978, pp. 17-20.

91. Huebert, B.J.; and Smith, J.: HNO_3 Vapor vs. Altitude at the Pawnee Grasslands. The CHON Photochemistry of the Troposphere, Nat'l. Center for Atmospheric Res. (Boulder, Colo.), 1980, pp. 67-71. (Available as NCAR/CQ-7+1980-ASP).

92. Okita, T.; Morimoto, S.; Izawa, M.; and Konno, S.: Measurements of Gaseous and Particulate Nitrates in the Atmosphere. Atmos. Environment, Vol. 10, No. 12, Dec. 1976, pp. 1085-1089.

93. Huebert, B.J.; and Lazarus, A.L.: Global Tropospheric Measurements of Nitric Acid Vapor and Particulate Nitrate. Geophys. Res. Lett., Vol. 5, No. 7, July 1978, pp. 577-580.

94. Huebert, B.J.: Nitric Acid and Aerosol Nitrate Measurements in the Equatorial Pacific Region. Geophys. Res. Lett., Vol. 7, No. 5, May 1980, pp. 325-328.

95. Huebert, B.J.; and Lazarus, A.L.: Tropospheric Gas-Phase and Particulate Nitrate Measurements. J. Geophys. Res., Vol. 85, No. C12, Dec. 1980, pp. 7322-7328.

96. Perner, D.; and Platt, U.: Detection of Nitrous Acid in the Atmosphere by Differential Optical Absorption. Geophys. Res. Lett., Vol. 6, No. 12, Dec. 1979, pp. 917-920.

97. Nash, T.: Nitrous Acid in the Atmosphere and Laboratory Experiments on Its Photolysis. Tellus, Vol. 26, 1974, pp. 175-179.

98. Noxon, J.; Norton, R.B.; and Marovich, E.: NO_3 in the Troposphere. Geophys. Res. Lett., Vol. 7, No. 2, Feb. 1980, pp. 125-128.

99. Delwiche, C.C.: The Nitrogen Cycle. Sci. Am., Vol. 223, No. 3, Sept. 1970, pp. 136-140.

100. Hardy, R.W.F.; and Halvcka, U.D.: Nitrogen Fixation: A Key to World Food? Science, Vol. 188, No. 4188, May 1975, pp. 633-643.

101. McElroy, M.B.; Elkins, J.W.; Wofsy, S.C.; and Yung, Y.L.: Sources and Sinks for Atmospheric N_2O. Rev. Geophys. & Space Phys., Vol. 14, No. 2, May 1976, pp. 143-150.

102. Levine, J.S.; Augustsson, T.R.; and Hoell, J.M.: The Ammonia Budget of the Atmosphere/Biosphere System. EOS, Vol. 61, No. 17, Apr. 1980, p. 239.

103. Levine, J.S.; Hays, P.B.; and Walker, J.C.G.: The Evolution and Variability of Atmospheric Ozone over Geological Time. Icarus, Vol. 39, No. 2, Aug. 1979, pp. 295-309.

104. Kasting, J.F.; and Donahue, T.M.: The Evolution of Atmospheric Ozone. J. Geophys. Res., Vol. 85, No. C6, June 1980, pp. 3255-3263.

105. Levine, J.S.; Augustsson, T.R.; Boughner, R.E.; Natarajan, M.; and Sacks, L.: Comets and the Photochemistry of the Paleoatmosphere. Comets and the Origin of Life. Edited by Ponnamperuma, C., D. Reidel pub-lishing Co., 1981.

106. Broecker, W.S.: Man's Oxygen Reserves. Science, Vol. 168, No. 3939, June 1970, pp. 1537-1538.

107. Machta, L.; and Hughes, E.: Atmospheric Oxygen in 1967 to 1970. Science, Vol. 168, No. 3939, pp. 1582-1584.

108. Fabian P.; and Pruchniewicz, P.G.: Meridional Distribution of Ozone in the Troposphere and Its Seasonal Variations. J. Geophys. Res., Vol. 82, No. 15, May 1977, pp. 2063-2073.

109. Danielsen, E.F.; and Mohnen V.A.: Project DUSTORM Report: Ozone Measurements and Meteorological Analyses of Tropopause Folding. ASRC-SUNY-PUB-394, (Contract N00014-76-C-0283), State University of New York at Albany, May 1976. (Available from DDDC as AD A032 555).

110. Crutzen, P.J.: Photochemical Reactions Initiated by and Influencing Ozone in Unpolluted Tropospheric Air. Tellus, Vol. 26, Nos. 1-2, Jan.-Apr. 1974, pp. 47-57.

111. Chameides, W.L.; and Stedman, D.H.: Tropospheric Ozone: Coupling Transport and Photochemistry. J. Geophys. Res., Vol. 82, No. 12, Apr. 1977, pp. 1787-1794.

112. Fishman, J.; Solomon, S.; and Crutzen, P.J.: Observational and Theoretical Evidence in Support of a Significant In Situ Photochemical Source of Tropospheric Ozone. Tellus, Vol. 31, No. 5, Oct. 1979, pp. 432-446.

113. Singh, H.B.; Viezce, W.; Johnson, W.B.; and Ludwig, F.L.: The Impact of Stratospheric Ozone on Tropospheric Air Quality. J. Air Poll. Control Assoc., Vol. 30, No. 9, Sept. 1980, pp. 1009-1017.

114. Kreuger, A.J.; and Minzner, R.A.: A Mid-Latitude Ozone Model for the 1976 U.S. Standard Atmosphere. J. Geophys. Res., Vol. 81, No. 24, Aug. 1976, pp. 4477-4481.

115. Chatfield, R.; and Harrison, H.: Tropospheric Ozone 2. Variations Along a Meridional Band. J. Geophys. Res., Vol. 82, No. 37, Dec. 1977, pp. 5969-5976.

116. Routhier, F.; Dennett, R.; Davis, D.D.; Wartburg, A.; Haagenson, P.; and Delany, A.C.: Free Tropospheric and Boundary-Layer Airborne Measurements of Ozone over the Latitudinal Range of 58° S to 70° N. J. Geophys. Res., Vol. 85, No. C12, Dec. 1980, pp. 7307-7321.

117. Crutzen, P.J.: SST's. Threat to the Earth's Ozone Shield. Ambio, Vol. 1, No. 2, Feb. 1972, pp. 41-51.

118. Rowland, R.S.; and Molina, M.J.: Chlorofluoromethanes in the Envinronment. Rev. Geophys. & Space Phys., Vol. 13, No. 1, Feb. 1975, pp. 50-52.

119. Meyer, A.D.; and Seitz, E.O.: Ultraviolette Strahlen ihre Erzeugung, Messung und Andwendung in Medizin, Biologie und Technik. de Gruter (Berlin), 1942.

120. Rambler, M.B.; and Margulis, L.: Bacterial Resistance to Ultraviolet Irradiation Under Anaerobiosis: Implications for Pre-Phanerozoic Evolution. Science, Vol. 210, No. 4470, Nov. 1980, pp. 638-640.

121. National Academy of Sciences, Climate Impact Committee: Environmental Impact of Stratospheric Flight. Washington, D.C., 1975.

122. Riehl, H.: Introduction to the Atmosphere. McGraw-Hill (N.Y.), 1972.

123. Schmidt, U.: Molecular Hydrogen in the Atmosphere. Tellus, Vol. 26, Nos. 1-2, Jan.-Apr. 1974, pp. 78-90.

124. Muenow, D.W.: High Temperature Mass Spectrometric Gas-Release Studies of Hawaiian Volcanic Glass: Pele's Tears. Geochimica et Cosmochimica Acta, Vol. 37, No. 6, June 1963, pp. 1551-1561.

125. Naughton, J.J.: Volcanic Flame: Source of Fuel and Relation to Volcanic Gas-Lava Equilibrium. Geochimica et Cosmochimica Acta, Vol. 37, No. 5, May 1973, pp. 1163-1169.

126. Mason, B.: Principles of Geochemistry. Wiley (N.Y.), 1966.

127. Chameides, W.L.: Tropospheric Odd Nitrogen and the Atmospheric Water Vapor Cycle. J. Geophys. Res., Vol. 80, No. 36, Dec. 1975, pp. 4989-4996.

128. Kok, G.L.: Measurements of H_2O_2 and HNO_3 in Rural Air. Geophys. Res. Lett., Vol. 6, No. 5, May 1979, pp. 325-328.

129. Kok, G.; and Nuttal, J.G.: Atmospheric Chemistry of Hydrogen Peroxide and Formaldehyde. The CHON Photochemistry of the Troposphere, Nat'l. Center for Atmospheric Res. (Boulder, Colo.), 1980, pp. 59-66. (Available as NCAR/CQ-7+1980-ASP).

130. Wang, C.C.; and Davis, L.I., Jr.: Measurements of Hydroxyl Concentrations in Air Using a Tunable UV Laser Beam. Phys. Rev. Lett., Vol. 30, 1974, pp. 349-352.

131. Wang, C.C.; Davis, L.I., Jr.; Wu, C.H.; Japar, S.; Niki, H.; and Weinstock, B.: Hydroxyl Radical Concentrations Measured in Ambient Air. Science, Vol. 189, No. 4205, Sept. 1975, pp. 797-800.

132. Perner, D.; Ehhalt, D.H.; Patz, H.W.; Platt, U.; Röth, E.P.; and Volz, A.: OH-Radicals in the Lower Troposphere. Geophys. Res. Lett., Vol. 3, No. 8, Aug. 1976, pp. 466-468.

133. Davis, D.D.; Heaps, W.; and McGee, T.: Direct Measurements of Natural Tropospheric Levels of OH via an Aircraft Borne Tunable Dye Laser. Geophys. Res. Lett., Vol. 3, No. 6, June 1976, pp. 331-333.

134. Campbell, M.J.; and Blankenship, W.: (Personal communication.) Average of measurements taken during June-Aug. 1978, at Washington State University (Pullman, Wash.).

135. Campbell, M.J.; Sheppard, J.C.; and Au, B.F.: Measurement of Hydroxyl Concentration in Boundary Layer Air by Monitoring CO Oxidation. Geophys. Res. Lett., Vol. 6, No. 3, Mar. 1979, pp. 175-178.

136. Davis, D.D.; Heaps, W.; Philen, D.; and McGee, T.: Boundary Layer Measurements of the OH Radical in the Vicinity of an Isolated Power Plant Plume: SO_2 and NO_2 Conversion Times. Atmos. Environment, Vol. 13, No. 8, Aug. 1979, pp. 1197-1203.

137. Campbell, M.J.; Sheppard, J.C.; and Blankenship, W.: Measurements of Hydroxyl Radical Concentrations in Boundary Layer Air. The CHON Photochemistry of the Troposphere, Nat'l. Center for Atmos. Res. (Boulder, Colo.), 1980, pp. 49-58. (Available as NCAR/CQ-7+1980-ASP).

138. Horne, R.A.: The Chemistry of Our Environment. Wiley (N.Y.), 1978.

139. Air Quality Criteria for Nitrogen Oxides. NAPCA-Publication No. AP-84, U.S. Environmental Protection Agency, Jan. 1971. (Available from NTIS as PB 197 333).

140. Swinnerton, J.W.; Linnenbom, V.J.; and Lamontagne, R.A.: The Ocean: A Natural Source of Carbon Monoxide. Science, Vol. 167, No. 3920, Feb. 1970, pp. 984-986.

141. Crutzen, P.J.; and Fishman, J.: Average Concentrations of OH in the Troposphere and the Budgets of CH_4, CO, H_2 and CH_3CCl_3. Geophys. Res. Lett., Vol. 4, No. 8, Aug. 1977, pp. 321-324.

142. Wofsy, S.C.; McConnell, J.C.; and McElroy, M.B.: Atmospheric CH_4, CO, and CO_2. J. Geophys. Res., Vol. 77, No. 24, Aug. 1972, pp. 4477-4493.

143. Seiler, W.: The Cycle of Atmospheric CO. Tellus, Vol. 26, Nos. 1-2, Jan.-Apr. 1974, pp. 116-135.

144. Barber, E.D.; and Lodge, J.P., Jr.: Paper Chromatographic Identification of Carbonyl Compounds as Their 2,4-Dinitrophenyl-Hydrazones in Automobile Exhaust. Anal. Chem., Vol. 35, No. 3, Mar. 1963, pp. 348-350.

145. Hatanaka, A.; and Harada, T.: Formation of Cis-3-Hexanal, Trans-2-Hexanal and Cis-3-Haxanol in Macerated Thea Sinensis Leaves. Phytochemistry, Vol. 12, 1973, pp. 2341-2346.

146. Lodge, J.P., Jr.; and Pate, J.B.: Atmospheric Gases and Particulates in Panama. Science, Vol. 153, No. 3734, July 1966, pp. 408-410.

147. Fushimi, K.; and Miyake, Y.: Contents of Formaldehyde in the Air Above the Surface of the Ocean. J. Geophys. Res., Vol. 85, No. C12, Dec. 1980, pp. 7533-7536.

148. Zafiriou, O.C.; Alford, J.; Herrera, M.; Peltzer, E.T.; and Cagosian, R.B.: Formaldehyde in Remote Marine Air and Rain: Flux Measurements and Estimates. Geophys. Res. Lett., Vol. 7, No. 5, May 1980, pp. 341-344.

149. Keeling, C.D.: The Carbon Dioxide Cycle: Reservoir Models to Depict the Exchange of Atmospheric Carbon Dioxide with the Oceans and Land Plants. Chemistry of the Lower Atmosphere. Edited by Rasool, S.I., Plenum Press, 1973, pp. 251-329.

150. Hoffert, M.I.: Global Distributions of Atmospheric Carbon Dioxide in the Fossil-Fuel Era: A Projection. Atmos. Environment, Vol. 8, No. 12, Dec. 1974, pp. 1225-1249.

151. Bolin, B.: The Carbon Cycle. Sci. Am., Vol. 223, No. 3, Sept. 1970, pp. 124-132.

152. Rasool, S.I.; and Schneider, S.H.: Atmospheric Carbon Dioxide and Aerosols: Effects of Large Increases on Global Climate. Science, Vol. 173, No. 3992, July 1971, pp. 138-141.

153. Manabe, S.; and Wetherald, R.T.: The Effects of Doubling the Concentration of CO_2 on the Climate of a General Circulation Model. J. Atmos. Sci., Vol. 32, No. 1, Jan. 1975, pp. 3-15.

154. Augustsson, T.R.; and Ramanathan, V.: A Radiative-Convective Model Study of the CO_2 Climate Problem. J. Atmos. Sci., Vol. 34, No. 3, Mar. 1977, pp. 448-451.

155. Chameides, W.L.; Liu, S.C.; and Cicerone, R.J.: Possible Variations in Atmospheric Methane. J. Geophys. Res., Vol. 82, No. 12, Apr. 1977, pp. 1795-1978.

156. Wang, W.C.; Yung, Y.L.; Lacis, A.A.; Mo, T.; and Hansen, J.E.: Greenhouse Effects Due to Man-Made Perturbations of Trace Gases. Science, Vol. 194, No. 4266, Nov. 1976, pp. 685-690.

157. Junge, C.E.; Chagnon, C.W.; and Manson, J.E.: Stratospheric Aerosols. J. Meteor., Vol. 18, 1961, pp. 81-108.

158. Crutzen, P.J.: The Possible Importance of CSO for the Sulfate Layer of the Stratosphere. Geophys. Res. Lett., Vol. 3, No. 2, Feb. 1976, pp. 73-76.

159. Environmental Protection Agency: Air Quality Criteria for Sulfur Oxides, Report AP-50 (Washington, D.C.), 1969, pp. 19-20.

160. Fujii, T.: Studies on the Air Pollution by Exhaust Gases of Aircraft (1). Taiki Osen Kenkyu, Vol. 8, 1975, p. 515.

161. Environmental Protection Agency: Air Pollution Emission Factors, Report AP-42 (Research Triangle Park, N.C.), 1973-1975.

162. Shinn, J.H.; and Lynn, S.: Do Man-Made Sources Affect the Sulfur Cycle of Northeastern States? Environmental Sci. & Tech., Vol. 13, 1979, pp. 1062-1067.

163. Cadle, R.D.: Trace Constituents Emitted to the Atmosphere by Volcanoes. Chemosphere, Vol. 2, No. 6, Nov. 1973, pp. 231-234.

164. Stoiber, R.E.; and Jepsen, A.: Sulfur Dioxide Concentrations to the Atmosphere by Volcanoes. Science, Vol. 182, No. 4112, Nov. 1973, pp. 577-578.

165. Jost, D.: Aerological Studies on the Atmospheric Sulfur-Budget. Tellus, Vol. 26, 1974, pp. 206-213.

166. Georgii, H.W.: Large Scale Spatial and Temporal Distribution of Sulfur Compounds. Atmos. Environment, Vol. 12, Nos. 1-3, Jan.-Mar. 1978, pp. 681-690.

167. Georgii, H.W.; and Meixner, F.X.: Measurement of the Tropospheric and Stratospheric SO_2 Distribution. J. Geophys. Res., Vol. 85, No. C12, Dec. 1980, pp. 7433-7438.

168. Georgii, H.W.; and Gravenhorst, G.: The Ocean as Source or Sink for Reactive Trace Gases. Pure and Appl. Geophys., Vol. 115, No. 3, 1977, pp. 503-511.

169. Maroulis, P.J.; Goldberg, A.B.; and Bandy, A.R.: Measurements of Tropospheric Background Levels of SO_2 on Project GAMETAG. EOS, Vol. 59, No. 46, Nov. 1978, pp. 1081-1082.

170. Jaschke, W.; Schmitt, R.; and Georgii, H.W.: Preliminary Results of Stratospheric SO_2-Measurements. Geophys. Res. Lett., Vol. 3, No. 9, Sept. 1976, pp. 517-519.

171. Garland, J.D.: Dry and Wet Removal of Sulfur From the Atmosphere. Atmos. Environment, Vol. 12, Nos. 1-3, Jan.-Mar. 1978, pp. 349-362.

172. Hicks, B.B.; and Liss, P.S.: Tellus, Vol. 28, 1976, pp. 349-354.

173. Katz, M.: Air Pollution Handbook. Edited by Magill, P.L.; Holden, F.R.; and Ackley, C., McGraw-Hill (N.Y.), 1956, pp. 2-1 to 2-56.

174. Robinson, E.; and Robbins, R.C.: Sources, Abundances, and Fate of Gaseous Atmospheric Pollutants. SRI Project PR-6755, Stanford Research Institute, 1968.

175. Kellog, W.W.; Cadle, R.D.; Allen, E.R.; Lazrus, A.L.; and Martell, E.A.: The Sulfur Cycle. Science, Vol. 175, No. 4022, Feb. 1972, pp. 587-596.

176. Hartstein, A.M.; and Forshey, D.R.: Coal Mine Combustion Products: Neoprenes, Polyvinyl Chloride Compositions, Urethane Foam, and Wood. U.S. Bureau of Mines Report Investigation, Vol. 7977, No. 15, 1974.

177. Tsifrinovich, A.N.; and Lulova, N.I.: Composition of Organo-Sulfur Trace Impurities in Gases. Neftepererab Neftekhim (Moscow), Vol. 6, 1972, pp. 33-35.

178. Tsuji, M.; and Okuno, T.: The GC Analysis of Carbonyl Sulfide Emitted by the Viscose Plant. Proc. of the 13th Symposium of the Japan Soc. of Air Pollution (Tokyo), 1972, p. 119.

179. Sandalls, F.J.; and Penkett, S.A.: Measurements of Carbonyl Sulfide and Carbon Disulfide in the Atmosphere. Atmos. Environment, Vol. 11, 1977, pp. 197-199.

180. Torres, A.L.; Maroulis, P.J.; Goldberg, A.B.; and Bandy, A.R.: Measurements of Tropospheric OCS on the 1978 GAMETAG Flights. EOS, Vol. 59, No. 46, Nov. 1978, p. 1082.

181. Maroulis, P.J.; Torres, A.L.; and Bandy, A.R.: Atmospheric Concentrations of Carbonyl Sulfide in the Southwestern and Eastern United States. Geophys. Res. Lett., Vol. 4, No. 11, Nov. 1977, pp. 510-512.

182. Hanst, P.L.; Speller, L.L.; Watts, D.M.; Spence, J.W.; and Miller, M.F.: Infrared Measurements of Fluorocarbons, Carbon Tetrachloride, Carbonyl Sulfide, and Other Trace Gases. J. Air Poll. Control Assoc., Vol. 25, 1975, pp. 1220-1226.

183. Bethge, P.O.; and Ehrenborg, L.: Identification of Volatile Compounds in Kraft Mill Emissions. Svensk Papperstidning, Vol. 70, 1967, pp. 347-350.

184. Saijo, T.; Tsujimoto, T.; and Takahaski, T.: Odor Pollution of Kashima District. Taiki Osen Kenkya, Vol. 6, 1971, p. 222.

185. Schlegel, H.G.: Production, Modification, and Comsumption of Atmospheric Trace Gases by Micro-Organisms. Tellus, Vol. 26, Nos. 1-2, Jan.-Apr. 1974, pp. 11-20.

186. Huntington, A.T.: The Collection and Analysis of Volcanic Gases from Mount Etna. Philosoph. Trans. Roy. Soc. of London, Series A, Vol. 274, 1973, pp. 119-128.

187. Mizutani, H.: Odor Pollution Research in Nagoya City. Taiki Osen Kenkyu, Vol. 8, 1973, p. 381.

188. Slatt, B.J.; Natusch, D.F.S.; Prospero, J.M.; and Savoie, D.L.: Hydrogen Sulfide in the Atmosphere of the Northern Equatorial Atlantic Ocean and Its Relation to the Global Sulfur Cycle. Atmos. Environment, Vol. 12, No. 5, May 1978, pp. 981-991.

189. Lovelock, J.E.: CS_2 and the Natural Sulfur Cycle. Nature, Vol. 248, No. 5449, Apr. 1974, pp. 625-626.

190. Maroulis, P.J.; and Bandy, A.R.: Measurements of Atmospheric Concentrations of CS_2 in the Eastern United States. Geophys. Res. Lett., Vol. 7, No. 9, Sept. 1980, pp. 681-684.

191. Challis, E.J.: The Approach of Industry to the Assessment of Environmental Hazards. Proc. Roy. Soc., Series B, Vol. 185, 1974, pp. 183-197.

192. Dickson, W.: Report No. 54, Institute of Freshwater Research (Drottningholm, Sweden), 1975, p. 8.

193. Shaw, R.W.: Acid Precipitation in Atlantic Canada. Environmental Sci. & Tech., Vol. 13, 1979, pp. 406-411.

194. Likens, G.E.: Acid Precipitation. Chem. Eng. News, Vol. 54, No. 48, 1976, pp. 29-44.

195. Davis, D.D.; Smith, G.; and Klauber, G.: Trace Gas Analysis of Power Plant Plumes via Aircraft Measurements: O_3, NO_x and SO_2 Chemistry. Science, Vol. 186, No. 4165, Nov. 1974, pp. 733-736.

196. Davis, D.D.; and Klauber, G.: Atmospheric Gas Phase Oxidation Mechanisms for the Molecule SO_2. Int. J. Chem. Kinetics Symposium, Vol. 1, edited by Benson, S.W., 1975, pp. 543-556. Conference held at Warrenton, Virginia, Sept. 16-18, 1974.

197. Graedel, T.E.: Sulfur Dioxide, Sulfate Aerosol and Urban Aerosol. Geophys. Res. Lett., Vol. 3, No. 3, Mar. 1976, pp. 181-184.

198. Cotton, F.A.; and Wilkenson, G.: Advanced Inorganic Chemistry. Wiley (N.Y.), 1966.

199. Burnett, W.E.: Air Pollution From Animal Wastes: Determination of Malodors by Gas Chromatographic and Organoleptic Techniques. Envrionmental Sci. & Tech., Vol. 3, 1969, pp. 744-749.

200. Nashida, K.; Honda, T.; and Tsuji, T.: The Effects of Ozone Deoderization Equipment for the Sewage Odor. Ashkuku no Kenkyu, Vol. 4, No. 20, 1975, pp. 24-30.

201. Man's Impact on the Global Environment. Report of the Study of Critical Environmental Problems (SCEP), M.I.T. Press (Cambridge, Mass.), 1970.

202. Smith, G.D.: Numerical Solution of Partial Differential Equations. Oxford University Press (London), 1965.

APPENDIX A

PHOTOCHEMICAL AND KINETIC DATA

The present model includes a total of 12 photolytic reactions and 114 chemical reactions. Table A1 lists the photolytic processes with their frequencies for a solar zenith angle of 45°. Table A2 lists the 114 chemical reactions with their rate expressions and references. For the photolytic processes in table A1, the unit is inverse seconds (s^{-1}). For the reactions in table A2, the units are $cm^3 s^{-1}$ for bimolecular processes and $cm^6 s^{-1}$ for termolecular processes.

Table A1. Photolytic reactions.

Photodissociation No.	Process	Rate (z=0), s^{-1}(45°)
1	$O_3 + h\nu \rightarrow O(^1D) + O_2$	6.3 E-6
2	$O_3 + h\nu \rightarrow O(^3p) + O_2$	3.0 E-4
3	$NO_2 + h\nu \rightarrow NO + O$	7.6 E-3
4	$NO_3 + h\nu \rightarrow NO_2 + O$	8.2 E-3
5	$NO_3 + h\nu \rightarrow NO + O_2$	2.0 E-3
6	$N_2O_5 + h\nu \rightarrow NO_2 + NO_3$	2.0 E-5
7	$HNO_3 + h\nu \rightarrow OH + NO_2$	1.6 E-7
8	$HNO_2 + h\nu \rightarrow OH + NO$	4.8 E-4
9	$H_2O_2 + h\nu \rightarrow 2\ OH$	1.6 E-6
10	$CH_2O + h\nu \rightarrow HCO + H$	2.0 E-5
11	$CH_2O + h\nu \rightarrow H_2 + CO$	6.6 E-5
12	$CH_3OOH + h\nu \rightarrow CH_3O + OH$	1.6 E-6

Table A2. Chemical reactions.

Reaction No.	Reaction	Rate Expression (mole - cgs units)	Reference
1	$CH_4 + OH \rightarrow CH_3 + H_2O$	2.4E-12*exp(-1710.0/T)	(a)
2	$CH_4 + O(^1D) \rightarrow CH_3 + OH$	1.3E-10	(a)
3	$CH_3 + O_2 + M \rightarrow CH_3O_2 + M$	2.2E-31*(300.0/T)$^{2.2}$	(a)
4	$CH_3O_2 + HO_2 \rightarrow CH_3OOH + O_2$	3.0E-11*exp(-500.0/T)	(b)
5	$CH_3OOH + OH \rightarrow CH_3O_2 + H_2O$	6.2E-12*exp (-750.0/T)	(a)
6	$CH_3O_2 + NO \rightarrow CH_2O + HNO_2$	0.0	(c)
7	$CH_3O_2 + NO_2 \rightarrow CH_2O + HNO_3$	0.0	(d)
8	$CH_3O_2 + NO \rightarrow CH_3O + NO_2$	8.0E-12	(a)
9	$CH_3O + O_2 \rightarrow CH_2O + HO_2$	5.0E-13*exp (-2000.0/T)	(a)
10	$CH_2O + OH \rightarrow HCO + H_2O$	1.7E-11*exp(-100.0/T)	(a)
11	$HCO + O_2 \rightarrow CO + HO_2$	5.0E-12	(a)
12	$CO + OH \rightarrow CO_2 + H$	1.35E-1*(1 + P_{atm})3	(a)
13	$CO + HO_2 \rightarrow CO_2 + OH$	1.0E-20	(e)
14	$H_2 + OH \rightarrow H + H_2O$	1.2E-11*exp(-2200.0/T)	(a)
15	$H + O_2 + M \rightarrow HO_2 + M$	5.5E-32*(300.0/T)$^{1.4}$	(a)
16	$O(^1D) + H_2O \rightarrow 2\ OH$	2.3E-10	(a)
17	$O(^1D) + H_2 \rightarrow H + OH$	9.9E-11	(a)
18	$HO_2 + OH \rightarrow H_2O + O_2$	4.0E-11	(a)
19	$OH + OH \rightarrow H_2O + O$	1.0E-11*exp(-500.0/T)	(a)
20	$HO_2 + HO_2 \rightarrow H_2O_2 + O_2$	2.5E-12	(a)
21	$H_2O_2 + OH \rightarrow HO_2 + H_2O$	1.0E-11*exp(-750.0/T)	(a)

Table A2. (Continued.)

Reaction No.	Reaction	Rate Expression (mole - cgs units)	Reference
22	$HO_2 + NO \rightarrow OH + NO_2$	3.4E-12*exp(250.0/T)	(a)
23	$HO_2 + NO_2 \rightarrow HNO_2 + O_2$	3.0E-14	(f)
24	$OH + NO_2 \overset{M}{\rightleftharpoons} HNO_3$	$2.6E-30*exp(300.0/T)^{2.9}$	(a)
25	$OH + NO \overset{M}{\rightleftharpoons} HNO_2$	2.0E-12	(g)
26	$HNO_3 + OH \rightarrow NO_3 + H_2O$	8.5E-14	(a)
27	$HNO_3 \rightarrow$ rainout	see text	(d)
28	$NO_2 + O_3 \rightarrow NO_3 + O_2$	1.2E-13*exp(2450.0/T)	(a)
29	$NO + O_3 \rightarrow NO_2 + O_2$	2.3E-12*exp(-1450.0/T)	(a)
30	$NO_3 + NO_2 \overset{M}{\rightleftharpoons} N_2O_5$	3.8E-12	(g)
31	$NO_3 + NO_2 \rightarrow NO + NO_2 + O_2$	2.3E-13*exp(-1000.0/T)	(h)
32	$NO_3 + NO \rightarrow 2\ NO_2$	8.7E-12	(i)
33	$NO + NO_2 + H_2O \rightarrow 2\ HNO_2$	6.0E-37	(j)
34	$N_2O_5 + H_2O \rightarrow 2\ HNO_3$	1.0E-20	(k)
35	$N_2O_5 \rightarrow NO_3 + NO_2$	5.7E-14*exp(-10600.0/T)	(g)
36	$O + O_2 + M \rightarrow O_3 + M$	$6.2E-34*(300.0/T)^{2.1}$	(a)
37	$O(^1D) + M \rightarrow O(^3p) + M$	3.2E-11	(l)
38	$OH + O_3 \rightarrow HO_2 + O_2$	1.6E-12*exp(-940.0/T)	(a)
39	$HO_2 + O_3 \rightarrow OH + 2\ O_2$	1.1E-14*exp(-580.0/T)	(a)
40	$OH + HNO_2 \rightarrow NO_2 + H_2O$	2.1E-12	(m)
41	$O(^1D) + CH_4 \rightarrow CH_2O + H_2$	1.4E-11	(a)
42	$N_2H_4 + H \rightarrow N_2H_3 + H_2$	9.9E-12*exp(-1200.0/T)	(n)
43	$N_2H_3 + N_2H_3 \rightarrow 2\ NH_3 + N_2$	$K_{43} << K_{44}$	(o)

Table A2. (Continued.)

Reaction No.	Reaction	Rate Expression (mole - cgs units)	Reference
44	$N_2H_3 + N_2H_3 \rightarrow N_2H_4 + N_2H_2$	6.0E-11	(o)
45	$N_2H_3 + H \rightarrow 2\ NH_2$	2.7E-12	(o)
46	$NH_3 + O \rightarrow NH_2 + OH$	6.6E-12*exp(-3300.0/T)	(n)
47	$NH_3 + O(^1D) \rightarrow NH_2 + OH$	2.5E-10	(a)
48	$NH_3 + OH \rightarrow NH_2 + H_2O$	2.3E-12*exp(-800.0/T)	(n)
49	$NH_3 + H \rightarrow NH_2 + H_2$	1.0E-16	(n)
50	$NH_2 + O \rightarrow HNO + H$	1.8E-12	(n)
51	$NH_2 + O \rightarrow NH + OH$	1.8E-12	(n)
52	$NH_2 + OH \rightarrow NH_3 + O$	1.0E-13	(n)
53	$NH_2 + H_2 \rightarrow NH_3 + H$	1.0E-16	(n)
54	$NH_2 + NO \rightarrow N_2 + H_2O$	2.1E-11	(n)
55	$NH_2 + NH_2 \rightarrow N_2H_4$	1.0E-10	(o)
56	$NH + NO \rightarrow N_2 + O + H$	4.7E-11	(n)
57	$NH + O_2 \rightarrow NO + OH$	0.0	(p)
58	$NH + NO \rightarrow N_2 + OH$	3.9E-11	(q)
59	$HNO + O_2 \rightarrow NO + HO_2$	2.1E-20	(n)
60	$HNO + M \rightarrow NO + H + M$	5.0E-08*exp(-24500.0/T)	(n)
61	$HNO + H \rightarrow NO + H_2$	5.0E-14	(n)
62	$HNO + HNO \rightarrow N_2O + H_2O$	4.0E-15	(n)
63	$H + H + M \rightarrow H_2 + M$	8.3E-33	(n)
64	$H_2S + OH \rightarrow HS + H_2O$	1.05E-11*exp(-200.0/T)	(a)

Table A.2. (Continued.)

Reaction No.	Reaction	Rate Expression (mole - cgs units)	Reference
65	$HS + O \rightarrow SO + H$	1.6E-10	(n)
66	$HS + O_2 \rightarrow SO + OH$	1.0E-13	(n)
67	$HS + NO \rightarrow$ products	1.0E-12	(r)
68	$SO + O_2 \rightarrow SO_2 + O$	7.5E-13*exp(-3250.0/T)	(n)
69	$SO + NO_2 \rightarrow SO_2 + NO$	1.5E-11	(s)
70	$CS_2 + O \rightarrow SO + CS$	3.1E-11*exp(-640.0/T)(f_{70} = 0.8)	(a)
71	$CS_2 + O \rightarrow S + COS$	3.1E-11*exp(-640.0/T)(f_{71} = 0.1)	(a)
72	$CS_2 + O \rightarrow S_2 + CO$	3.1E-11*exp(-640.0/T)(f_{72} = 0.1)	(a)
73	$CS + O \rightarrow S + CO$	2.2E-11	(n)
74	$CS + O_2 \rightarrow SO + CO$	<3.0E-18	(s)
75	$CS + O_2 \rightarrow COS + O$	<3.0E-18	(s)
76	$S + O_2 \rightarrow SO + O$	2.2E-12	(t)
77	$SO_2 + OH\ (+M) \rightarrow HSO_3\ (+M)$	(8.2E-13*M)/(7.9E17 + M)	(u)
78	$SO_2 + HO_2 \rightarrow SO_3 + OH$	2.0E-17	(v)
79	$SO_2 + CH_3O_2 \rightarrow SO_3 + CH_3O$	<3.3E-15	(w)
80	$SO_3 + H_2O \rightarrow H_2SO_4$	9.1E-13	(n)
81	$SO_2 + O \rightarrow SO + O_2$	(2.1E-10/$_T$0.5)*exp(-9980.0/T)	(n)
82	$HS + H \rightarrow S + H_2$	2.5E-11	(n)
83	$S + H_2 \rightarrow HS + H$	2.2E-25	(n)
84	$H_2S + H \rightarrow HS + H_2$	1.29E-11*exp(860.0/T)	(n)
85	$COS + H \rightarrow HS + CO$	2.2E-14	(n)
86	$COS + OH \rightarrow HS + CO_2$	5.7E-14	(a)
87	$CS_2 + OH \rightarrow HS + COS$	1.9E-13	(a)

Table A2. (Continued.)

Reaction No.	Reaction	Rate Expression (mole - cgs units)	Reference
88	$S + CS_2 \rightarrow S_2 + CS$	6.5E-13	(n)
89	$S + COS \rightarrow S_2 + CO$	2.8E-12*exp(-2050.0/T)	(n)
90	$SO + SO \rightarrow S + SO_2$	3.0E-15	(n)
91	$SO + SO_3 \rightarrow 2\ SO_2$	2.0E-15	(n)
92	$SO_2 + CH_3\ (+M) \rightarrow CH_3SO_2$	3.0E-13	(n)
93	$HS + HS \rightarrow H_2S + S$	1.2E-11	(n)
94	$CH_3SH + O \rightarrow CH_3 + HSO$	1.9E-12	(x)
95	$CH_3SH + O \rightarrow CH_3SO + H$	1.9E-12	(x)
96	$CH_3SH + O \rightarrow CH_3SOH$	1.9E-12	(x)
97	$CH_3SH + OH \rightarrow$ products	3.4E-11	(y)
98	$CH_3SCH_3 + O \rightarrow CH_3SO + CH_3$	4.8E-11	(z)
99	$CH_3SCH_3 + O \rightarrow CH_2S + CH_3O$	6.3E-11	(x)
100	$CH_3SCH_3 + OH \rightarrow$ products	6.08E-12*exp(134.0/T)	(aa)
101	$COS + O \rightarrow SO + CO$	2.1E-11*exp(-2200.0/T)	(a)
102	$H_2S + O \rightarrow HS + OH$	2.4E-12*exp(-1300.0/T)	(a)
103	$SO + O_3 \rightarrow SO_2 + O_2$	2.5E-12*exp(-1050.0/T)	(n)
104	$SO_2 + O + M \rightarrow SO_3 + M$	3.4E-32*exp(-1130.0/T)	(n)
105	$HSO_3 + OH \rightarrow SO_3 + H_2O$	1.0E-11	(bb)
106	$SO_2 \rightarrow$ washout	3.8E-6*(10-z)/10	(bb)
107	$HSO_3 \rightarrow$ washout	2.3E-5*(10-z)/10	(bb)
108	$H_2SO_4 \rightarrow$ washout	2.3E-5*(10-z)/10	(bb)
109	$CH_3O_2 + CH_3O_2 \rightarrow 2\ CH_3O + O_2$	2.6E-13	(a)

Table A.2. (Continued.)

Reaction No.	Reaction	Rate Expression (mole - cgs units)	Reference
110	$HNO_3 + O \rightarrow NO_3 + OH$	3.0E-17	(a)
111	$HNO_2 + O_3 \rightarrow HNO_3 + O_2$	5.0E-19	(a)
112	$NO + HO_2 \rightarrow HNO_3$	1.4E-13	(a)
113	$NO_3 + H_2O \rightarrow HNO_3 + OH$	2.3E-26	(a)
114	$H + HNO_3 \rightarrow$ products	1.0E-13	(a)

References for kinetic data:

(a) Chemical Kinetic and Photochemical Data for Use in Stratospheric Modeling. Evaluation Number 2, JPL Publication 79-27. (Available from NASA.)

(b) Levy, H., II: Photochemistry of Minot Constituents in the Troposphere. Planetary and Space Sci., Vol. 20, No. 6, June 1973, pp. 575-591.

(c) Pate, C.T.; Finlayson, B.J.; and Pitts, J.N., Jr.: A Long Path Infrared Spectroscopic Study of the Reaction of Methyl-Peroxy Free Radicals with Nitric Oxide. J. Am. Chem. Soc., Vol. 96, No. 21, Oct. 1974, pp. 6554-6558.

(d) Chameides, W.L.; and Stedman, D.H.: Tropospheric Ozone: Coupling Transport and Photochemistry. J. Geochem. Res., Vol. 82, No. 12, Apr. 1977, pp. 1787-1794.

(e) Davis, D.D.; Payne, W.A.; and Stief, L.J.: The Hydro-Peroxyl Radical in Atmospheric Chemical Dynamics: Reaction with Carbon Monoxide. Science, Vol. 179, No. 4070, Jan. 1973, pp. 280-282.

(f) Chemical Kinetics and Photochemical Data for Modeling Atmospheric Chemistry, edited by Hampson, R.F.; and Garvin, D., NBS Technical Note 866, National Bureau of Standards (Gaithersburg, Md.).

Table A2. (Continued.)

(g) Baulch, D.L.; Drysdale, D.D.; Horne, D.G.; and Lloyd, A.C.: Evaluated Kinetic Data for High Temperature Reactions. Homogeneous Gas Phase Reactions of the H_2-N_2-O_2 System, Vol. 2. Chemical Rubber Company Press (Cleveland, Ohio), 1973.

(h) Chemical Kinetics Data Survey 7. Tables of Rate and Photochemical data for Modeling the Stratosphere, edited by Garvin, D.; and Hampson, R.F., Report NBSIR 74-430, National Bureau of Standards (Gaithersburg, Md.), 1974.

(i) Harker, A.B.; and Johnston, H.S.: Photolysis of Nitrogen Dioxide to Produce Transient O, NO_3, and N_2O_5. J. Phys. Chem., Vol. 77, No. 9, Apr. 1973, pp. 1153-1156.

(j) Chan, W.H.; Nordstrum, R.J.; Calvert, J.G.; and Shaw, J.H.: An IRFTS Spectroscopic Study of the Kinetics and the Mechanism of the Reactions in the Gaseous System HONO, HO, HO_2, H_2O. Chem. Phys. Lett., Vol. 37, No. 3, Feb. 1976, pp. 441-446.

(k) Morris, E.D., Jr.; and Niki, H.: Mass Spectrometric Study of the Hydroxyl Radical with Formaldehyde. J. Chem. Phys., Vol. 64, Aug. 1971, pp. 1991-1992.

(l) Davidson, J.A.; Sadlowski, C.M.; Schiff, H.I.; Streit, G.E.; Howard, C.J.; Jennings, D.A.; and Schmeltekopf, A.L.: Absolute Rate Constant Determinations for the Deactivation of $O(^1D)$ by Time Resolved Decay of $O(^1D) \rightarrow O(^3p)$ Emission. J. Chem. Phys., Vol. 64, No. 1, Jan. 1976, pp. 57-62.

(m) Cox, R.A.: The Photolysis of Gaseous Nitrous Acid - A Technique for Obtaining Kinetic Data on Atmospheric Photo-Oxidation Reactions. Proceedings of the Symposium on Chemical Kinetics Data for the Lower and Upper Atmosphere, edited by Benson, S.W.. Wiley - Interscience (N.Y.), 1975, pp. 379-398.

(n) Reaction Rate and Photochemical Data for Atmospheric Chemistry - 1977. Edited by Hampson, R.F.; and Garvin, D., National Bureau of Standards Special Publication 513, U.S. Government Printing Office (Washington, D.C.), 1978.

(o) Atreya, S.K.; Donahue, T.M.; and Kuhn, W.R.: The Distribution of Ammonia and Its Photochemical Products on Jupiter. Icarus, Vol. 31, No. 3, July 1977, pp. 348-355.

(p) McConnell, J.C.: Atmospheric Ammonia. J. Geophys. Res., Vol. 78, No. 33, Nov. 1973, pp. 7812-7821.

Table A2. (Continued.)

(q) Gordon, S.; Mulac, W.; and Nangia, P.: Pulse Radiolysis of Ammonia Gas, 2, Rate of Disappearance of the $NH_2(X_2B_1)$ Radical. J. Phys. Chem., Vol. 75, No. 14, July 1971, pp. 2087-2093.

(r) Bradley, J.N.; Trueman, S.P.; Whytock, D.A.; and Zaleski, T.A.: Electron Spin Resonance Study of the Reaction of Hydrogen Atoms with Hydrogen Sulfide. J. Chem. Soc. London, Faraday Transactions I, Vol. 69, No. 2, Feb. 1973, pp. 416-425.

(s) Schofield, K.: Evaluated Chemical Kinetic Rate Constants for Various Gas Phase Reactions. J. Phys. Chem. Reference Data, Vol. 2, No. 1, Jan. 1973, pp. 25-84.

(t) Davis, D.D.; Klemm, R.B.; and Pilling, M.: A Flash Photolysis-Resonance Fluorescene Kinetics Study of Ground-State Sulfur Atoms: I. Absolute Rate Parameters for Reaction of $S(^3p)$ with $O_2(^3\Sigma)$. Int. J. Chem. Kinetics, Vol. 4, No. 4, July 1972, pp. 367-382.

(u) Moortgat, G.K.; and Junge, C.E.: The Role of SO_2 Oxidation for the Background Stratosphere Sulfate Layer in the Light of New Reaction Rate Data. Pure and Appl. Geophys., Vol. 115, Nos. 4-6, 1977, pp. 759-774.

(v) Burrows, J.P.; Cliff, D.I.; Harris, G.W.; Thrush, B.A.; and Wilkinson, J.P.T.: World Meterorological Organization Technical Note No. 511, 1978, pp. 25-28. (Available from W.M.O., Geneva, Switzerland).

(w) Whitbeck, M.R.: A Kinetic Study of CH_3O_2 and $(CH_3)_3CO_2$ Radical Reactions by Kinetic Flash Spectroscopy. Paper presented at 12th Informal Conference on Photochemistry, National Bureau of Standards (Gaithersburg, Md.), June 28, 1976.

(x) Slagle, I.R.; Graham, P.E.; and Gutman, D.: Direct Identification of Reactive Routes and Measurements of Rate Constants in the Reactions of Oxygen Atoms with Methanethiol, Ethanethiol, and Methylsulfide. Int. J. Chem. Kinetics, Vol. 8, No. 3, May 1976, pp. 451-458.

(y) Atkinson, R.; Perry, R.A.; and Pitts, J.N., Jr.: Rate Constants for the Reactions of the OH Radical with CH_3SH and CH_3NH_2 over the Temperature Range 299-426 K. J. Chem. Phys., Vol. 66, No. 4, Feb. 1977, pp. 1578-1581.

(z) Lee, J.H.; Timmons, R.B.; and Stief, L.J.: Absolute Rate Parameters for the Reaction of Ground State Oxygen with Dimethyl Sulfide and Episulfide. J. Chem. Phys., Vol. 66, No. 4, Feb. 1977, 1578-1581.

Table A2. (Concluded.)

(aa) Kurylo, M.: Flash Photolysis Resonance Fluorescence Investigation of the Reaction of OH Radicals with Dimethyl Sulfide. Chem. Phys. Lett., Vol. 58, No. 2, Sept. 1978, pp. 233-237.

(bb) Turco, R.P.; Hamill, P.; Toon, O.B.; Whitten, R.C.; and Kiang, C.S.: A One-Dimensional Model Describing Aerosol Formation and Evolution in the Stratosphere: I. Physical Processes and Mathematical Analogs. J. Atmos. Sci., Vol. 36, No. 4, Apr. 1979, pp. 699-717.

APPENDIX B

THE CONTINUITY EQUATION

The continuity equation can be written in either number density form or mixing ratio form. In the present one-dimensional tropospheric photochemical model, the mixing ratio form is used. The vertical profile of a long-lived species is then expressed as

$$\frac{\partial \phi_i}{\partial z} = Q_i(n_j) - L_i(n_j)Mf_i \tag{B1}$$

where ϕ_i is the vertical flux (molecules cm^{-2} s^{-1}) of the ith species; $Q_i \times (n_J)$ are the chemical production terms; $L_i(n_j)Mf_i$ are the chemical loss terms of the ith species; M is the total number density (molecules cm^{-3}), f_i is the mixing ratio of the ith species, and M and f are related by the expression

$$f_i = \frac{n_i}{M} \tag{B2}$$

where n_i is the number density of the species under consideration. The vertical flux of the ith species ϕ_i can be written in terms of a parameterization K_z:

$$\phi_i = -K_z\ M \left[\frac{\partial f_i}{\partial z}\right] \tag{B3}$$

The term K_z is an empirical constant (cm^2 s^{-1}) usually called the "eddy diffusion coefficient." The word "eddy" is somewhat of a misnomer since it indicates that the diffusive process occurs on a small scale. On the contrary, most vertical transport in the troposphere takes place on a very large scale. Substitution of equation (B3) into equation (B1) yields

$$\frac{\partial}{\partial z} \quad K_z\ M \left[\left(\frac{\partial f_i}{\partial z}\right)\right] = -Q_i(n_j) + L_i(n_j)\ Mf_i \tag{B4}$$

Because equation (B4) usually depends on many species other than the ith, it is a highly coupled, nonlinear, partial differential equation that has to be solved numerically.

In the case of short-lived species, the chemistry dominates the vertical distribution. For these species the vertical transport terms [i.e., the terms on the left-hand side of eq. (B4)] can be neglected. This condition is known as photochemical equilibrium (PCE). If the PCE assumption is justified, the solution of equation (B4) is simplified considerably, since we can solve explicitly for f_i:

$$f_i = \frac{Q_i(n_j)}{L_i(n_j)M} \tag{B5}$$

Hence, in the cases where PCE can be used, a high degree of computational efficiency, both in terms of time and money, can be reached.

The present one-dimensional global tropospheric photochemical model calculates the continuity equation in the mixing ratio form, previously given in equation (B4). By expanding the derivative with respect to altitude and rearranging the terms in equation (B4) we obtain

$$K_z M \frac{\partial^2 f_i}{\partial z^2} + \frac{\partial}{\partial z}(K_z M)\frac{\partial f_i}{\partial z} - L_i(n_j) M f_i + Q_i(n_j) = 0 \tag{B6}$$

After dividing this equation by M, we obtain

$$K_z \frac{\partial^2 f_i}{\partial z^2} + \frac{1}{M}\frac{\partial}{\partial z}(K_z M)\frac{\partial f_i}{\partial z} - L_i(n_j) f_i + \frac{Q_i(n_j)}{M} = 0 \tag{B7}$$

Equation (B7) defines a system of equations for each species f_i. A finite-difference scheme is used to solve the equations (ref. 202). The finite-difference equations are defined as

$$\frac{\partial^2 f}{\partial z^2} \rightarrow \frac{f_{k+1} - 2f_k + f_{k-1}}{\Delta z^2} \quad \text{(for second-order equations)} \tag{B8}$$

and

$$\frac{\partial f}{\partial z} \rightarrow \frac{f_{k+1} - f_{k-1}}{2\Delta z} \quad \text{(for first-order equations)} \tag{B9}$$

Substituting these equations into equation (B4), rearranging terms, and dropping the species index i and subscript z on K_z, we obtain

$$f_{k+1}\left[\frac{K_k}{\Delta z^2} + \frac{A}{2\Delta z}\right] + f_k\left[\frac{2K_k}{\Delta z^2} - L\right] + f_{k-1}\left[\frac{K_k}{\Delta z^2} - \frac{A}{2\Delta z}\right] = \frac{Q}{M} \tag{B10}$$

The term A represents

$$\frac{1}{M}\frac{\partial(K_z M)}{\partial z}$$

and the index k refers to the spatial derivative z. Equation (B10) can be written in finite-difference form as

$$\vec{A} \cdot f_{k+1} + \vec{B} \cdot f_k + \vec{C} \cdot f_{k-1} = \vec{D} \tag{B11}$$

APPENDIX C

BOUNDARY CONDITIONS

Two types of boundary conditions are available to solve the continuity equation. We can either specify a mixing ratio f_i or a flux ϕ_i upward or downward at the upper or lower boundaries. In general, the boundary condition can be written as

$$a_i \cdot \frac{\partial f_i}{\partial z} + b_i \cdot f_i = c_i \tag{C1}$$

If we specify a mixing ratio f_i at the lower boundary, $a_i = 0$, $b_i = 1$, and equation (C1) becomes

$$f_i = c_i \tag{C2}$$

or, in finite-difference form,

$$\vec{B}_\ell \cdot f_\ell = \vec{D}_\ell \tag{C3}$$

where the subscript ℓ is used to denote "lower boundary." If a mixing ratio is specified at the upper boundary, $a_i = 1$, $b_i = 0$, and equation (C1) becomes

$$a_i \cdot \frac{\partial f_i}{\partial z} = c_i \tag{C4}$$

In finite-difference form (with subscript u for "upper boundary"):

$$\vec{B}_u \cdot f_u + \vec{C}_u \cdot f_u = \vec{D}_u \tag{C5}$$

This result is obtained from an expansion of equation (C4)

$$\frac{f_u - f_{u-1}}{\Delta z} = c_u \tag{C6}$$

This can be arranged to

$$f_u - f_{u-1} = c_u \, \Delta z \tag{C7}$$

which in finite-difference form can be written as equation (C5), with

$$\vec{B}_u = 1, \ \vec{C}_u = 0, \text{ and } \vec{D}_u = c_u \, \Delta z$$

For an upward or downward flux across the upper boundary, the boundary condition reduces to

$$\frac{\partial f(\phi)_u}{\partial z} = c(\phi)_u \tag{C8}$$

The finite-difference form looks similar to equation (C5):

$$\vec{B}(\phi)_u \cdot f(\phi)_u + \vec{C}(\phi)_u \cdot f(\phi)_u = \vec{D}(\phi)_u \tag{C9}$$

In this case, $\vec{B}(\phi)_u = 1$, $\vec{C}(\phi)_u = -1$, $\vec{D}(\phi)_u = \vec{C}(\phi)_u + \vec{C}(\phi)_u \, \Delta z$, and $\vec{A}(\phi)_u = 0$. For a flux, upward or downward across the lower boundary, equations (C8) and (C9) are still valid, except in this case, $\vec{B}(\phi)_\ell = -1$, $\vec{C}(\phi)_\ell = 1$, $\vec{D}(\phi)_\ell = \vec{C}(\phi)_\ell \, \Delta z$ and $\vec{A}(\phi)_\ell = 0$.

Equation (B11) from Appendix B, together with equations (C3) and (C5), forms a so-called "block tridiagonal" system of equations given by

$$\begin{bmatrix} \vec{B} & \vec{A}_\ell & 0 & . & . & . & . & 0 \\ \vec{C}_2 & \vec{B}_2 & \vec{A}_2 & 0 & . & . & . & 0 \\ 0 & \vec{C}_3 & \vec{B}_3 & \vec{A}_3 & . & . & . & 0 \\ . & . & . & . & . & . & . & . \\ 0 & . & . & 0 & \vec{C}_{u-1} & \vec{B}_{u-1} & & \vec{A}_{u-1} \\ 0 & . & . & . & 0 & \vec{C}_u & & \vec{B}_u \end{bmatrix} \begin{bmatrix} f_\ell \\ f_2 \\ f_3 \\ . \\ f_{u-1} \\ f_u \end{bmatrix} = \begin{bmatrix} \vec{D}_\ell \\ \vec{D}_2 \\ \vec{D}_3 \\ . \\ \vec{D}_{u-1} \\ \vec{D}_u \end{bmatrix} \tag{C10}$$

There are several numerical techniques available to solve the tridiagonal matrix described by equation (C10). In the present model, a Gaussian elimination method without pivoting is used (ref. 202).

APPENDIX D

CONVERGENCE CRITERIA

The model imposes two separate convergence criteria, one for the species in photochemical equilibrium and one for the species that are calculated using the continuity equation. The number of iterations needed is a strong function of the initial profiles that are prescribed. In general, the flow of the calculations of the model is as follows: first, the initial profiles for all species are prescribed. Second, the reaction rate constants are calculated. Next, the incident solar radiation is calculated and, based on these results, the photodissociation rates are computed. The model then calculates the vertical profiles of the short-lived species in photochemical equilibrium. Finally, the long-lived species that are transported are calculated. The vertical profiles that are obtained for the species are compared to the previous iteration and recalculated until the convergence criteria is achieved. For the short-lived species, the convergence criteria are

$$\left| 1 - \frac{(n_i)_1}{(n_i)_2} \right| < 10^{-6} \tag{D1}$$

and for the transported species the criteria are

$$\left| 1 - \frac{(n_i)_1}{(n_i)_2} \right| < 10^{-4} \tag{D2}$$

Computationally, the photochemical equilibrium species are calculated much more rapidly than the transported species; therefore, a somewhat more stringent convergence criterion can be imposed on the PCE species. With reasonably close initial guesses of the vertical profiles (i.e., vertical profiles within a couple of orders of magnitude of the final profiles), convergence is achieved after three or four iterations for the short-lived species and five to six iterations for the long-lived species.

LANGLEY RESEARCH CENTER
3 1176 00511 3320